OÉ Gaillimh
NUI Galway

A Study of Black Carbon and Related Measurements from Ireland's Atmospheric Composition and Climate Change (AC^3) Network

A Thesis

Submitted by

Teresa Kristine Spohn

for the degree of

Doctor of Philosophy

School of Physics, College of Science and Engineering,

Ryan Institute's Centre for Climate & Air Pollution Studies,

National University of Ireland Galway.

Academic Supervisor: Professor Colin O'Dowd

March 2021.

Table of Contents

List of Tables

List of Figures

List of Abbreviations

µg/m3	micrograms/metre cubed
AC3	Atmospheric Composition and Climate Change
ACMCC	Aerosol Chemical Monitoring Calibration Center
ACSM	Aerosol Chemical Speciation Monitor
ACTRIS	Aerosols, Clouds, and Trace Gas Infrastructure
AGAGE	Advanced Global Atmospheric Gases Experiment
alpha (α)	Angtrom Absorption Exponent
AMS	Aerosol Mass Spectrometer
AOD	Aerosol Optical Depth
ATN	Attenuation
BB	Biomass Burning
BC	Black Carbon
BC6	880nm wavelength of aethalometer
CAMS	Copernicus Atmospheric Monitoring System
CEDS	Community Emissions Data System
CLRTAP	Convention on Long-Range Transboundary Air Pollution
CMIP6	Coupled Model Inter-comparison Project phase 6
CPC	Condensation Particle Counter
CRI	Common Representative Intermediates
CRP	Carnsore Point
DC	Direct Current
DEMC	Differential Electrical Mobility Classifier
EC	Elemental Carbon
ECAC	European Center for Aerosol Calibration
ECMWF	European Centre for Medium-range Weather Forecasting
EEA	European Environmental Agency

EMEP	European Monitoring and Evaluation Programme
EPA	Environmental Protection Agency
EU	European Union
GAW	Global Atmospheric Watch
GENEMIS	Generation and Evaluation of Emission Data
GHG	Green House Gas
ICOS	Integrated Carbon Observation System
IMP	Intensive Monitoring Period
IMPLICIT	IMProving inversion modeL Capability in Ireland
IPCC	International Panel on Climate Change
MAAP	Multi-Angle Absorption Photometer
MAC	Mass Absorption Cross-section
MHD	Mace Head
MLH	Malin Head
MOSAIC	Model for Simulating Aerosol Interactions and Chemistry
MYJ	Mellor-Yamada-Janjic
NAMBLEX	North Atlantic Marine Boundary Layer Experiment
ng/m3	nanograms/metre cubed
NILU	Norwegian Institute for Air Research
NUIG	National University of Ireland, Galway
OC	Organic Carbon
PARFORCE	New Particle Formation and Fate in the Coastal Environment
PASS	Photo Acoustic Soot Spectrometer
PBL	Planetary Boundary Layer
pcc	particles per cubic centimetre
PI	Principle Investigator
PM	Particulate Matter

PM1	PM smaller than 1 micron
PM10	PM smaller than 10 microns
PM2.5	PM smaller than 2.4 microns
PMF	positive matrix factorization
ppb	parts per billion
PSAP	Particle Soot Absorption Spectrometer
PSI	Paul Scherrer Institute
RF	Response Factor
SIRTA	Site Instrumental de Recherche par Télédétection Atmosphérique
SLCF	Short-Lived Climate Forcer
SMPS	Scanning Mobility Particle Sizer
SOA	Secondary Organic Aerosol
STILT	Stochastic Time-Inverted Lagrangian Transport Model
TC	Total Carbon
TEOM	Tapered Element Oscillating Microbalance
TXB	Transboundary
UCD	University College Dublin
UK	United Kingdom
UV	Ultra-Violet
VOC	Volatile Organic Compound
WACCM	Whole Atmosphere Community Climate Model
WHO	World Health Organisation
WMO	World Meteorological Organization
XPS	X-Ray Photoelectron Spectroscopy
YSU	Yonsei University

Declaration

I hereby declare that none of the work described in this thesis has been presented to this or any other university in support of an application for a higher degree.

Teresa K. Spohn

Statement of Contribution to Work Presented

I performed the entire literature review in Chapter 1. While the network was already in existence, I helped in setting up and maintaining most of the instruments on the network which involved frequent visits to the stations listed in Chapter 2. I also processed the data from the EMEP campaign for organic carbon, elemental carbon, and total carbon. Data for the ACSM were provided by others in our research group. I was responsible for validating the AE33 against the AE16 aethalometer and the MAAP in Chapter 3, however ACSM calibration was performed by others in Paris. All the data analysis in Chapters 4 and 5 was conducted by me, however high volume sampler and data for stations not on the network were downloaded from the Irish Environmental Protection website. The modelling data in Chapter 6 were provided by members of our research team at NUIG and Douglas Lowe from Manchester University.

Abstract

A national aethalometer network for monitoring black carbon was developed at three Irish regional stations (Mace Head, Malin Head, and Carnsore Point) as part of Ireland's Atmospheric Composition and Climate Change (AC^3) Network in 2017. This work provides an extensive analysis of black carbon in combination with other network data in order to assess the broader scope of the network's capabilities to monitor the impact of local, regional, and trans-boundary air masses on the measurements. Results show 33% of black carbon arrives at Carnsore Point from the east, while the wind is only from that direction 14% of the time. A comparison of the aethalometer biomass burning function against levoglucosan indicates the instrument default settings are adequate for this environment. Analysis of organic carbon and PM1 organics measurements showed PM1 organics comprise only between 40-60% of total organic matter. This is confirmed through the mass closure experiment for both PM10 and PM2.5. High particle counts were evaluated using a CPC and SMPS and occur most frequently in the summer months during low tides, with very small particle diameters indicative of new particle formation. The Covid-19 lockdown restrictions impacted regional pollution levels as indicated by a 5.6% reduction in ozone measured at rural stations compared to a 13.7% increase in suburban areas. The study concludes with a preliminary look at how the network data can be applied toward modelling applications, laying the groundwork for future research and improved models and emissions inventories.

Acknowledgements

This work would not have been possible without the kindness and generosity of my supervisor, Professor Colin O'Dowd, who took me on as his student and provided me with the extra time and funding needed to complete my degree. My sincerest thanks for everything you have done to help me.

Great thanks also to my co-supervisor, Dr. Damien Martin, for all your patience and understanding. You kept me on track and continuously challenged me to achieve my best.

My gratitude extends to all those at NUIG, the School of Physics, and the Centre for Climate and Air Pollution Studies, and those affiliated who have been there to help and support me these last years. Particular thanks go to: Dr. Michael Geever, for the weekly data updates and troubleshooting at Carnsore Point; Dr. Jana Preissler, for always being available to help me with Python programming issues; Chunsui Lin, for helping me get a grasp on the ACSM data; Liz Coleman, Mark Neary, and Clare Noone for WRF-Chem and server support; Douglas Lowe from Manchester University for the use of his WRF-Chem data; Derek Coburn, Stuart Haries, and James Nallen, for their technical support; and my fellow students in the office and the break room who made me laugh and smile even when I felt I couldn't.

Additionally, I would like to thank all those outside of the university who have been there for me during what has been the most difficult time in my life, especially: My parents, Bruce and Ingrid Spohn; my sister, Jennifer Spohn; my dearest friends: Niall, Christine, Ger, Marina, Maya, and Kathy. I owe a huge debt of gratitude to my master's supervisor, Prof. Bernhard Rappenglueck from the University of Houston for his on-going support and feedback, which gave me the confidence I needed to succeed. And last but not least, very special thanks to Grzegorz for helping to keep me focused when I was running out of steam at the end.

Funding for this project was provided by the Irish Research Council, and the Irish Environmental Protection Agency (EPA Ireland).

Dedication

In Memoriam G. Paul Roberts

1. Introduction

1.1 Motivation

Climate change is the biggest challenge facing the world today, threatening the very existence of humanity. Extreme weather, rising sea levels, and melting polar ice are already starting to have devastating effects on civilisation world-wide. While the earth naturally cycles through periods of warming and cooling at regular intervals, it has been shown that the warming trend has rapidly increased since the 1900's, the time of the industrial revolution, indicating that human activities are to blame [*Hegerl et al.*, 2019].

In the interest of self-preservation, it has become crucial to study and understand the changes that are happening, in order to at least mitigate the impact on our environment. To this end, governments and organisations around the world have funded research, set up monitoring networks, and signed agreements to regulate substances which are not only harmful to human health, but detrimental to the Earth's climate as well. It is a very broad area of research, with some topics already well understood, while others remain are still under investigation.

Every contribution, however small, can help to construct the bigger picture, and it is the focus of this study to investigate the nature and source of aerosols, in particular Black Carbon (BC) in Ireland, using measurements from a three-node monitoring network at coastal stations on opposing sides of the country. This will improve emissions inventories and model inputs by providing a better understanding of long-range transport of pollutants. Ultimately it may lead to policies and regulations regarding emissions on a national or international scale, aimed at containing the impact humans have on Earth's climate.

1.2 Background

Green house gases (GHGs) are those which contribute to the warming of the atmosphere. The two most potent ones are Carbon Dioxide (CO_2) and Methane (CH_4), but also include Ozone (O_3), Carbon Monoxide (CO), water vapour (H_2O), and Nitrous Oxide (N_2O). Black Carbon (BC) is actually a particulate that acts to trap heat through absorption of sunlight, but has been shown to have similar warming effects as CO_2 and CH_4 in the atmosphere [*Kleefeld et al.*, 2002; *Ravishankara et al.*, 2009]. It is considered a Short-Lived Climate Forcer (SLCF), meaning that its atmospheric life-time is relatively short, lasting only days to months, rather than years. The graphics in **Figure 1** show the impact on warming and cooling of the atmosphere of various species, with the right panel focusing specifically on BC emissions. There is still very high uncertainty in the measurements, and more research is needed to fully understand these processes.

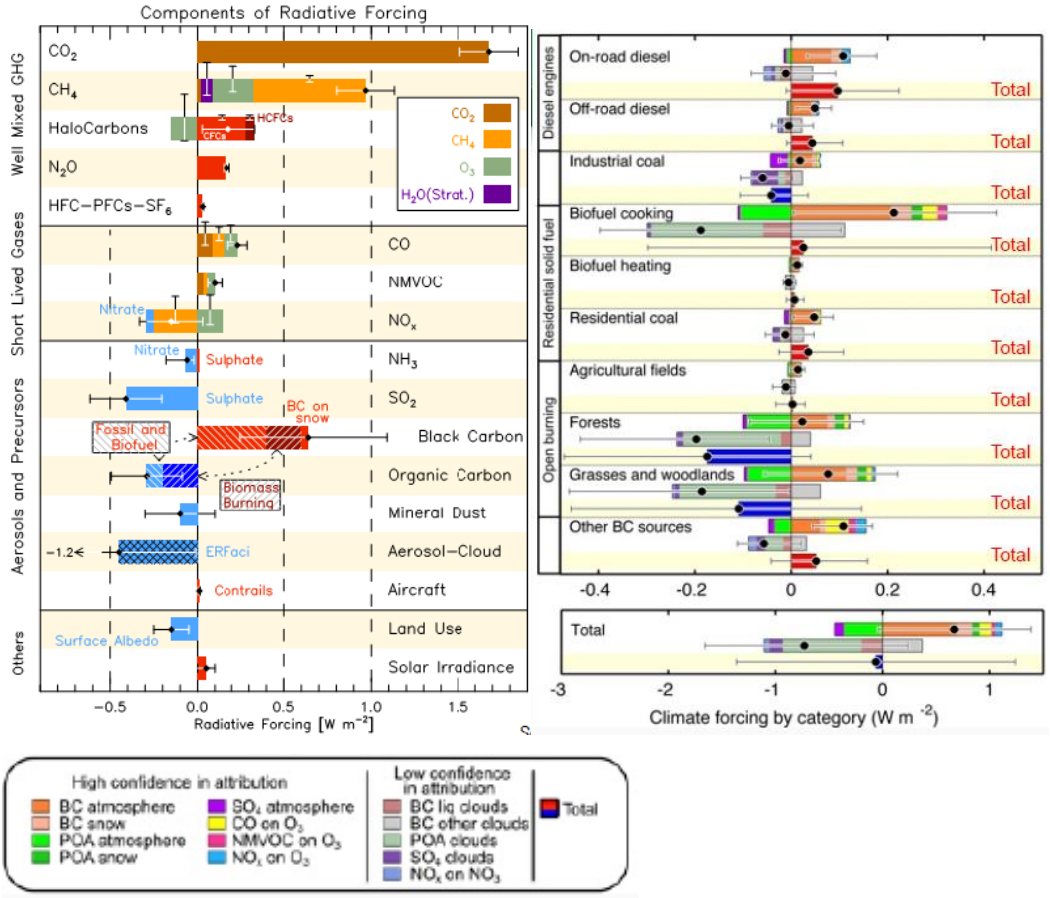

Figure 1 The above infographics from the IPCC, 2013 (left) and Bond et al 2013 (right) show the relative warming or cooling effects of various species of climate forcers, with a focus on Black Carbon in the right panel.

The warming of the Earth's atmosphere is a result of changes in the radiative balance of energy being reflected, absorbed, or radiated from the surface or the atmosphere. GHGs and aerosols increase or decrease the amount of solar radiation received by the earth by absorbing or reflecting energy within the atmosphere. To some extent this is normal and desirable, as it keeps the planet at a comfortable temperature for sustaining life, however, an excess of GHGs will cause the global temperatures to rise too high, causing polar ice to melt, sea levels to rise, and extreme weather phenomena. It has been shown that the amount of CO_2 has increased by over 40% since pre-industrial times, to over 400ppb as measured at the Moana Loa Observatory in Hawaii. As a result of these increases in GHGs, the average global surface temperature has already increased by about more than 1°C since 1880 according to the National Aeronautics and Space Association Goddard Institute for Space Studies [*NASA*, 2019], and continues to increase at a much faster rate than before.

Based on the available information, the most recent report by the International Panel on Climate Change (IPCC 2018) predicts that global temperatures will have increased as a result of human activities by 1.5°C between the years 2030 and 2052, and that immediate and drastic action must be taken to avoid the temperature rising above 2°C , which would have catastrophic consequences for life on the planet [*Masson-Delmotte et al.*, 2018]. Extensive research is being conducted world-wide in an attempt to mitigate the effects of rising temperatures by gaining a better understanding of the chemical and physical characteristics of the gases and aerosols involved, and finding effective ways to halt or slow the process.

In an effort to contribute to this global undertaking, this study will investigate the atmospheric composition at Irish coastal stations based on the measurements of black carbon, which is a form of particulate matter, and the contribution of biomass burning, as well as other related measurements on the network.

1.2.1 Particulate matter

Particulate matter (PM) encompasses a wide variety of substances in the atmosphere from black carbon to sea salt. It is typically classed by size in microns, ranging from PM10 down to PM1. It has been shown to have both environmental and health impacts, depending on composition, type, and size. Some types of PM scatter light in the atmosphere and have a relative cooling effect, whereas others, such as black carbon absorb heat and cause the temperature to increase. Particles smaller than PM2.5 are known to cause respiratory illnesses and premature death as they are able to enter the bloodstream through the lungs. Certain types such as black carbon are also known carcinogens [*Grahame et al.*, 2014].

As there are many natural and anthropogenic sources of PM, understanding and regulating the human contribution to PM is important to minimise the adverse effects on climate and air quality. The Irish Environmental Protection Agency [*EPA-Ireland*, 2020a] monitors PM10 and PM2.5 at sites across the country, and found that while Ireland is still in compliance with EU regulations on daily and annual limits, it exceeded the World Health Organisation (WHO) daily limits for PM10 at 14 out of 30 stations, and 25 out of 30 stations for PM2.5 in 2019. Five of these stations also exceeded the WHO's annual limit for PM2.5 that year. The biggest anthropogenic source of PM2.5 in Ireland is home heating, specifically solid fuel burning.

1.2.2 Black Carbon

The main focus of this study is on Black Carbon (BC), a type of carbonaceous aerosol formed by incomplete combustion that falls into the category of PM1. Its sources are both natural (i.e. wildfires and volcanoes) and anthropogenic, with fossil fuels from traffic and domestic heating being the main contributors, making it useful as an anthropogenic tracer. Named for its light absorbing properties, it acts to trap heat in the atmosphere, thus behaving like a greenhouse gas, and is considered a strong short-lived climate forcer by the International Panel on Climate Change (IPCC)[*Alexander et al.*, 2013]. It is also a hazardous pollutant, affecting air quality and the human respiratory system when inhaled.

Studies have been done on BC as early as the 1950's, when London fog was a concern, and soot was the most visible pollutant. In the decades since then BC was largely disregarded and dismissed as insignificant in terms of climate, despite measurements indicating otherwise [*Novakov and Rosen*, 2013]. It is only since the beginning of the 21st century that BC has once again moved to the forefront of scientific investigation, with studies showing that it is being transported to remote regions of the planet, such as the arctic, affecting global temperatures and weather patterns through absorption of solar energy as well as albedo through atmospheric scattering and deposition on snow and ice. The study by Bond et al. [*Bond et al.*, 2013] has contributed the most comprehensive study of BC to date, much of which is being used as the source of information by the IPCC and other agencies. According to a study by Ramanthan and Carmichael [*Ramanathan and Carmichael*, 2008] BC is the second most potent climate forcer next to carbon dioxide (CO_2), and a simple reduction in BC emissions would have an immediate and positive impact on the radiative budget of the Earth's atmosphere.

1.2.3 Biomass Burning

Recently it was discovered that carbonaceous aerosols from biomass burning (BB) such as forest fires and residential wood burning, also known as brown carbon, affect the ultra violet (UV) light absorption in the atmosphere in addition to BC's absorption in the visible and near infrared spectrum [*Martinsson*, 2014]. Studies have been conducted in order to accurately distinguish and quantify the contribution of both BC and BB [*Garg et al.*, 2016; *Healy et al.*, 2017; *J. Sandradewi et al.*, 2008a], yet there is still very high uncertainty in the measurements.

Most of these studies are based on the model developed by Sandradewi et al. (2008a), which has since been incorporated into the aethalometers, enabling these instruments to apportion a percentage of the BC mass as BB. It relies on the Angstrom absorption coefficient or alpha (α) values for fossil fuel and wood (biomass) burning, which is the wavelength dependency of the absorption of the carbonaceous aerosol, which is typically between 0.9-1.0 for fossil fuel, and generically assigned the value of 2 in aethalometers for wood burning. The higher the α, the greater the wavelength dependence on absorption. This method appears

to work quite well in environments where the combustion types are known and limited to only a few types, such as the studies in the Swiss Alps, where wood burning was the primary biomass fuel in winter. However, the study by Garg et al. (2016) found that in India, where there are numerous sources of biomass burning, ranging from home cooking/heating, to crop and garbage burning, the α values for BB were not only much higher than 2, they varied based on combustion efficiency (flaming vs. smouldering), which in turn varied by moisture content and other factors. While Ireland does not produce nearly as much black or brown carbon as India, here there are also many variable sources of biomass burning, including turf (peat), which studies such as Healy et al. (2017) have shown to have very high α values, ranging from 7-11, as well as very high humidity in the atmosphere which might reduce combustion efficiency in wood or peat.

1.3 Monitoring Networks

As a result of the urgent need to mitigate Climate Change, as well as improve air quality, BC is currently of particular interest to governments and environmental agencies world-wide, and monitoring networks are being set up to gain a better understanding of BC concentration and distribution.

Ireland has been monitoring atmospheric aerosols since at least 1958 at Mace Head, and has since expanded the station to host a suite of the most sophisticated instrumentation for studying the unique conditions in this environment, which is generally considered the most pristine air in the northern hemisphere, with 60% of air masses coming from the Atlantic Ocean. As a result, Mace Head has been incorporated into the world's atmospheric monitoring networks, including Global Atmospheric Watch (GAW), World Meteorological Organisation (WMO), and EMEP (European Monitoring and Evaluation Programme), and has thus become renowned as the subject of many studies and monitoring campaigns. [*NUIG*, 2019].

Among the over 500 publications involving the Mace Head Atmospheric Research Station, there have been many relating to atmospheric aerosol and Black Carbon,

even including unusual events such as the eruption of the Icelandic volcano Eyjafjallajokull in 2010 [*C O'Dowd et al.*, 2011], and major international campaigns such as NAMBLEX (North Atlantic Marine Boundary Layer Experiment) [*Heard et al.*, 2006]. Notably, an early study of the seasonal variation of black carbon in the marine atmosphere was conducted at Mace Head for the period from 1989-1996 by Cooke et al. [*Cooke et al.*, 1997], using an older model aethalometer, providing an opportunity to build on this research by looking at changes over time with the advantage of more modern technology. Research at Mace Head is on-going, and it continues to be a valuable location for atmospheric research.

However, for Ireland it is insufficient to rely on one monitoring station alone in order to gain insight into the atmospheric conditions affecting air quality, climate, and weather. While other studies, such as the doctoral thesis by Paul Buckley [*Buckley*, 2019] and publications by Lin et al. [*Lin et al.*, 2017; *Lin et al.*, 2019] have been done intermittently at locations around the country in order to investigate the impacts of black carbon, thus far there has not been a cohesive monitoring network collecting atmospheric data within Ireland. In recent years, two other stations at Carnsore Point and Malin Head have begun regular measurements as part of Ireland's Transboundary Network. The current aim is to unite the stations into a single network, the Atmospheric Composition and Climate Change (AC^3) Network, which will provide a more comprehensive overview of the atmospheric conditions in Ireland. A brief description of the networks to be incorporated follows.

1.3.1 The Integrated Carbon Observation System (ICOS)

Figure 2 ICOS Measurement Stations in Europe taken from ICOS website

As part of various international agreements and protocols, Ireland is required to report annual emissions of GHGs [*EPA-Ireland*, 2016]. To do this, historically emissions inventories have been input into models producing a bottom up approach of emissions estimates. The Intergovernmental Panel on Climate Change (IPCC) [*Intergovernmental Panel on Climate*, 2006] provides a three tiered framework for making GHG estimates. Tier 1 consists of very generic data concerning potential sources such as agriculture or industry on a global scale. Tier 2 allows for country specific emission inventories based on land use and livestock demography, and Tier 3 would include very specific information on a very local scale, such as inventories of individual farms. Previous studies [*Y-H Chen and Prinn*, 2006; *Derwent et al.*, 2006; *Misselbrook et al.*, 2011; *J Wang et al.*, 2010] have found that using Tier 1 data routinely leads to over-prediction of GHGs by the models, along with huge uncertainties. In the absence of any country specific inventories, Ireland has been using Tier 1 data for the annual estimates, thus exceeding the limits set, for example, by the Kyoto Protocol. According to the most recent trends and projections of GHGs provided by the EPA Ireland (2020), GHG's have been reduced by 4% in 2019 compared to 2018, but Ireland is still not on track

to meet its commitments to the EU Effort Sharing 2020 target of achieving a 20% reduction compared to 2005 levels, having only reduced GHGs by 7% since then.

While GHGs are emitted by almost all sectors, such as industrial processes, waste, transport, and agriculture, the Irish Agriculture and Food Development Authority, Teagasc, [*Murphy*, 2015] are working on a detailed Tier 2 inventory for methane, the main agricultural source of GHG. However this is difficult because so many environmental variables affect emissions, such as temperature, rainfall, type of livestock (as well as age, weight, type of feed, etc.), seasons, and location, many of which are constantly changing, and it is not enough to simply know the number of livestock and land use to determine accurate emissions estimates. It would also be a never-ending task to keep up with the current numbers, and not a practical approach to solving the problem.

The Integrated Carbon Observation System (ICOS) is a European endeavor to measure and quantify the anthropogenic effects on the carbon cycle and climate change. It is subdivided into the areas marine, ecosystems, and atmospheric research. The atmospheric component of ICOS consists of a network of 100 monitoring stations throughout Europe, which have been measuring CO_2 and CH_4 since 2009. The purpose of the network is to provide high quality data on greenhouse gas (GHG) emissions to policy makers both on a global and regional scale, on which major decisions concerning standards and compliance can be based. Part of this involves using the measured data to improve models and emissions inventories, as these are still fraught with uncertainties. Having actual measurements eliminates the need for estimates, and will greatly improve the accuracy of both current and predicted emissions reporting [*ICOS*, 2016].
Three potential ICOS monitoring stations exist to date in Ireland: the Met Eireann Observatory at Malin Head (MLH) in the north in County Donegal, Mace Head Atmospheric Research Station (MHD) in the west in County Galway, and an EPA site at Carnsore Point (CRP) in the southeast in County Wexford [*EPA-Ireland*, 2016]. Currently Malin Head and Carnsore Point are compliant with ICOS standards for Class 2 stations, and Mace Head only lacks the required flask sampling capacity for a

Class 1 station, as Carnsore Point recently upgraded its meteorological measurement equipment. According to the ICOS Station Specifications [*ICOS*, 2015], the difference between a Class 1 and Class 2 station is the ability to continuously monitor CO (Carbon Monoxide) in addition to CO_2 and CH_4, obtain weekly flask samples of gases such as N_2O and SF_6 (Sulfur Hexafluouride), and measure boundary layer height. For all stations there are minimum equipment standards to ensure the best quality data and homogeneity throughout the network. Additionally the stations must be capable of measuring windspeed within 0.5 m/s, wind direction within 1 degree, temperature within 0.1 degree Celsius, relative humidity within 1%, and pressure within 0.1hPa, which only a limited number of meteorological stations are capable of. Tables on page 176 in Appendix C illustrate the ICOS requirements and the current state of compliance of the Irish stations. Data validation and verification procedures are subject to equally high standards. There is a well-defined system in place, through which station Principle Investigators (PIs) can flag and tag data before it is uploaded to a central server. The mechanisms in place for both quality control and quality assurance ensure that the end-product is to the highest standard.

The main concern now, before Ireland can officially join ICOS, is the potential of local contamination at the sites, as Malin Head is increasingly affected by traffic, and Carnsore Point is surrounded by agricultural land used for grazing livestock. ICOS requirements state that for coastal sites the top level should be sufficiently high to avoid local interference. Because of this, the air inlets at Carnsore Point are being moved to a higher elevation, and BC and CO_2 data at Malin Head are being evaluated as part of this study to determine whether the local sources are impacting the measurements.

1.3.2 Black Carbon and the Transboundary Network (TXB)

In addition to the greenhouse gases measured by ICOS, black carbon data are being collected at Mace Head, Malin Head, and Carnsore Point as part of the Transboundary Network since 2004 [*Leinert*, 2008]. The Transboundary Network was developed by the Irish Environmental Protection Agency (EPA Ireland) in

cooperation with the Irish weather service, Met Éireann, in response to the requirements of the European Monitoring and Evaluation Programme (EMEP). The EMEP protocol was established in 1984 and originated from the 1979 CLRTAP (Convention on Long-Range Transboundary Air Pollution) in Geneva. Its three main objectives are [*Fagerli et al.*]:

1. Collection of emissions data
2. Measurements of air and precipitation quality
3. Modelling of atmospheric transport and deposition of air pollutants

While the EPA's main focus is on air quality, health effects, and EU compliance, the EMEP focuses on long-term data collection of transboundary pollution. The Transboundary Network links these objectives and unifies them in a common purpose.

Currently the Transboundary Network comprises of four stations: Malin Head (County Donegal), Mace Head (County Galway), Carnsore Point (County Wexford), and Oak Park (County Carlow). Valentia (County Kerry) was previously involved in data collection and is currently undergoing upgrades and maintenance in order to be an active monitoring station again in the near future. The defining characteristic of these stations is their location, mostly at or near the coast, with the ability to monitor incoming, or transboundary pollution.

The network includes a suite of instruments for monitoring the atmospheric composition at the stations. These include a Tapered Element Oscillating Microbalance (TEOM), Condensation Particle Counter (CPC), nephelometer, high volume sampler, and aethalometer, which will be described in more detail later. Although all of the instrument measurements are of interest, this study focuses primarily on the aethalometers, which measure black carbon.

In 2016 the older Magee Scientific AE16 Aethalometers at Malin Head and Carnsore Point were replaced by new model AE33 Aethalometers, capable of distinguishing between "black" (traffic/industrial) and "brown" (biomass burning) carbon, and in 2018 Mace Head was also equipped with an AE33. Previous studies in Switzerland

[*J. Sandradewi et al.*, 2008c] and India [*Garg et al.*, 2016] have investigated the effectiveness of the algorithm used by the aethalometer to determine the percentage of biomass burning, and have found a number of variables which might impact the accuracy of the instrument calculation. The ability to correctly apportion the amount of black and brown carbon measured at the Irish sites would be very useful in determining whether there is any local interference from traffic, for example, at Malin Head.

Black carbon is a key component of the Transboundary Network, as it is an important tracer of anthropogenic pollution. In a November 2018 press release, The Irish EPA stated that although Ireland is still within the EU limits for air quality for PM (which includes BC), pollution from transport and solid fuel burning are above the World Health Organisation's (WHO) guidelines and need to be addressed. In an effort to better understand and improve the situation, the first results of the network measurements are presented in this study, including seasonal variations, as well as local, regional, and transboundary influences based on air mass trajectories. The contribution of biomass burning as reported by the instruments will be compared to calculations using different variables, i.e. Angstrom exponent, which seems to impact the results of other studies and varies widely depending on the fuel type and other factors. Ancillary aerosol measurements will be used to determine the number and size distribution of particles, though these may not necessarily be BC, given that the coastal sites are relatively unpolluted and sea spray or sea salt are likely the biggest contributors to measured aerosols. As BC is an anthropogenic tracer, its absence, for example in "clean" Atlantic air will be used to elucidate the high aerosol particle count events which frequently occur in the summer months along the coasts of Ireland.

1.3.3 Intensive Measurement Period

Occasionally special monitoring campaigns take place which include the Irish stations, and this was the case during the time of this study. In Winter 2018 Ireland participated in an intensive measurement period (IMP), conducted by the European Monitoring and Evaluation Programme (EMEP), along with several other European countries and including both rural and urban sites, which took place from

December 2017 to March 2018, as part of an effort to establish a European-wide uniform system for the collection and monitoring of carbonaceous aerosols, which could be used for model validation. All data from the campaign are being uploaded to the EBAS online database (http://ebas.nilu.no/) in order to establish a long-term record [*Aas et al.*, 2018]. The EBAS database is an online resource hosting atmospheric chemical and physical composition data submitted by participants of various programs and networks such as EMEP, GAW (Global Atmospheric Watch), ACTRIS (Aerosols, Clouds, and Trace Gas Infrastructure) for use in international monitoring and research projects. It is owned and operated by the Norwegian Institute for Air Research (NILU).

In addition to the overarching goal of data collection, the primary purpose of this campaign was to achieve more accurate alpha (α) values to determine the BB contribution to aethalometer measurements, as well as compare filter sampled elemental carbon to the black carbon (BC, or BC6 when specifically using the 880nm wavelength data) collected using aethalometers. This was done through simultaneous measurements of aethalometer BC, and elemental carbon (EC), organic carbon (OC), and total carbon (TC) collected from a high-volume sampler. Measurements of the wood burning tracer levoglucosan will be used to validate the BB measurements of the aethalometer and assess the BB contribution to TC, as well as establish site-specific α values for the aethalometers. The collection and processing of high-volume sampler data was performed by colleagues from University College Dublin (UCD) and submitted to NILU by our research group at NUI Galway along with data from the AE33. NILU will conduct further processing on the data, and it will be made publicly available through their ebas database.

For the purpose of this study, daily averages of BC, EC, OC, TC, and levoglucosan only from the Irish stations Carnsore Point (CRP), Mace Head (MHD), and Malin Head (MLH) were analysed, with the addition of a temporary site at University College Dublin (UCD), a suburban site where an aethalometer was stationed for the duration of the campaign, and the initial results are presented here.

1.4 Objectives

With these motivations and available resources, this work sets out to accomplish the following objectives:

1. Analyse the measurement data from the newly established network, including instrument validation and inter-comparison.

2. Examine the relationship between black carbon and other measurements in order to gain insight about the atmospheric composition.

3. Evaluate the performance of the aethalometer in-built biomass burning algorithm at coastal stations.

4. Investigate the contribution of local, regional, and transboundary pollution to air masses reaching the stations.

5. Prepare data for use in models and emissions inventories.

The following chapter describes in more detail the stations, instrumentation, and analytical methods selected for this purpose.

2. Methodology

The data analysed in this study were collected from the instruments at the three coastal Irish monitoring stations, with the exception of the temporary campaign site in Dublin, and compared to other model and observation data from the Irish EPA, European Environmental Agency (EEA), and the UK Black Carbon Network. The stations, instruments, and analytical methods selected are described here to provide a general overview of scope of the work.

2.1 Monitoring Stations

In 2016 a Black Carbon Network was established for collecting black carbon data in Ireland. It consists of three stations co-located with the Irish Environmental Protection Agency's (EPA) Transboundary Network (TXB) [*Leinert*, 2008]. These are Mace Head, Malin Head, and Carnsore Point, all coastal sites ideally located for monitoring air pollution transported from outside Ireland.

2.1.1 Mace Head

Mace Head (MHD) is located in County Galway in the west of Ireland near Carna, with the predominant wind coming off the Atlantic Ocean, providing clean background air for sampling. The site is owned and operated by the National University of Ireland, Galway, since 1958, and host to several other networks and measurement campaigns, such as Global Atmospheric Watch (GAW), World Meteorological Organization (WMO), Advanced Global Atmospheric Gases Experiment (AGAGE), European Monitoring and Evaluation Programme (EMEP), and the Integrated Carbon Observation System (ICOS). Thus, it is a valuable resource for long-term measurements of other trace gases and aerosols.

2.1.2 Malin Head

As shown in **Figure 3** Malin Head (MLH) is the northern most point of Ireland, located in County Donegal, and in close proximity to Northern Ireland, United Kingdom. It is owned by Met Eireann, and also part of the TXB and in the process of being incorporated into ICOS. As with Mace Head, the prevailing wind at Malin Head comes from the Atlantic Ocean, however, the site is only 30km away from the Northern Irish border and the city of Londonderry, therefore it is likely to pick up

transboundary pollution when the winds are from the southeast. As there are also a regional road (R242) and some houses immediately to the south of the station, the "polluted sector" (direction from which the majority of pollution arrives at the station) will be considered between 90-180 degrees unless otherwise specified. The clean Atlantic air arrives from what will be defined as the "clean sector" between 270-360 degrees.

2.1.3 Carnsore Point

Carnsore Point (CRP) is located in County Wexford, in the southeast extremity of Ireland, about 10km from Rosslare Harbour. It is an EPA station, and like Malin Head, is a member of the TXB and preparing for participation in ICOS. Carnsore Point receives the majority of air masses from the west, coming across the country over land, but is also in a suitable position to measure incoming pollution from the United Kingdom and mainland Europe.

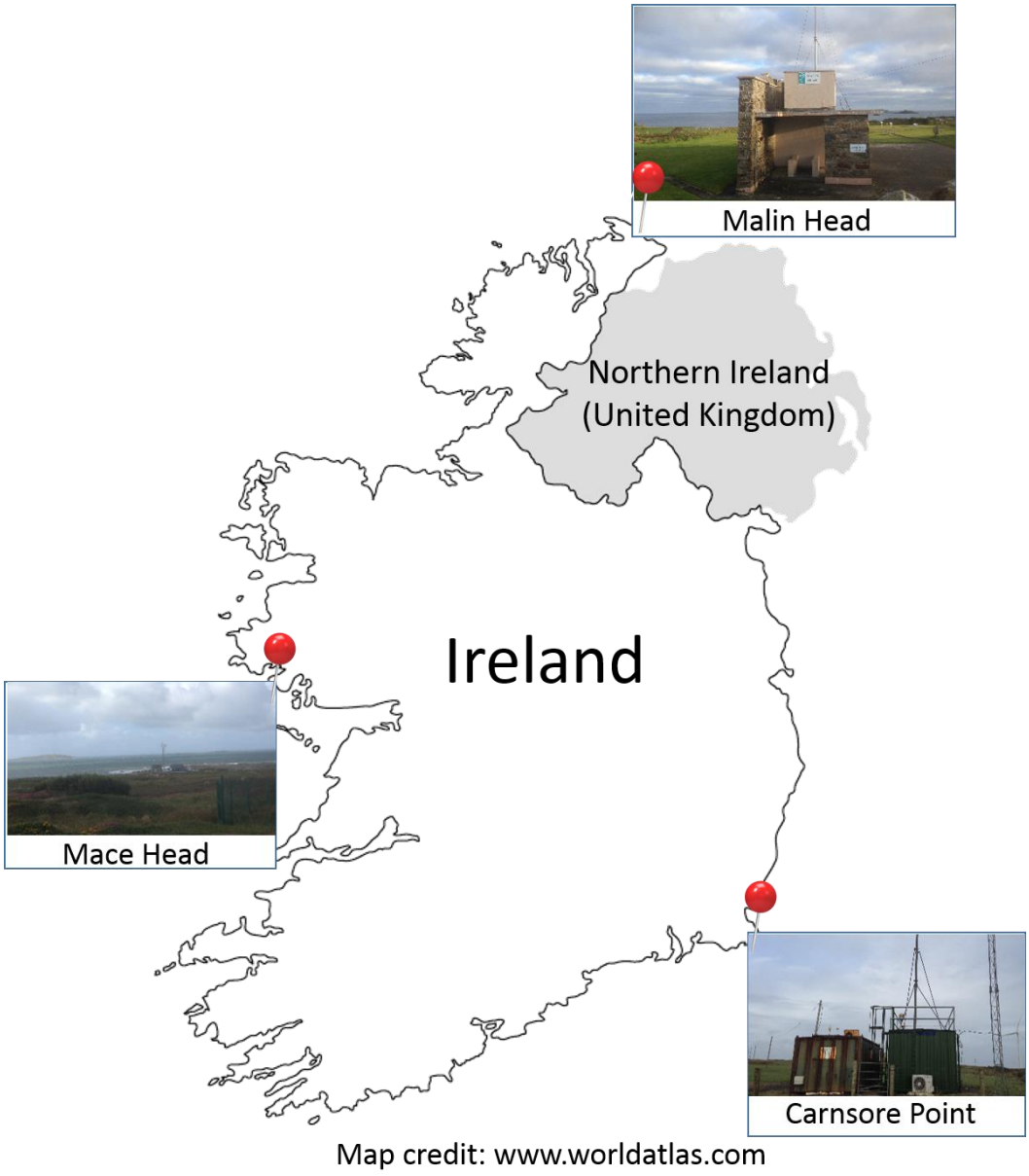

Figure 3 Ireland's Black Carbon Network

2.2 Instrumentation

The stations are equipped with a wide range of instrumentation for a multitude of purposes, as illustrated in Table 1. This study will focus only on the ones described in the section below, which combine to ideally represent the atmospheric aerosol composition and effects of transboundary pollution.

Table 1 Instruments at each station, grey colouring indicates not used in this study

Mace Head	Malin Head	Carnsore Point
AE33 (Dec 2017-Mar 2020)	AE33 (Jun 2016-Mar 2020)	AE33 (Jun 2016-Mar 2020)
CPC	CPC (Apr 2017-Mar 2020)	CPC (Jul 2016-Mar 2020)
TEOM	Fidas (May 2018-Mar 2020)	TEOM (Jun 2016-Mar 2020)
Picarro	Picarro (May-Jul 2018)	Picarro
Flask samples N_2O, CFCs, halocarbons	Ozone (Jan 2017-Oct 2020)	Ozone (Jan2017-Oct 2020)
High Volume Sampler (Dec 2017-Apr 2018)	High Volume Sampler (Dec 2017-Apr 2018)	High Volume Sampler (Dec 2017-Apr 2018)
SMPS	SMPS (Apr-May 2019)	Nephelometer
AMS	ACSM (Sep-Nov 2018)	ACSM (Aug 2016-Aug 2017)

2.2.1 Aethalometer

Historically BC has been measured in a number of different ways, ranging from the British “Black Smoke” standard of the 1950’s, defined as the darkness of the stain on a filter, to X-Ray Photoelectron Spectroscopy (XPS) measuring the kinetic energies of substances irradiated by X-Rays, to various heat and light attenuation methods [*Novakov and Rosen*, 2013]. These eventually led to the development of the current BC measurement technologies such as the Multi-Angle Absorption Photometer (MAAP), Photo Acoustic Soot Spectrometer (PASS), and Particle Soot Absorption Spectrometer (PSAP), as described in detail by [*Martinsson*, 2014].

The Magee Scientific Aethalometers in this study are currently the most commonly used instruments for measuring BC, for their ease of operation and ability to acquire near real-time data. The Aethalometer measures the attenuation of light through a quartz filter tape based on the Beer-Lambert Law and the accumulation of particles on the filter using the formulas depicted in on page 177 in Appendix C. Air samples are drawn in at a constant rate, and the tape advances once

attenuation has reached a set level. Older models such as the AE16 used a single light source with a wavelength of 880nm, at which BC absorbs most strongly. The newest version of the Aethalometer, the AE33, uses seven wavelengths of light, ranging from 370nm-950nm, which includes 880nm, and takes measurements at two separate spots on the filter tape simultaneously to eliminate errors due to filter loading [*Drinovec et al.*, 2014].

The benefit of having seven wavelengths is the added ability of the instrument to estimate a percentage of biomass burning (BB) contribution using an algorithm developed by [*Jisca Sandradewi et al.*, 2008b] which calculates the difference in absorption in the ultraviolet wavelengths (mostly by brown carbon) and the near infrared wavelengths (only by black carbon). While Aethalometers have a proven record of accurate BC measurements, as demonstrated over several years in comparisons with other instruments and confirmed again in this study, the BB function is not yet very reliable, especially given the different parts of the world and environments the instruments operate in, and the wide variety of substances classed as biomass.

The Irish Black Carbon Network, as it exists today was established in June 2016. Previously the stations had been measuring BC intermittently using the older model AE16 Aethalometers, which were replaced at Malin Head and Carnsore Point with state of the art AE33 Aethalometers when work commenced on the network. The AE16 at Carnsore Point was left operating at the station in order to compare the data to the newer instruments. Beginning in June 2017, a second AE33 was tested at Malin Head, before transferring the instrument to Mace Head in December 2017. It was connected to the same inlet as the MLH AE33, and after two months a dryer was added to one instrument to see if it had a significant impact on the measurements. Two months later a dryer was added to the second instrument and a comparison was made of the two instruments.

All three AE33's are set to record data at one minute intervals, with flow rates of 5 l/m (spot 1 and spot 2 combined flow), and the attenuation (ATN) level set to 70 (default setting is 120) to account for lower BC levels at the coastal locations and a manufacturer problem with the filter tape of measurements where ATN > 50. In

August 2017, Magee-Scientific announced a new filter tape and the discontinuation of previous versions due to optical non-linearity at short wavelengths which did not affect BC, however caused significant variance in the BB detection [*Magee-Scientific*, 2017]. The filter tape problem has been resolved since December 2017 with the installation of improved tape (part number 8060). The instruments use the default settings of 470nm for the lower wavelength, 950nm for the upper wavelength, 7.7 as the mass absorption cross-section of BC, and Angstrom exponents of alpha traffic (α_{tr}, fossil fuel related) =1 and alpha wood burning (α_{wb}, biomass related) =2 to calculate the percentage of BB contribution.

The data were processed using Python Pandas, and recalculated as needed into 5-minute, 30- minute, 1 hour, or daily averages both to smooth the data and to match it to time averages of other instruments. In the case of BB, which is reported as a percentage of BC, the ng/m^3 of BB were calculated before resampling, and the BB percentage of BC was recalculated from the proportion of BB ng/m^3 and BC ng/m^3 after resampling.

2.2.2 Multi-Angle Absorption Photometer (MAAP)

Prior to the AE33 being moved to Mace Head, BC had been measured there by a Multi-Angle Absorption Photometer (MAAP), which is currently still in operation. The MAAP uses both absorption and scattering properties of particles on a filter measured at three different angles to a light source to determine BC concentration [*Petzold and Schönlinner*, 2004].

Many comparisons between the MAAP and AE33 have been done, such as the recent TROPOS research institute's inter-comparison study [*TROPOS*, 2018], in which the instruments agree very well. This is important for data continuity in establishing a long-term record of measurements, as well as comparing data from different places. Although both instruments measure with similar precision, the AE33 is a more cost-effective piece of equipment, with the added capability of multi-wavelength measurements for determining the biomass burning contribution. For these reasons the AE33 is more commonly replacing the MAAP as the standard for measuring BC.

A brief section shows a comparison of the MHD MAAP to the AE33, demonstrating excellent agreement between the two instruments, yet only AE33 data are being used for data analysis. Nevertheless, the MAAP data are available for future analysis, to look at annual or decadal trends in BC concentrations.

2.2.3 Tapered Element Oscillating Microbalance (TEOM)

The Thermo Fisher Scientific Tapered Element Oscillating Microbalance (TEOM) is an instrument used to measure the mass concentrations of particulate matter (PM). It does this by drawing heated air through a filter at the end of a tapered glass tube, collecting particulate matter in the process, and mass change is detected by frequency changes in the oscillation of the tapered end of the tube and calculated with a spring-mass equation [*Thermo-Fisher-Scientific*, 2016].

The TEOM is a low-cost, easy to use, low-maintenance instrument frequently used to monitor concentrations of ambient particulate matter world-wide, for the purpose of long-term measurements as well as compliance to environmental standards and exposure limits. The technology was developed for this purpose in the early 1990's [*Patashnick and Rupprecht*, 1991], and has since evolved to higher time resolution sampling with more accurate measurements. It has been used successfully in mass-closure equations in previous studies.

A TEOM has been nearly continuously monitoring the mass concentration of PM10 (particles of 10 microns or less) in 5 minute time resolution since June of 2016 at Carnsore Point, and data from this instrument were recalculated into 24 hour averages and used for the total mass in a mass-closure equation, which attempts to model several subsets of particulate and compare them to the actual mass concentration.

2.2.4 High Volume Sampler

All three monitoring stations are operating DIGITEL DHA-80 high volume samplers, which collect 24 hour filter data that are then analysed for a series of ions (calcium, chlorine, sodium, magnesium, potassium, ammonium, sulphate, and nitrate), as well as levoglucosan, elemental carbon (EC), organic carbon (OC), and total carbon (TC). As the name implies, a high volume of air is pumped through the filter, at 500 litres/minute, and particles of size PM10 and smaller are trapped on a quartz fibre filter. The filters change automatically every 24 hours, and small sections of them are sent to a laboratory for analysis, where a Sunset Laboratory Carbon Aerosol Analyser is used to separate the aerosols through a multiple stage process that includes chemical immersion, heating, and burning off of the various species incrementally as described in detail by [*Birch and Cary*, 1996].

High volume sampler data obtained from the Irish EPA were used in this study both in the mass closure equation, comparing levels of the various ions to the total mass concentrations measured by the TEOM at CRP and the Fidas (described in the next section) at MLH, and the black carbon analysis during the EMEP campaign. Data from previous years were obtained from EBAS, a long-term online database hosted by NILU (the Norwegian Institute for Atmospheric Research) at http://ebas.nilu.no/ and used to show trends of the aerosols over time.

2.2.5 Fidas

Since May 2018 a Palas Fidas 200E has been in operation at MLH. This is an aerosol spectrometer capable of simultaneously distinguishing between PM1, PM2.5, PM4, and PM 10 sized particles at a very high time resolution and, as the only instrument capable of this, is currently the European standard for fine dust monitoring. In addition to long-term monitoring, this instrument is useful in detecting particle events such as volcanic eruptions [*Palas*, 2019].

The Fidas uses Lorenz-Mie scattered light analysis of single particles to determine particle size [*Palas*, 2019]. It has a flow rate of 0.3 m^3/hour and data are in one-minute time resolution. In contrast to the TEOM, which measures actual mass, the Fidas operates by measuring the number of scattered light impulses produced as particles pass through an optically differentiated measurement volume illuminated by white light, and converts them to a mass by multiplying by a correlation factor corresponding to different sources of environmental aerosol and applying a separation curve for size distribution.

In this study PM10 data from the Fidas are recalculated into 24-hour resolution for comparison to the high-volume sampler, and used as a measure of total mass concentration, in the same way TEOM data from CRP are used in the mass closure equation. As BC falls mainly into the PM1 size range, data are also analysed to determine the contribution of BC to total PM1. A further section will explore the Fidas data by itself in more detail.

2.2.6 Condensation Particle Counter (CPC)

Malin Head and Carnsore Point are host to TSI Condensation Particle Counters (CPC), model 3775. These instruments take in particle laden air which is introduced into a continuous flow butanol rich particle free sheath air and cooled. As the supersaturation increases, the particles, or condensation nuclei are activated into droplets which then scatter light efficiently and the individual particle light pulses are detected. The highest supersaturation reached is sufficient to activate 4 nm ammonium sulphate nuclei, which is the smallest particle size the instruments are capable of detecting. At low concentrations, the instruments work in single particle mode counting each pulse on a photodetector produced by a particle passing through the sensing zone, and switch to photometric mode at higher concentrations above 50,000 particles per cubic centimetre (pcc), where they can measure up to 10^7 pcc. In photometric mode particle count is determined by the total light scattered by the particles in the form of a DC voltage from the photodetector and calculated from a correction factor obtained through a calibration process involving known quantities of sodium chloride [*TSI*, 2007]. If the limit of 10^7 pcc is exceeded, the amount of aerosol entering the CPC needs to be diluted in order to get accurate counts. The instruments are collecting data in one-minute time resolution since July 2016 at CRP and April 2017 at MLH.

The CPC is able to work on its own, simply as a particle counter, or in conjunction with a Scanning Mobility Particle Sizer (SMPS), described later, which then provides a size distribution of the particles as well.

Previous studies have observed that extremely high particle counts occur at Mace Head during periods of low tide and high solar radiation [*De Leeuw et al.*, 2002], though it was not certain whether this was a local phenomenon or happens at other coastal areas as well. Using the CPC data in the absence of BC (less than 50ng/m^3) and the “clean air” wind sectors at the stations in conjunction with tidal and meteorological observations, this study will demonstrate that these events do take place at Carnsore Point and Malin Head under similar conditions.

2.2.7 Picarro

Each of the three stations is equipped with a Picarro cavity ring-down spectrometer for measuring methane (CH_4), carbon dioxide (CO_2), water vapour (H_2O), and in the case of Malin Head, an upgraded model (G2401) capable of measuring carbon monoxide (CO) as well. A cavity ring-down spectrometer works by sending a laser beam through a cavity, reflecting off multiple mirrors to produce a several kilometre long path length, turning the laser off, and measuring the "ring-down" effect that occurs as the light within the cavity gradually extinguishes. Since each gas absorbs light at a certain wavelength, the laser is tuned across these wavelengths, and the concentration of gases is calculated to parts per billion (ppb) precision from the difference in ring-down between an empty cavity and one with gases [*Picarro*, 2019]. The instruments are set to record data in one-minute intervals.

The Picarro instruments were selected for use in the ICOS network, as they are one of the two types of instruments deemed suitable by ICOS for long-term yet high precision measurements of methane. Their relatively low maintenance and ease of use makes them ideal for monitoring at remote locations, such as the Irish coastal stations, where they can be left unattended for months at a time.

In this study, specifically the CO data from Malin Head are used to assess the effects of local pollution from traffic on the measurements at the station using their ratio to BC as an indicator of combustion. All Picarro data are routinely sent to and validated by ICOS to establish a long-term record.

2.2.8 Aerosol Chemical Speciation Monitor (ACSM)

From August 2016 to August 2017, an Aerodyne ACSM was set up to take 30-minute measurements at Carnsore Point. This instrument measures the PM1 mass loadings of NO_3, NH_4, SO_4, Cl, and organics using a quadrupole mass spectrometer. It consists of three vacuum chambers that are differentially pumped by three turbo pumps, and an aerodynamic lens which focuses a particle beam through the first two chambers into the third chamber where they are vaporised by an oven at about 600°C. The resulting vapour is ionized with electron impact and characterised by the mass spectrometer [*Ng et al.*, 2011]. The ACSM is a smaller (more portable) and less expensive version of the Aerodyne Aerosol Mass Spectrometer (AMS), which is currently the highest standard of aerosol monitoring. An AMS is being used at Mace Head as well.

As most organics are assumed to fall into the PM1 category, the organics data from the ACSM were recalculated to 24-hour averages and used to supplement the mass closure equation at Carnsore Point along with the high-volume sampler data in this study.

An ACSM was also temporarily available at Malin Head for three months in Fall of 2018, such that some of the organics data could be used in a mass closure experiment for that station, however the size cut-off on this instrument was PM2.5 allowing for larger particle size measurements. The ACSM has until now been operated by other members of the research group, who have made the data available for this study, but the instrument will be permanently relocated to Malin Head in the near future to augment the existing network. This instrument's ability to distinguish between different species can be used in conjunction with the other measurements to present a more accurate profile of the aerosol loading in the atmosphere.

2.2.9 Scanning Mobility Particle Sizer (SMPS)

As part of the network expansion, a Palas Universal Scanning Mobility Particle Sizer (U-SMPS) model 2100 with a 8-1200 nm particle diameter detection range was installed at Malin Head in April 2019. This instrument will supplement the PM measurements by providing more information on the particle size distribution. It works using a Differential Electrical Mobility Classifier (DEMC) to charge particles to a known charge distribution and classifying them by the way they traverse an electrical field, then counting them using a Condensation Particle Counter (CPC) and applying an inversion algorithm to calculate particle size.

According to the product description at the Palas website (https://www.palas.de/en/product/usmps2050x_2100x_2200x#datasheet), aerosol is passed through a dryer and Kr-85 bipolar neutralizer before entering the DEMC, where it is mixed with a dry, particle-free sheath air. The DEMC consists of an inner and outer column, to which a voltage is applied. The aerosol passes through the annular space between the cylinders, and negatively charged particles are precipitated along the positively charged inner cylinder rod depending on their particle electrical mobility. The voltage changes continuously, and so different sizes of particles move through the system and are transferred to a particle sensor to determine concentration. This is done via a Condensation Particle Counter (CPC), the operation of which is described in section 2.2.6.

The instrument at Malin Head is set up to record data at 3-minute intervals with a particle detection range of 0-10^8 particles per cubic centimetre. The size distribution is classed into 67 bins ranging from 7.2nm-777.7nm on an exponential scale. Due to the very recent installation of this instrument, only a few months of data are currently available, which is nevertheless sufficient to investigate its ability to detect in-situ aerosol formation at a coastal site. Of particular interest is its potential for measuring particle growth events linked to high particle counts.

2.3 Analytical Methods

For clarity and simplicity, the analytical methods used in this study will be grouped here in relation to achieving the main objectives, as there is some overlap within various sections that are inter-related. The diagram in **Figure 4** provides an overview of the topics covered, and how they fit within the framework of the objectives. The main objectives are in the bold boxes on top, with their related subcategories below them. Note that Biomass Burning, being a subset of BC, spans multiple categories. The BB methodology for each objective will be explained in section 2.3.3.

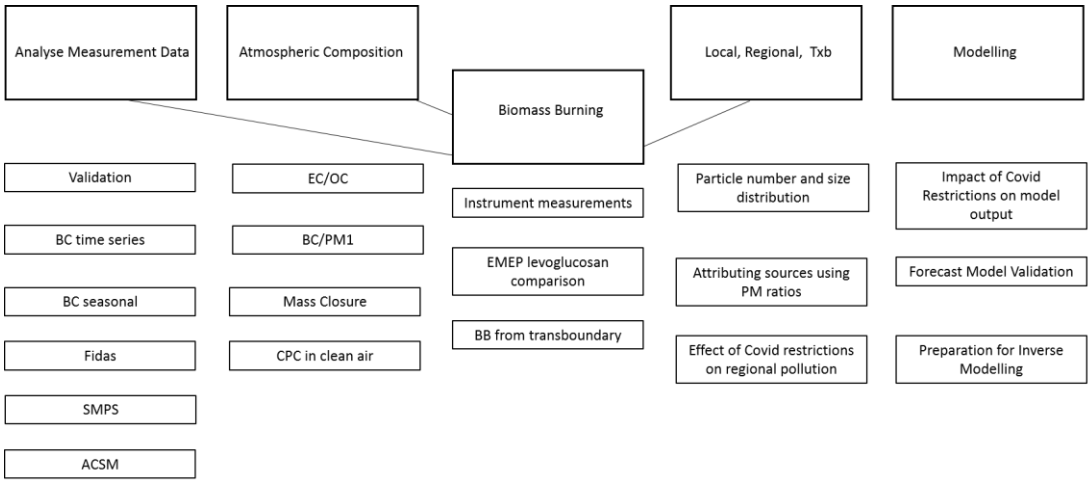

Figure 4 Diagram of objectives and sub-objectives

2.3.1 Analyse the measurement data

This work begins with the validation of the instruments used in the study, primarily the AE33's in order to ensure data continuity from older models and for comparability between instruments. Validation of network instruments is important enough to merit its own chapter, as it provides the foundation for the analysis conducted. The scatter plot method was selected, having proved effective in other AE33 inter-comparison studies, such as those by [*Laing et al.*, 2020] and [*Cuesta-Mosquera et al.*, 2021], in showing how well two instruments agree, and by how much they differ. The Malin Head Fidas validation was based on comparisons to

other studies in similar environments, and the ASCM validation was conducted by a different research group and is only presented here for reference.

Chapter 4 begins with the measurements obtained from the instruments, showing their time series, seasonality, and relationship to BC or the absence thereof. It is a basic presentation of so far unpublished data, giving an overview of the network measurements.

2.3.2 Atmospheric composition

The analysis in Chapter 4 continues with a deeper exploration of the atmospheric composition, made possible by the combination of instruments on the network. It incorporates the EMEP campaign data, which gives insight into the aerosol size distribution of black and organic carbon, and their contribution to PM. The results of this analysis lead to further elucidating the mass closure equation, which was conducted based on a previous study in Ireland [*Jennings et al.*, 2006]. A mass closure equation is simply the sum of individual atmospheric components compared to a total PM mass, with the aim of minimising the unknown factor and gaining an understanding of the atmospheric composition of a particular location.

2.3.3 Evaluate biomass burning algorithm

Biomass burning, as a subset of BC, of course is closely tied to every section related to BC. The AE33 has an in-built algorithm to determine the biomass burning contribution as a percentage of BC. It does this by comparing the attenuation at the lower 470nm to the attenuation at the higher 950nm wavelength based on alpha values for traffic and biomass burning. The full formula is shown on page 179 (Appendix C), adapted for the Igor Pro [*Wavemetrics*, 2014] script (provided by the Paul Scherrer Institute) which was used to calculate BB by changing variable inputs. As the BB algorithm of the AE33 has so far not been tested in clean, coastal environments, one of the objectives of this work is to observe its performance. In Chapter 4 the basic measurements are first presented as reported by the instrument, then compared with results of other studies, and finally calculated based on the EMEP levoglucosan measurements. Chapter 5 evaluates local and regional pollution based on the wind speed and wind direction from which BB primarily arrives at Malin Head.

2.3.4 Investigate local, regional, and transboundary pollution

Differentiating between local, regional, and transboundary pollution is of great interest to authorities seeking to regulate pollution, and the network is ideally suited for this purpose. Chapter 5 is devoted to this topic, showing how the instrument measurements and meteorology can be used to distinguish different events and sources. It also evaluates the network's ability on a regional scale by investigating the impact of Covid-19 lockdown restrictions on the remote rural stations, as the main focus of such studies has thus far been on urban areas.

2.3.5 Prepare data for use in models and emissions inventories

One future use of network data will be to inform and improve models and emissions inventories. To this end, Chapter 6 seeks to explore how current models compare to the actual measurements, as well as prepare data for input into inverse models. This is done by comparing the NUIG and Manchester University model BC output to AE33 measurements and adapting a spike removal algorithm previously used for trace gases to BC. A separate section examines how the Covid-19 lockdown impacted the models.

Given these objectives analysis methods, the following chapter begins with instrument validation, providing confidence in the measurements for further analysis.

3. Validation

Instrument and data validation are of utmost importance in the initial phase of setting up a network. By comparing the measurements from different instruments to each other, we can guarantee compatibility with past measurements and gain confidence in the performance of each instrument. This will lay a solid foundation for continuous long-term measurements providing data that can be relied upon.

The following chapter shows comparisons of the legacy AE16 to the new AE33 at Carnsore Point, and two co-located AE33's at Malin Head, demonstrating the difference in noise when a dryer is added to one instrument. Results of a comparison of the MHD AE33 to the MAAP are included as well, since MHD only recently began AE33 measurements, and the instruments agree well enough that MAAP measurements may be substituted for the time period since the BC network was established. Finally, the Malin Head Fidas PM2.5 and PM10 ratios are compared to other studies which found similar values, and the results of the ACSM calibration and inter-comparison are presented.

3.1 AE16 vs AE33

The AE16 at Carnsore Point has been continuously collecting BC data since January 2015. In July 2016 the new seven wavelength AE33 was installed, and both instruments have been running in parallel for over a year. A data comparison of the AE16 (which measures BC only at 880nm) and the AE33's 880nm BC channel was conducted for the period of overlap to ensure data continuity. Only data from December 2017 onward are displayed here, as a new filter tape was installed on the AE33 at that time. The plots in **Figure 5** below show excellent agreement between the two instruments; however, the slope indicates that the AE33 is picking up about 30% more BC than the AE16. This is likely due to the AE33 being newer with specially calibrated lamps, and having more advanced technology, i.e. the dual spot measurements, which provide for greater sensitivity and accuracy. A comparison of the AE16 BC to the uncorrected (spot 1) 880nm data of the AE33 shows slightly better agreement between the two instruments.

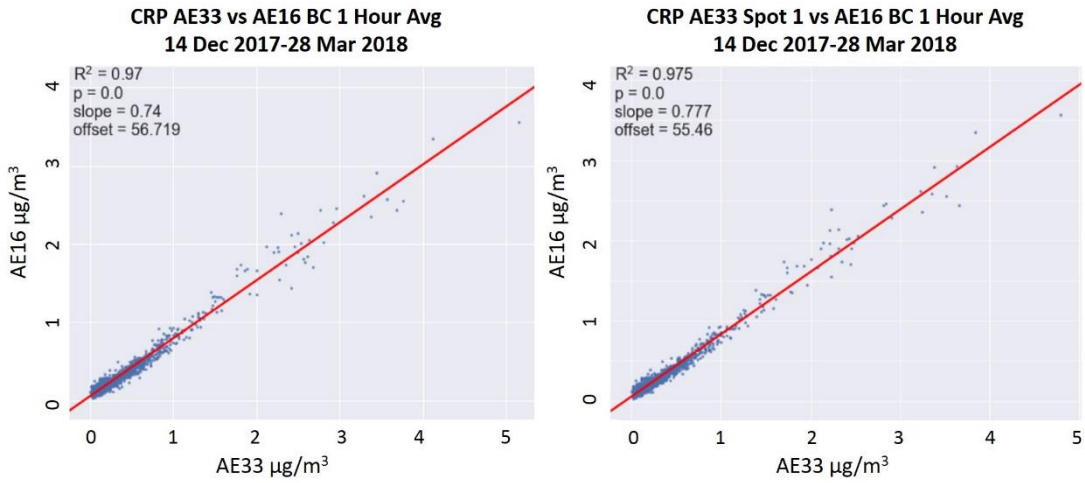

Figure 5 Correlation plots of CRP AE16 vs AE33 880nm BC (left) and CRP AE16 vs AE33 spot1-uncorrected (right)

3.2 AE33 vs AE33

3.2.1 Same Inlet

In June of 2017 a second AE33 was installed on the same inlet as the original AE33 at Malin Head. This instrument has since been transferred to Mace Head, where there were previously a MAAP and an AE16 in operation. The purpose of comparing the same instruments to each other is to determine whether their measurements differ significantly, and if so, when and why. Due to a problem with the filter tape, only data for the period after the tape was replaced are being used in this comparison. As illustrated in the plots below (**Figure 6**), the two instruments agree very well at the 880nm wavelength, and any systematic differences are within manufacturer specifications.

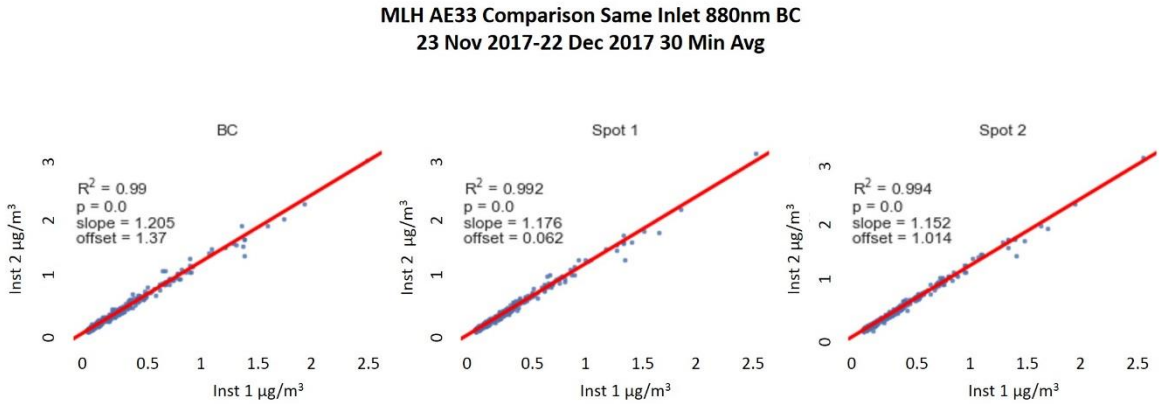

Figure 6 MLH AE33's on same inlet, comparison of BC6, spot 1, and spot2

3.2.2 With Dryer

On 21 August 2017 a dryer was installed on the original MLH AE33 to observe any changes in the measurements. As can be seen in the graph below, the data are visibly less noisy, especially at the lower values, after the dryer is installed. A dryer was installed on the second MLH AE33 on 12 October 2017, and the instrument comparison in the previous section shows both instruments using dryers. While a dryer is an optional accessory for the AE33, it is manufacturer recommended, and does make a difference, particularly in an environment with low levels of pollution, where the instruments are measuring close to their detection limit, as the instruments are sensitive to variations in relative humidity.

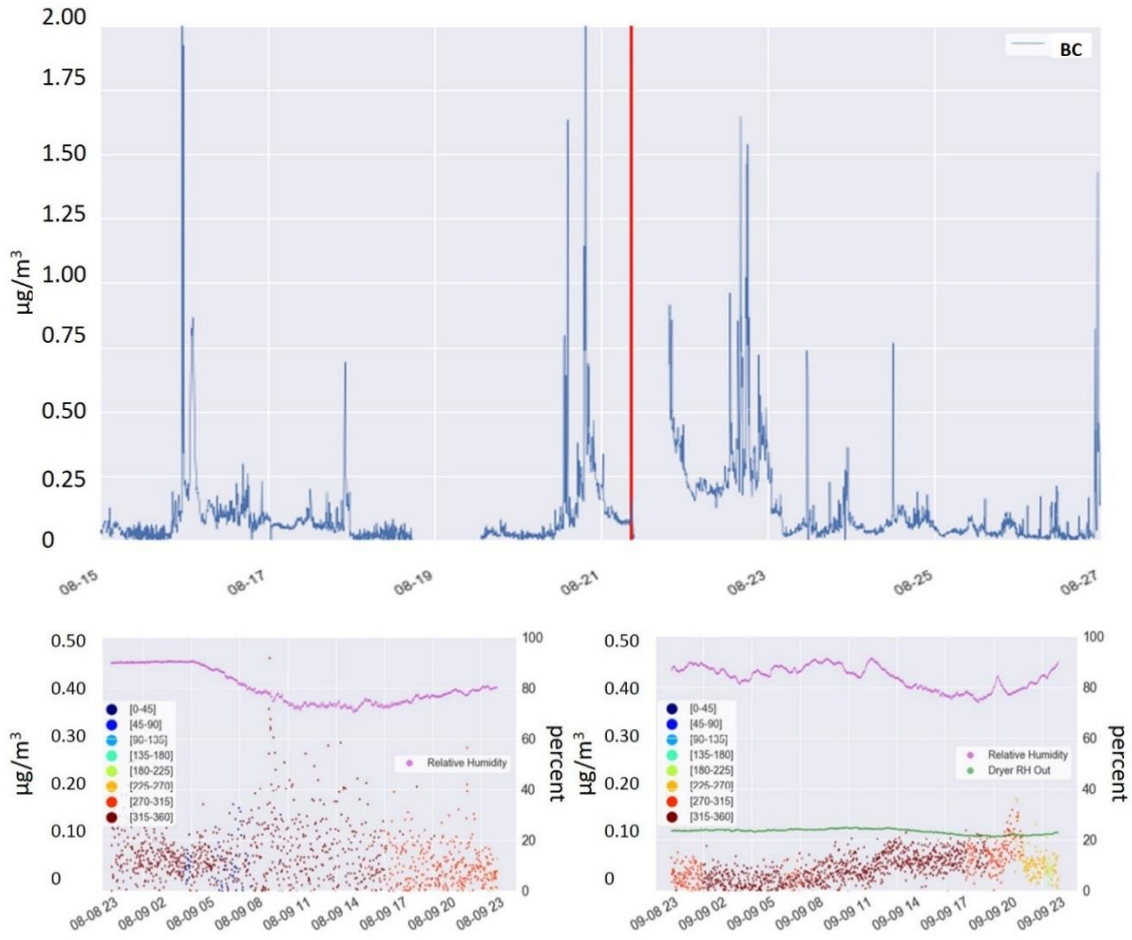

Figure 7 MLH AE33 time series of 880nm BC. A dryer was installed on 08-21 (red line top plot) resulting in less noisy measurements. The bottom two plots are of two days with similar conditions before and after dryer was installed.

Table 2 Statistical comparison of the two similar days before and after the dryer was installed. Count and mean in the 315-360 sector are nearly equal, but standard deviation with dryer is less than half.

	9-10 August 2017 (Before Dryer)			9-10 September 2017 (After Dryer)		
	Count	Mean	Stdev	Count	Mean	Stdev
0-45	85	45.18	50.96	0	N/A	N/A
45-90	0	N/A	N/A	0	N/A	N/A
90-135	0	N/A	N/A	0	N/A	N/A
135-180	0	N/A	N/A	0	N/A	N/A
180-225	0	N/A	N/A	16	38.5	15.48
225-270	10	18.1	25.79	133	54.59	29.88
270-315	388	28.96	54.04	318	49.55	36.77
315-360	957	45.37	83.22	971	38.11	29.68

3.3 AE33 vs MAAP

Upon its arrival at MHD, the AE33 was compared to the MAAP instrument. The two instruments agree extremely well, but the AE33 measures consistently higher than the MAAP, particular during times of low BC concentrations, as shown in the plot below (**Figure 8**). This instrument was also measuring about 15% higher than the MLH AE33, so it is most likely calibrated differently. A scatter plot of hourly averages of the two instruments (not shown) has an R^2 value of 0.956 and a slope of 0.851. According to an inter-comparison study by the Leibniz Institute for Tropospheric Research (TROPOS) and the European Center for Aerosol Calibration (ECAC)[*TROPOS*, 2018], AE33 aethalometers typically measure up to 35% higher BC than the MAAP, and that "such differences can be caused by different sensitivities depending on aerosol type."

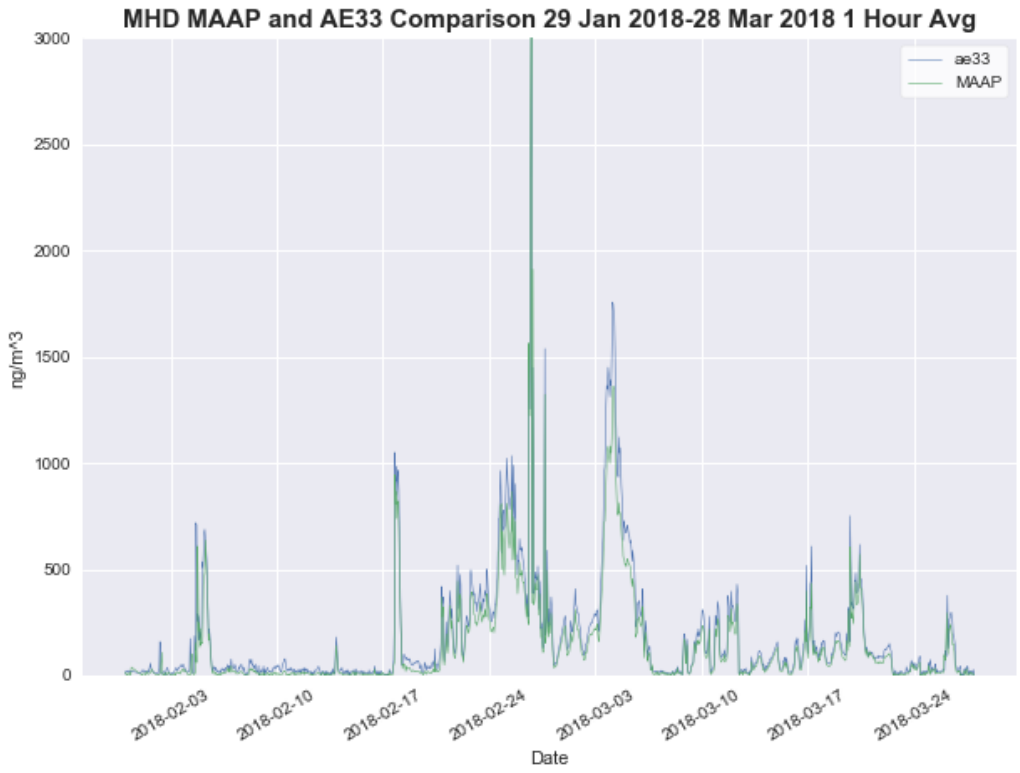

Figure 8 MHD AE33 and MAAP time series

3.4 Malin Head Fidas

As there are no other Fidas instruments currently on the network, the Malin Head PM2.5/PM10 ratios are compared to those of other studies, i.e. in the UK, which found similar results. Presented here is the scatter plot of PM2.5 and PM10 for the first year (May 2018-May 2019) the Fidas has been measuring at Malin Head. The results are in agreement with other background sites, such as those reported by [*Munir*, 2017], where the PM2.5/PM10 ratio was on average 0.65, as well as a study by [*Dinoi et al.*, 2017] which found the ratios to be 0.68 at a coastal site in Italy, and a further investigation by [*Querol et al.*, 2004] which claims rural background ratios to be between 0.6-0.8 in countries throughout Europe.

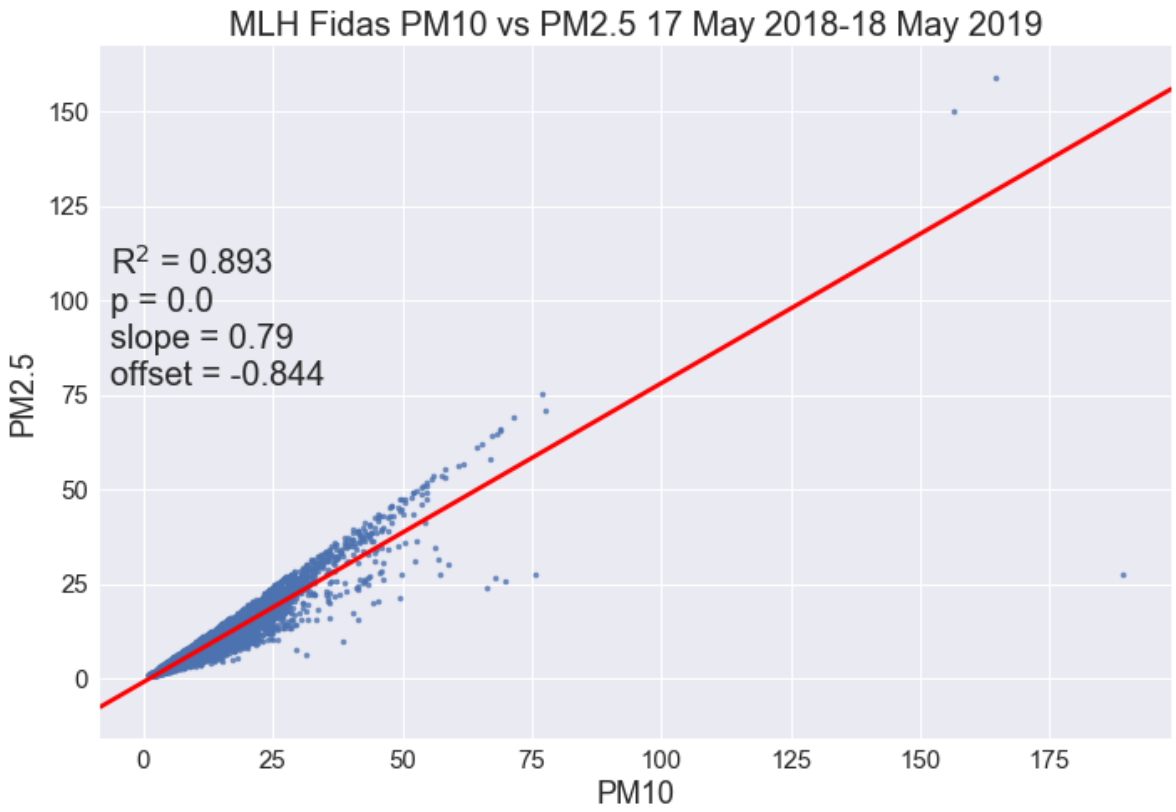

Figure 9 MLH Fidas PM2.5 vs PM10 May 2018-May 2019

3.5 ACSM Calibration Results

In November 2018 the ACSM instrument was shipped to Paris, France for an inter-comparison and calibration campaign at the Aerosol Chemical Monitoring Calibration Center (ACMCC), part of SIRTA (Site Instrumental de Recherche par Télédétection Atmosphérique), where it was compared to other aerosol chemical speciation monitors as well as the SIRTA reference instrument. The tests consisted of three parts: First all the instruments were compared to the SIRTA reference instrument and to each other using the robust median of the instruments and a Z-score analysis; then a calibration was performed using monodisperse (300 nm) ammonium nitrate and ammonium sulfate nebulized particles to obtain a nitrate response factor (RF) which was applied to the raw data; and finally the first test was repeated, the results of which are shown in **Figures 10-11** below, taken from the ACMCC report, ACTRIS 2 (ECAC-ACMCC) Intercomparison of Aerosol Chemical Speciation Monitors, November 2018. The overall conclusion was that the instrument compared very well both to the SIRTA and other instruments, well within the 30% error range, and its performance was further improved through calibration and tuning.

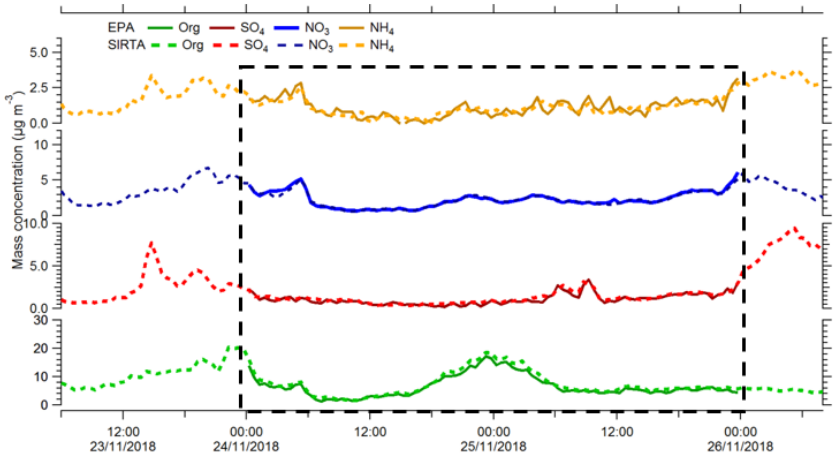

Figure 10 ACSM compared to SIRTA reference after calibration, black rectangle denotes inter-comparison period

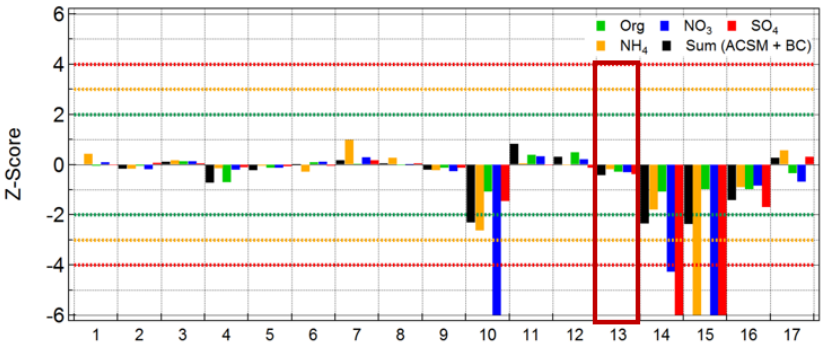

Figure 11 ACSM compared to other instruments after calibration, red rectangle highlights results of this instrument

After all instrument validation was successfully conducted, analysis of the data could proceed. The next chapter provides both basic and in-depth analysis of the data collected so far on the newly established network.

4. Data Analysis

This chapter concurrently addresses three main objectives:
First, it provides a basic analysis of the network data collected from the instruments, including some later additions toward the end of the chapter. Second, it attempts to gain insight into the atmospheric composition of the coastal stations through more complex analysis, i.e. through a mass closure equation and comparison of different measurements as they relate to black carbon or the absence thereof. Third, biomass burning is investigated both in terms of direct instrument measurements and in comparison to other studies.

4.1 Black Carbon Time Series

Figure 12 depicts a basic comparison of all three stations for one year. Some seasonal variation is visible, with expected increases of BC in wintertime due to an increase in home heating, particularly solid fuel heating. Carnsore Point stands out as having the highest levels of BC, with an annual median of 132 ng/m^3, and a maximum of 9410 ng/m^3, as this station is most vulnerable to pollution from outside the country, despite the majority of air masses arriving across land from within Ireland. Malin Head has an annual median of 109 ng/m^3, with a maximum of 7331 ng/m^3. Mace Head is the least polluted, with mostly clean air from the Atlantic and no significant nearby sources of BC. The annual median BC at MHD was 33 ng/m^3, with a maximum of 9575 ng/m^3. Several periods of prolonged regional pollution were detected by all the stations in February, June, July, and November. BC below 50 ng/m^3 can be considered background levels, as previously defined by [*Grigas et al.*, 2017].

Figure 13 shows the corresponding BB measurements from the aethalometers at the three stations in 2018. This follows a similar pattern to the BC, with higher percentages during the winter months and during periods of regional pollution. The BB contribution at MLH seems to be more impacted by local sources in the winter, as the measurements begin to deviate then.

A frequency distribution of BC was conducted for the three stations using Igor Pro's multi-curve fitting package, with BC plotted in 100 lognormal bins on the x axis ranging from 0.01 to 10,000 (the approximate maximum BC concentration), and the frequency of occurrence in percent on the y axis. The BC distribution at all three stations tends to be bimodal, with the initial peak being in the low, unpolluted range, and the secondary peak in the moderate pollution range. Carnsore Point follows this pattern too; however, it also has three smaller peaks in the highly polluted range. Unlike the other two stations, CRP receives much of its air from inland rather than the sea, which may account for the higher concentration in the initial peak, but the higher levels of BC (over 1000 ng/m^3) are indicative of stronger pollution sources, such as Dublin, ferry/ship traffic, or transboundary from the UK. **Figure 14** shows the frequency distributions for the three stations for 2018.

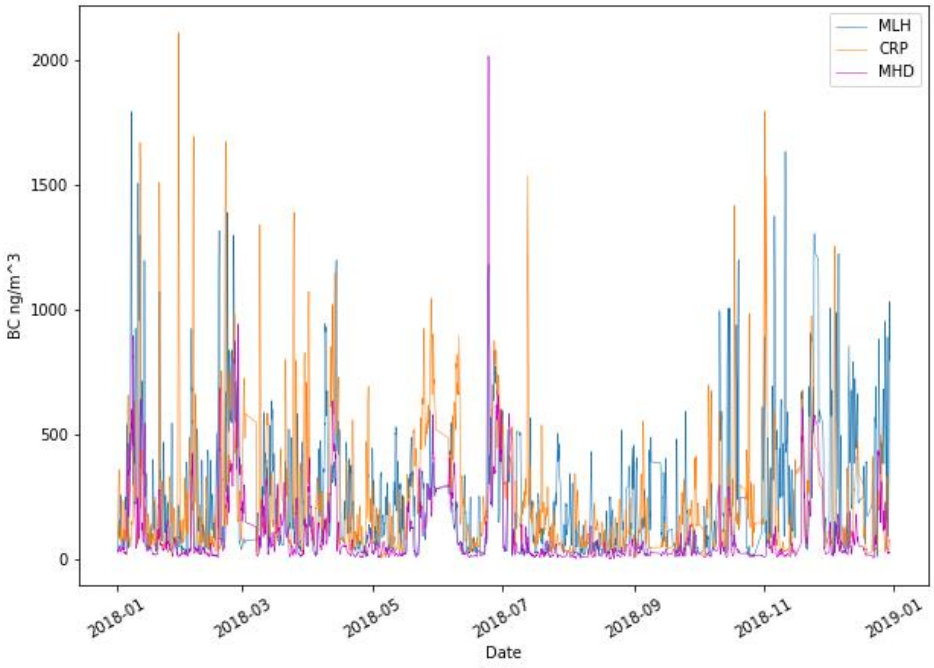

Figure 12 12-hour rolling average BC for the three stations in 2018

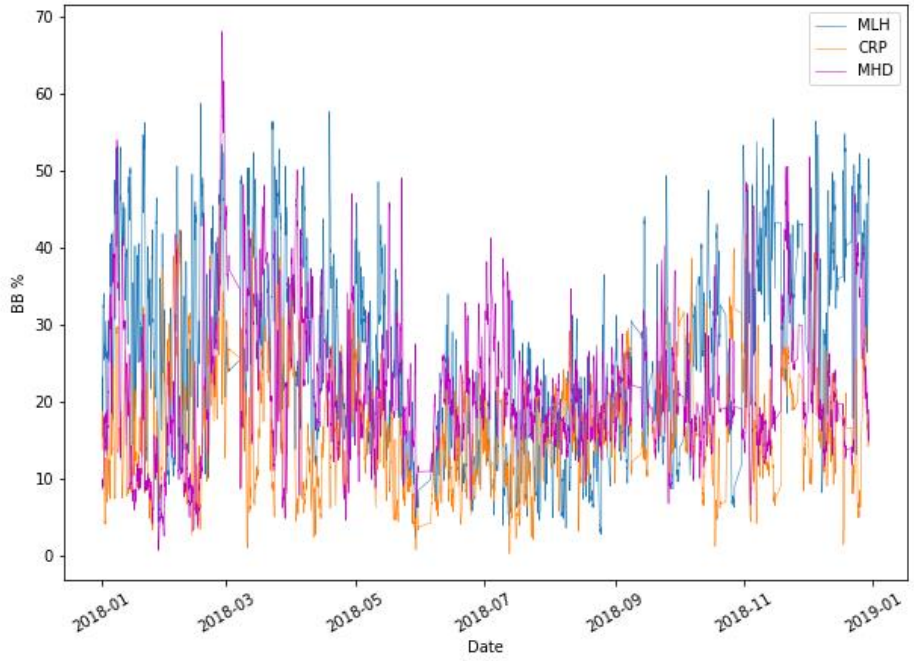

Figure 13 12-hour rolling average BB for the three stations in 2018

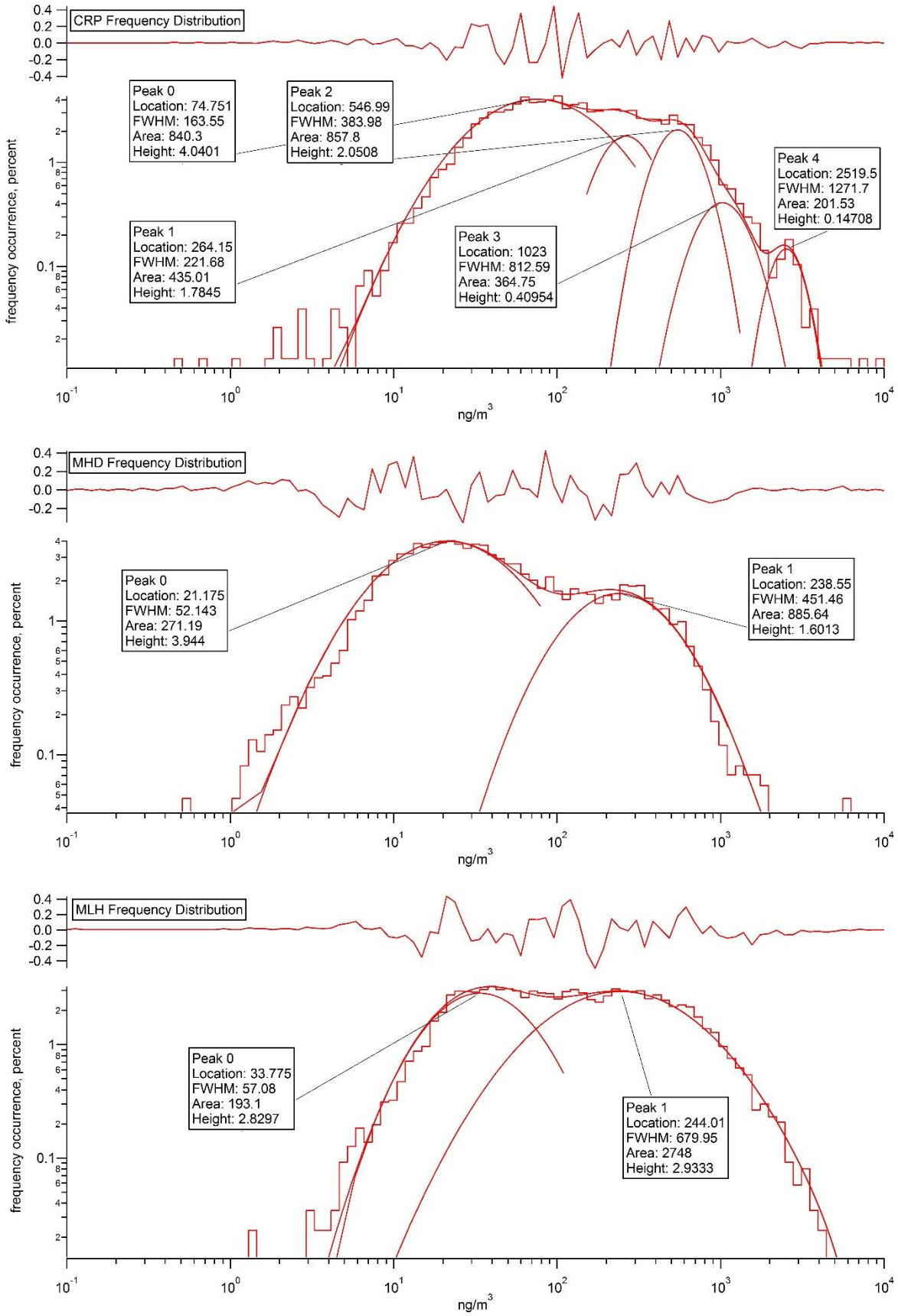

Figure 14 Frequency Distributions of BC for 2018 (top plots on each graph are residuals of the fit)

4.2 Seasonal Comparison of Black Carbon

The BC data from the three stations were analysed in more detail by season and plotted together with wind direction to provide a visual concept of when and where the highest sources of BC were coming from. This was done by grouping data for each season by 45-degree wind sectors. The pie graphs show the average concentration by wind sector, and the time series are colour-coded by wind sector using the same colour scheme. All three stations measured the highest concentrations of BC in winter, due to an increase in home heating. Mace Head showed no unusual trends, however, both Malin Head and Carnsore Point had surprisingly high levels of BC on their respective seaward sides, which may be indicative of ship traffic in the area. The BC to the east of Carnsore Point was extremely high, especially in winter, when seas are rough and there is less ship traffic, so much of the BC may actually be coming from Wales and England. In fact, the wind only came from the East (45-135 degrees) 14% of the time in the whole year, yet 33% of the BC measured at CRP is from that sector. The majority of BC at Malin Head appears to come from the East-Southeast (90-180 degrees) sector, which is in the direction of Northern Ireland. Wind roses for all stations and seasons can be found on pages 180-181 of Appendix C.

The seasonal time series in **Figures 15-17** allow for a closer look at the BC measurements at the stations. The wind direction at Carnsore Point is predominantly from the south/southwest, yet prolonged levels of elevated BC occur during periods when the wind is from the east. Winds from the north also carry increased concentrations of BC from Dublin or possibly nearby villages, particularly in fall and winter.

Mace Head, in comparison, has very low concentrations of BC throughout the year, with increases only when the wind is from the east, or from inland, making it ideal for estimating background levels. Much of the BC reaching the site is from local or regional sources, however there may be some transboundary pollution being carried across the country in certain conditions [*Huang et al.*, 2001].

Similar to Mace Head, Malin Head has very low BC concentrations when the wind is from the north, or marine sector, however, BC levels are considerably higher than either of the other stations when the wind direction is from the land, particularly

from the south. There is a definite local influence caused by a regional road immediately to the south of the station and nearby residences, but quite likely also a heavy impact of transboundary pollution from Northern Ireland. The difficulty lies in distinguishing the difference between local and regional influences with the measurements currently available.

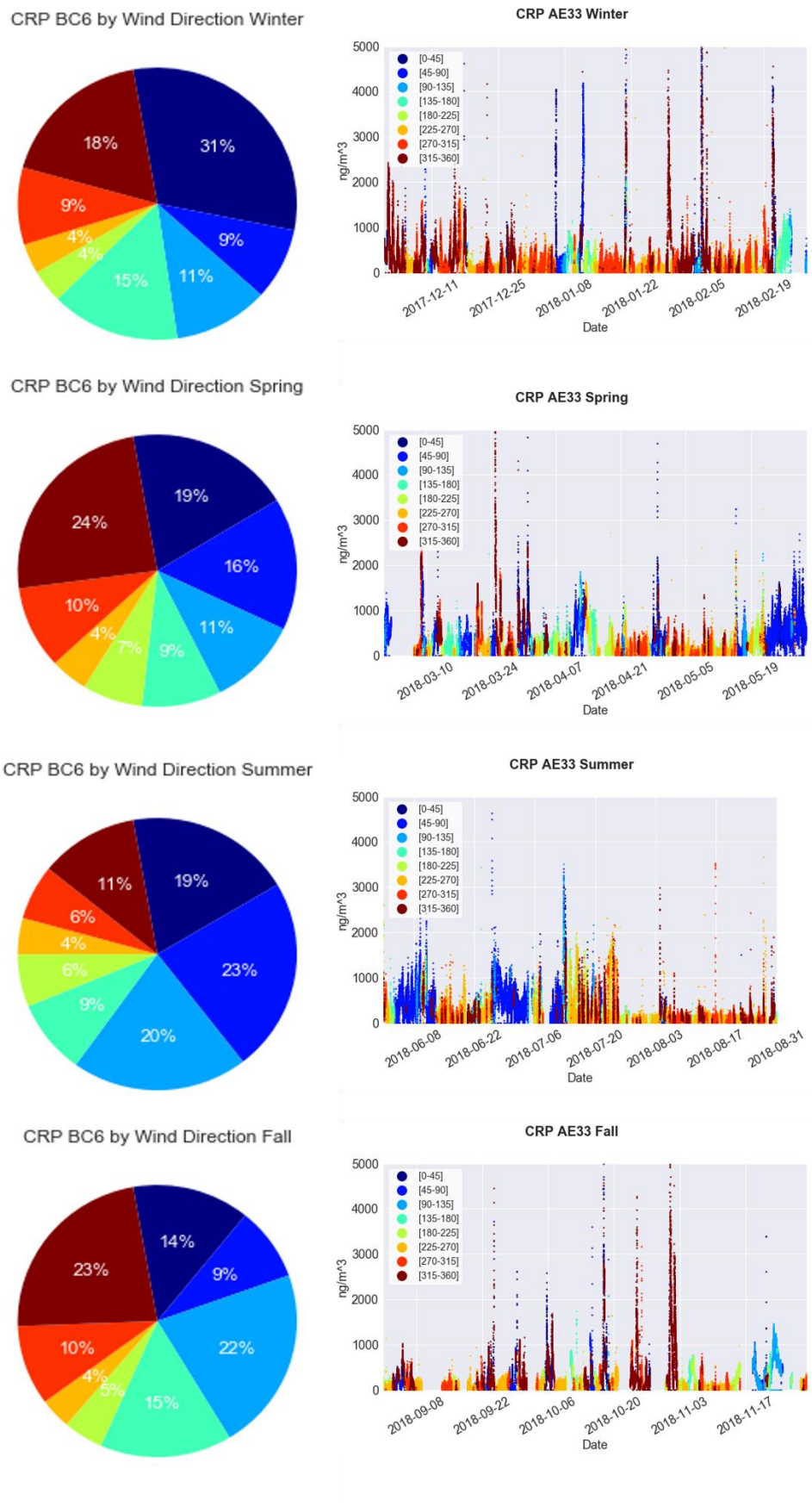

Figure 15 Carnsore Point seasonal BC by wind direction

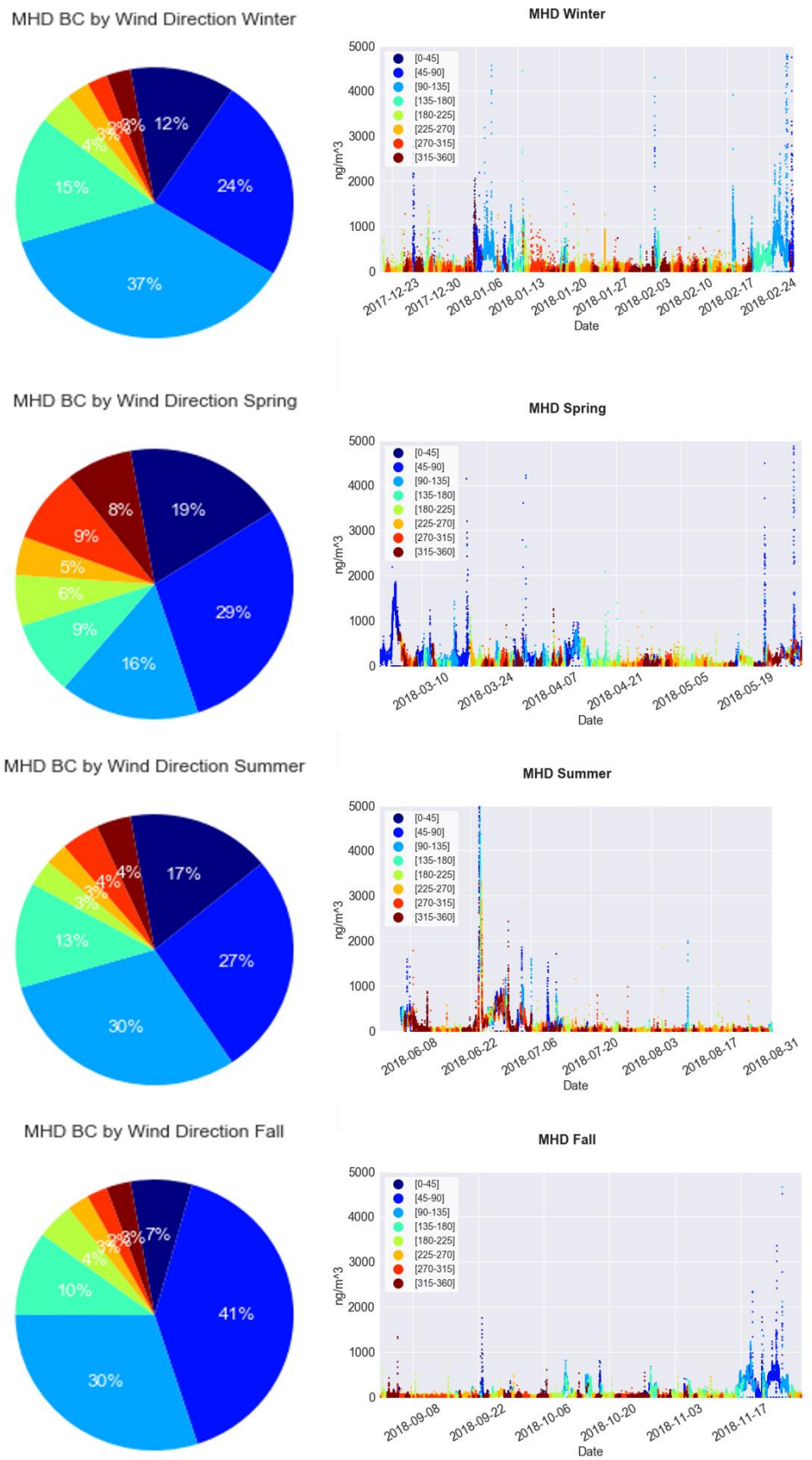

Figure 16 Mace Head seasonal BC by wind direction

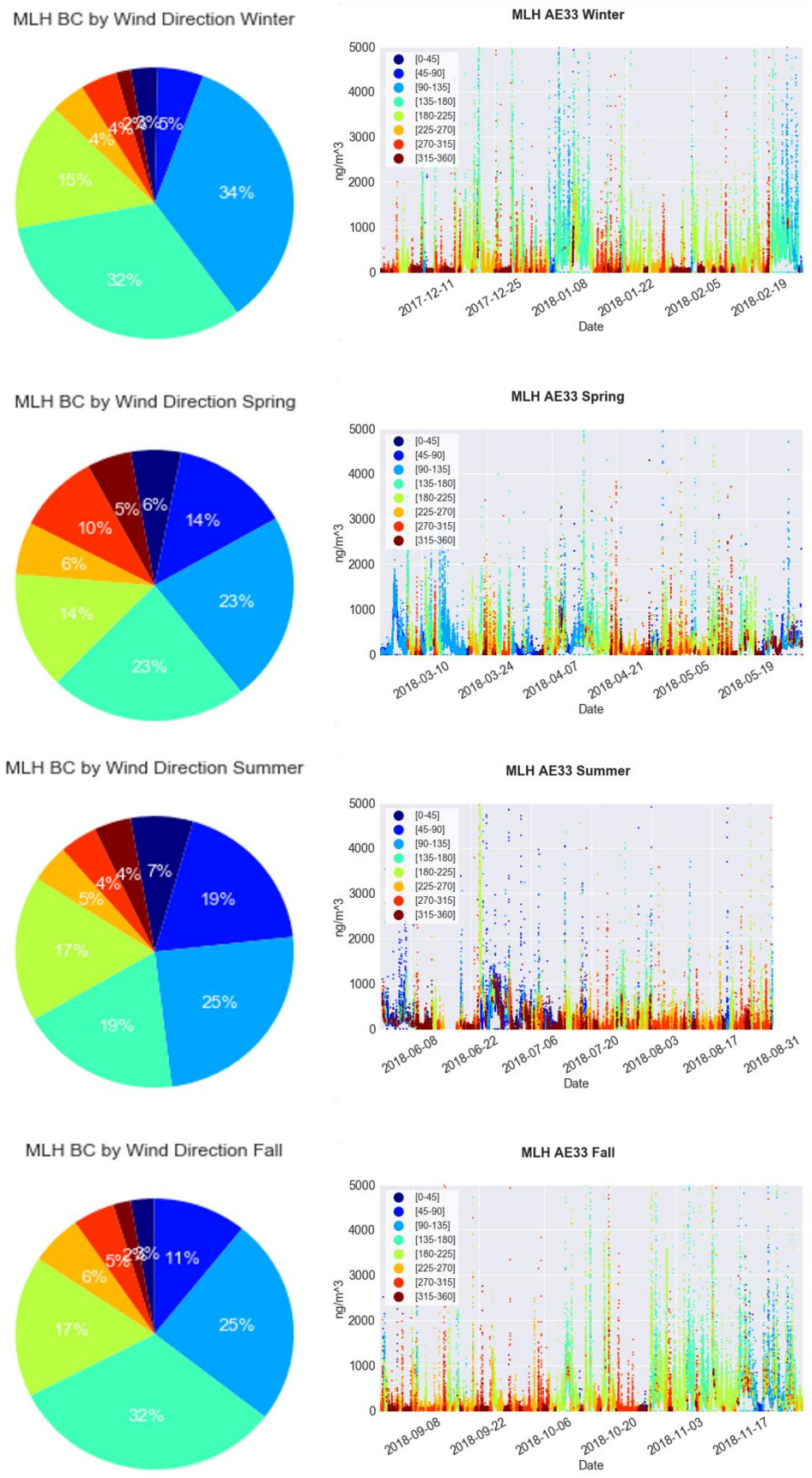

Figure 17 Malin Head seasonal BC by wind direction

As in the previous section, a frequency distribution was done for the stations by season, and the following figure (**Figure 18**) compares the results of summer and winter. The distributions are remarkably similar in both seasons at all of the stations; however, Mace Head appears to have a strong local influence during the winter, as higher pollution levels at that station are typically from local sources. This is not apparent at Malin Head, where the proximity of local sources would make it more likely to have higher levels of BC.

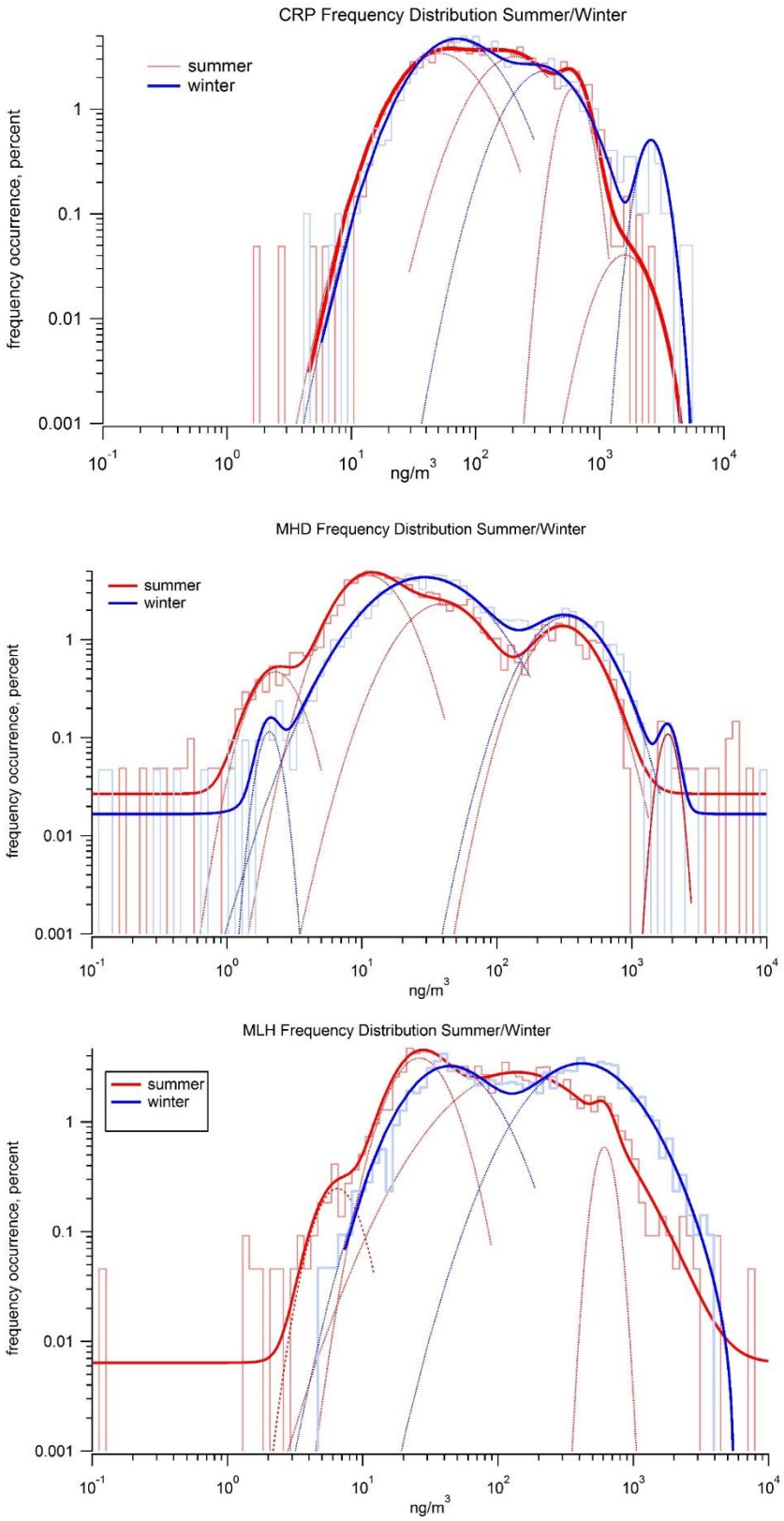

Figure 18 Frequency distribution by summer/winter

4.3 Brown Carbon Source Apportionment

The study aimed to assess whether Malin Head data could be used to provide a unique opportunity to test the AE33's inbuilt algorithm, developed by [*Jisca Sandradewi et al.*, 2008b] to calculate the brown carbon or Biomass Burning (BB) percentage of the total measurement. The station is located very near to a regional road (R242) which has seen a roughly 20% increase in traffic since its inclusion in a tourist route known as the "Wild Atlantic Way" in 2014 (estimate based on nearest traffic count data on the route at An Clochan Liath Dungloe, https://www.tii.ie/roads-tolling/operations-and-maintenance/traffic-count-data/). Spikes in BC are indicative of vehicular emissions, thus likely not to contain significant amounts of BB. By identifying these spikes and applying the algorithm to the data using different inputs, improvements might be made in order to obtain more accurate estimates of BB. The formula relies on the fact that BB absorbs better in the lower (370nm, 470nm) wavelengths, while BC absorbs only at the higher wavelengths (880nm, 950nm). A key factor is a variable called the Angstrom Absorption Exponent, commonly referred to as α (alpha). This is the dependence of the aerosol optical thickness on wavelength, and varies, in this case, with the type of fuel being burnt and how it is being burnt to produce the BC. The instrument defaults are 1 for BC and 2 for BB, yet it has been shown in other papers as Garg et al. [*Garg et al.*, 2016] that α values tend to be much higher for BB, in the range of 7-10 for example for turf (peat), a common heating fuel in Ireland.

Unfortunately, it is rare that conditions at Malin Head are such that individual spikes of BC can be identified as almost certainly traffic related, i.e. the wind is from the south (direction of the road) and BC is near background levels of under 100 ng/m^3. Only a handful of cases exist in the current dataset, where the measurements rose significantly above the previous measurement for the duration of one minute, and then returned to the previous level while the wind direction was between 135 and 225 degrees (south quadrant). The problem is that in most cases the levels before and after the spikes are not "clean" background concentrations, but between 300 and 600 ng/m^3, meaning that there is some regional pollution, which may or may not contain BB.

While there is no way to know the exact percentages of BB in the sampled air without being able to clearly distinguish the traffic cases from the regional pollution or knowing whether or not the alpha values are correct, the instruments are capable of showing trends in BB percentage over time. Below are monthly averages of BB for Carnsore Point, Mace Head, and Malin Head for the period of January to December 2018, showing a decrease by nearly half between the winter and summer at the stations. Interestingly, when data where BC is greater than 100 ng/m^3 are filtered out, leaving essentially background levels of BC with their respective BB values, there is little change between winter and summer BB. However, when BC6 values below 1000 ng/m^3 are filtered out, the corresponding BB averages are higher in the winter and lower in the summer than they are in the complete data series, which confirms there is a definite impact of home heating on BB in the winter time. Until more precise measurements of BB can be made, this approach at least allows for the basic analysis of trends in BB, as well as a comparison of the stations relative to each other.

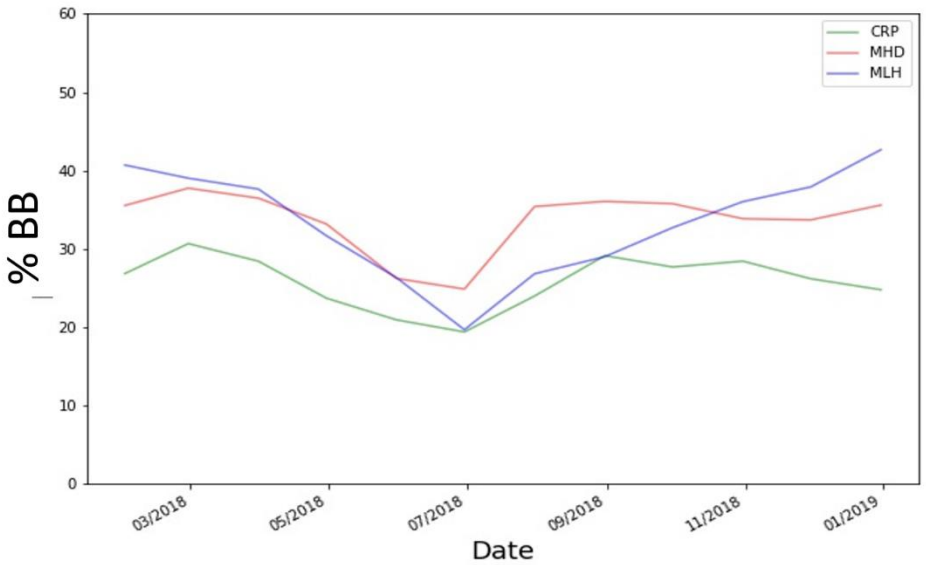

Figure 19 Monthly Average BB percent for CRP (green), MHD (red), and MLH (blue).

In a recent study [*Zotter et al.*, 2017] experimented with alpha values for traffic and wood burning at various locations throughout Switzerland, and determined the "ideal" values to be 0.9 (α_{tr}) and 1.68 (α_{wb}), however these numbers may not apply

to other regions of the world where different fuel sources, i.e. peat (which has much higher α values according to [*Garg et al.*, 2016]), are more commonly burned. Other studies have tried to obtain the BB contribution to total carbon (TC) using the ratio of organic carbon (OC)/elemental carbon (EC), such as [*Pio et al.*, 2011], but this relies on several assumptions. In that study OC is defined as the sum of secondary OC + fossil fuel OC + bio fuel OC + biomass burning OC and EC is equated to the sum of biomass burning EC + fossil fuel EC, so that under certain conditions (an urban environment in winter), OC is approximately equal to $OC_{fossil\ fuel}$ and EC is approximately equal to $EC_{fossil\ fuel}$, which they found was not actually the case unless measured inside a heavily trafficked tunnel, and even less so in rural areas, where there was always some background level of OC.

Using an Igor Pro script developed by the Paul Scherrer Institute (PSI), it was possible to test different alpha values on the aethalometer data. The formula used is the same as that programmed into the instrument and yields the same results as the instrument when the instrument default alpha and mass absorption cross-section (MAC) values are used (see equation page 179 in Appendix C).

When applying the alpha values of 0.9 (α_{tr}) and 1.68 (α_{wb}) derived by Zotter et al., 2017 to the data from the three Irish stations, the BB percentage is nearly double that of the BB percentage reported with the instrument default settings of 1 (α_{tr}) and 2 (α_{wb}), and in fact seems unbelievably high for monthly values at between 60-80% vs the 20-40% with the default alpha values. **Figure 20** shows the difference in BB when using the instrument default values vs. the values recommended by Zotter et al., 2017.

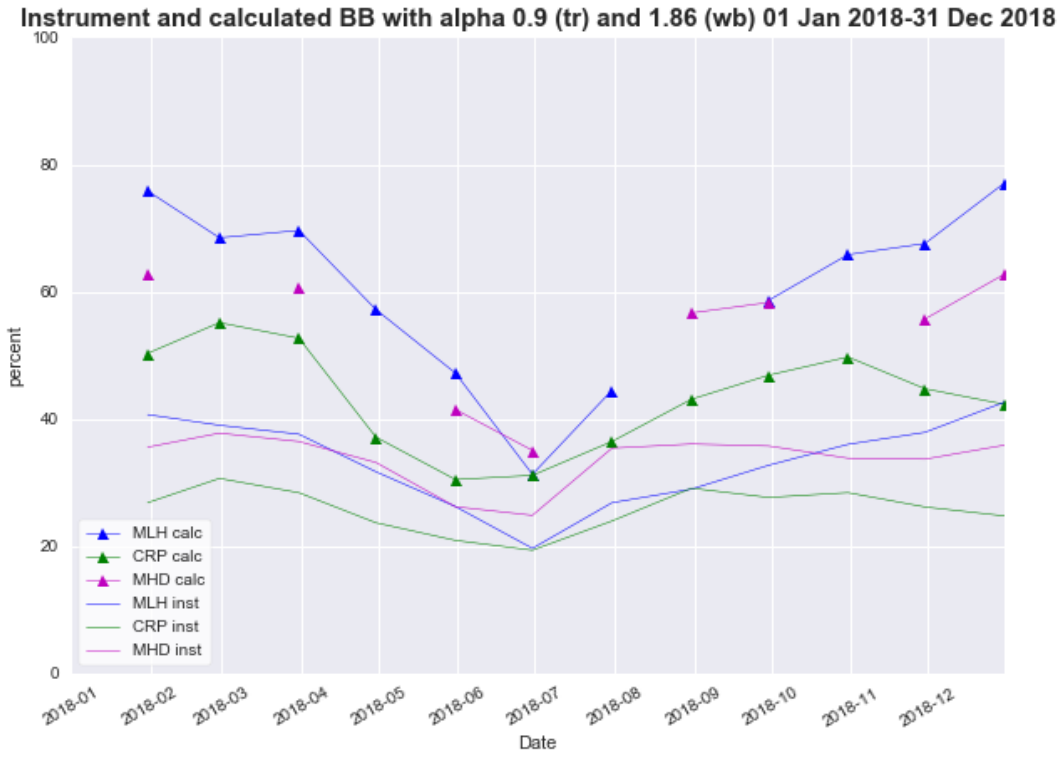

Figure 20 Monthly BB percentage using instrument and calculated alpha values

Looking at the above figure, it is hard to say which values are correct, without knowing what they should actually be. A study by [*Helin et al.*, 2018] on BC source apportionment in Finland found that the BB contribution varies greatly between urban and suburban areas, particularly in winter. Most of the air reaching the Irish stations contains regional pollution, which is more dispersed from its sources, however particularly at MLH there can be local influences resulting in higher concentrations, which seemed to be reflected in the BB time series in the previous section.

4.4 Evaluation of EC/OC from EMEP Intensive Monitoring Period

The source apportionment of BB clearly requires further study, and for this purpose EMEP/ACTRIS conducted an intensive measurement period (IMP) in Winter 2018. As mentioned previously, this involved collection of daily averages of aethalometer BC, and elemental carbon (EC), organic carbon (OC), and total carbon (TC) collected from a high-volume sampler.

As shown in the following scatter plot (**Figure 21**), the EC and BC agree quite well at all stations, though slightly less at Mace Head. This is most likely because Mace Head is the least polluted environment of the stations, and levels of BC are frequently below the detection limit of the instruments.

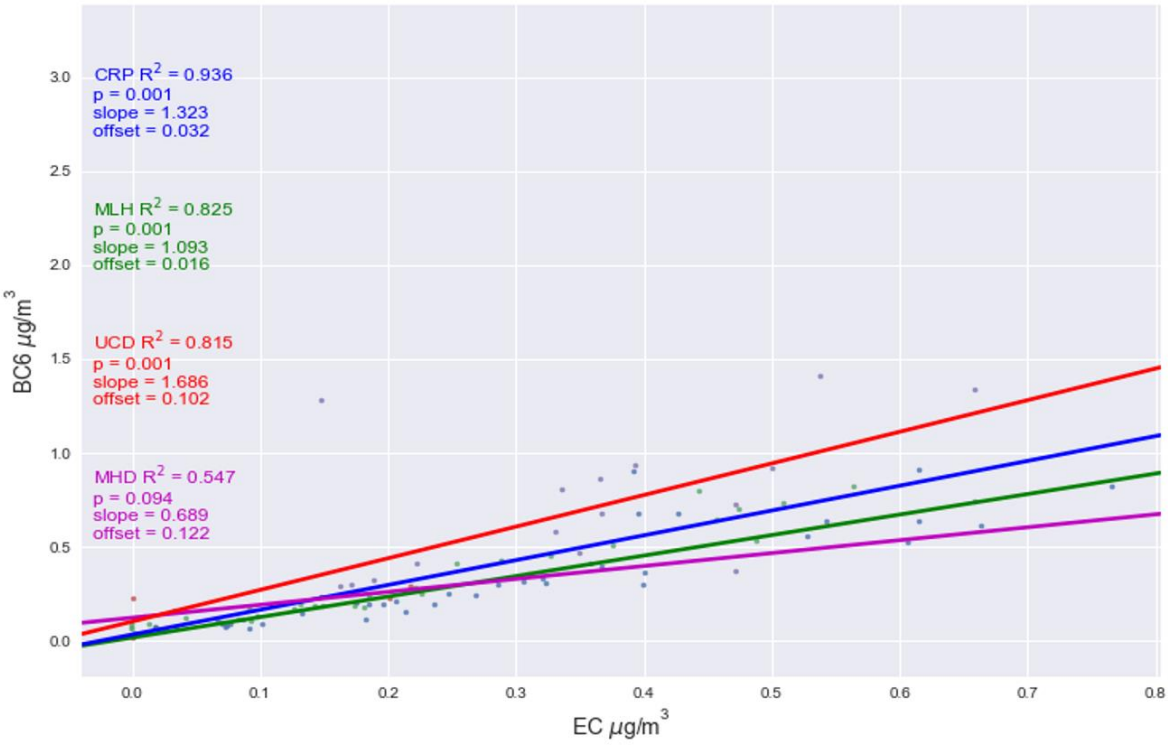

Figure 21 Elemental Carbon from high-volume sampler vs Aethalometer Black Carbon (BC6) for the four Irish sites

The following time series (**Figure 22**) also show good agreement between EC and BC, and the ratios of BC/EC are typical for rural areas according to a study by [*Salako et al.*, 2012] which looked at the variation in these ratios across various parts of the world, and also determined that higher correlations were likely a result of similar sources. A large part of the TC is comprised of OC, which constitutes a large fraction of organic matter.

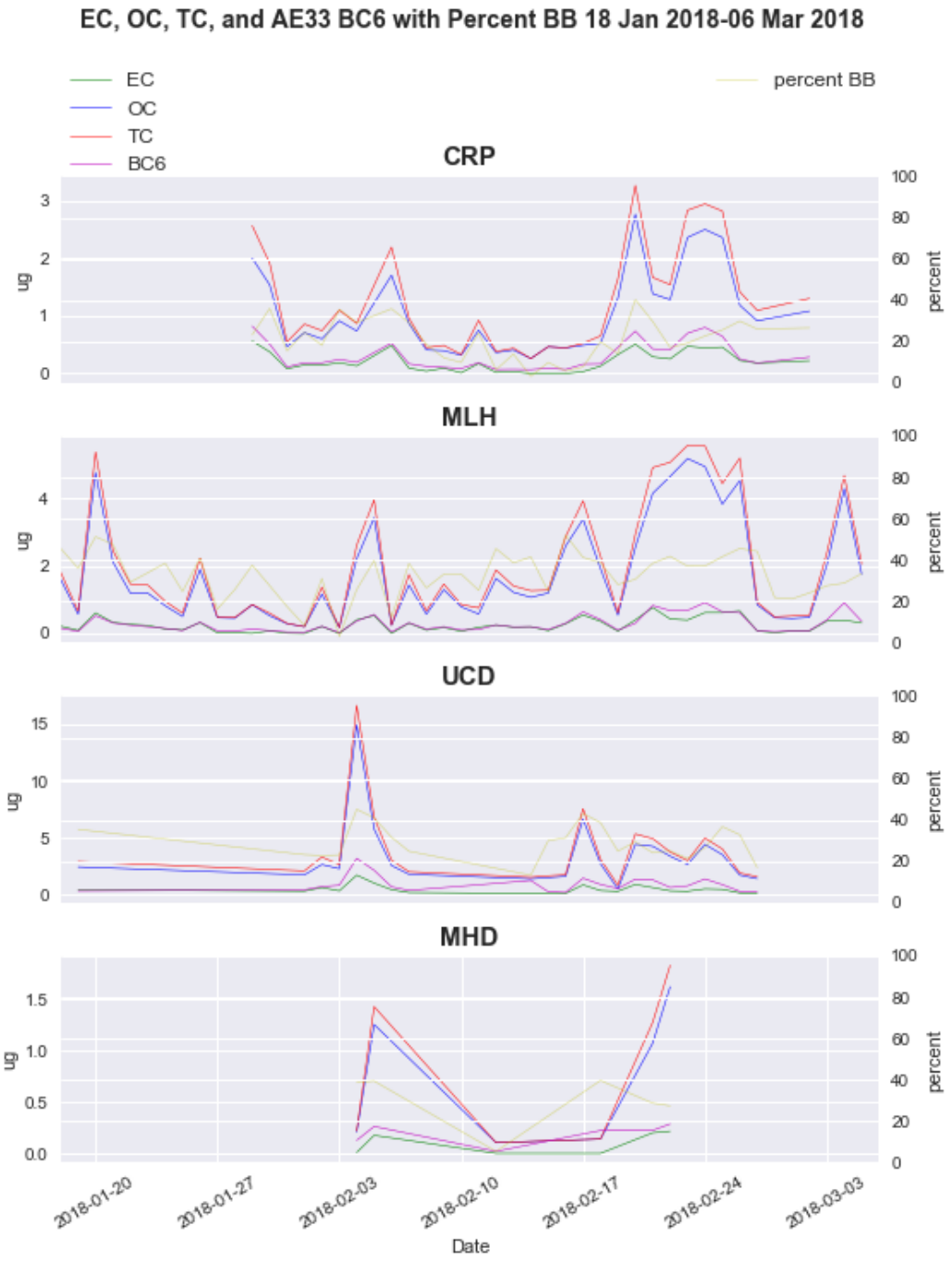

Figure 22 Total Carbon, Elemental Carbon, Organic Carbon, Black Carbon (left axis) and Biomass Burning Percent (right axis)

Table 3 Organic Carbon/Elemental Carbon ratios

	Count	Mean	Std. Dev.
CRP	27	7.05	5.19
MHD	6	51.21	65.27
MLH	43	8.83	6.20
UCD	22	7.11	2.21

Table 4 Organic Carbon/Total Carbon ratios

	Count	Mean	Std. Dev.
CRP	27	0.85	0.05
MHD	6	0.92	0.06
MLH	43	0.88	0.04
UCD	22	0.86	0.06

A breakdown of the OC/EC ratio and the OC/TC ratio shows that OC is in fact at least seven times higher than EC, ignoring MHD here due to a limited number of data points resulting from a large number of negative EC values. This is in accordance with previous studies such as [*Pio et al.*, 2011] and [*Krzysztof et al.*, 2017] who found similar results, particularly in rural and remote regions, and as noted by [*Bougiatioti et al.*, 2013], OC/EC ratios greater than 2 are indicative of secondary organic aerosol (SOA) formation. Another study by [*H Wang et al.*, 2017] demonstrated that significant amounts of both OC and EC (between 25-33%) fall into the PM2.5 and larger category, and [*Bougiatioti et al.*, 2013] found that 74% of the total OC and 79% of EC is in the PM1 size category. As shown in **Table 4** above, organic carbon also comprises over 80% of the total carbon, and thus may account for a large part of the organics measured at the stations. This will be taken into account in the section on mass closure.

Organics were measured with the AMS at Mace Head and ACSM at UCD during the EMEP campaign, albeit only particles in the PM1 category. PM1 organic carbon has not been very thoroughly investigated, and so it is difficult to find relevant studies showing its contribution to the total PM1 mass. One paper by [*Godec et al.*, 2012] showed that the wintertime PM1 organic carbon in a suburban area of Zagreb, Croatia constituted 19.88% of the total PM1 measured as well as an additional 23.76% of PM2.5 and 24.15% of PM10. It demonstrates that organic carbon contributes a large fraction to the total mass in each size category. Organic matter

(OM), of which organic carbon is a subset, must therefore be even larger in all size categories. Indeed, when plotting the PM10 organic carbon against the PM1 organic matter for MHD and UCD, the ratio was less than 1, and the time series consistently showed the measured OM as less than the OC. Therefore, an attempt was made to find how much OM PM10 there should be based on OM/OC ratios found in previous studies, such as one by [*H. S. El-Zanan et al.*, 2005], which found OM/OC ratios of on average 2.07 (ranging from 1.58 at Indian Gardens, Arizona to 2.58 at Mt. Rainier, Washington) for remote regions of the U.S, which were higher than other results cited by that study, and the ratio of 1.4 (the estimated average molecular weight per carbon weight derived from theoretical and lab studies in the 1970's, as explained by [*Turpin and Lim*, 2001]) commonly used in mass reconstruction. **Table 5** outlines values found in other studies for different types of environments. It is noteworthy that the "coastal" locations have the highest OM/OC ratios, even when they are urban environments.

Table 5 Literature OM/OC ratios

	OM/OC	**Location**	**Source**
Urban	1.56	Phoenix, AZ	[*Ruthenburg et al.*, 2014]
	1.59	Avg. 14 Chinese cities (winter)	[*Xing et al.*, 2013]
	1.6	Los Angeles, CA Denver, CO	[*Turpin and Lim*, 2001]
Rural	1.77	Olympic, WA	[*Ruthenburg et al.*, 2014]
	1.78	Acadia National Park, ME	[*H. S. El-Zanan et al.*, 2005]
	1.9	K-puszta, rural Hungary	[*Kiss et al.*, 2002]
Coastal	1.91	Hong Kong, China	[*X Chen and Yu*, 2007]
	2.1	Crete, Greece	[*Bougiatioti et al.*, 2013]
	2.16	Atlanta, GA	[*Hazem S. El-Zanan et al.*, 2009]

Applying a simple formula, $OC_{PM10} * x = OM_{PM10}$, where x is the OM/OC PM10 ratio, and solving this equation using a range of site appropriate OM/OC ratios from previous studies, the calculated OM_{PM10} can be used to derive the percentage of OM_{PM1} of the total OM. The results of this are shown in the **Table 6** below, and

while it is still uncertain exactly which OM/OC ratio is most appropriate for each station, it is evident that 1.4 is too low for both. For MHD it appears to be a minimum of 2, and for UCD 1.59 seems to be a reasonable ratio. This implies that nearly half of the organic matter is larger than PM1. El-Zanan (2005) notes that the ratios increase as the OM is transported over long distances and the aerosols age and become more oxygenated and polar during secondary organic aerosol (SOA) formation, so it is likely, also based on the calculations below, that the UCD ratio will be lower than MHD, as it is located in an urban area and MHD is a remote rural/coastal environment. The paper also notes that ratios will tend to be lower during the winter months due to less photo-chemical activity.

A previous study involving Mace Head [*Yttri et al.*, 2007] found that OM comprised 8.9% of PM10 at that station, using a conversion factor of only 1.4, which according to these latest measurements, could mean that a much larger percentage of OM falls into the coarse particle category. The study by [*Ruthenburg et al.*, 2014] shows seasonal variations at all sites and suggests a single estimate cannot be representative of the OM/OC ratio for any location. Factors such as plankton blooms which, according to[*Cavalli et al.*, 2004], occur near the coasts of Ireland in the Spring and Fall, can add significant amounts of organic matter to the atmosphere, thus increasing the OM/OC ratio. Future measurements will be able to determine these numbers more accurately, but for now it is possible to at least estimate them.

Table 6 MHD and UCD OM/OC ratio ranges and OM_{PM1} percent

	OM/OC range	OM_{PM1} % of OM
MHD	1.91-2.16	56-63
UCD	1.56-1.6	42.8-44

Analysis of the levoglucosan results yielded higher alpha values than both the instrument default setting (2) and the literature recommended value (1.68) [*Zotter et al.*, 2017] for the biomass burning component, but still not significantly higher than the instrument default. Shown here are the correlation plots of the "wood burning" contribution (BC_{wb}) to levoglucosan, keeping the α_{tr} set at 1 and changing the α_{wb} to obtain the lowest y intercept, followed by the daily average BB percentage time series along with levoglucosan based on these values. For all 4 locations, the α_{wb} was around 2.2, which is reasonably close to the default setting of 2. Increasing the α_{wb} resulted in the BB percentage almost disappearing completely, and decreasing α_{wb} , as demonstrated using the recommended value of 1.68, caused BB to exceed 100% almost the entire time, which is highly unlikely given that these are daily averages. The last plot shows the monthly averages for the year with seasonal cycle for the instrument default settings compared to the new levoglucosan based alpha values.

There are of course limitations to this method, as levoglucosan is removed from the atmosphere at a faster rate than BC [*Helin et al.*, 2018], and it is mainly a wood burning tracer, whereas much of the biomass burning in Ireland is from peat. Nevertheless, there is a strong correlation (r^2= 0.83) of BC_{wb} to levoglucosan, and as can be seen in the time series, levoglucosan levels are frequently high, especially during this winter campaign.

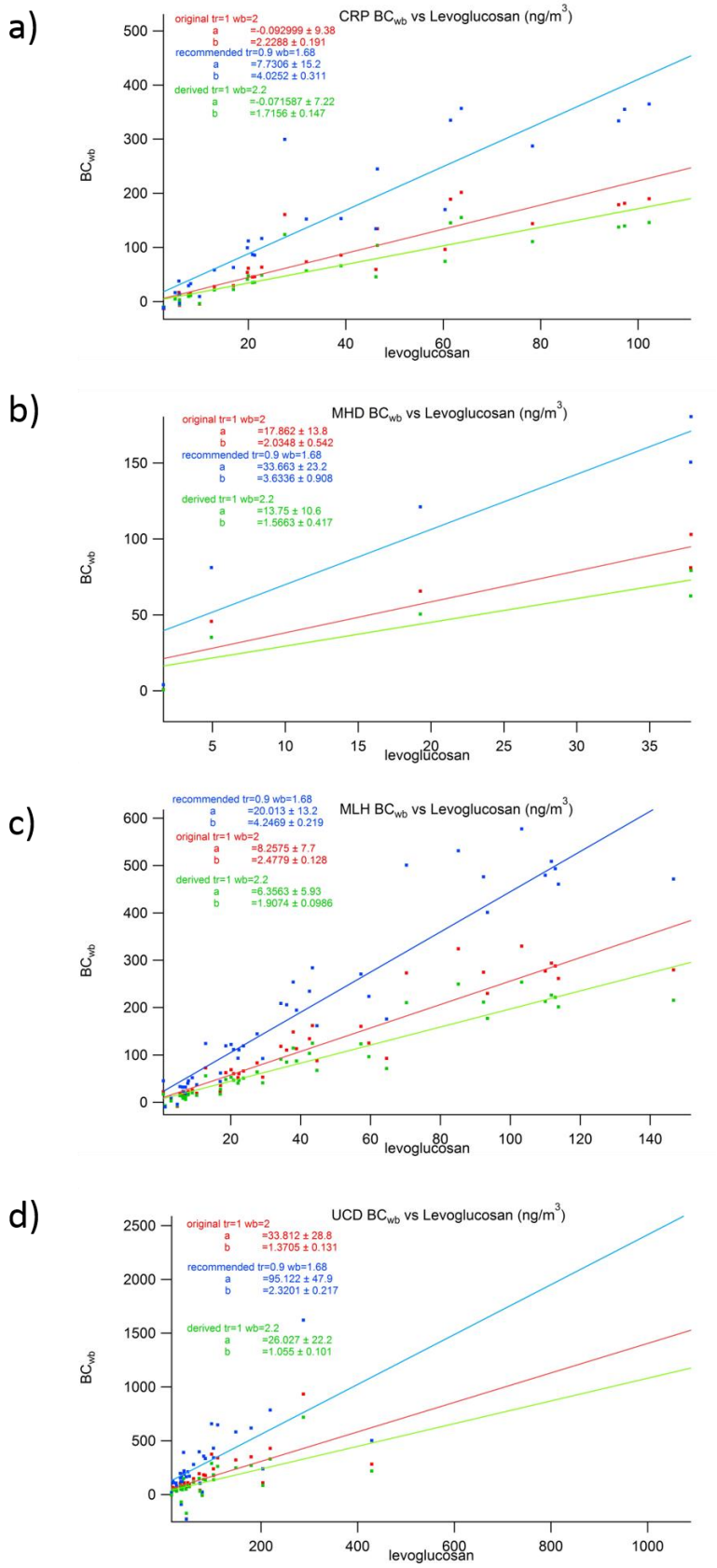

Figure 23 BC$_{wb}$ vs Levoglucosan for all 4 locations during the EMEP campaign.

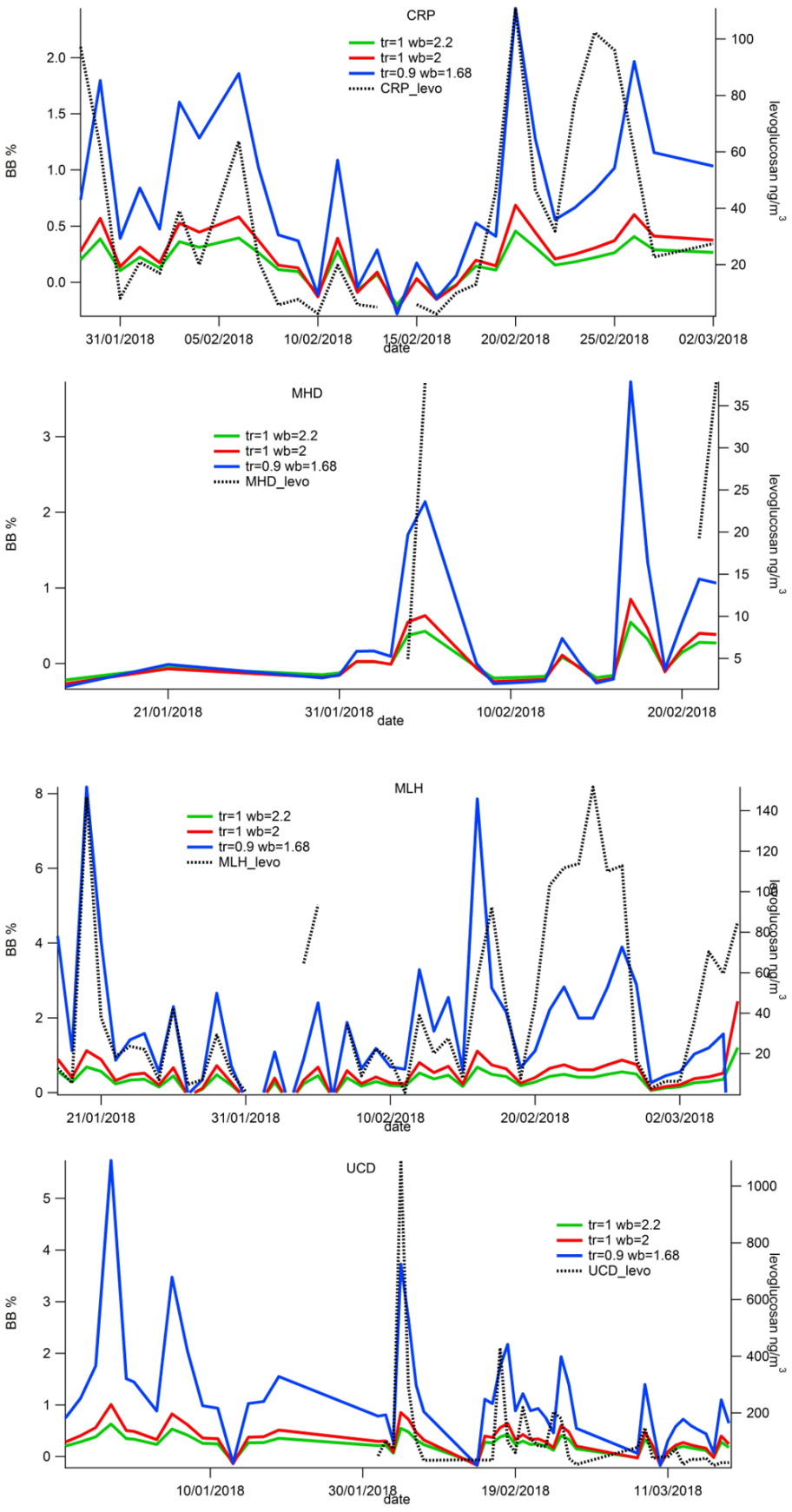

Figure 24 Time series of BB percent and Levoglucosan

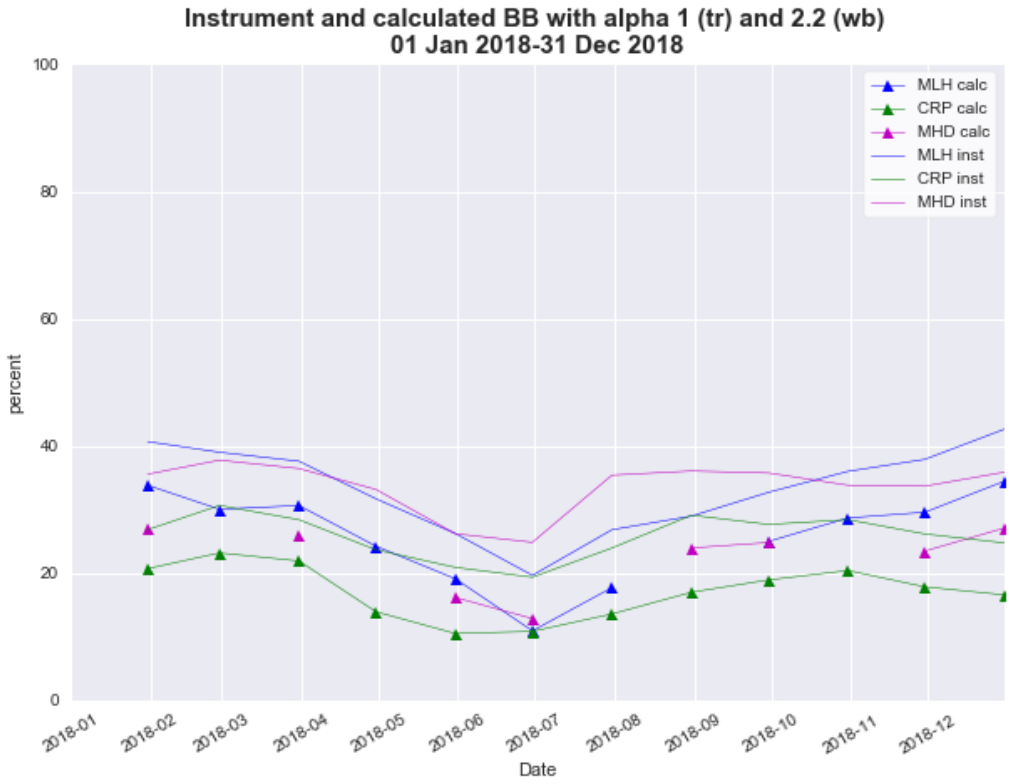

Figure 25 Seasonal cycle of BB using levoglucosan derived alpha values

4.5 Black Carbon as a Fraction of PM1

A preliminary analysis was conducted on the first year of Fidas data, from the time the instrument was installed at Malin Head in May 2018 until May 2019. The data show that the lowest percentage of BC of the total PM1 originates from the polluted sector, as can be seen in **Table 7**, even though these correspond to the highest BC concentrations, indicating that there are other sources of PM1 in the polluted sector where PM1 is highest. Higher percentages of BC are associated with lower PM1 concentrations in the clean air sector where both BC and PM1 are lowest. The following time series plot (**Figure 26**) also shows reasonably good agreement between BC and PM1, indicating a common source of both BC and PM1 with highest levels during the winter months.

Table 7 Mean ng/m3 and standard deviation of PM1, BC6, and Percentage BC of total PM1 at MLH by wind sector

	Count	PM1		BC6		Percent BC6 of PM1	
		Mean	Stdev	Mean	Stdev	Mean	Stdev
0-45	29178	2871.98	2824.44	85.6	196.88	3.71	29.96
45-90	39981	4835.3	4462.8	251.13	579.8	2.65	27.7
90-135	26976	8265.63	8032.65	426.73	594.25	2.58	10.72
135-180	55009	8850.65	8651.81	595.22	739.6	1.87	11.61
180-225	105704	5517.8	6995.59	368.9	900.67	2.56	11.52
225-270	84181	3425.19	2763.05	95.58	241.85	5.55	30.84
270-315	65245	3293.25	2974.07	95.93	342.42	5.73	39.0
315-360	35146	2608.98	2280.13	54.78	197.39	4.15	41.25

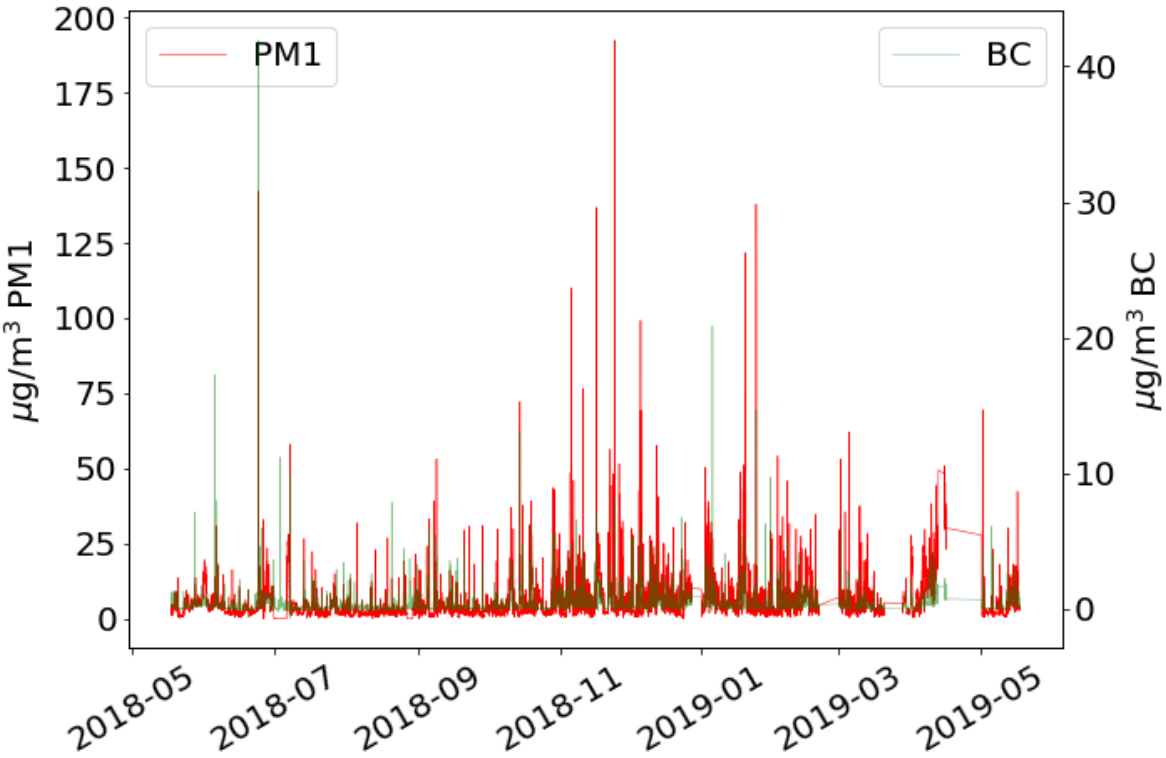

Figure 26 MLH AE33 BC6 and Fidas PM1 time series 12-hour rolling average

4.6 Mass Closure Experiment

It is a common practice to use models to compare the sum of individual species to a total measured mass, and there are many methods used to do this. In 2006, Jennings et al. [*Jennings et al.*, 2006] conducted a mass closure experiment on data from 2002 using measurements of certain substances such as Sulphate (SO_4^{2-}), Sodium (Na^+), Calcium (Ca^{2+}), and Nitrate (NO_3^-) to estimate the contribution of sea salt (2.54 x Na^+), resuspended dust (4.3 x non-sea salt Ca^{2+}), BC, secondary inorganic material (1.29 × NO_3^- +1.38 × non-sea salt SO_4^{2-}), and organics to the total aerosol in the atmosphere. Their method used five sampling locations around Ireland, including one coastal site at Wicklow Head on the east coast of Ireland, about 100km south of Carnsore Point (referred to as site C in **Table 8** below). 24-hour filter samples were collected and analysed gravimetrically, chemically, and thermally to determine which species were present and in what quantity. The sum of the five categories was then compared to the total gravimetric mass, the results of which are shown in **Table 9**.

The same mass closure model used by Jennings et al. (2006) was applied to data collected by the high volume sampler, TEOM, AE33, and ACSM at Carnsore Point. Here are the results of this analysis compared to the PM10 of site C of the original. As atmospheric levels of Sulphate have been shown to have decreased by about 50% since 2002 based on the trend for Carnsore Point in **Figure 27**, an attempt was made to extrapolate 2002 concentrations from the current dataset to compare them to the values in the original study as well. The results are quite similar, and within 10%. An important factor that could affect the results is that the ACSM was only measuring PM1 data, and many of the organics fall into the PM2.5 range, as can also be seen in the results of the original study. Other differences can be accounted for by a number of factors, including meteorological conditions, instrumental accuracy, and possible errors in the model.

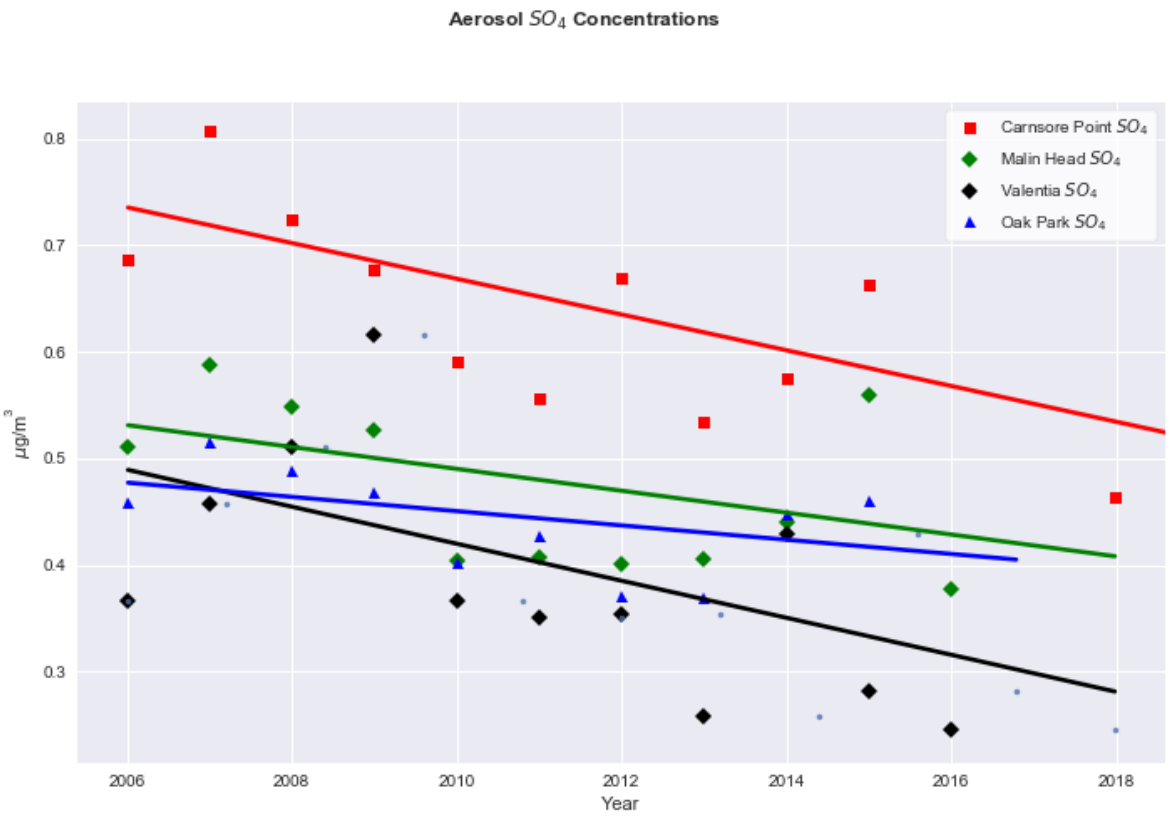

Figure 27 Sulphate concentrations annual averages

Table 8 Mean reconstructed component concentrations (µg/m3) and their contributions to PM mass (%) in Ireland by Jennings et al. 2006. Site C is the coastal site in this study.

Fractions	Sites	EC	Organics	Secondary	Sea salt	Resuspended dusts	Other
PM_{10}	A	7.9 (22%)	9.0 (25%)	4.8 (13%)	3.2 (9%)	6.5 (18%)	6.1 (14%)
	B	3.1 (14%)	3.9 (17%)	4.5 (20%)	3.2 (14%)	4.7 (21%)	2.8 (12%)
	E	3.0 (13%)	4.3 (18%)	4.1 (17%)	4.2 (18%)	3.5 (15%)	4.8 (20%)
	C	0.5 (3%)	1.1 (6%)	4.3 (23%)	7.4 (40%)	1.2 (6%)	4.0 (22%)
	D	0.4 (4%)	1.0 (10%)	3.2 (30%)	2.3 (22%)	1.0 (10%)	2.4 (24%)
$PM_{2.5}$	A	7.3 (33%)	7.4 (33%)	3.8 (17%)	0.7 (3%)	0.6 (3%)	2.6 (12%)
	B	3.0 (26%)	3.5 (29%)	3.4 (29%)	0.6 (5%)	0.5 (4%)	0.8 (7%)
	E	2.9 (23%)	3.8 (30%)	3.3 (26%)	0.8 (7%)	0.5 (4%)	1.2 (10%)
	C	0.5 (6%)	1.1 (14%)	3.3 (44%)	1.1 (15%)	0.3 (4%)	1.2 (16%)
	D	0.4 (7%)	1.0 (16%)	2.5 (42%)	0.6 (11%)	0.2 (3%)	1.3 (21%)
$PM_{2.5-10}$	A	0.6 (4%)	1.6 (11%)	1.1 (7%)	2.5 (17%)	5.9 (39%)	3.3 (22%)
	B	0.1 (1%)	0.4 (4%)	1.1 (10%)	2.6 (25%)	4.2 (41%)	1.9 (19%)
	E	0.2 (2%)	0.6 (5%)	0.9 (8%)	3.4 (30%)	3.1 (27%)	3.2 (28%)
	C	0.02(0.2%)	0.1 (1%)	1.1 (9%)	6.3 (56%)	0.9 (8%)	2.8 (25%)
	D	0.01(0.3%)	0.05 (1%)	0.6 (14%)	1.7 (39%)	0.8 (18%)	1.2 (28%)

Table 9 Mass Closure using 2017 CRP data with extrapolation back to 2002 assuming higher BC and SO4 values at that time

	Sea Salt		Resusp		BC		Inorganic		Organic		Other		TEOM
	µg/m³	%	µg/m³	%	µg/m³	%	µg/m³	%	µg/m³	%	µg/m³	%	µg/m³
2017	7.05	40.01	0.63	3.58	0.24	1.36	2.91	16.52	0.60	3.41	6.19	35.13	17.62
2002	7.05	35.86	0.63	3.20	0.61	3.10	4.67	23.75	0.60	3.05	6.1	31.03	19.66

Looking at the Carnsore Point mass closure by season in **Table 10** below, it is interesting to note the large sea salt contribution during the winter, and generally the highest levels of all categories, resulting in the lowest unknown component. Likewise, summer has the lowest percentages in each category and the highest percentage unknown. Particularly BC and organics are much lower in the summer months than in other seasons. Further study is needed to determine the types of organics contributing seasonally, as the sources are both natural and anthropogenic.

Table 10 CRP Mass Closure by Season August 2016-August 2017

	Sea Salt		Resusp		BC		Inorganic		Organic		Other		TEOM
	µg/m3	%	µg/m3	%	µg/m3	%	µg/m3	%	µg/m3	%	µg/m3	%	µg/m3
Spring	6.96	36.55	0.59	3.10	0.22	1.16	4.20	22.06	0.62	3.26	6.45	33.88	19.04
Summer	6.31	36.33	0.50	2.88	0.14	0.81	2.18	12.56	0.46	2.64	7.78	44.79	17.37
Fall	6.13	37.42	0.51	3.11	0.29	1.77	2.59	15.81	0.64	3.91	6.22	37.98	16.38
Winter	9.88	53.78	1.07	5.82	0.38	2.07	3.17	17.26	0.74	4.03	3.13	17.04	18.37

With the addition of the Fidas instrument at Malin Head, it became possible to perform the same mass closure experiment using data from that station for one year with the PM10 mass from the Fidas and compare it to Carnsore Point, albeit without the organics contribution because the ACSM was not available at MLH for the entire year. It is important to note that the ACSM at Carnsore Point was measuring only PM1 data, and at Malin Head it was measuring PM2.5, which, given that a large amount of organics are in the range between PM1-PM2.5, could have an impact on the comparisons. The ACSM was at MLH only for a brief period, from September-November 2018, so **Table 11** shows the results of the PM10 mass closure for that time, compared to CRP Fall (September-November 2016).

During the time of the ACSM measurements at Malin Head, there is a considerably greater contribution (8.88%) of organics to the total mass than at Carnsore Point, probably due to much of it falling into the PM2.5 category. The much higher unknown contribution at Malin Head in **Table 12** without organics seems to confirm this. From previous calculations we know that roughly between 40-60% of the total OM is PM1 at UCD and MHD, depending on the OM/OC ratio, so it should be possible to improve the mass closure equation by applying this to the ACSM PM1 organics.

Assuming that about 50% of organics are larger than PM1, doubling the ACSM PM1 organics at CRP in the Fall period would increase the mass to 1.28µg/m^3 and their percentage of total PM10 mass would increase to 7.8% thereby reducing the unknown to 34%. For the full year at CRP, the calculated organics are 1.2µg/m^3 making up 6.8% of total PM10 mass, reducing unknown to 31.7%. These numbers agree well with the MLH PM2.5 organic percentage of the total PM10 mass as well as with the studies by [*Jennings et al.*, 2006] and [*Yttri et al.*, 2007] who used

OM/OC conversion factors of 1.5 and 1.4 respectively. When applying a factor of 1.4 to calculate OC at CRP in Fall, the result is 0.91 µg/m^3, which is remarkably close to the average OC of 0.96 µg/m^3 from EMEP winter campaign. This could mean that CRP has a similarly low OM/OC ratio to Dublin, especially during the Fall/Winter time.

Table 11 Malin Head Mass Closure with organics Sep-Nov 2018 and CRP Sep-Nov 2016

	Sea Salt		Resusp		BC		Inorganic		Organic		Other		PM10
	µg/m^3	%	µg/m^3	%	µg/m^3	%	µg/m^3	%	µg/m^3	%	µg/m^3	%	µg/m^3
MLH	5.36	48.00	0.37	3.33	0.22	1.97	0.79	7.10	0.98	8.88	3.42	30.70	11.14
CRP	6.13	37.42	0.51	3.11	0.29	1.77	2.59	15.81	0.64	3.91	6.22	37.97	16.38

Following are the results of one year from the Malin Head mass closure compared to Carnsore Point without the organics contribution at MLH, as there is no overlap of measurements during this time. Note that the time periods are not identical (CRP is from August 2016-August 2017 and MLH is from May 2018-December 2018), but the percentages still agree quite well over a one-year time period. **Figure 28** below shows the scatter plots of the mass closure vs the total mass for the two stations based on the table. The final plot shows the MLH mass closure including the ACSM organics, and it is noteworthy that both the slope and r^2 are similar to CRP then. Interestingly, there is also a much higher contribution of inorganic matter at CRP, nearly double that at MLH, both in the seasonal and one-year comparisons.

Table 12 Carnsore Point and Malin Head Mass Closure comparison one year without MLH organics

	Sea Salt		Resusp		BC		Inorganic		Organic		Other		PM10
	µg/m^3	%	µg/m^3	%	µg/m^3	%	µg/m^3	%	µg/m^3	%	µg/m^3	%	µg/m^3
MLH	3.62	37.00	0.31	3.20	0.25	2.60	1.70	17.36	n/a	n/a	3.91	39.94	9.79
CRP	7.05	40.01	0.63	3.58	0.24	1.36	2.91	16.52	0.60	3.41	6.19	35.13	17.62

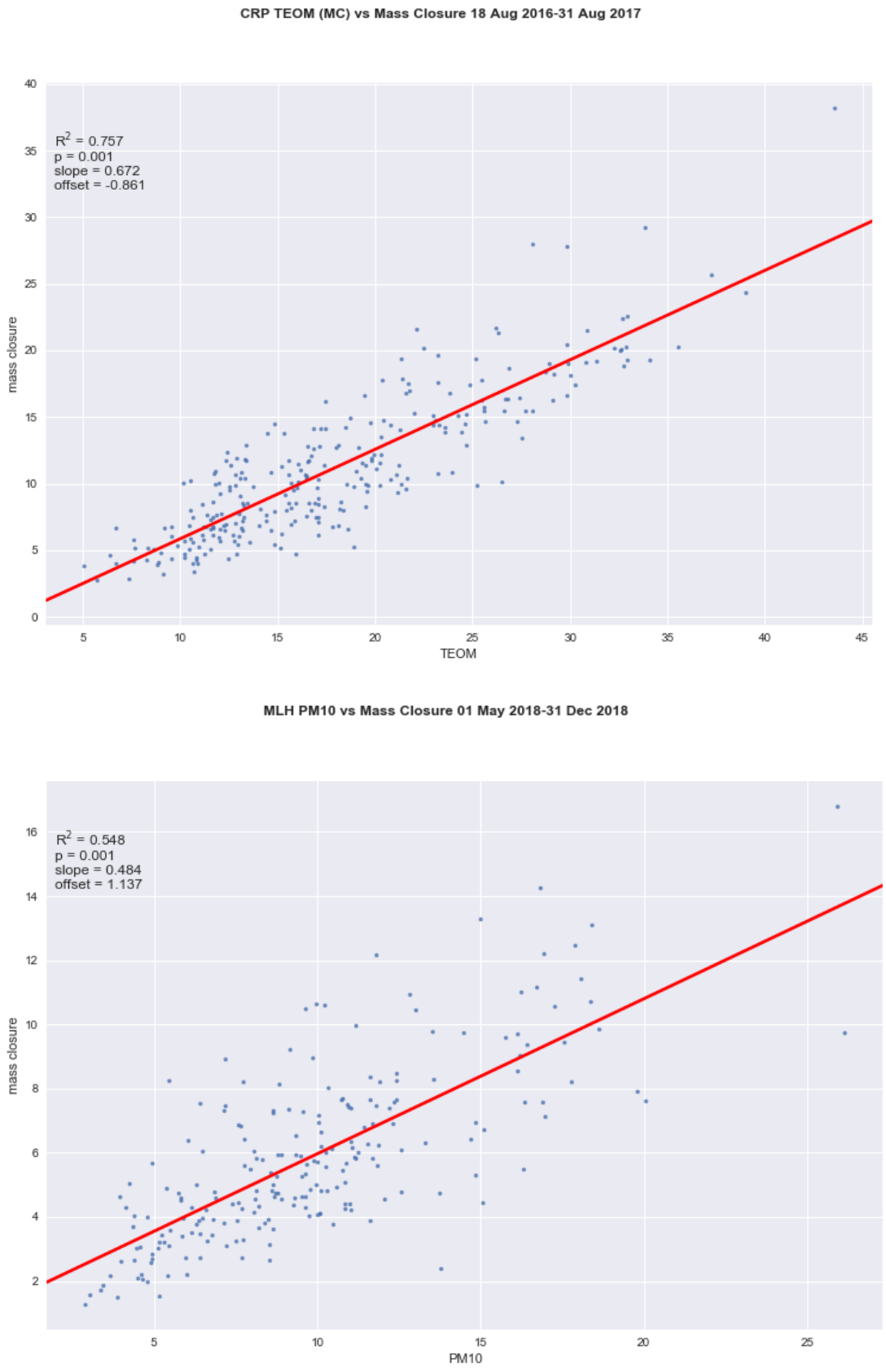

Figure 28 Total mass vs Mass Closure for CRP and MLH. Note that MLH plot does not include organics.

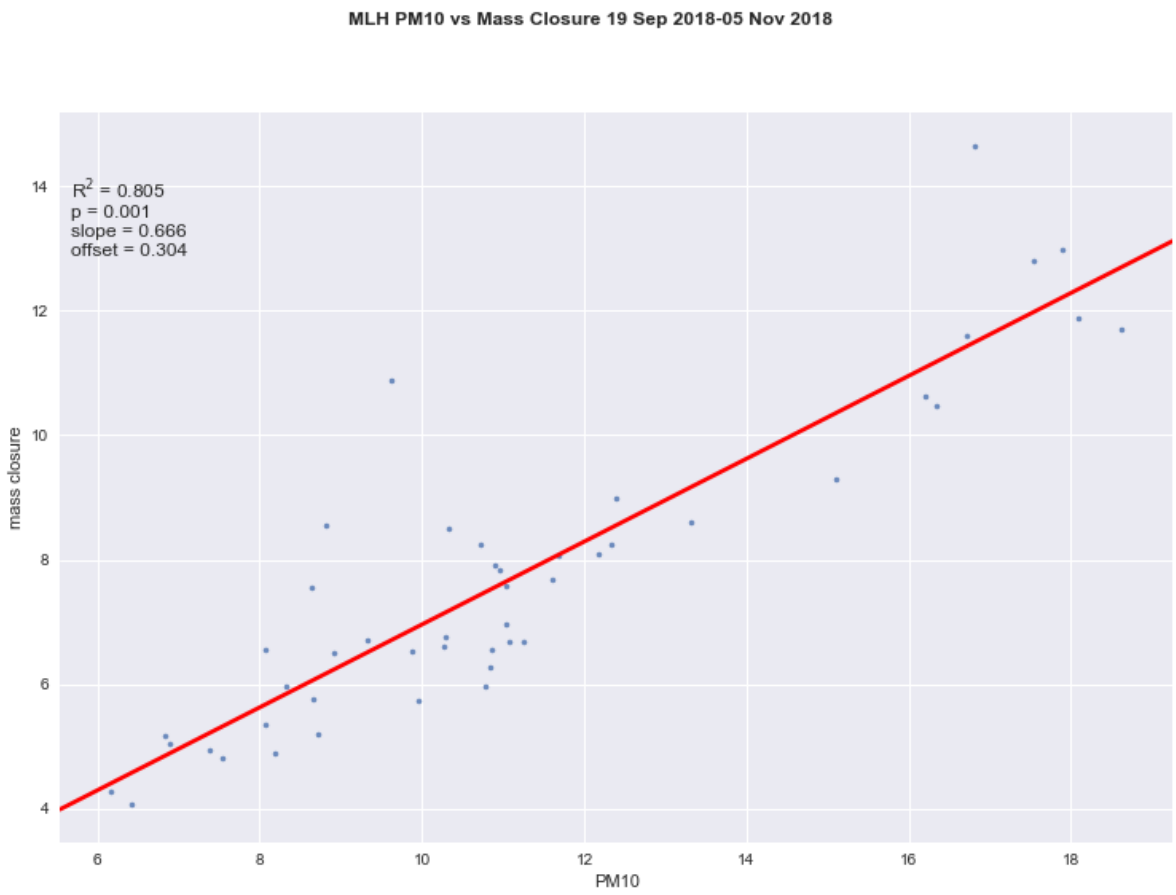

Figure 29 MLH total mass vs mass closure with ACSM organics

As a large portion of organics seem to fall into the category of PM2.5 or below, and the Fidas is capable of distinguishing particle sizes, it makes sense to evaluate the mass closure equation as the sum of species measured by the ACSM (NH_4, SO_4, NO_3, Cl, and organics) with its PM2.5 cut-off, plus BC from the aethalometer in order to see how much of the particulate matter is accounted for in this smaller size category. Following are the results of this mass closure using daily averages of Fidas PM2.5, ACSM, and AE33 BC6 in micrograms/m^3.

Indeed, only about 40% of the total PM2.5 is accounted for using this method on the entire dataset, as opposed to between 60-70% using the PM10 data. This could be due to the lack of ability to measure the sea salt contribution, which is the highest contributor to the total mass in the coarse particle fraction, but most likely adds a significant amount to the fine particle total as well. The absence of Calcium (Ca^{2+}) measurements in the ACSM data may also contribute a small amount to the

unaccounted mass, as this is used in the PM10 mass closure as an indicator of resuspended dust.

When separated into clean and polluted air sectors, it becomes evident that sea salt does play a major role even in the PM2.5 aerosol composition. Looking at only the polluted air sector, the unknown is reduced to 35%, which is comparable to the PM10 mass closure. Being a coastal station, most likely even the polluted air sector contains a significant amount of sea salt, which if taken into account would reduce the unknown even further. The clean air sector on the other hand, has an even greater unknown percentage than the overall total, with generally much lower concentrations of every measured species, as can be expected in “clean” air.

Just as in the PM10 mass closure, organics are a key contributor to the PM2.5 total mass, and represent a similar percentage here as in the 2002 study results in **Table 8**, where organics comprised 14% of the total PM2.5 at the coastal site (C). Very little is known about the nature of these organics, and much more research is needed to understand the origins of this major factor in atmospheric composition and its influence on the environment.

Table 13 MLH PM2.5 mass closure

	SO_4		NO_3		BC		NH_4		Cl		Organic		Other		PM2.5
	$\mu g/m^3$	%	$\mu g/m^3$	%	$\mu g/m^3$	%	$\mu g/m^3$	%	$\mu g/m^3$	%	$\mu g/m^3$	%	$\mu g/m^3$	%	$\mu g/m^3$
All	0.5	6.77	0.24	3.25	0.23	3.11	0.59	7.98	0.08	1.1	1.38	18.67	4.37	59.13	7.39
Poll.	0.9	8.49	0.93	8.77	0.55	5.19	0.97	9.15	0.15	1.4	3.38	31.89	3.72	35.09	10.6
Clean	0.4	5.7	0.07	0.99	0.07	0.99	0.48	6.85	0.06	0.8	0.62	8.84	5.31	75.75	7.01

The PM2.5 to mass closure scatter plot shows almost no correlation between the total mass and the mass closure and confirms that about 60% of the total mass is not accounted for using all the available data. Again, this is likely due to the absence of sea salt measurements, as this is a primary component of the atmosphere at coastal stations. When separating the data into clean and polluted air sectors (using 270-360 degrees for the "clean" sector, as previously defined), there is a definite correlation of 0.751 between the PM2.5 and ACSM measurements in polluted air, similar to the results of the ACMCC comparison of the ACSM to Fidas where the r^2 was 0.85 for PM1 measurements, which were conducted in a far more polluted environment near Paris, France [*ACMCC*, 2018]. The clean air sector has almost no correlation as there are far fewer pollutants and a much greater amount of sea salt arriving from that direction. Of course, it should be taken into consideration that these are only a few months' worth of data, and only from the Fall season, which may not be representative of the overall PM2.5 composition. Only continued long-term measurements will be able to show this more accurately, and hopefully combined with other instrument data, will provide a better understanding of the particulate matter in the atmosphere.

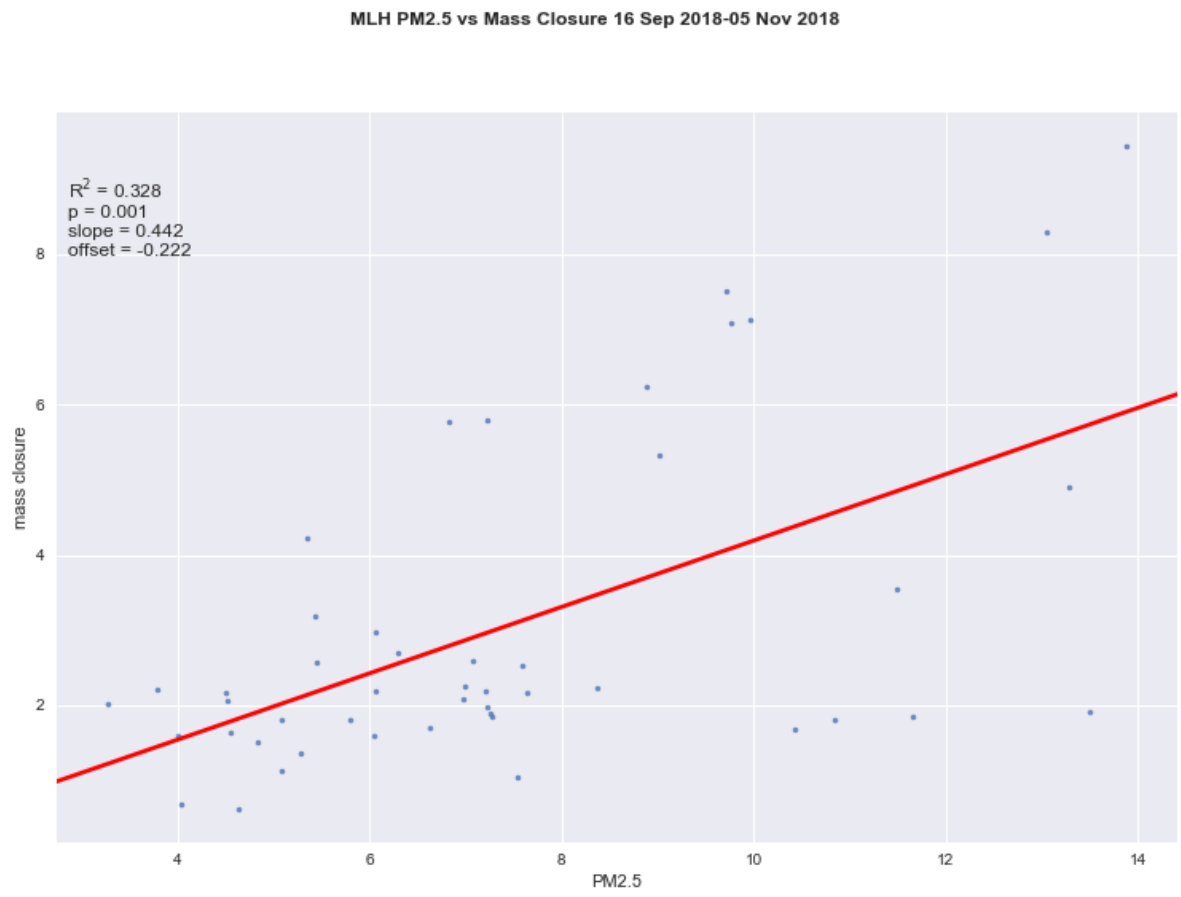

Figure 30 MLH PM2.5 vs ACSM and BC mass closure

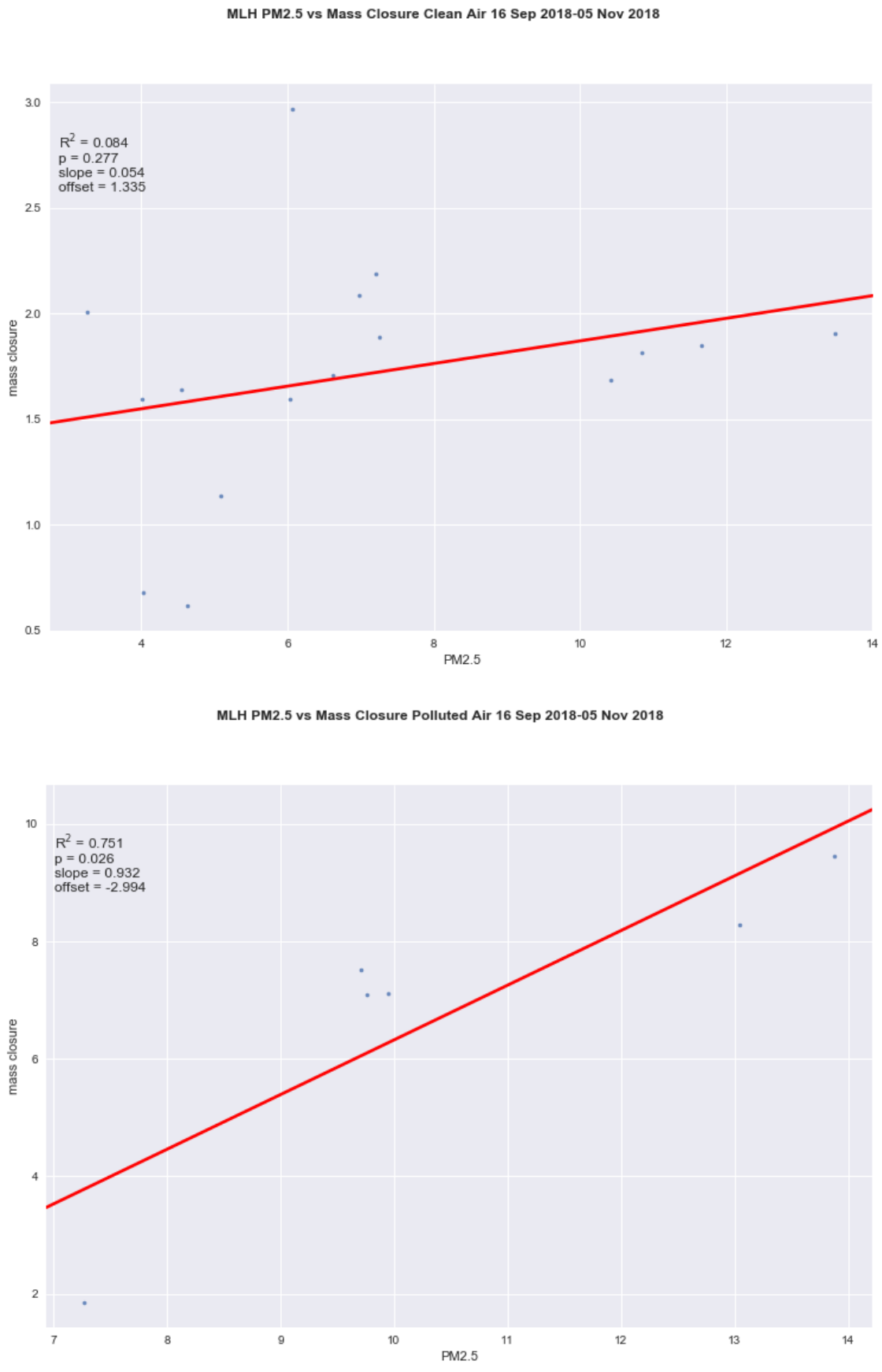

Figure 31 MLH PM2.5 Mass Closure, top: clean air, bottom: polluted air

4.7 Analysis of CPC Events in Clean Air

Previous studies by [*C D O'Dowd and Hoffmann*, 2005] and [*De Leeuw et al.*, 2002] at Mace Head during the PARFORCE (New Particle Formation and Fate in the Coastal Environment) campaign showed that extremely high particle counts occurred under certain conditions (low tide, high solar radiation, low relative humidity), often overwhelming the CPC and requiring dilution of the air flow. Though the exact nature of these aerosols is still unknown, they appear to be linked to exposed seaweed in the intertidal zone, which releases various gases and biogenic compounds when stressed from lack of water and exposure to sunlight. The studies showed that the high particle events occurred both in clean and polluted air masses, though there were some differences in particle numbers depending on the source region. Nevertheless, it appears the high particle counts are mainly the result of naturally occurring in-situ aerosol formation which could have a large impact on the radiative properties of the atmosphere both directly and indirectly (through cloud formation), and it is important to know how much can be attributed to natural sources. The previous studies focused on Mace Head, so now it is of interest to see if these events occur at other network stations under similar conditions. Since the CPC only measures the number of particles in the atmosphere, without providing information about their size or composition, BC will be used here as a tracer for polluted air, in order to examine periods of "clean air" when BC levels are at their lowest, yet CPC particle count is very high.

A "high" particle count for the CPC is anything over 20,000 particles per cubic centimetre (pcc). Generally, the clean air sector at Carnsore Point is between 45-135 degrees, and between 270-360 degrees at Malin Head. BC under 50 ng/m^3 is considered clean air. This study focuses on particle counts above 20,000 during which the air is from the clean sector at the stations with BC concentrations below 50 ng/m^3.

The histogram in **Figure 32** shows the number of occurrences by particle count by season in the clean air sector between 45-135 degrees, for periods when BC was under 50 ng/m^3, from May 2017-May 2018 at Carnsore Point. Based on this, it is very clear that the majority of high particle counts occur during the summer, occasionally in spring and fall, and very rarely in winter.

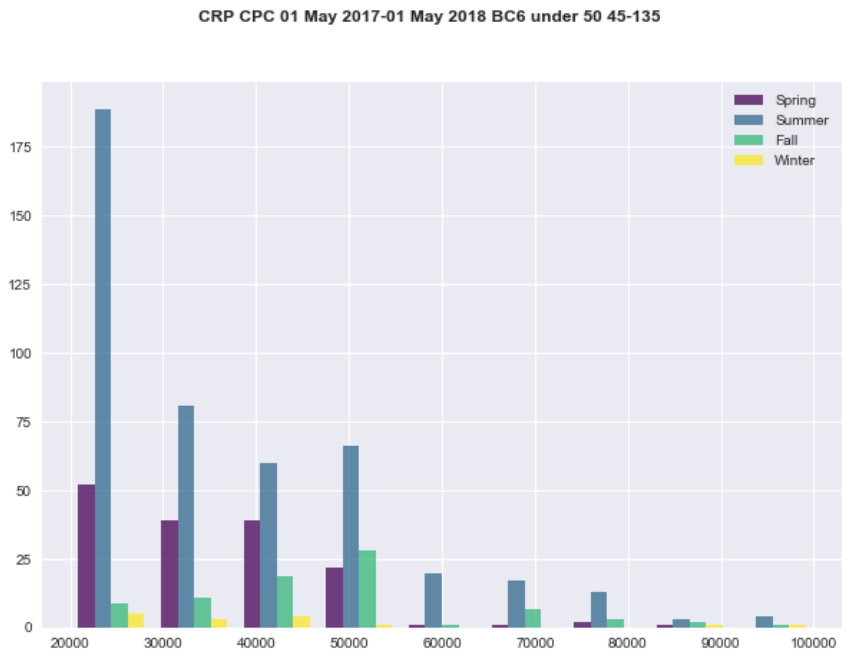

Figure 32 Number of occurrences by particle count by season in the clean air sector at CRP

Likewise, the high particle counts in the clean air sector at Malin Head occur most frequently in the summertime, although generally the number of occurrences is less than at Carnsore Point. **Figure 33** shows these data for the MLH station for the same time period as CRP above.

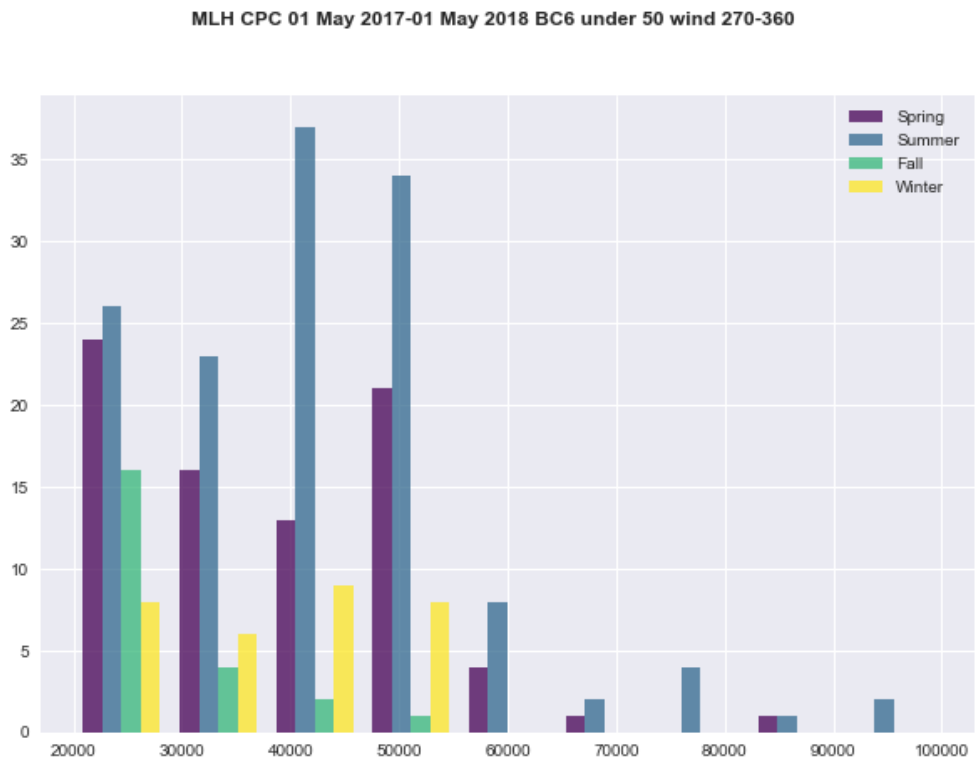

Figure 33 Number of occurrences by particle count by season in the clean air sector at MLH

Analysis of the CPC data in conjunction with BC concentration, tidal observations (obtained from the Integrated Marine Observations website http://www.marine.ie/Home/site-area/data-services/real-time-observations/tidal-observations-imos) and meteorological data, as well as ozone show that the high particle events at CRP do occur under similar conditions as at MHD, during low tide in the middle of the day when solar radiation is highest (coinciding with highest temperatures), and RH below 80%. Ozone does not appear to be affected by the high particle events, reaching its daily maxima during peak solar radiation each day without any significant increases or decreases before, during, or after the particle event occurs. A previous study by [*Whitehead et al.*, 2010] suggested that ozone was depleted during such events based on vertical deposition fluxes of ozone, however without vertical wind measurements this could not be tested for CRP. ACSM measurements also could not provide more information on the composition of the aerosol, due to its 30-minute time resolution being inadequate to detect the rapid formation and growth of particles. Shown below is a series of high particle events which occurred at CRP in June 2018. Such events occur at MLH too and will be discussed in more detail in a later section together with the SMPS, which can be used to demonstrate particle growth.

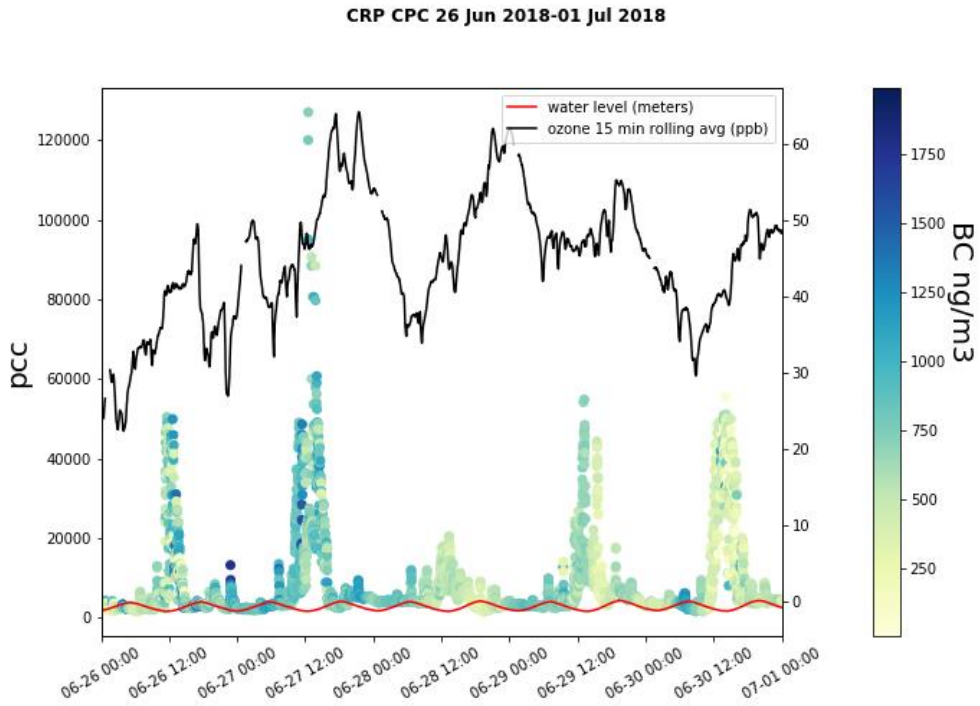

Figure 34 CRP CPC particles per cubic centimetre (left axis) coloured by BC concentration with tide level and ozone (right axis)

4.8 Expansion of the Network

As part of the constant improvements to the network, more instruments are being added to expand the measurement capabilities. The previous sections focused mainly on black carbon and included some of these ancillary measurements. In this section the emphasis will be on data from the three newest additions: the Fidas, ACSM, and SMPS. As part of the data analysis objective, the data from these instruments are presented here in their entirety, as well as seasonally when possible, will give additional insight into the aerosol loading at the stations, and provide a broader perspective using the combined measurements.

4.8.1 Fidas Measurements

As mentioned previously, the Palas Fidas 200E has been collecting data at Malin Head since May of 2018. One year of data are now available for analysis, and the results are presented here. The first plot shows the daily average time series of PM1, PM2.5, and PM10 for the year. It can be observed that, as with BC, the particle concentrations are generally higher in the winter than in the summer with some unusually high concentrations in April-May of 2019. In the following ratio plots there is nearly double the amount of PM10 to PM2.5, and again that much more PM2.5 than PM1 for most of the year, with low ratios in summer months when PM10 is lowest, and the notable exceptions in the above-mentioned April-May of 2019 where there appears to be a large proportion of fine particles. The scatter plots of PM2.5 to the other PM categories in **Figure 37** show good correlation indicative of common sources, however there is a strong bimodal distribution, which bears further investigation, and will be looked at in more detail by season.

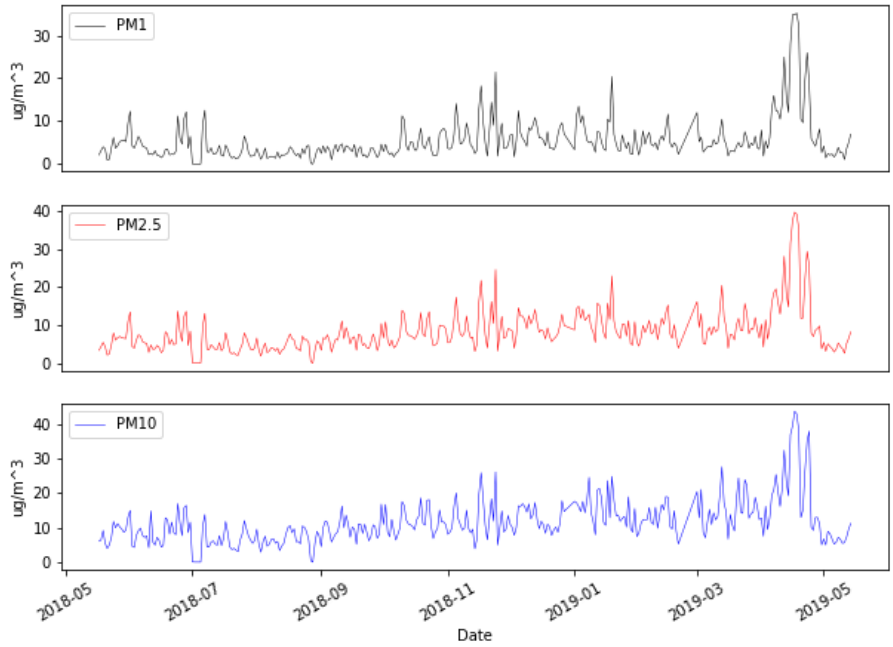

Figure 35 Fidas annual time series, daily average

Figure 36 MLH Fidas ratio time series, daily average

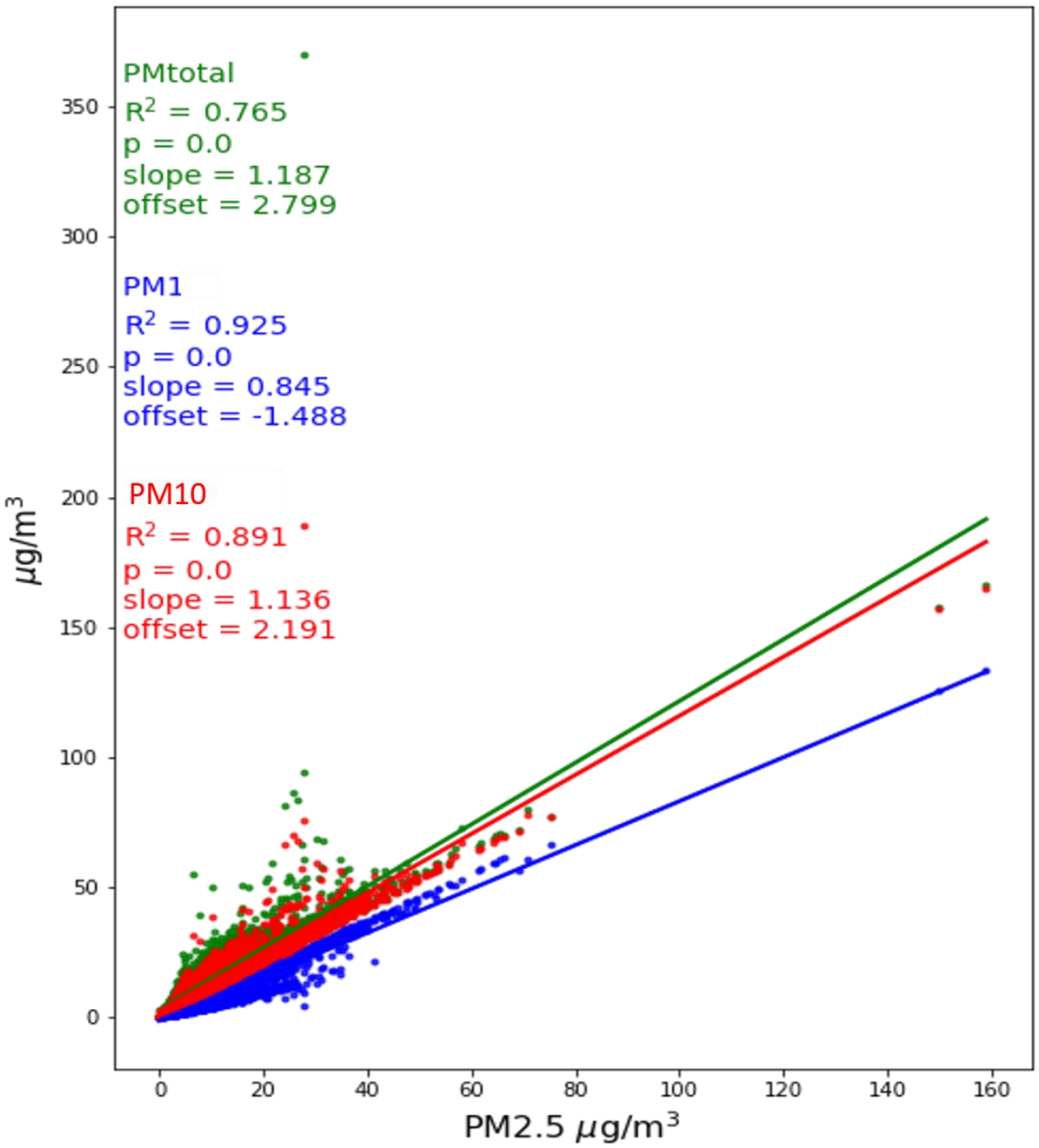

Figure 37 Fidas PMtotal, PM1, and PM10 compared to PM2.5

The following wind roses show from which direction and at which wind speeds the PM in each category is most prominent. All of them have higher concentrations at higher wind speeds, but the smaller particle sizes tend to come mostly from the southeast (direction of houses, road, and Northern Ireland) whereas the larger particle sizes, most likely sea salt, are associated with the marine sector, and corroborate previous studies [*Ovadnevaite et al.*, 2012] in which sea salt in the atmosphere is the result of waves breaking due to high wind speeds.

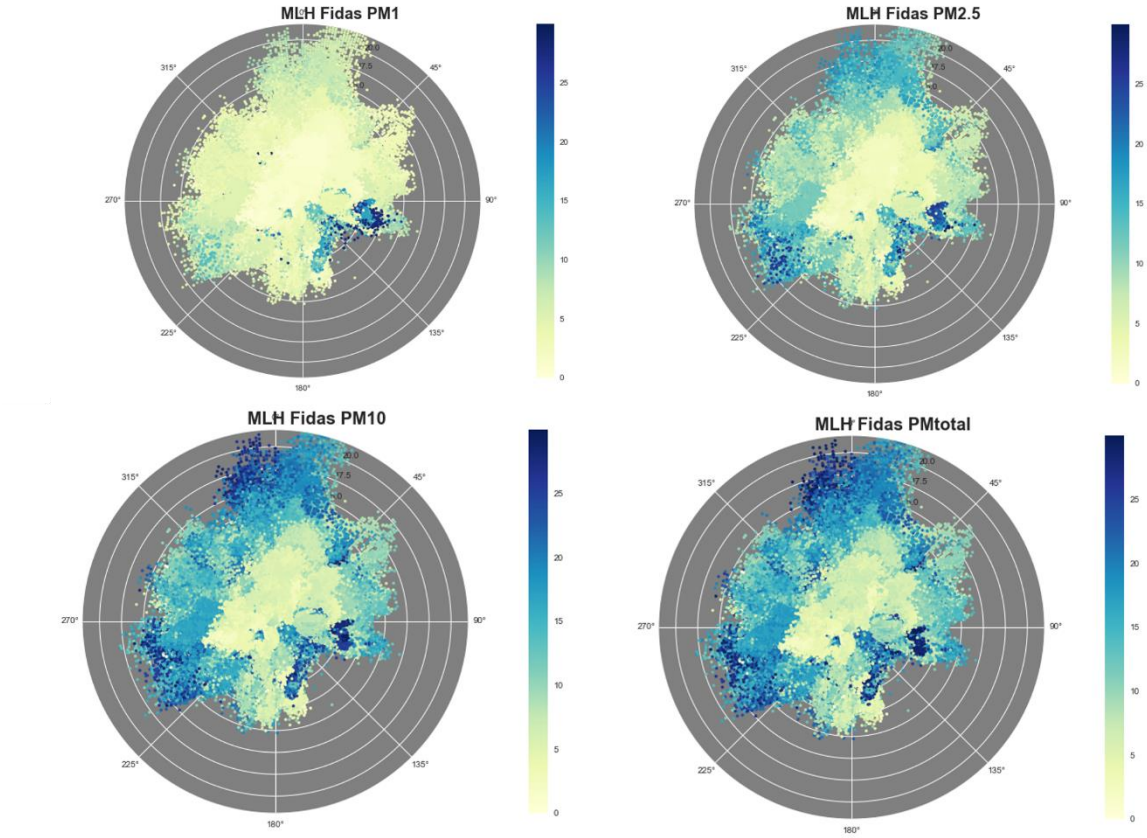

Figure 38 MLH Fidas wind roses for full year in µg/m³

Broken down by seasons, the wind roses show a very clear distinction between summer and winter, especially for PM1. In winter PM10 and PMtotal are very similar, particularly in the marine sector, most likely due to higher winds and the resulting sea salt aerosol produced. PM1 is always highest from the southeast quadrant, which is the direction of the houses and road, as well as the city of Londonderry, Northern Ireland. In the fall, very high wind speeds from the southeast seem to contribute large amounts of PM of all sizes most likely across a longer distance. High levels of PM1 in the winter are associated with lower wind speed, thus indicating more local sources.

When comparing PM2.5 to PM10 and PMtotal, the correlation in the wintertime is 0.87 and 0.8 respectively, whereas in summer the r^2 is only 0.67 and 0.4. The bimodal distribution seen in the previous scatter plot is still evident, though not as pronounced in the seasonal plots. The summer and winter plots for PM10 and PMtotal vs PM2.5 can be found on pages 181-183 in Appendix C for reference.

Interestingly, when the PM2.5 versus PM10 plots are broken down by season and wind direction, the bimodal distribution reappears. It is especially pronounced in the summertime from the marine sector, and only very slight during the winter months. The slope is also slightly higher during the summertime in all wind sectors but particularly from the north, whereas in winter it tends to be closer to 1. This is indicative of different sources both natural and anthropogenic, which will be discussed in more detail later.

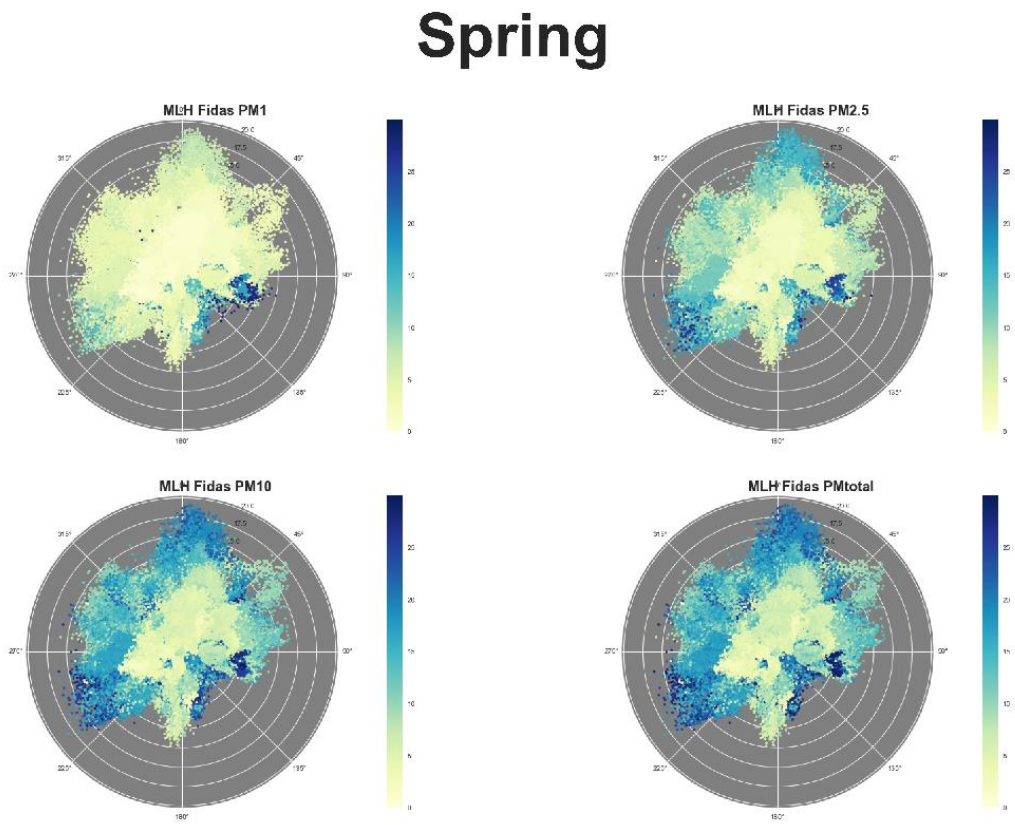

Figure 39 MLH Fidas Spring wind roses in µg/m³

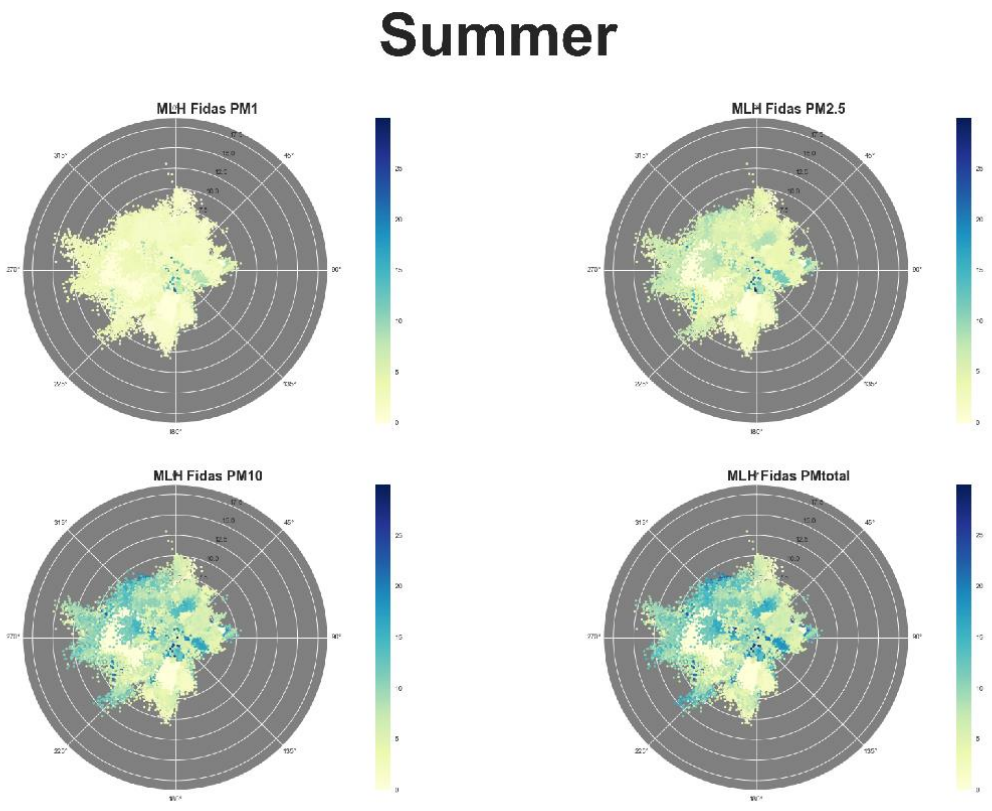

Figure 40 MLH Fidas Summer wind roses in µg/m³

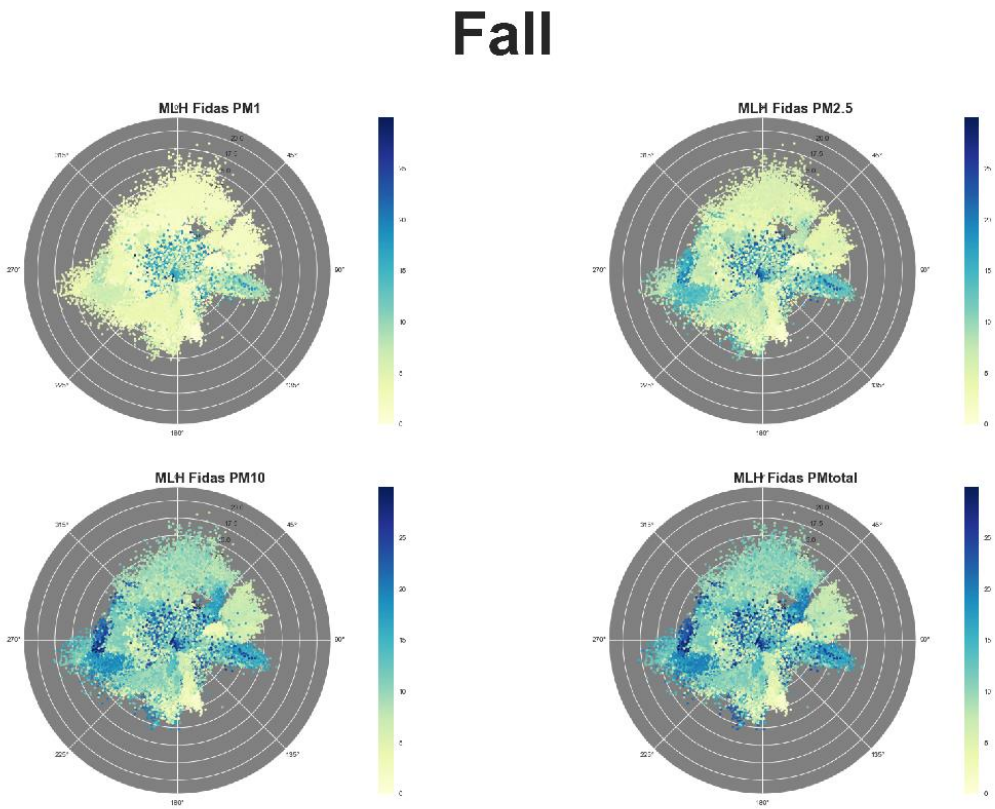

Figure 41 MLH Fidas Fall wind roses in µg/m³

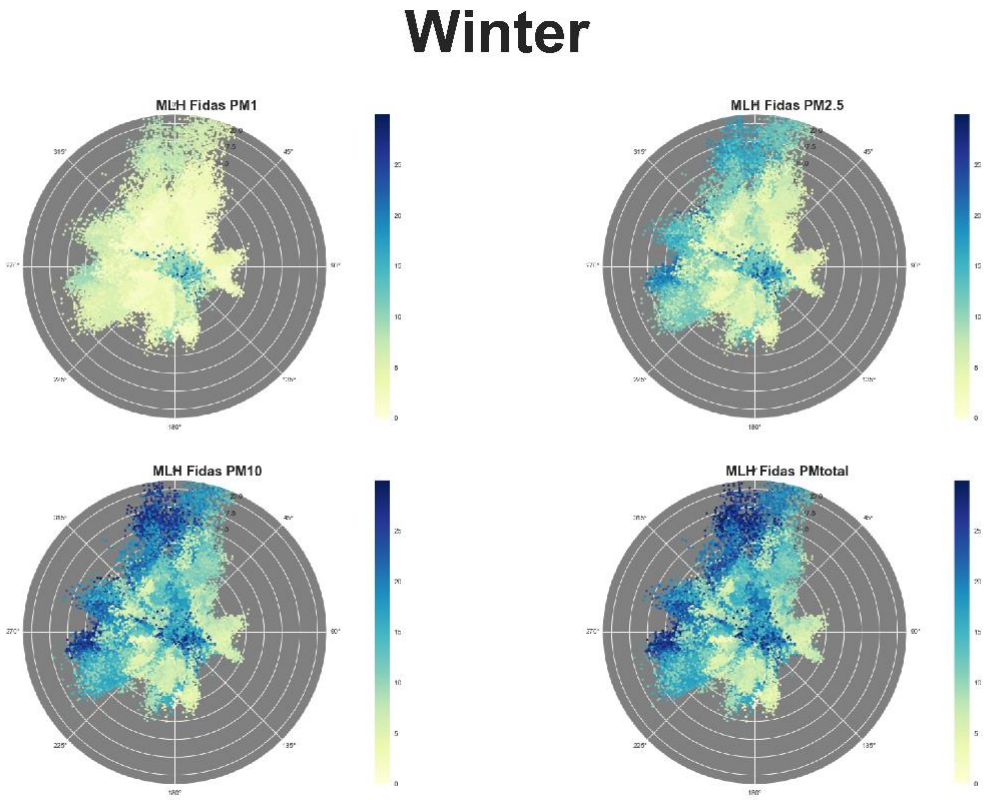

Figure 42 MLH Fidas Winter wind roses in µg/m³

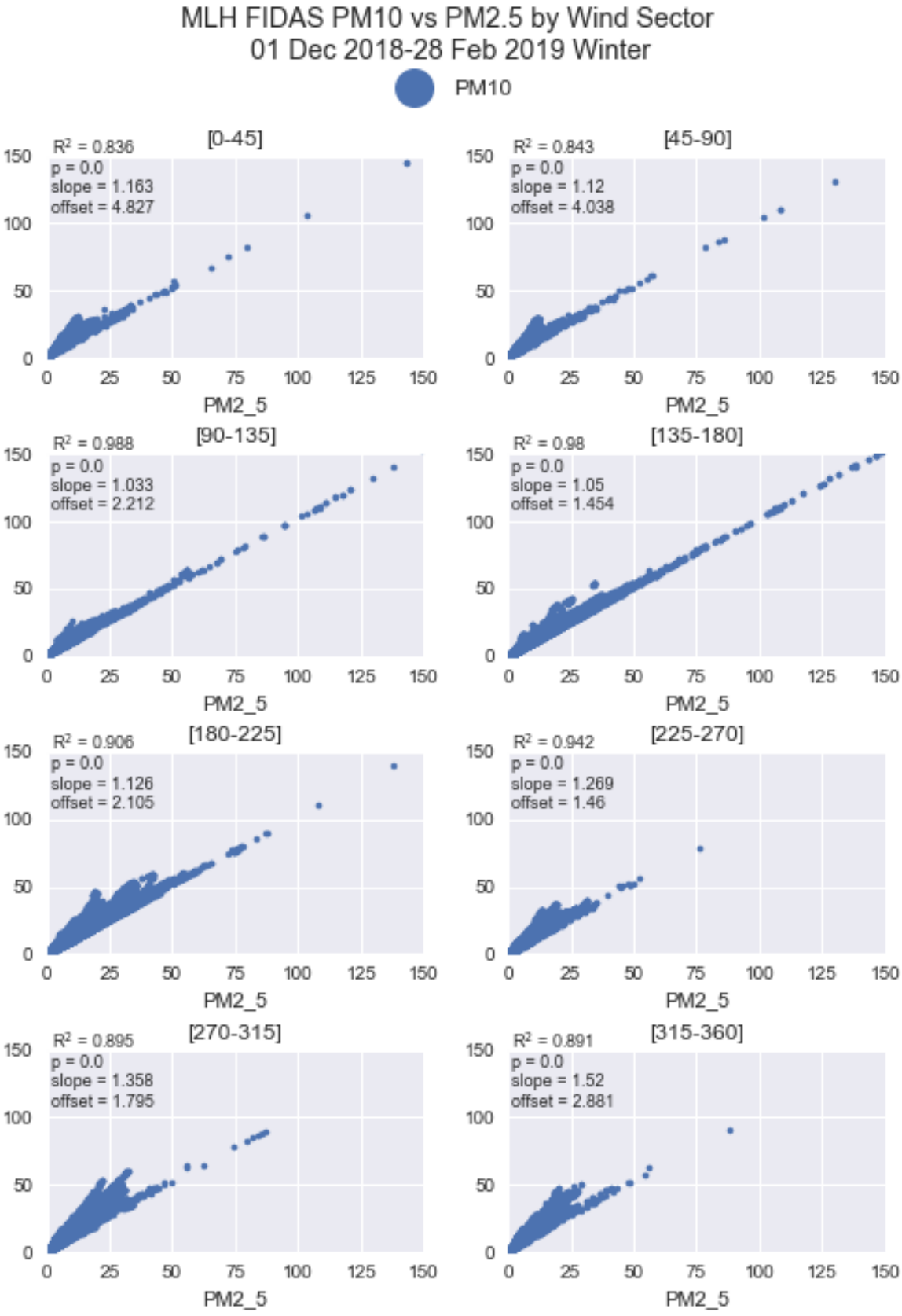

Figure 43 MLH Fidas PM2.5 vs PM10 by wind sector Winter in µg/m³

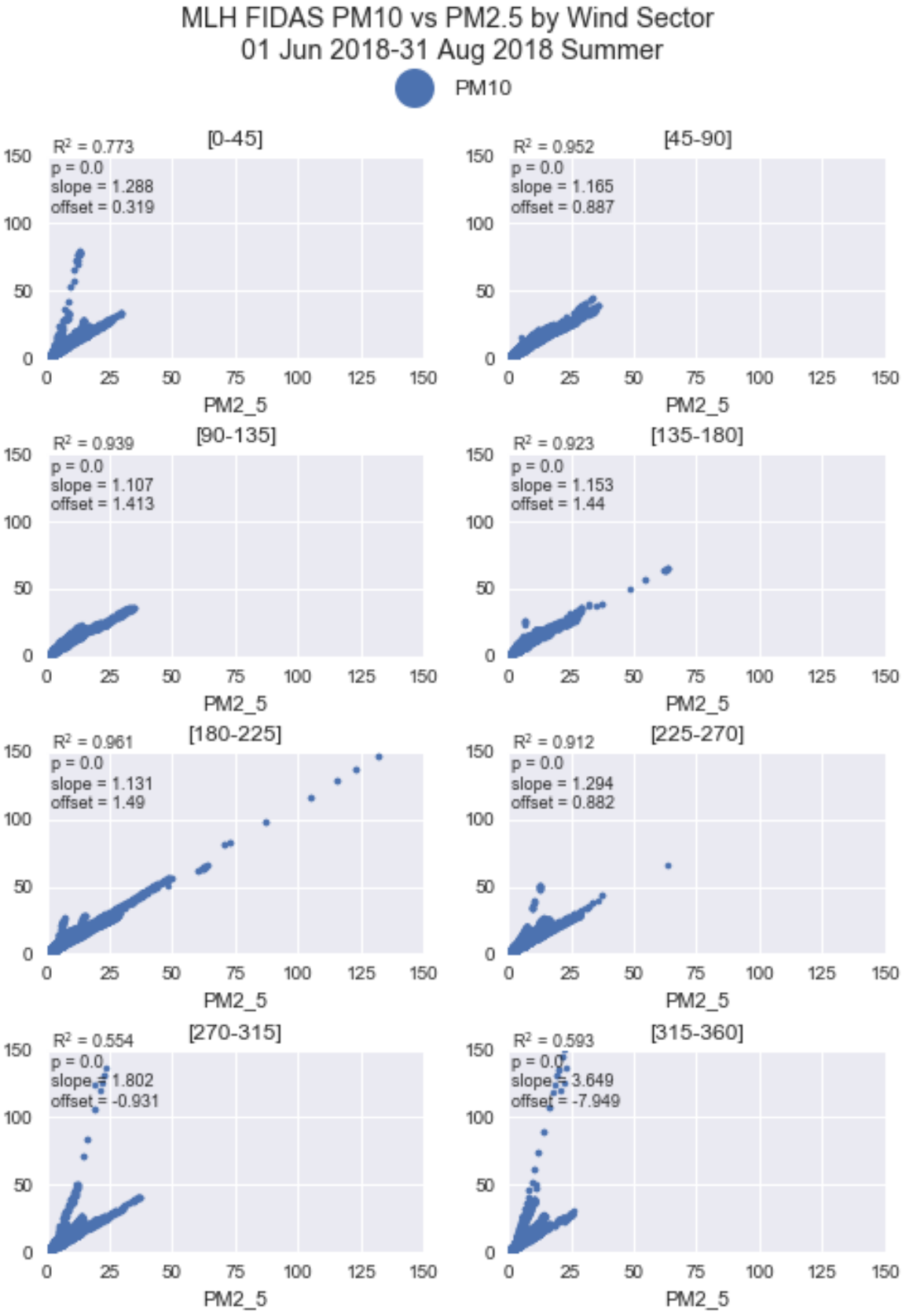

Figure 44 MLH Fidas PM2.5 vs PM10 by wind sector Summer in µg/m³

4.8.2 ACSM Measurements

An ACSM was collecting data at Carnsore Point for one year, from August 2016-August 2017, operated by other members of the NUIG research group, who have made the data available for use in this study. In their recent paper [*Lin et al.*, 2019] evaluated the composition of winter-time PM1 aerosol at Carnsore Point using data from the ACSM and AE33. This section will expand on their work, showing the seasonal variations over the course of a year and attributing a percentage to transboundary pollution based on wind direction.

The following bar graphs show the ACSM species and BC along with BB (in percent as measured by the AE33) for each season. Organic aerosol and Nitrate (NO_3) dominate in every season except summer, when Sulfate (SO_4) plays a prominent role. Looking at these graphs, it appears that certain wind sectors have higher concentrations than others, and when splitting the directions into east (with 0-180 degrees classed as transboundary) and west (between 180-360 as inland), between 61% (fall) and 70% (spring) of the PM1 arrives from outside Ireland depending on the season, even though the wind is only from the east (incorporating all wind between 0-180 degrees) about 28% of the time (only 15% in summer). The pie charts below illustrate this using the sum of all ACSM species and BC. Looking at BB% in the same way, on average the highest percentage of BB originates within Ireland (23, 16, 24, and 28 percent for spring, summer, fall, and winter respectively), probably from local sources, compared to the easterly direction where the average is 18, 13, 16, and 22 percent for each of the seasons. BC, on the other hand, is still higher coming from outside Ireland than from within, as shown previously, between 1.5-2 times depending on the season.

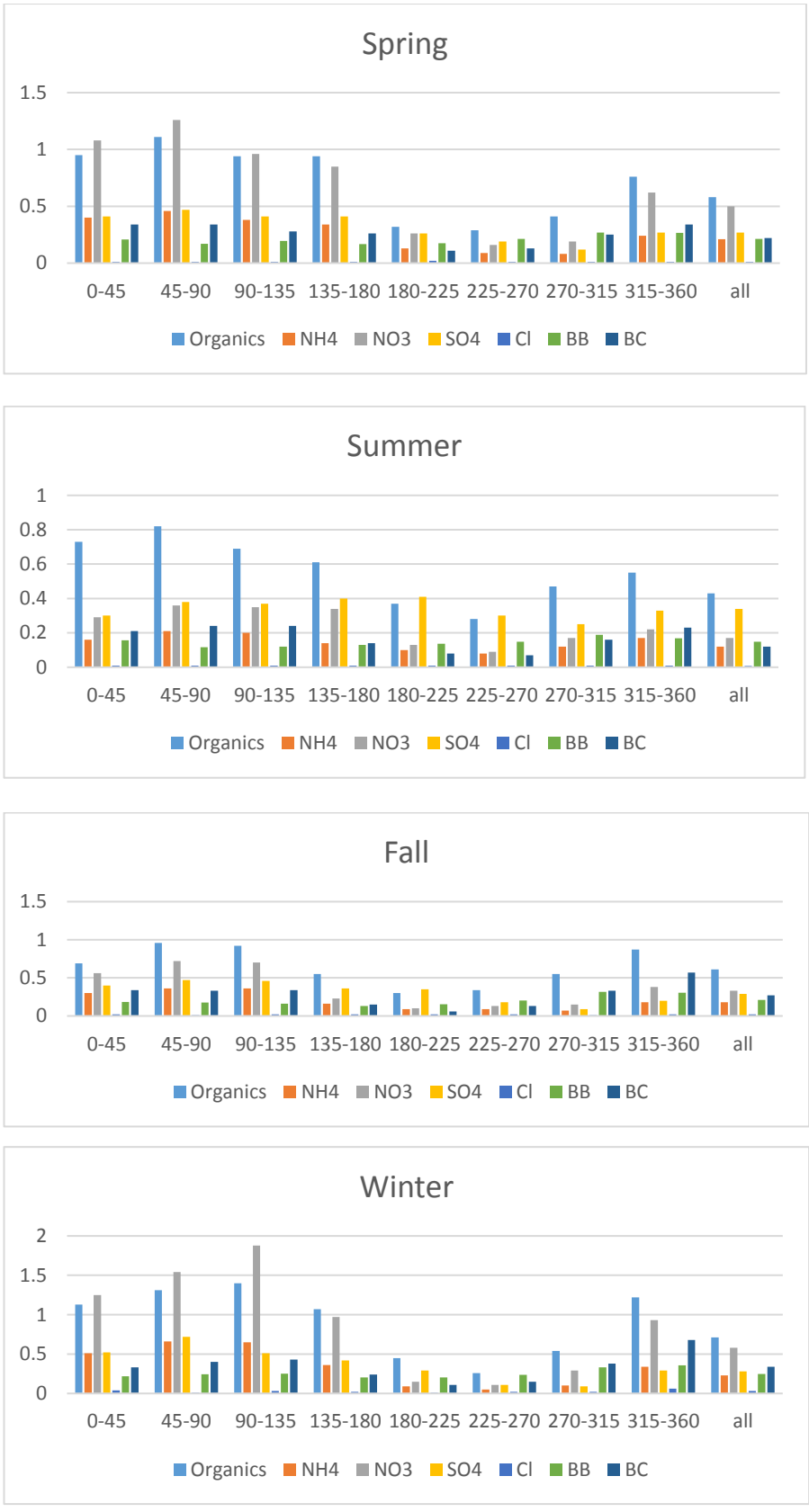

Figure 45 CRP ACSM and AE33 by wind sector and season

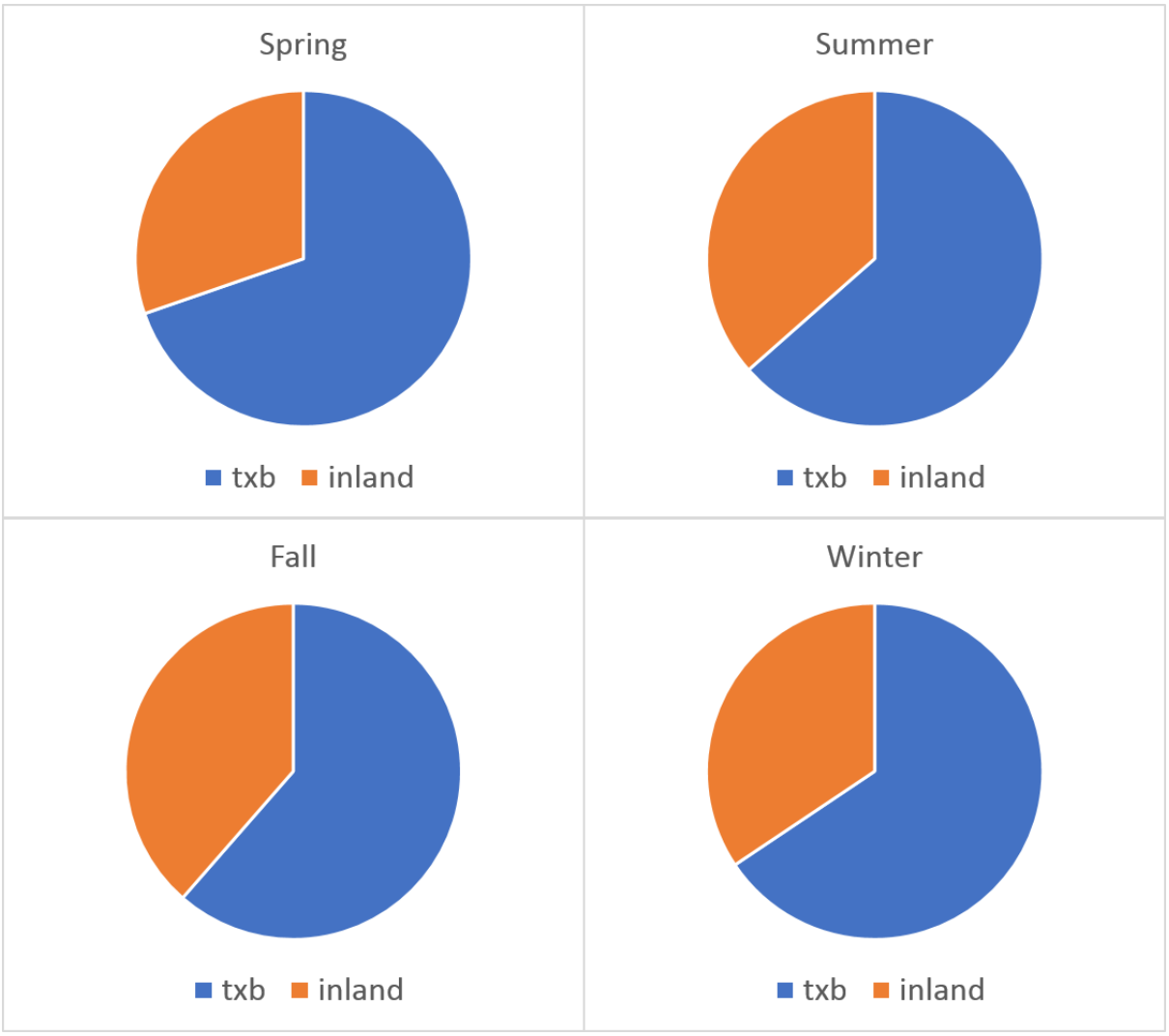

Figure 46 ACSM Total + BC transboundary (0-180) vs inland (180-360)

Another interesting comparison is the ratio of ACSM PM1 (plus BC) to the mass concentration of the TEOM. This should give an indication of how much of the total mass is made up of PM1. In winter, this is between 50-80%, mainly from the transboundary direction. The ACSM PM2.5 to Fidas mass closure at Malin Head showed the ACSM accounting for only about 44% of PM2.5 mass in the fall (actually only 25% of the PM2.5 in the clean sector), and therefore even less of the total PM mass. The ratios at CRP indicate PM1 makes up between 20-30% of total mass in the fall, depending on wind sector. At MLH, the Fidas PM1/PM10 ratio is 0.39 in the fall, and ranges from 0.39 (fall) to 0.47 (summer).

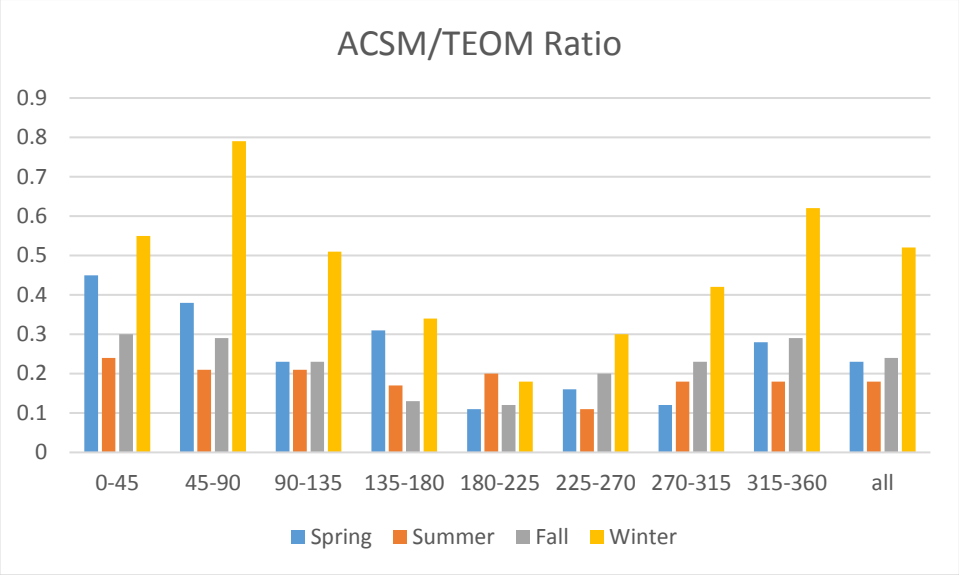

Figure 47 CRP ACSM/TEOM ratio

The ACSM was at Malin Head for a short period, from September-November 2018, before being moved to France for a calibration campaign and will be installed at Malin Head again in the near future. As the instruments had different size cut-offs (CRP was PM1 and MLH was PM2.5), and there are no overlapping time periods of measurements, only a general comparison can be made between the two stations for similar time periods (September-November), as shown in the following time series plots.

The levels of organics at MLH are much higher than at CRP, however this could be due to the measurements being made in different years under different conditions, as MLH tends to have more polluted air in the immediate vicinity of the station, and also because, as indicated by the mass closure experiment, significant amount of organics are larger than PM1, which was the limiter at CRP. As shown previously, in both the mass closure and EMEP data analysis, OC is the major contributor to total carbon, and constitutes a large fraction of PM2.5 organics. Chlorine levels at CRP are extremely low, but the ACSM is known to have difficulties in measuring it.

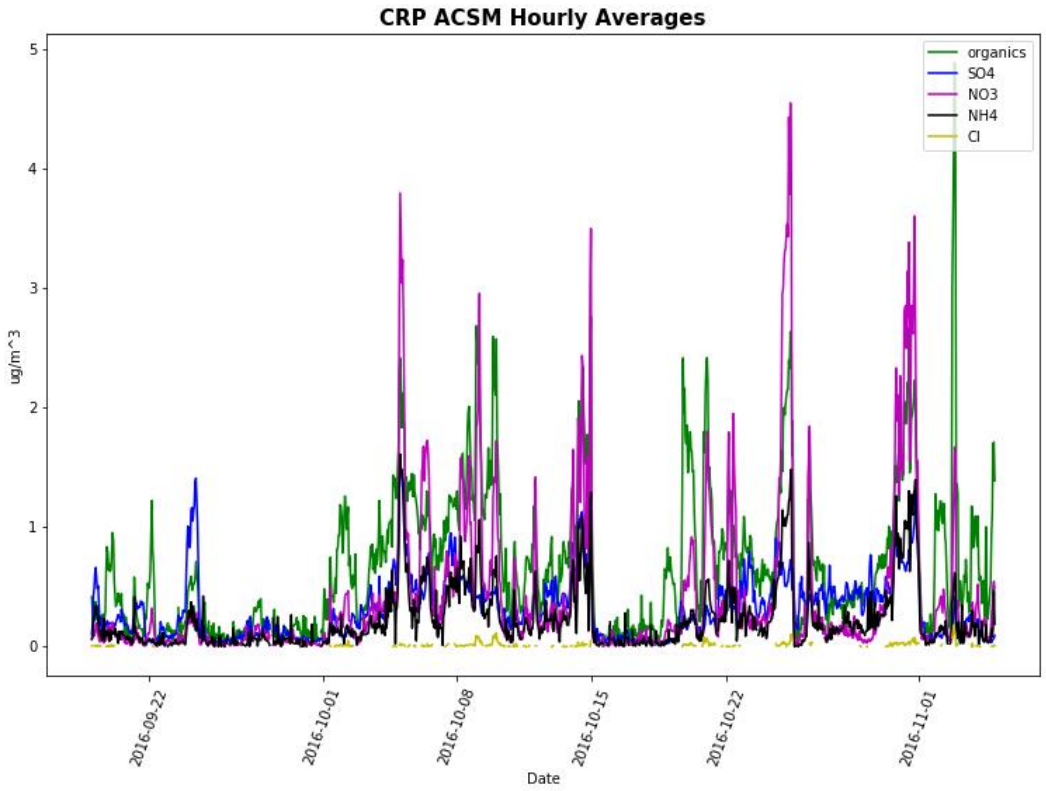

Figure 48 CRP ACSM time series September-November 2016

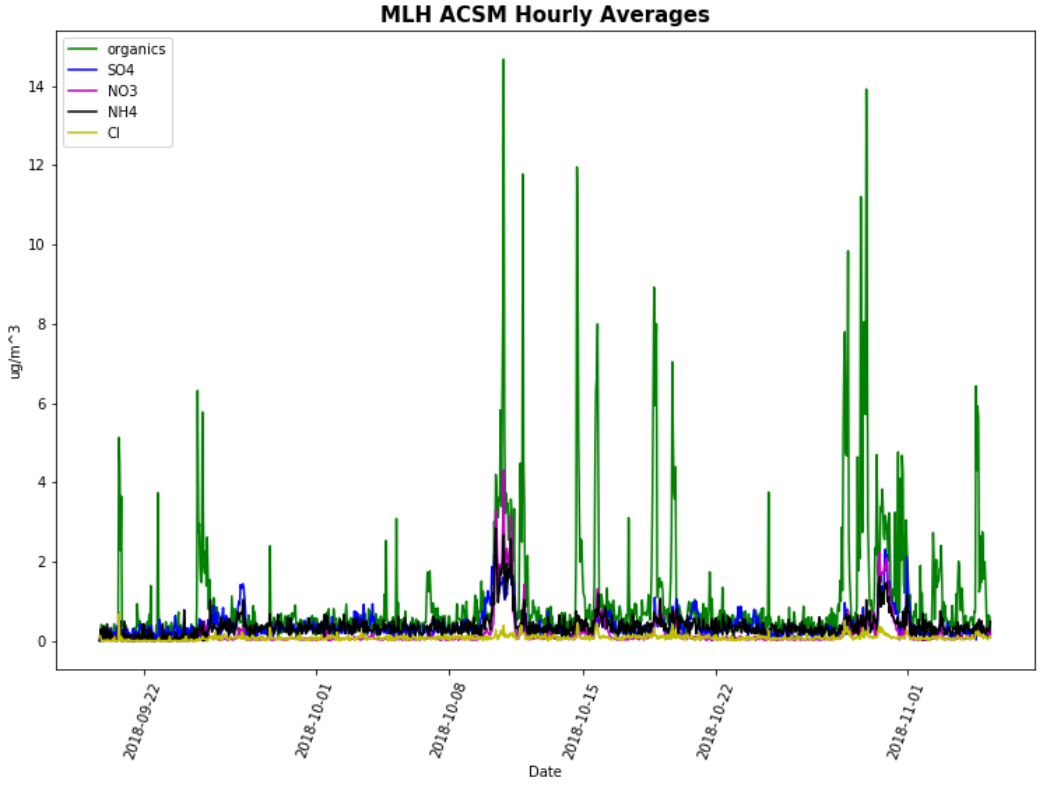

Figure 49 MLH ACSM time series September-November 2018

Both time series plots exhibit periods of regional pollution, and a further breakdown by wind sector in **Tables 14-15** shows that the majority of it comes from the east (the direction of the sea) at CRP and at MLH most of the pollution is from the south southeast, except for Chlorine which is also prominent from the north northwest (the sea) as demonstrated by the wind roses. Most notably, the wind at CRP only comes from the east (0-180 degrees) about 26% of the time, yet the highest levels of all species are recorded from this wind direction. This is a strong indicator of transboundary pollution, as there are no local sources from these directions, and the levels and duration are typical of regional pollution, which tends to last several days. The lower wind speeds associated with higher pollution levels at Malin Head may suggest some local influences in the area, though they are comparable to wind speeds at Carnsore Point carrying high levels of pollution. Note that the scale for Cl on the wind roses is only from 0-0.10 micrograms to make it visible, as the levels are very low at both stations. Only Cl, organics, and SO_4 wind roses are shown, as the NH_4 and NO_3 wind roses exhibit similar patterns and concentrations.

The ACSM is a powerful tool to enhance the existing measurements at the stations, and future long-term measurements will be much improved by its ability to distinguish between individual species. It has already proven invaluable in the mass closure equation making it possible to compare data at higher time resolution than the daily averages provided by the high-volume samplers.

Table 14 CRP ACSM by Wind Sector (mean and std dev)

Wind Sector (degrees)	Occ (%)	Wind (m/s)		Organics (µg/m³)		NH_4 (µg/m³)		NO_3 (µg/m³)		SO_4 (µg/m³)		Cl (µg/m³)	
0-45	6	3.42	1.9	0.93	0.68	0.45	0.41	0.82	0.94	0.45	0.32	0.02	0.02
45-90	9	3.56	1.79	0.97	0.57	0.39	0.32	0.78	1.03	0.47	0.2	0.01	0.01
90-135	5	3.97	1.49	1.06	0.5	0.42	0.34	0.83	0.82	0.52	0.3	0.01	0.02
135-180	6	4.88	2.48	0.49	0.34	0.17	0.15	0.19	0.21	0.3	0.19	0.01	0.01
180-225	15	4.83	2.5	0.27	0.23	0.11	0.11	0.09	0.11	0.29	0.28	0	0
225-270	34	4.1	1.62	0.32	0.3	0.1	0.11	0.12	0.22	0.17	0.16	0.01	0.01
270-315	16	3.43	1.44	0.58	0.37	0.09	0.08	0.16	0.12	0.09	0.06	0.01	0.01
315-360	10	3.13	1.1	1.1	0.84	0.25	0.21	0.54	0.55	0.24	0.16	0.03	0.03

Table 15 MLH ACSM by Wind Sector (mean and std dev)

Wind Sector (degrees)	Occ (%)	Wind (m/s)		Organics (µg/m³)		NH_4 (µg/m³)		NO_3 (µg/m³)		SO_4 (µg/m³)		Cl (µg/m³)	
0-45	3	9.46	2.73	0.38	0.16	0.26	0.11	0.04	0.02	0.24	0.08	0.06	0.04
45-90	1	4.37	1.62	0.47	0.23	0.24	0.1	0.08	0.08	0.26	0.06	0.1	0.04
90-135	0.64	2.12	0.83	1.88	2.29	0.32	0.16	0.15	0.06	0.44	0.23	0.12	0.11
135-180	11	3.37	1.65	2.96	2.77	0.79	0.6	0.79	0.87	0.7	0.55	0.13	0.09
180-225	32	4.23	2.02	1.25	1.54	0.38	0.22	0.2	0.31	0.43	0.36	0.09	0.07
225-270	18	6.04	2.09	0.55	0.77	0.31	0.16	0.06	0.06	0.33	0.21	0.07	0.06
270-315	26	5.41	1.79	0.48	0.5	0.27	0.16	0.04	0.02	0.26	0.13	0.06	0.05
315-360	8	6.63	2.07	0.34	0.19	0.24	0.14	0.03	0.02	0.22	0.11	0.05	0.04

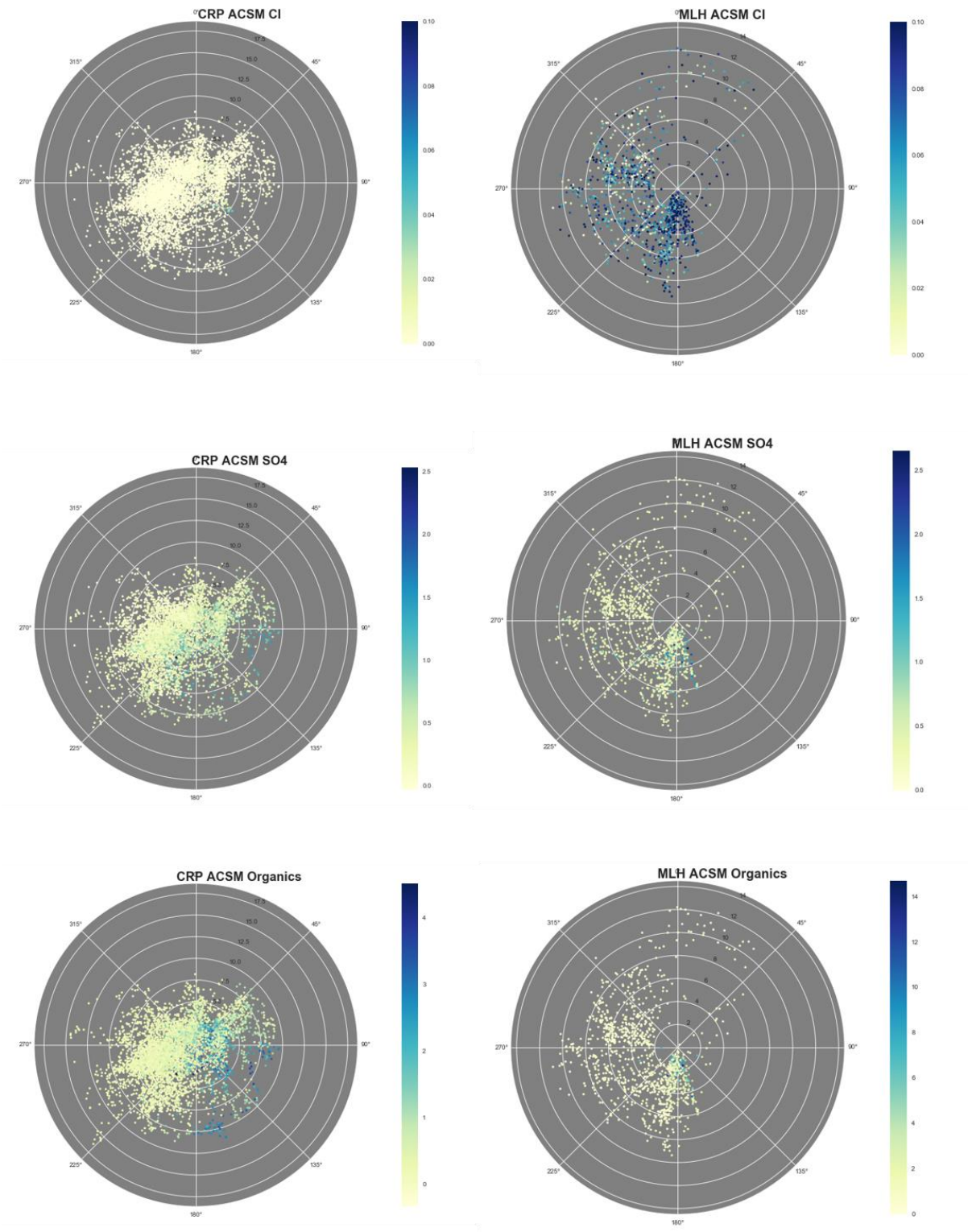

Figure 50 CRP and MLH ACSM wind roses in µg/m³

4.8.3 SMPS Measurements

The high particle events observed at Mace Head and Carnsore Point occur at Malin Head as well under the same conditions described previously, but here we have the addition of the SMPS instrument to provide information on the size distribution and particle growth. While this SMPS is a bit limited with a minimum detection size of 8nm, it can be used in conjunction with the CPC which is able to detect particles down to 4nm diameter, and the differences between these measurements can illustrate how many particles must exist in the smaller diameter size range.

Below is a time series of CPC high particle events at Malin Head in May 2019, overlaid with the ratio of CPC counts/SMPS total particle counts. It is interesting to observe that although the CPC consistently measures more particles than the SMPS for the high particle events, during periods of higher pollution (represented here as BC concentration), the CPC detects only about 20 times more particles than the SMPS, whereas during periods of clean air, the CPC measures more than 120 times the number of particles than the SMPS, which would indicate that under these conditions there are many more newly produced particles smaller than the detection limit of the SMPS. The following curtain plot of the SMPS data reflects the high particle events measured by the CPC and also shows the highest concentrations occurring in the lower size range at or below 10nm in the clean air events.

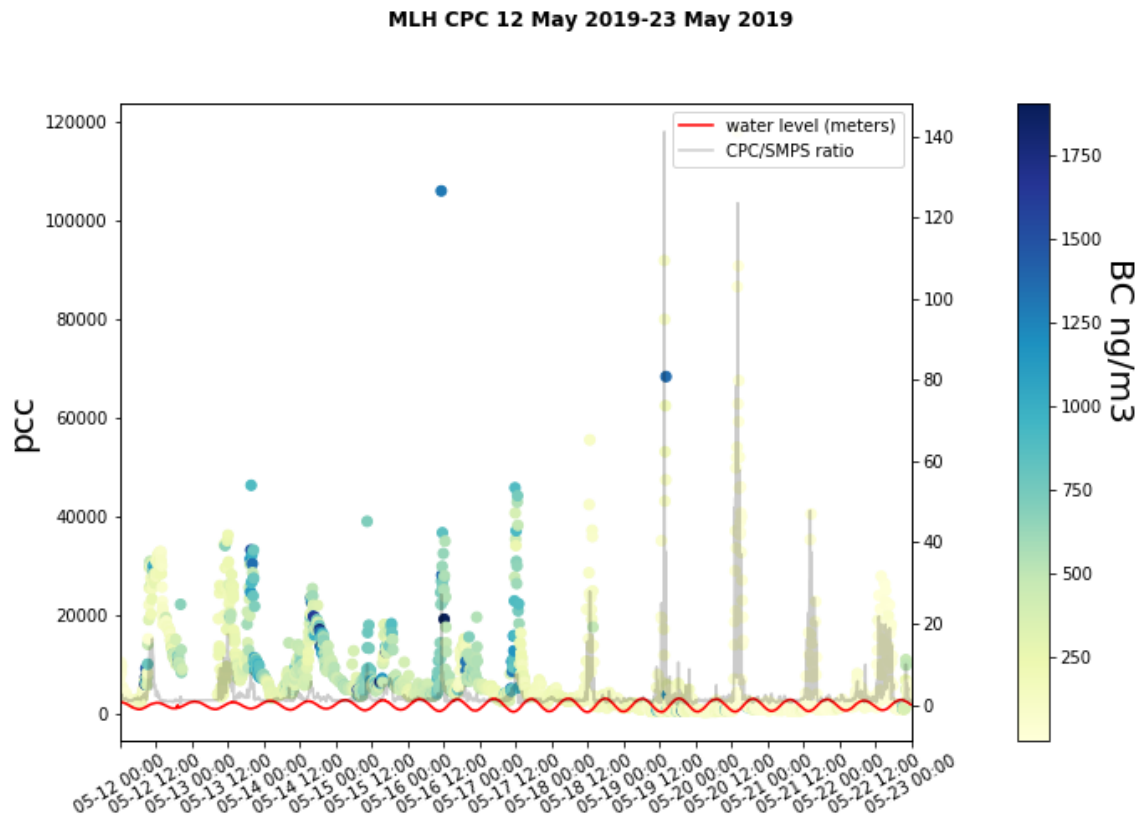

Figure 51 MLH CPC coloured by BC concentration with tides and CPC/SMPS ratio overlay

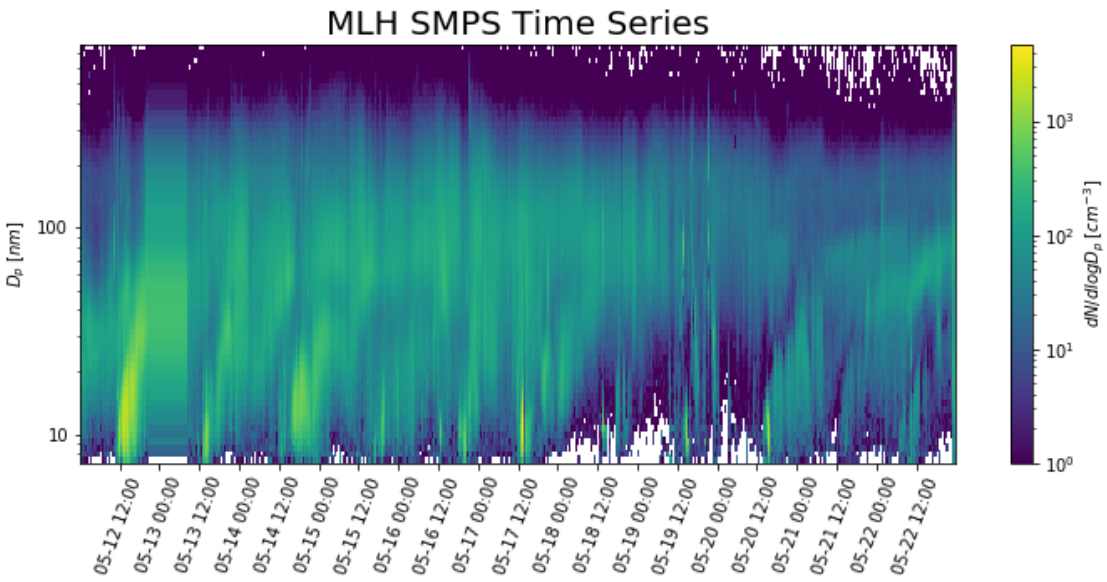

Figure 52 MLH SMPS curtain plot 12-23 May 2019

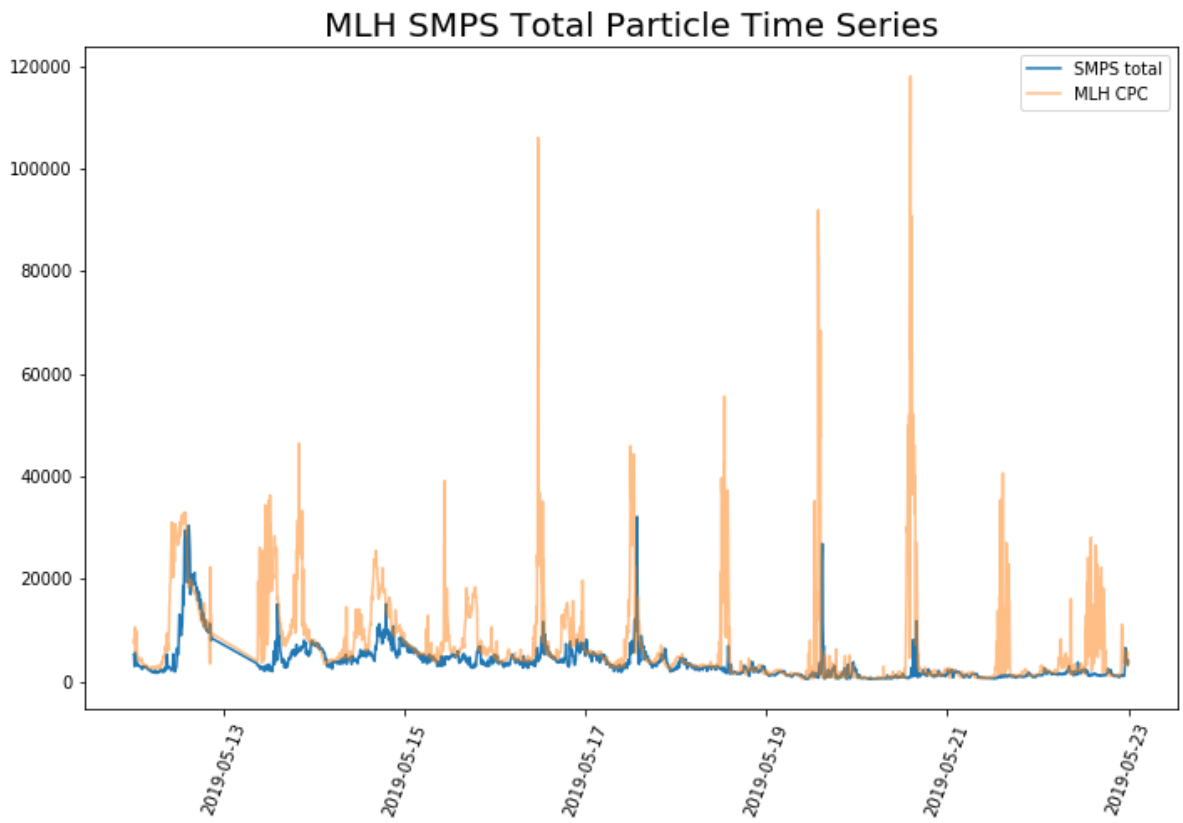

Figure 53 MLH CPC and SMPS total counts

The plot above of CPC and SMPS particle counts shows a distinct time delay between the CPC measuring particle maxima and the SMPS detecting them. The time interval between the peaks of the two instruments and the difference in particle concentration suggests particle growth is occurring and that there are fewer of the larger particles than the original smaller ones, meaning that either they are coagulating to form larger particles, or being scavenged by larger particles. In some cases they may not grow at all, for example, on 22 May there is a burst of small particles detected by the CPC, which never reached a size detectable by the SMPS.

The time delay between CPC and SMPS peaks is between 1-2 hours, with differences in peaks between 3,000 to over 100,000 pcc. The more polluted events tend to have longer times between peaks and lower differences in particle concentrations. The SMPS size distribution for these events will be shown in a later section.

5. Local, Regional, and Transboundary Influences

This chapter will be broken down into four subcategories discussing the results presented previously and how they relate to local, regional, and transboundary production of aerosols. It will look at the broader picture of the combined measurements, thus demonstrating the potential of the monitoring network as it exists, as well as opening up opportunities for future expansion and improvement.

5.1 Black Carbon and Biomass Burning

Based on the BC analysis in chapter 4, it is evident that the highest levels at Carnsore Point are being recorded when the wind is from the east, even though this only occurs a small fraction of the time. Depending on the season, this could be 60-70% of the BC measured at the station. At Malin Head, the majority of BC arrives from the southeast, in the direction of Northern Ireland, and the pattern of elevated BC over periods of several days indicates it is more often regional and not local. Mace Head receives around 88% of BC from the east, and what little does arrive from the west is usually recirculated [*Huang et al.*, 2001]. The average wintertime BC at CRP from the east is 427ng/m^3, whereas at MHD it is only 274ng/m^3, meaning there is considerably less BC being transported from within the country to MHD than to CRP from outside.

When combined with the CO measurements from the Picarro, the AE33 data at Malin Head revealed that there are strong traffic related sources near the station based on a high CO/BC ratio at low wind speed, but the BB related BC seems to be more diffused or transported from a longer distance based on higher wind speed. It is noteworthy that these measurements were from the summertime, and it is therefore likely that there was more traffic and less biomass burning in the vicinity of the station than at other times of year. The pie charts below show the percent of BB at CRP by wind sector and season. Here it is visible that nearly equal amounts of BB come from the east and west, although in summer the average BB is about 16% while in winter it is 22%.

These data are corroborated by Fidas measurements, which show the highest PM1 concentrations from the same wind direction as BC, and the ACSM confirms there is

non-traffic related regional pollution by showing the presence of species such as NO_3, NH_4, and SO_4 in that wind sector. At CRP yet again, as with BC, the highest levels of pollution measured by the ACSM originate from the east, although the wind is least frequently from that direction.

The combination of this suite of instruments along with meteorological data and air mass trajectories makes it possible to demonstrate that transboundary pollution does occur. However, it will be necessary to perform some kind of inverse modelling in the future to determine the exact sources and locations of emissions.

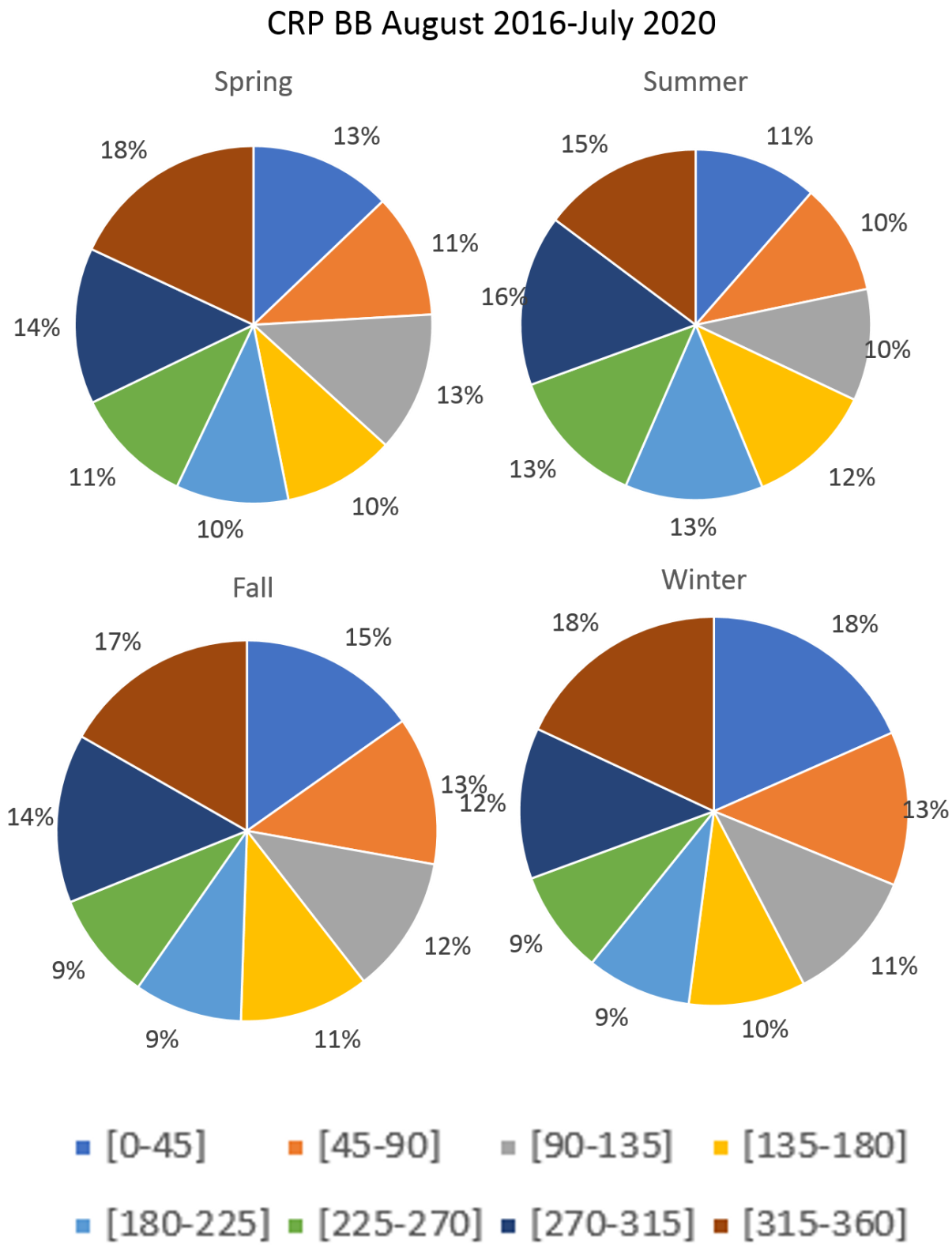

Figure 54 CRP BB by season and wind direction (degrees)

5.2 Particle Number and Size Distribution

The previous SMPS section demonstrated how the instrument could be used in conjunction with the CPC to gain insight into new particle formation and growth, which are a source of natural in-situ production of aerosol. This section will examine some of these events to see if and how much particles are growing and compare the differences between size distributions in very clean air and air mixed with regional pollution. As the period of 12-23 May 2019 had daily high particle events with both very clean and somewhat polluted air masses, it will be used again here.

First, the size distribution histogram was plotted for each event, and all exhibited a similar pattern, with a higher primary peak below 10nm diameter and a lower secondary peak around 80nm diameter. The magnitude of the primary peaks varied from as low as 200 to over 1600 counts, yet the secondary peaks were consistently between 100-200. An example of more polluted air on 17 May and clean air on 20 May is shown in **Figures 55-56** to illustrate the similarities.

Size distribution during the events demonstrates high concentration in the smaller particle range but particle growth cannot be established based on these data. A recent paper by [*Sarangi et al.*, 2015] applied a method comparing changes in the geometric diameter mean over time to determine the growth rate during periods where the particle diameter mode was increasing in SMPS measurements in New Delhi, India, and found a growth rate of 15.4nm/hour depending on conditions. This was quite high compared to other studies around the world cited in that study, which all reported growth rates less than 10nm/hour, with the exception of Mexico City at 11.6nm/hour. Growth rates in large cities were higher than in rural areas, yet no coastal environments were shown. Here an attempt is made to apply this method to the MLH SMPS data, to see if the particle growth rate can be determined.

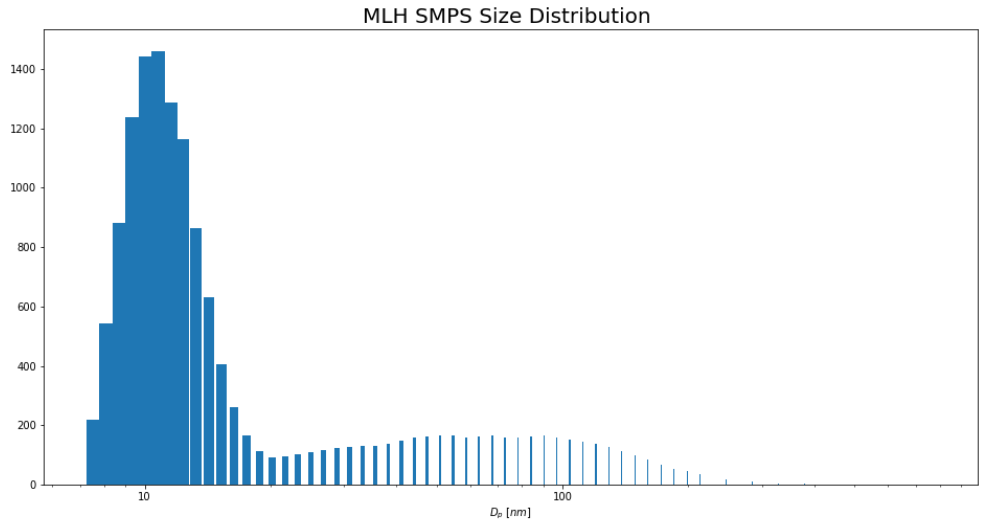

Figure 55 MLH SMPS size distribution for 17 May 2019 13:00-14:00 with polluted air

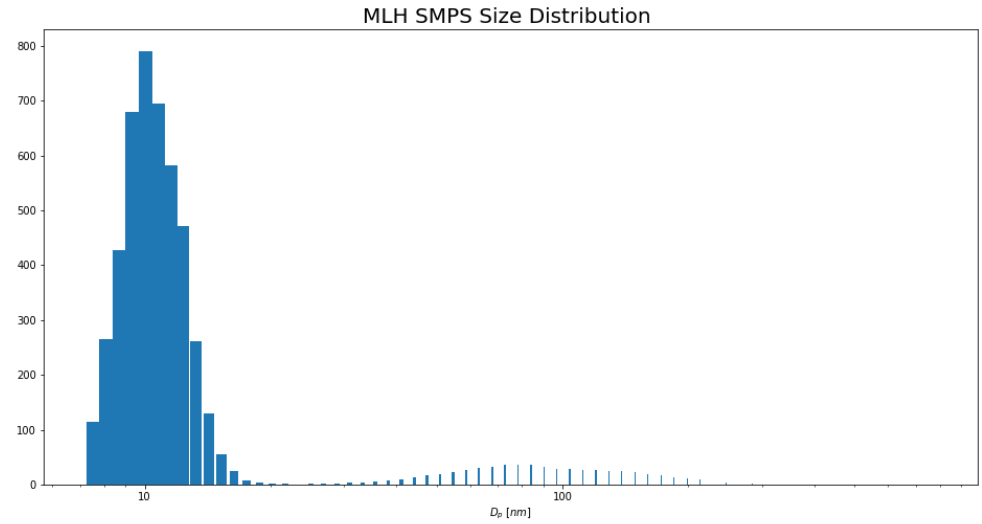

Figure 56 MLH SMPS size distribution for 20 May 2019 15:00-16:00 with clean air

Plotting the particle diameter mode over time, along with particle counts yields the following results. In the New Delhi study, there was a clear increase from particles smaller than 10nm to over 150nm in the span of three hours, and based on this the authors were able to perform a regression, the slope of which was the growth rate.

In the cases shown below, it appears that the particle size during the event jumps from under 10nm to over 80nm in less than one hour. However, the particle count for the 80nm particles is very low, similar to the time prior to the event, which may mean the particles are not actually growing, or rather, continuing to grow, as the previous section showed that they must have grown from a size detectable by the CPC to one which the SMPS could measure. According to [*Vana et al.*, 2008], regional growth events such as those in the New Delhi study cannot be as easily measured in coastal environments with a Eularian method, due to the events being linearly connected to a point source, so they devised a new classification system for coastal particle formation based on their appearance on a particle diameter and concentration time series. Apart from rain-induced events (Class V), Class IV (mixed type events) were the most common at Mace Head. In these events it was clear particle formation occurred but could not be clearly defined as a "banana" (Class I), "hump" (Class II), or "apple" (Class III), due to the air mass passing over multiple point or line sources. Another study at Mace Head by [*Ehn et al.*, 2010] attempted to calculate particle growth rates based on the time air travelled from the source area (exposed seaweed at low tide) to the monitoring station, and found incredibly high growth rates depending on travel time. In air reaching the station within 10 seconds, particles were estimated to grow at 260nm/h, whereas a travel time of 30 minutes reduced this growth rate to 1.61nm/h. The available cases at MLH appear to be mostly Class IV (mixed) events, though Class II "hump" events seem to occur quite often as well, as seems to be the case for both the 17 and 20 May examples. Not knowing the exact source area of the particle formation makes it impossible to calculate a growth rate based on travel time, and could be the topic of future study.

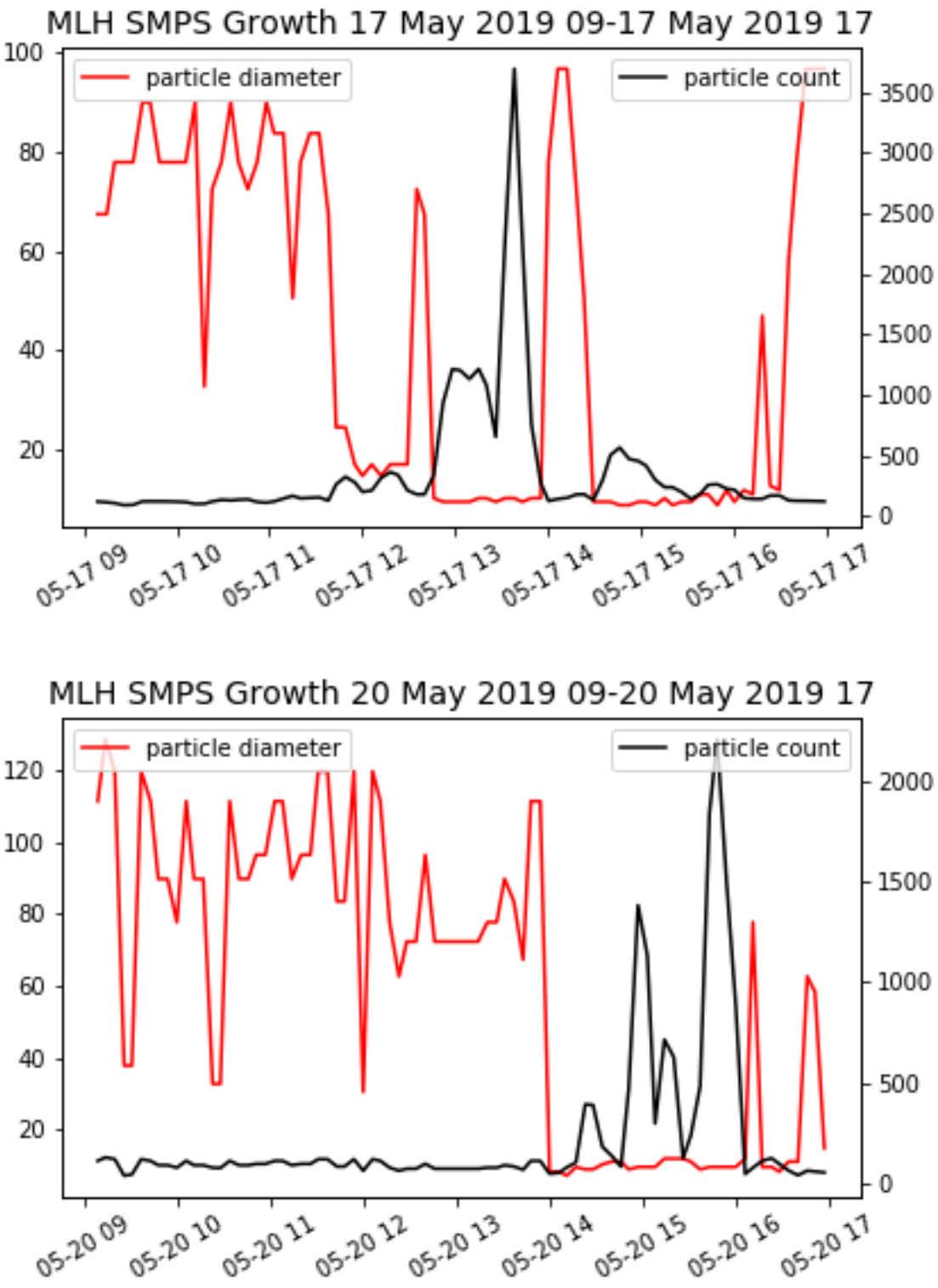

Figure 57 MLH SMPS Particle diameter (nm) mode time series

5.3 Attributing Sources of Aerosols using PM Ratios

Many studies have been conducted trying to interpret the relationship between coarse (PM10) and fine (PM2.5 or PM1) particulate matter in order to obtain meaningful results about the sources from which they originate. In the previous section it was unclear where at Malin Head the high particle events are occurring, but more information could be gained from examining the ratios of the PM2.5/PM10 by wind sector.

Typically, fine particulate tends to originate from combustion sources, while coarse particulate is most often of natural origins, such as sea salt or mineral dust. Although there is considerable cross-over of sources between the categories, as a general indicator, the ratio of PM2.5/ PM10 can be used as a marker for particle origin. Higher ratios are attributed to more anthropogenic influences, when a greater fraction of the PM10 (or PMtotal) is comprised of fine particulate, and lower ratios having more natural origins, as posited by [*Sugimoto et al.*, 2015]. However, as was shown previously at MLH, the in-situ production of particles on the coast can contribute greatly to the PM1 and thereby to the PM2.5 mass.

A study by [*Speranza et al.*, 2014] plotted results of PM ratios from other studies on a triangle in order to see how the Agri Valley in Northern Italy compares to them. On this plot, locations are placed based on their PM1/PM10, PM2.5/PM10, PM1/PM2.5, and (PM2.5-PM1)/(PM10-PM1) ratios, and clusters of points are indicative of similar environments, i.e. urban, suburban, rural, arid, etc. They found that although the Agri Valley would normally be considered a rural environment due to its location, the amount of industry there placed it in the same category as large cities such as Vienna. Below is the triangle plot from this study showing where Malin Head Fidas ratios fit in for annual values. It appears to be consistent with more rural areas (left side of triangle), but with its larger PM10 component from sea salt, it has some commonalities with arid sites (bottom right of triangle). The study noted that this may be different depending on seasons, and as was previously shown from the MLH Fidas measurements, the concentration and ratios of the different PM categories do vary considerably by time of year.

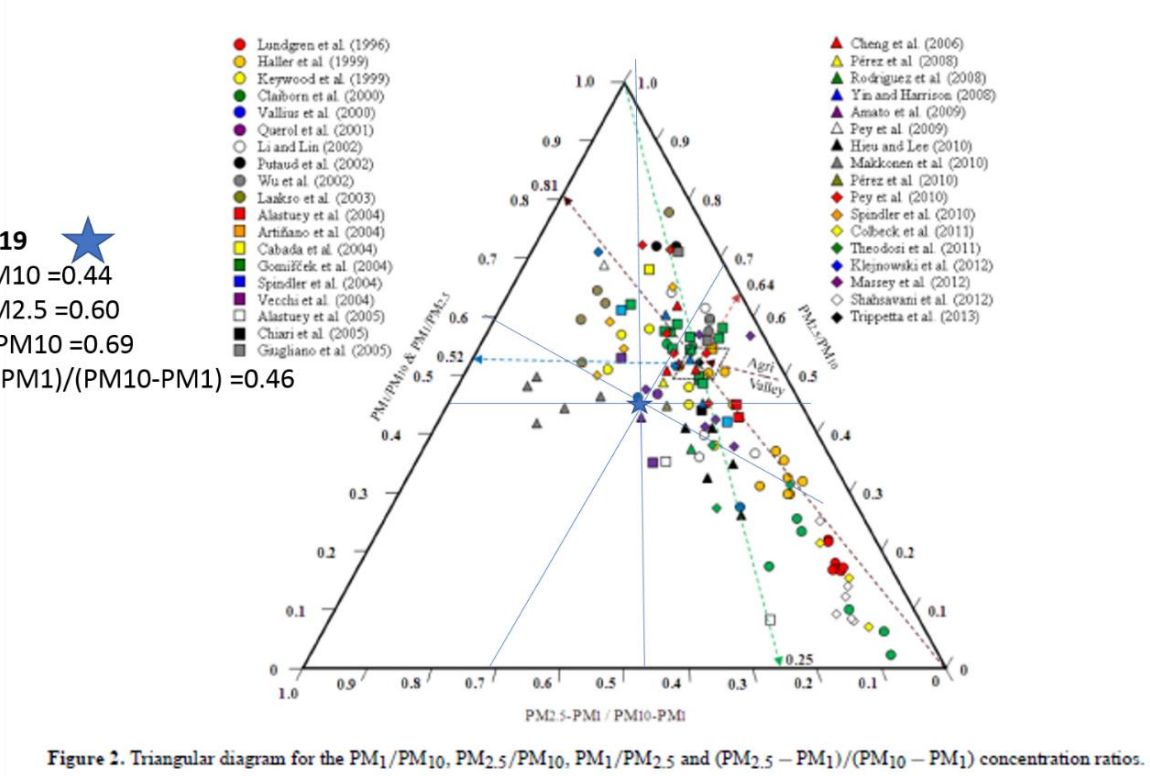

Figure 2. Triangular diagram for the PM_1/PM_{10}, $PM_{2.5}/PM_{10}$, $PM_1/PM_{2.5}$ and $(PM_{2.5} - PM_1)/(PM_{10} - PM_1)$ concentration ratios.

Figure 58 Triangle plot from Speranza et al. (2014) with MLH fidas ratios

The Fidas measurements presented in this study seem to show mixed results over the entire year, but when divided by season and wind direction, there is a distinct difference in the ratios. Below are wind roses for Fidas PM2.5/PM10 for summer and winter at Malin Head, and for a clean, rural, coastal environment in the summer, the PM2.5/PM10 ratios are very high, possibly due to the PM concentrations of all sizes being lowest at this time of year, yet still indicating that the largest fraction falls into the PM2.5 range. In particular, the sector between 225-315 degrees, directly west of the station seems to yield a very high percentage of PM2.5 relative to PM10, meaning it is likely of biogenic origin and could be related to open ocean nucleation and possibly coastal new particle formation events. By contrast, the winter wind rose shows the highest PM2.5/PM10 ratios from the southeast of the station, which other measurements concur is the direction of the highest levels of anthropogenic pollution, and relatively low PM2.5/PM10 ratios linked to high wind speeds from the north, which are indicative of sea spray. This shows that in a coastal environment such as Malin Head or Mace Head, the PM ratios can be influenced by other factors, and a high PM2.5/PM10 is not necessarily the result of anthropogenic pollution.

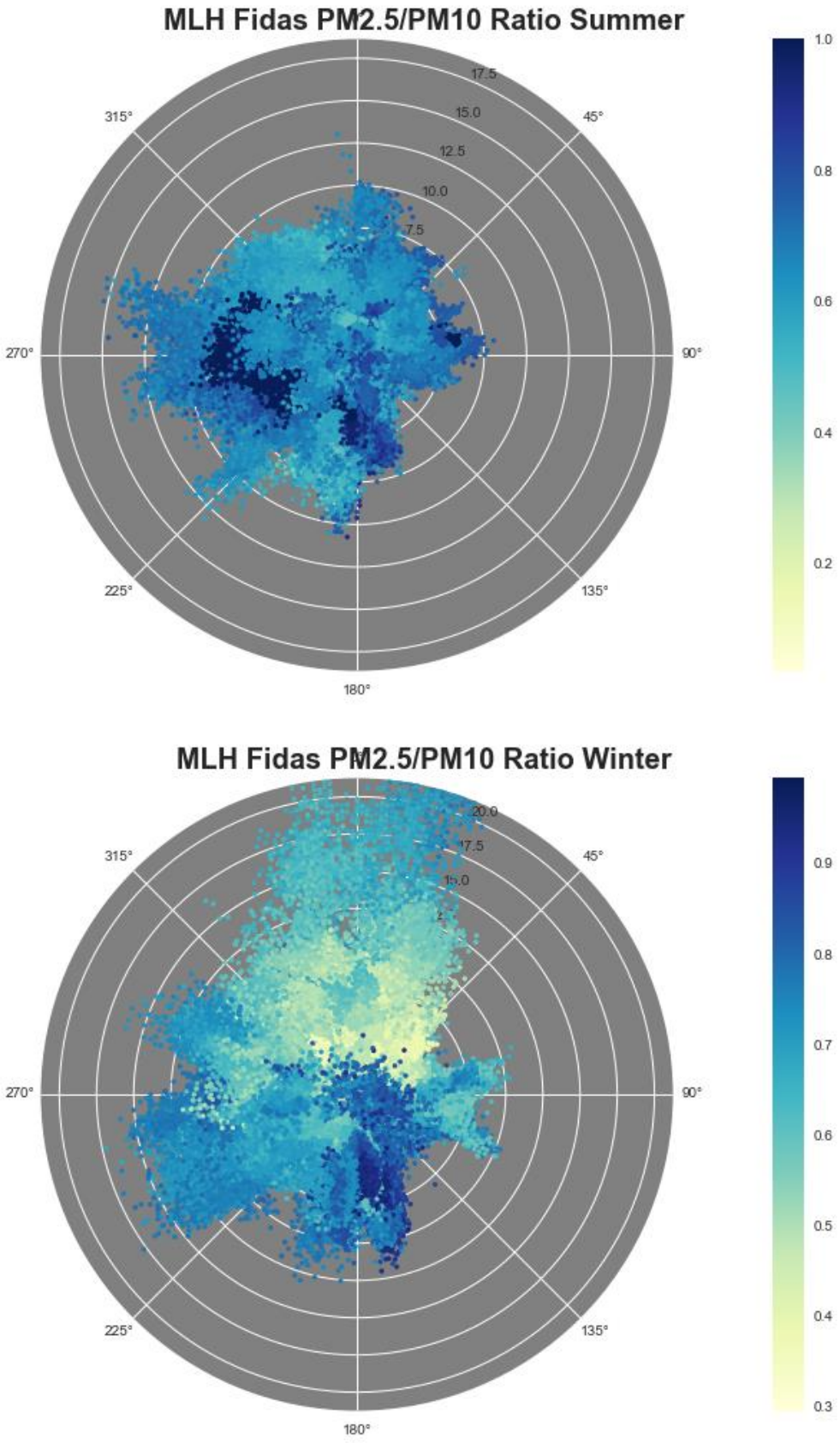

Figure 59 MLH PM2.5/PM10 ratio wind roses for summer and winter

5.4 Effect of Covid-19 Pandemic on Regional Pollution

With the Covid-19 pandemic currently affecting the entire world, it has been observed in other places such as China, Italy, and the USA that pollution levels have dropped significantly as a result of less traffic and industry. Already the Irish EPA has reported a 50% reduction in Nitrogen Dioxide (NO_2), which is the primary pollutant emitted by road traffic for Dublin after lockdown restrictions were put in place according to a recent press release [*EPA-Ireland*, 2020b]. While these changes are most visible in cities and highly industrial areas, this section will examine if changes on a regional scale are detectable in Ireland. Black carbon measurements were not widely available, therefore in order to do this, ozone (O_3) and PM measurements from the three network stations in conjunction with available ozone, PM10, PM2.5, and NO_2 data (downloaded from the European Environmental Agency website [*EEA*, 2020]) from ten other sites across the country operated by the Irish Environmental Protection Agency will be analysed for the lockdown period from 28 March-19 May 2020, as well as pre-lockdown (January-February 2020) and compared to the same time periods of the previous three years. To account for meteorology and seasonal cycles, the average of three previous years of data will be used to assess changes.

Figure 60 Irish EPA stations (yellow pins)

5.4.1 Observations

Ozone is a harmful secondary pollutant formed by photolysis of vehicular emissions of Nitric Oxide (NO) and Nitrogen Dioxide (NO_2), collectively known as NO_x, and Volatile Organic Compounds (VOCs), and so may be affected by a reduction in these pollutants. It is being measured at the rural sites Mace Head, Malin Head, Carnsore Point, Valentia, and Monaghan, as well as suburban background sites of Bray, Castlebar, Cork Bishopstown, Kilkenny, Laois, and Clonskeagh (Dublin). Cork City and Rathmines (Dublin) are classed as urban traffic sites.

Looking at the differences between 2020 ozone concentrations and the previous 3-year average, some interesting patterns emerge. As shown in the time series in **Figures 61-62**, areas considered suburban background experienced a slight increase in ozone occurs during lockdown in May, on average 13.7% (a two-tailed t-test showed a significant p value of 0.03), and seemingly higher the closer a site is to traffic emissions. In rural areas there is an average 5.6% decrease in ozone during the same time period, which the two-tailed t-test did not prove as significant, with a p value of 0.16. The two urban traffic sites in Cork City and Rathmines (Dublin) showed no clear pattern relating to lockdown. By comparison, ozone was slightly higher than previous years in February (before lockdown), an average of 7.46% across all sites. The boxplots in **Figure 63** illustrate typical examples of rural and suburban sites and show that there is no obvious upward or downward trend in ozone over the years. Boxplots for the other stations can be found on page 184 in Appendix C.

It is noteworthy that at both suburban background and rural sites, the average monthly ozone is lower than the previous years' average for the entire period after lockdown, with sharp increases toward the beginning of October when another lockdown came into effect. Plotting the ozone percent change by latitude showed no obvious relationship and is therefore not shown here. The main factor influencing whether or not ozone increased or decreased at a particular site appears to be its proximity to traffic, and hence NO_x emissions.

One possible reason for the sudden increase in ozone in the suburban areas could be what has become known as the "weekend effect," described by [*Atkinson-*

Palombo et al., 2006] and references therein. This, as the name suggests, mainly occurs on weekends in suburban areas, when ozone increases as a result of fewer NO_x emissions, and possibly more sunlight from lower BC levels, associated with traffic. Especially the amount of ozone titration through NO would have an effect if the NO_x concentrations are reduced.

As ozone formation in rural areas is more dependent on VOC concentrations than on NO_x, the reduction in ozone is more difficult to explain. As discussed by [*Kroll et al.*, 2020] there is a complex and non-linear chemistry involved, which depends on the types of VOC's and their ratio to NO_x, that determines whether ozone or secondary organic aerosol (SOA) is formed. Without more detailed measurements of VOCs, it is impossible to determine if the amount was reduced or increased due to anthropogenic emissions (less traffic, more cleaning agents), or if this affected the ratio to NO_x in such a way that SOA formation increased.

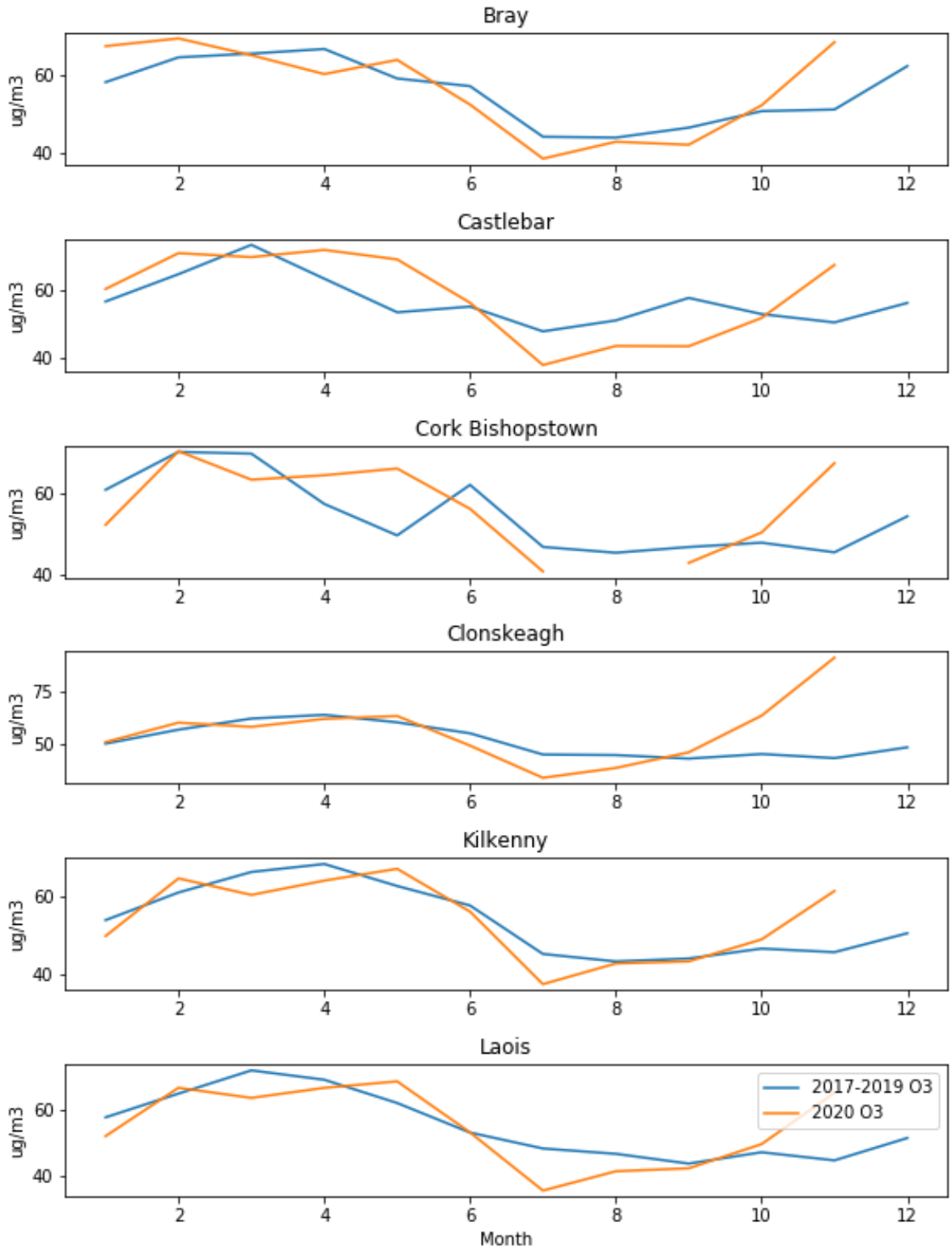

Figure 61 Suburban Background Ozone

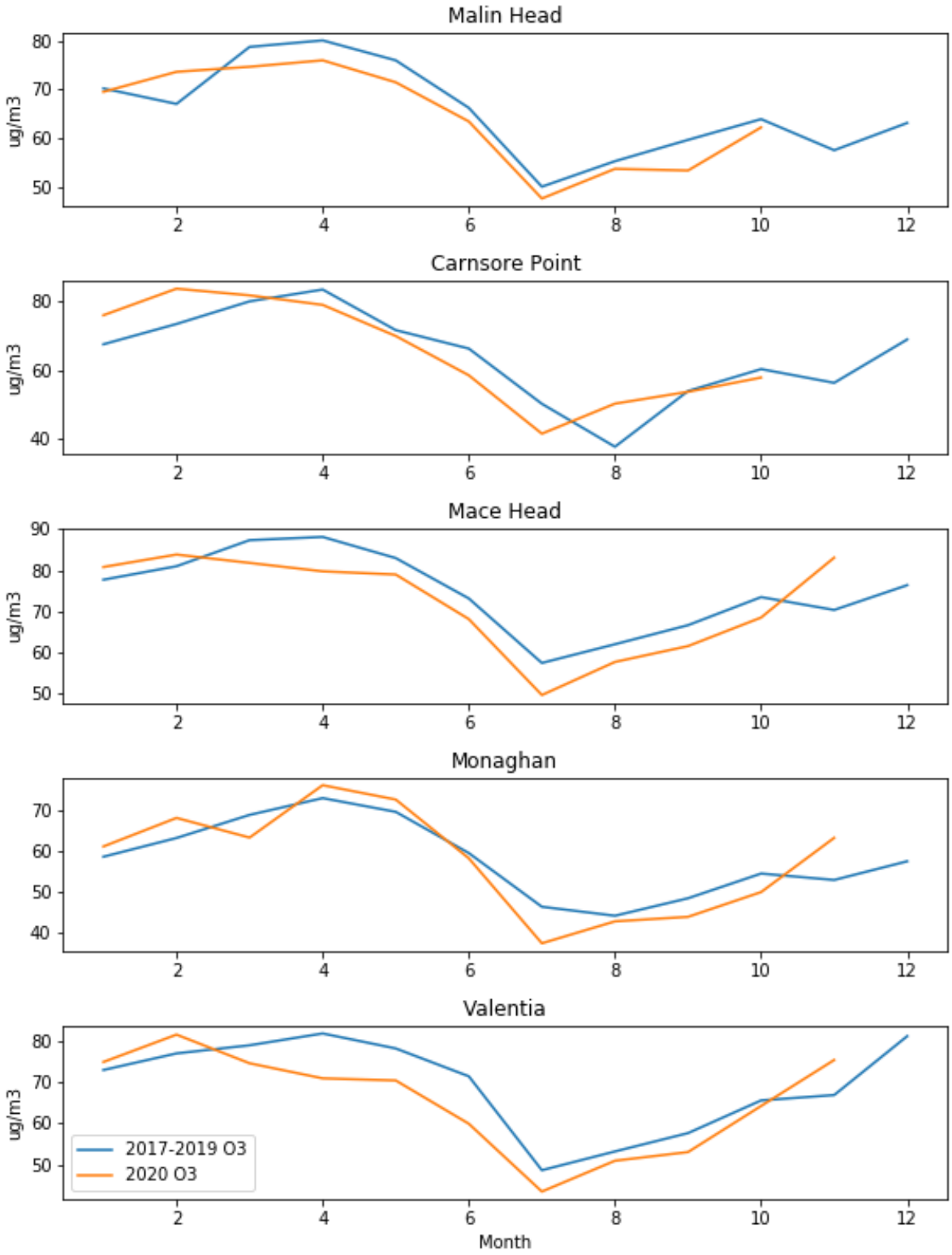

Figure 62 Rural Ozone

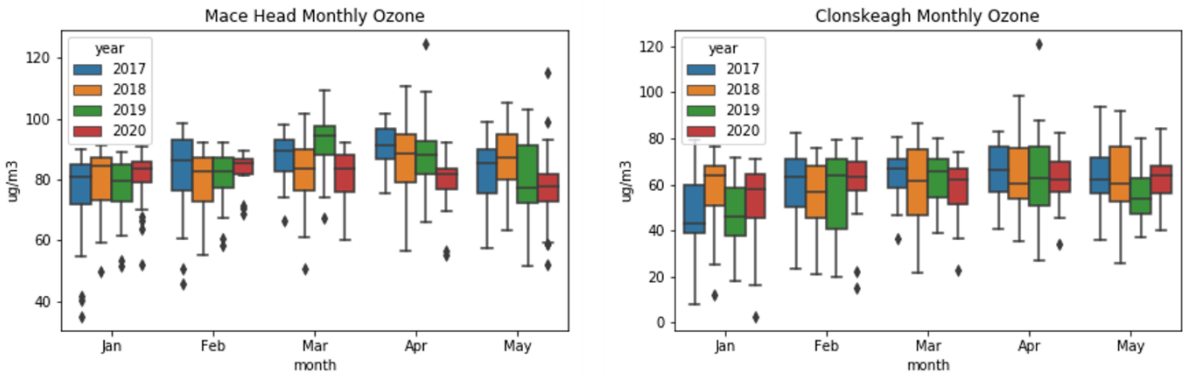

Figure 63 Comparison of rural (Mace Head) and suburban (Clonskeagh) ozone

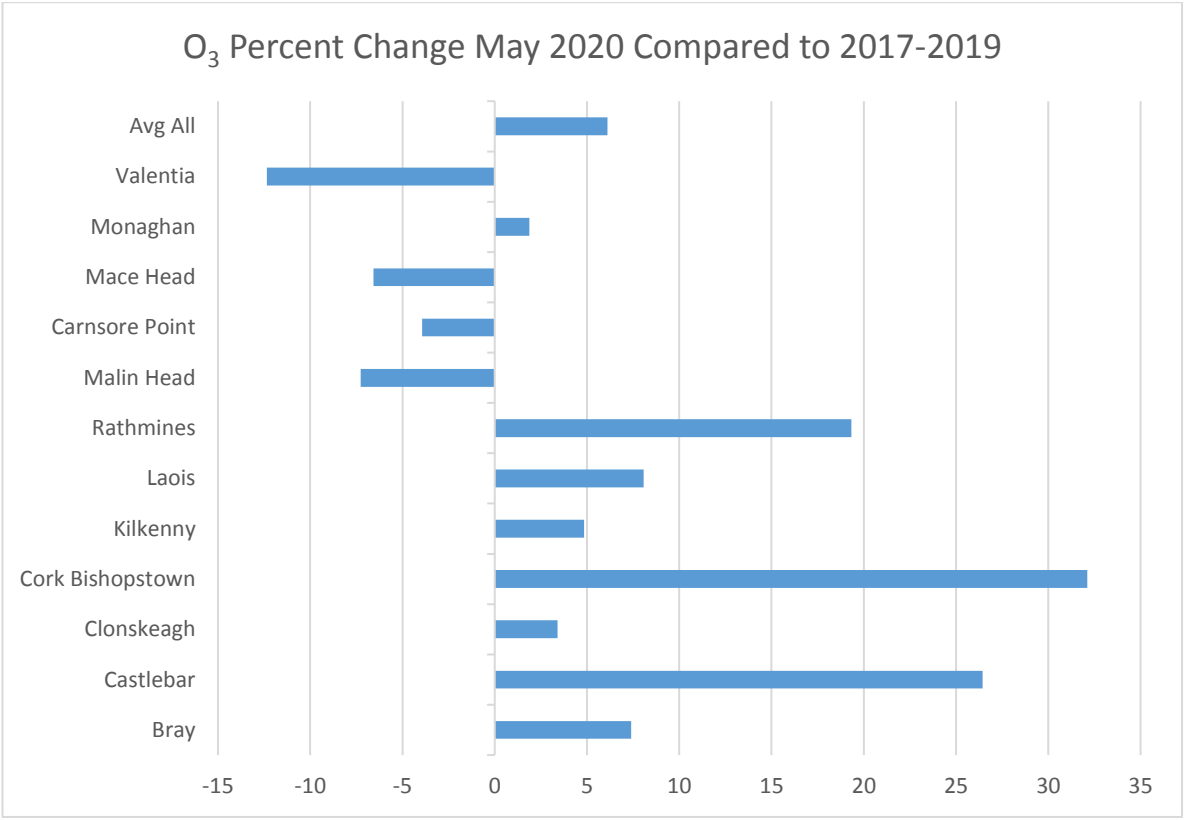

Figure 64 Percent change in ozone between 2020 and the average of 2017-2019

Nitrogen dioxide (NO_2) is primarily emitted by vehicles, and therefore a key indicator of traffic related changes in pollution. It is measured at five of the sites that also measure ozone, only one of which is rural. The below comparison with ozone shows that the rural site (Monaghan) has significantly lower NO_2 levels than the other stations, although its ozone levels are about the same as the others. Monaghan differed from the other rural sites in that it experienced a 1.88% increase in ozone during the lockdown period. The reduction in NO_2 as a result of

lockdown is clearly visible in **Figure 65**, especially in the urban area of Rathmines, which likely experienced the greatest decrease in vehicle emissions. Seasonality is accounted for by comparing to the previous three-year average.

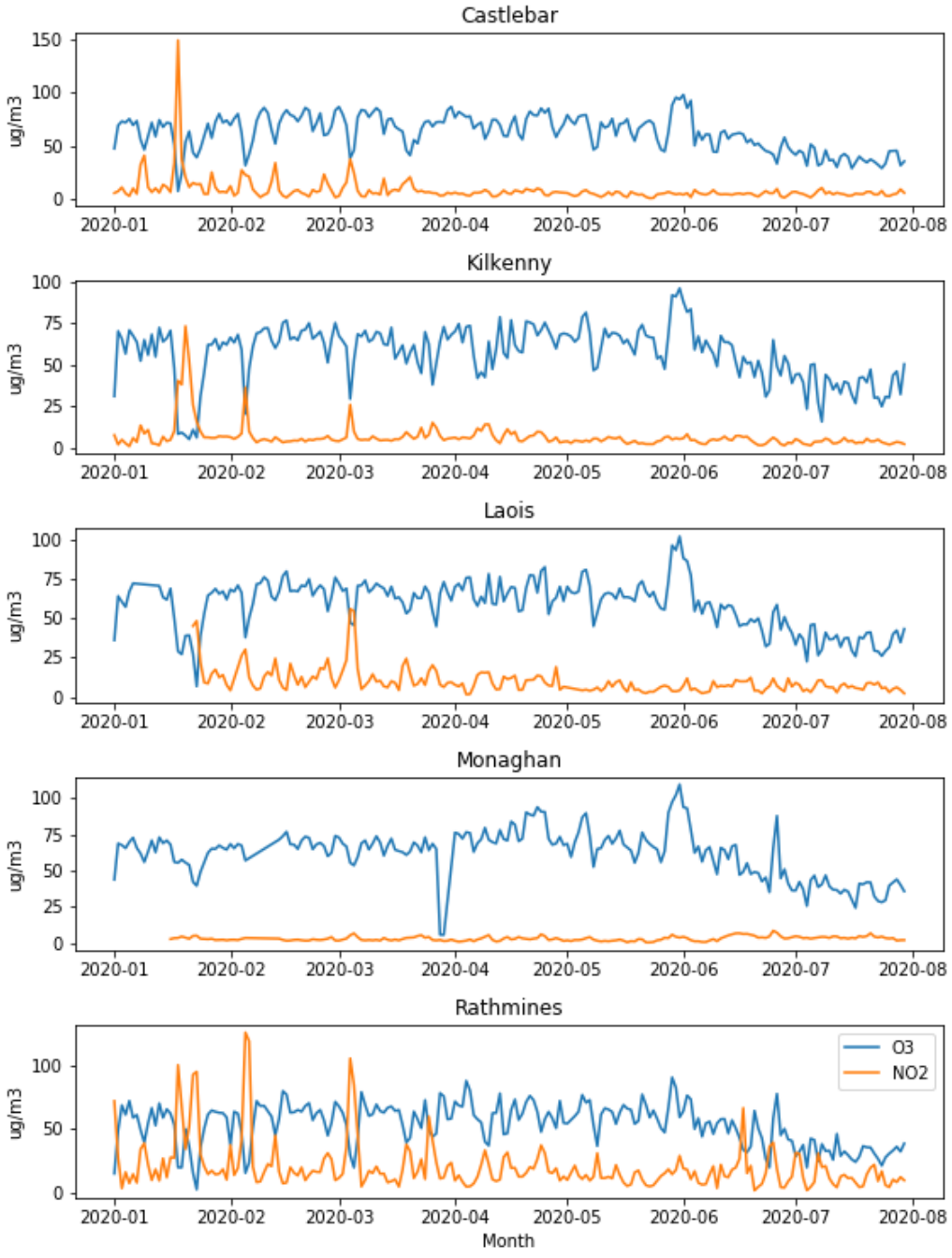

Figure 65 NO_2 and Ozone daily averages comparison

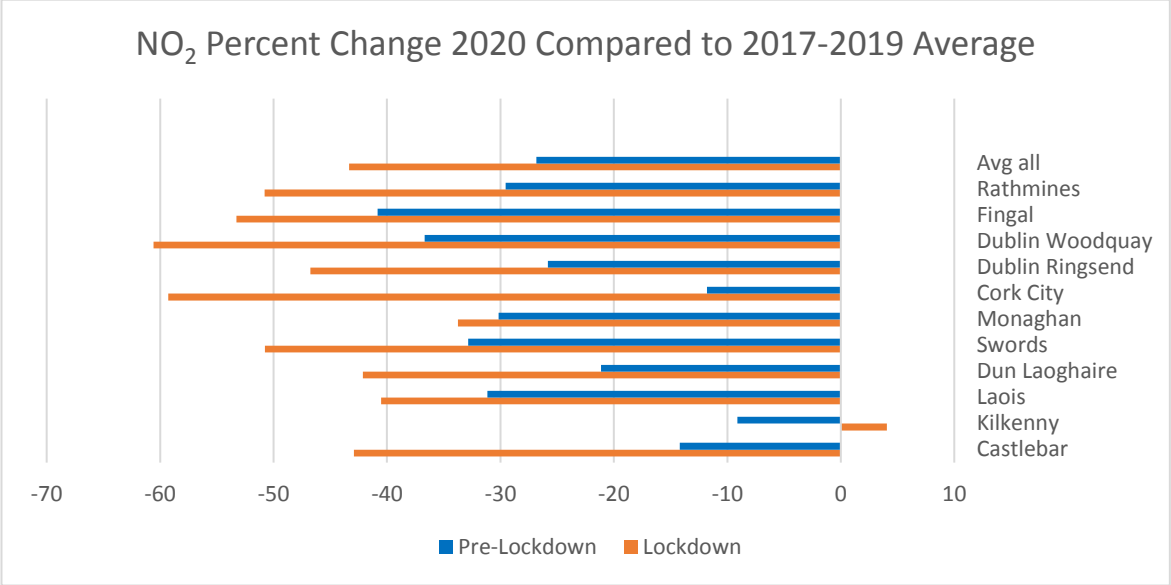

Figure 66 Percent change in NO_2 compared 2017-2019. Pre-lockdown is 1 Jan-28 Feb, Lockdown is 28 Mar-19 May.

There are five Dublin sites measuring NO_2 (but not O_3), which were included here for comparison. Dun Laoghaire and Swords are background suburban sites, whereas Dublin Ringsend, Woodquay, and Fingal are categorized as urban traffic. As the chart above shows, all stations had lower levels of NO_2 in 2020 than in previous years, however the difference increased everywhere except Kilkenny during the lockdown period. The heaviest traffic area of Dublin Woodquay is associated with the largest decrease (60.6%) compared to the previous years' average, and the average decrease over all Dublin sites was 50.7%, consistent with the EPA's report [*EPA-Ireland*, 2020b]. NO_2 concentration depends largely on emissions, chemistry, and meteorology, and the largest source of emissions, traffic, had not changed compared to previous years, meaning that the reduction is likely due to changes in meteorology, which will be looked at in more detail later. The following boxplots for Dublin Woodquay and Kilkenny indicate that there was no visible upward or downward trend in previous years, and this holds true for all sites (boxplots pages 185-187 Appendix C). The plots below reflect this as well, with Kilkenny being the only station to show a net increase in NO_2 during the lockdown. The reason for Kilkenny exhibiting a different pattern than the other stations is likely local or regional influences such as agricultural activity.

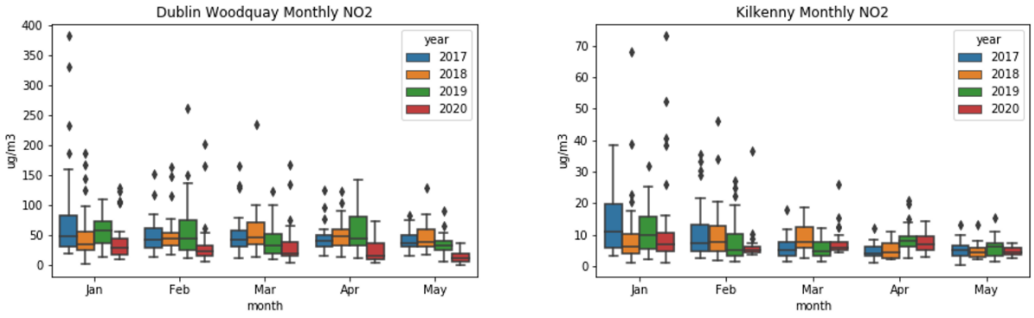

Figure 67 NO_2 Boxplots for Dublin Woodquay and Kilkenny

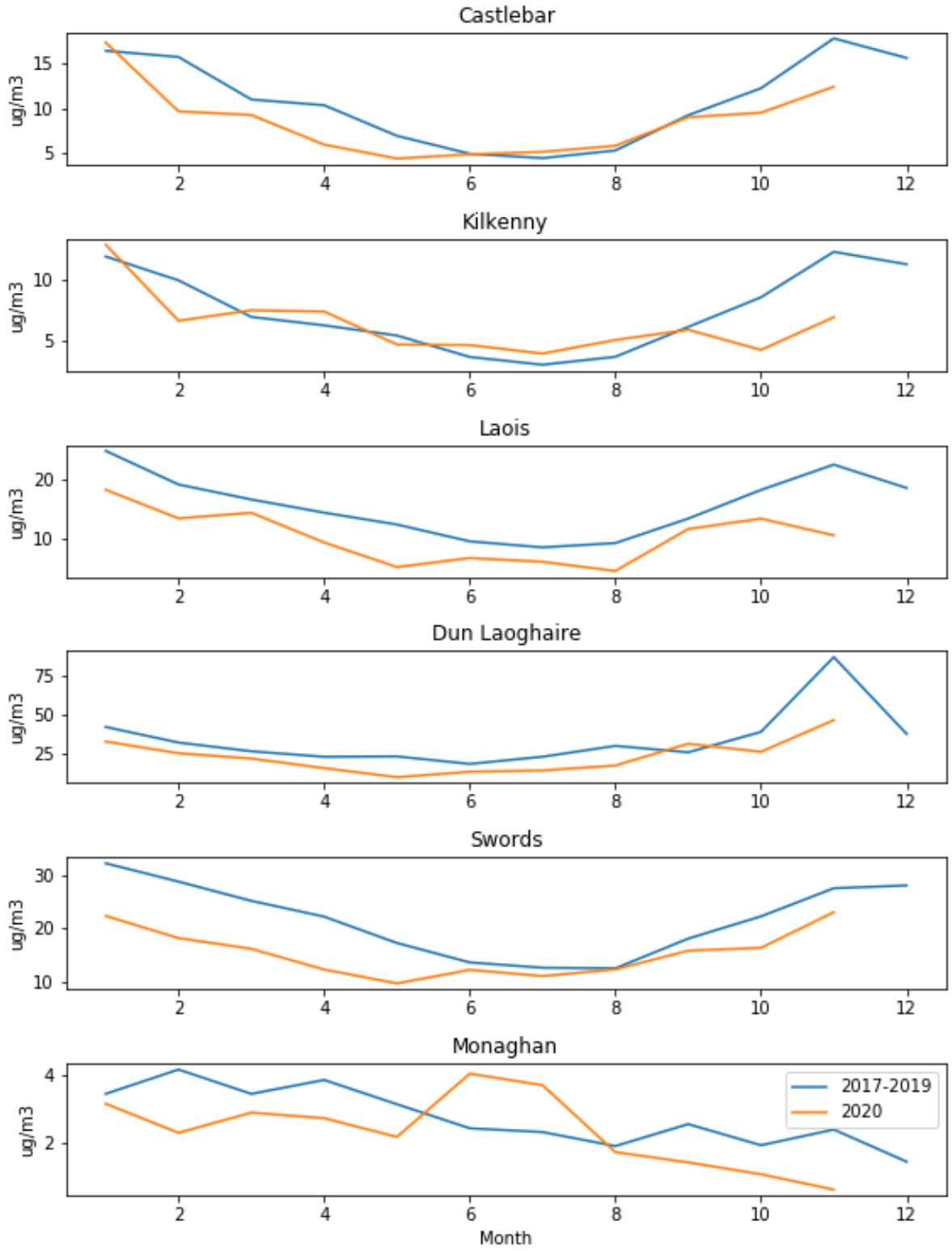

Figure 68 Suburban background (and Monaghan rural) NO_2 comparison 2020 to average of 2017-2019

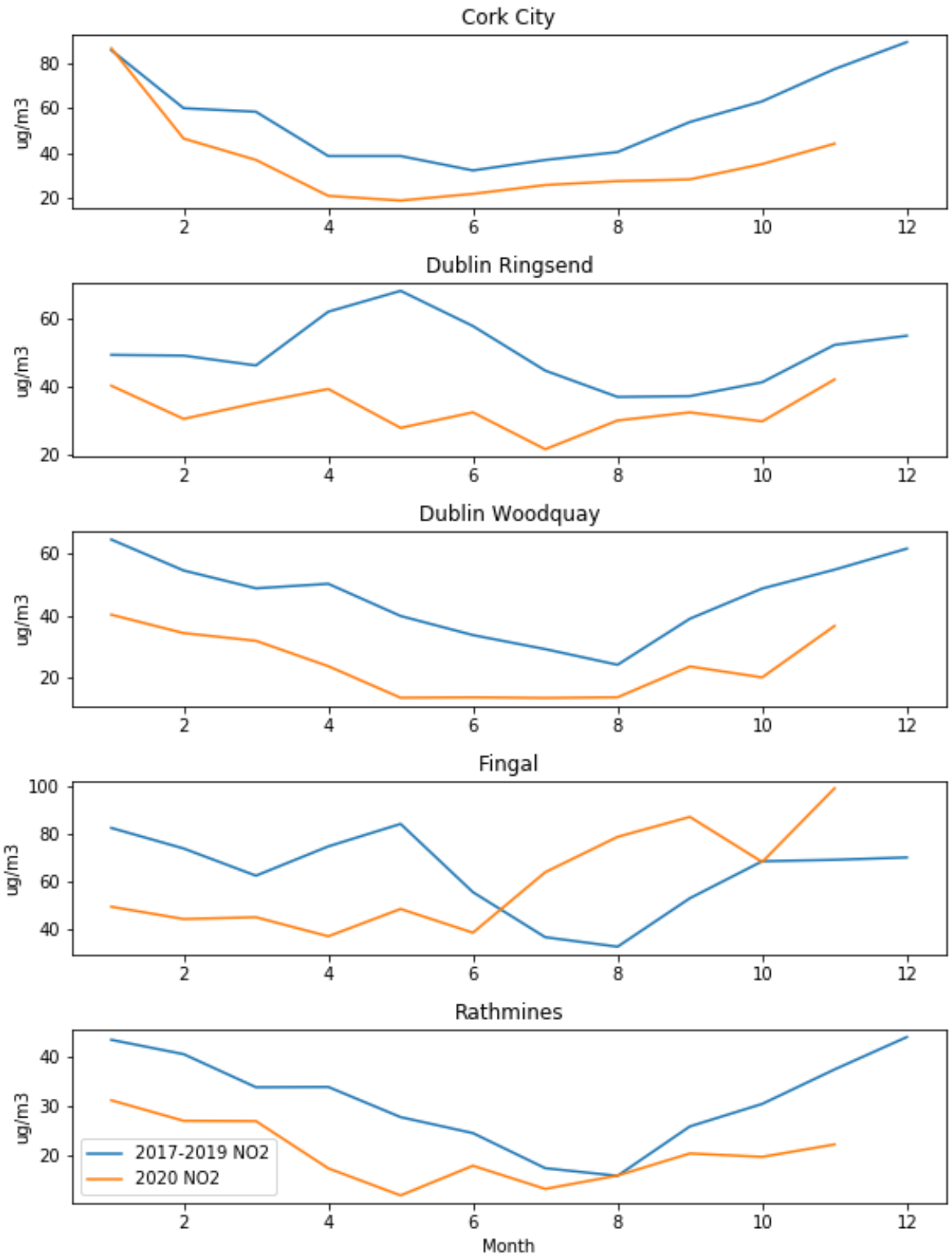

Figure 69 Urban NO_2 comparison 2020 to average of 2017-2019

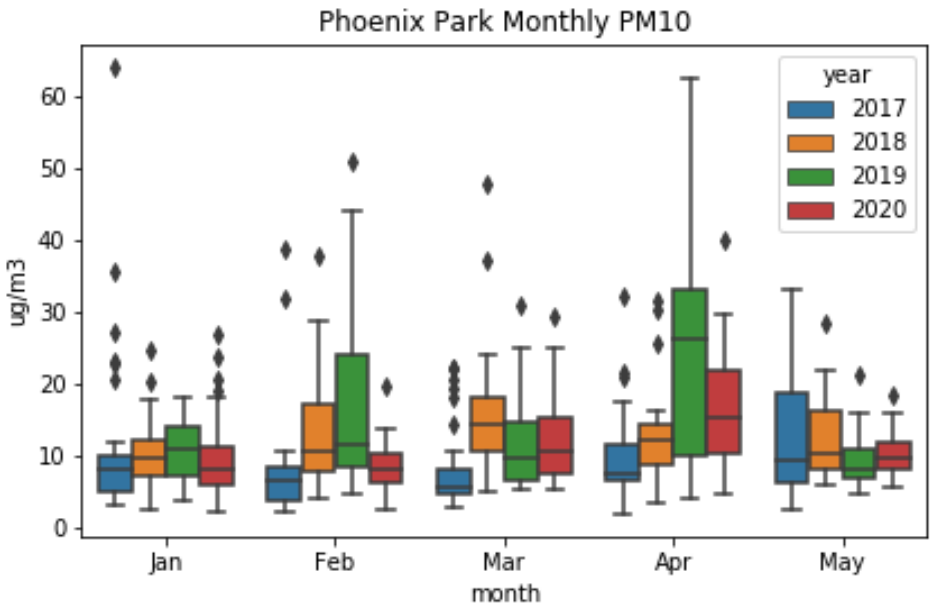

Figure 70 Box plot of PM10 at suburban site Phoenix Park (Dublin)

Although most of the sites do have some available PM10 measurements, only seven of them had consistent enough data sets to complete this analysis. These were Dublin Ringsend, Rathmines, Inchicore, Ballyfermot, Phoenix Park, Cork City, and Castlebar. Only four sites measure PM2.5, all of them urban traffic apart from Malin Head, yet due to insufficient data an analysis could not be conducted. When comparing the 2020 PM10 measurements from the stations to the average of 2017-2019, PM10 did not change considerably before or during lockdown, and there was no consistent pattern in the percent change. This is likely due to the complex nature of PM, which has many sources and varied composition. The boxplots show only April 2019 being anomalously high compared to other years, which is reflected across all stations (boxplots page 187 Appendix C). As shown by [Coleman et al., 2020], wind speeds in the months of January and February were higher than the 2016-2019 average for those months, and may have caused dispersion of PM leading to lower concentrations in most areas, whereas there was less precipitation in the months after lockdown began which could mean fewer particles were washed out. Castlebar on the west coast of Ireland may have experienced increased sea salt as a result of the higher wind speeds. The composition of aerosols will vary by season and type of site, i.e. Malin Head PM10 is largely made-up of sea salt, as

previously shown in the mass closure experiment, but other factors such as an increase in home heating and decrease in road traffic due to lockdown could have resulted in similar levels of PM from different sources than usual.

As the Malin Head Fidas instrument has the ability to measure different PM size categories simultaneously, these data were further evaluated, and showed there were some clear changes after the lockdown comes into effect in Ireland. The time series below shows a distinct reduction in the signal variability of PM1 and PM2.5 after lockdown begins (the average standard deviation for PM1 before lockdown was 1.00 and after lockdown 0.36, for PM2.5 before lockdown 1.60 and after lockdown 0.57), which could be related to less local traffic that would otherwise produce BC and road dust in the area. PM10 by comparison seems relatively unchanged with an average standard deviation of 1.05 before and 1.08 after lockdown, and with Malin Head being a coastal station, the sea salt component of these coarse particles would not be expected to change.

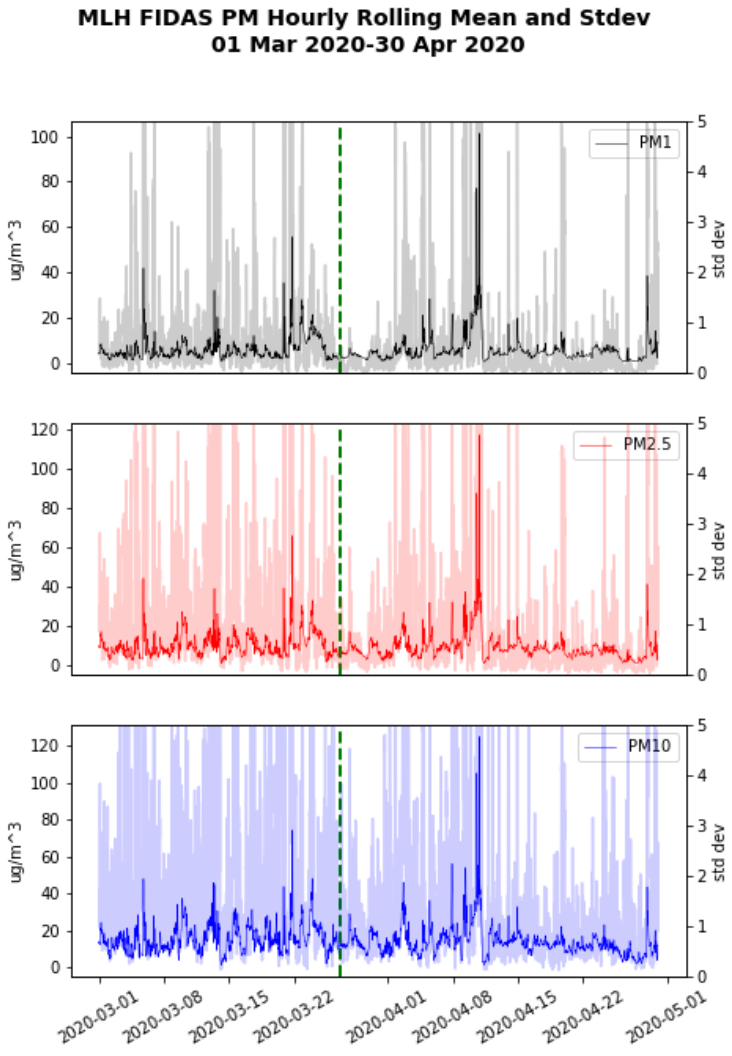

Figure 71 MLH Fidas PM hourly rolling time series on left axis with standard deviation in lighter colour on right axis (green dashed line denotes beginning of lockdown in Ireland)

Meteorology can affect all of the above species, so this was evaluated compared to previous years as well. The most noteworthy changes in 2020 were the aforementioned windspeed and precipitation, although the wind roses also show a slight shift in wind direction to the southwest in January and February, which may have had the effect of bringing more Atlantic background air to Dublin than continental air from the south. Higher wind speed would lead to greater dispersion in urban areas, not only of PM, but also NO_2, and could be a factor in the lower NO_2 concentrations before lockdown, as shown for example by [*Dragomir et al.*, 2015] . Solar radiation remained similar to previous years before lockdown, but was somewhat higher in April and May of 2020, which could affect ozone chemistry.

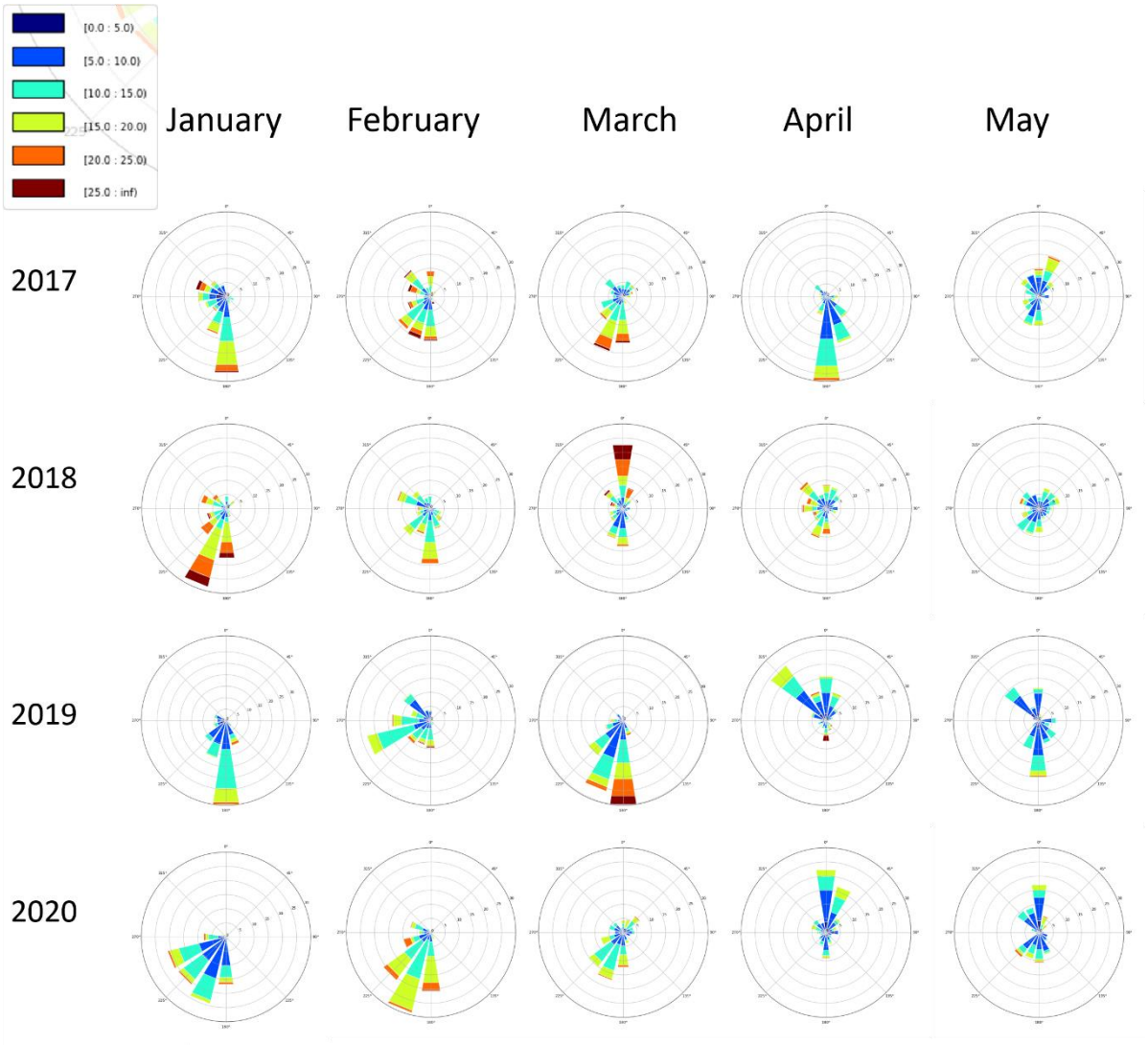

Figure 72 Dublin airport wind roses, scale is 0-30 knots for speed, colours represent frequency of occurrence.

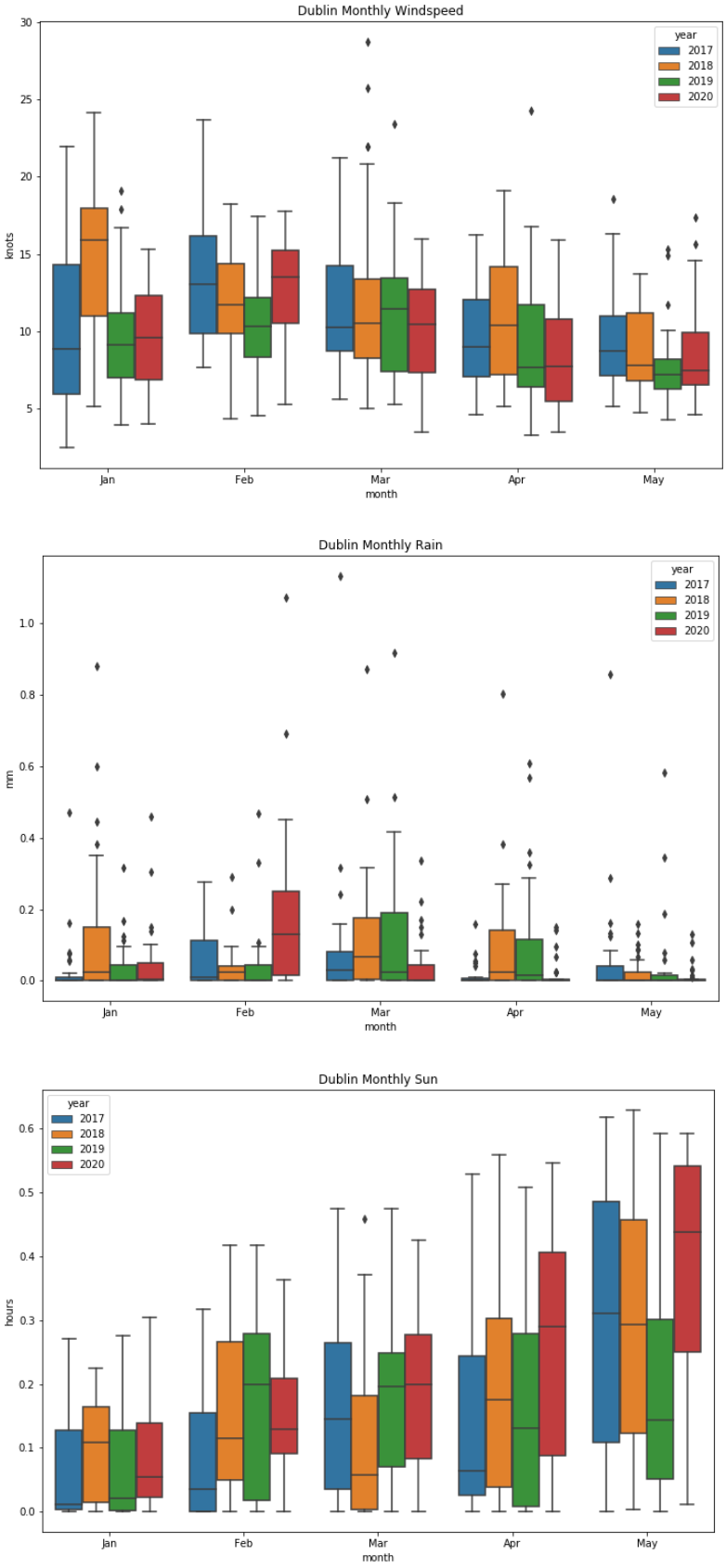

Figure 73 Dublin Airport meteorology

5.4.2 Comparison to Literature

To put all of these results into perspective, it is informative to look at related measurements and studies. While a plethora of new literature showing reduced emissions in various parts of the world has emerged in the wake of the pandemic, here the focus will be on two articles which are most relevant to the observations in Ireland.

A recent study by [*Lee et al.*, 2020] examined in-situ measurements at over 150 monitoring stations across the UK. Using the same methodology applied here of comparing 2020 values to the previous 3 years, they were able to show an average 11% rise in ozone in urban background areas of the UK after lockdown came into effect. They also found a slight increasing trend in ozone over multiple years. Solar radiation plays a major role in ozone formation, and the UK study demonstrated that the southern regions which had more sunlight and warmer temperatures during this period experienced greater increases in ozone compared to Scotland and Northern Ireland.

The increase in ozone in the suburban background sites of 13.7% in Ireland agrees well with the UK study by Lee et al., however no upward trend could be discerned over time, with the more rural stations actually trending slightly downward. There was also no correlation between latitude and ozone concentration. These differences are likely due to fewer stations in Ireland with a shorter timeframe of measurements.

[*Menut et al.*, 2020] performed a modelling study comparing “business as usual” emissions to estimated reduced emissions based on how many fewer vehicles were on the road, and calculated that for Ireland this would result in a 2.7% reduction in ozone in urban areas, and a 2.34% reduction in ozone in rural areas. They also predicted a 37.3% and 29.5% decrease in NO_2 in urban and rural areas respectively. PM2.5 was expected to be 11.1% (urban) and 11.7% (rural) lower in Ireland.

Comparing the results from that study to the observations in Ireland, the average rural decrease of 5.6% in ozone is slightly higher than predicted for Ireland by Menut et al., yet close enough to be within the margin of error. While there was a short-term increase in suburban background ozone in May after the lockdown began, for the most part ozone did decrease in Ireland both in rural and suburban areas compared to previous years, though the percentage varies depending on the site's proximity to traffic. The NO_2 predictions of the reduced emissions modelling scenario match very closely with the observations for both rural and urban environments, however the PM2.5 did not reduce as predicted, indicating some other source of PM not related to traffic.

5.4.3 Comparison to Satellite

Satellite images from NASA's Aura/OMI (https://so2.gsfc.nasa.gov/no2/no2_index.html) during the lockdown period between 28 March and 19 May 2020 also show reductions in NO_2 compared to previous years of about 27% (±13% over the time period) overall in Dublin. This is less than the average decrease in NO_2 of 50.7% (±6.2% of the site averages) measured in-situ across all the Dublin sites, likely due to the satellite comparison covering a larger time scale for previous years (2015-2019), and possible inaccuracies due to grid resolution. The image below is only a representative sample as it is part of an animated time series. The satellite analysis is focused on Dublin; however, the maps do show the entire country. Here it is noteworthy that areas such as Kilkenny seem to have slightly higher than usual NO_2 concentrations, which is consistent with in-situ measurements from that station. According to [*Duffy et al.*, 2020], transport made up 40.6% of the national total NO_x in Ireland, but agriculture accounted for 32.4% of NO_x emissions. As Kilkenny is located in a largely agricultural part of Ireland, it is likely that the 4% increase in NO2 compared to previous years is related to that.

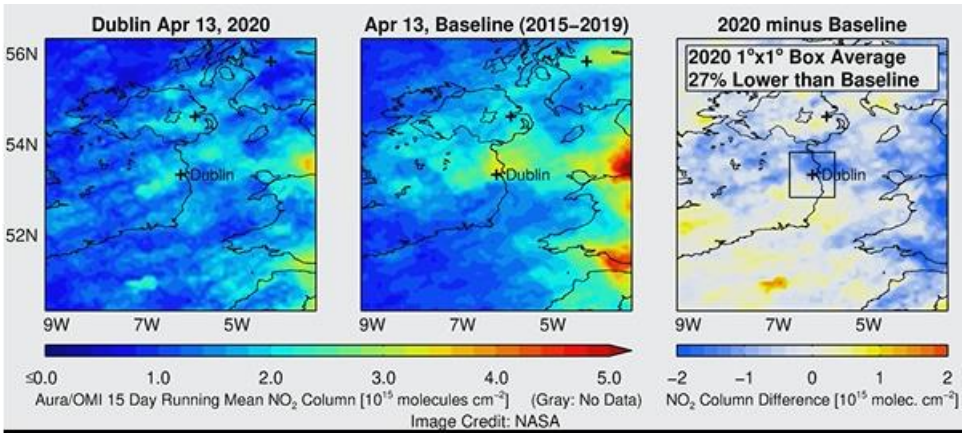

Figure 74 NASA Aura/OMI NO2 column images over Ireland

5.4.4 Comparison to Emission Inventory

While NO_2 was greatly reduced in most places as a result of less vehicular traffic during lockdown, O_3 appears to have remained fairly constant before and after lockdown, as the daily averages show it to be well within the range of northern hemisphere background concentrations reported by [*Vingarzan*, 2004] of 20-45 ppb at all stations, even accounting for the springtime high. Apart from a brief increase in suburban areas compared to previous years from a possible "weekend effect" after lockdown, O_3 was generally lower in 2020 than before. Ozone concentration depends on a number of factors, with both natural and anthropogenic sources. Its longer lifetime of about 20 days in the troposphere allows it to be transported over long distances, which is why there is a fairly constant background level.

The production and loss of ozone depends mainly on meteorology and the ratio of VOC/NO_x. This relationship is often depicted in the form of an ozone isopleth diagram (see page 183, Appendix C), as explained by [*Division on Earth and Life et al.*, 2000], with NO_x on the y-axis and VOCs on the x-axis, and lines of constant value of ozone (isopleths) plotted as the maximum resulting from the different combinations of NO_x and VOCs. A diagonal line from the origin at bottom left to top right on these charts is representative of the 8:1 ratio of VOC/NO_x, and anything to the right of this line is considered NO_x limited (characteristic of rural or suburban areas, where a reduction in NOx results in lower ozone), whereas to the left is VOC limited (in highly polluted inner cities, where in order to reduce ozone, VOCs must be reduced). Due to the curvature of the isopleths, it is possible in a VOC limited environment for ozone to actually increase when NO_x is lowered, until the ratio crosses to the other side of the ridge line which results in reduced ozone. This also is part of the "weekend effect" in urban areas.

VOCs are a broad category of chemical compounds, many of which come from natural sources such as trees. Without measurements of these compounds, it is impossible to know how the concentrations and composition have changed, thus affecting the VOC/NO_x ratio. The Informative Inventory Report for Ireland [*Duffy et al.*, 2020] estimates only 4% of total VOCs are related to transport. This is a very small amount compared to the over 40% of NO_x attributed to transport, and so it is

likely that the reduction in NO_2 would result in a higher VOC/NO_x ratio after lockdown, creating a more NO_x limited environment which would account for the somewhat lower O_3 levels in 2020.

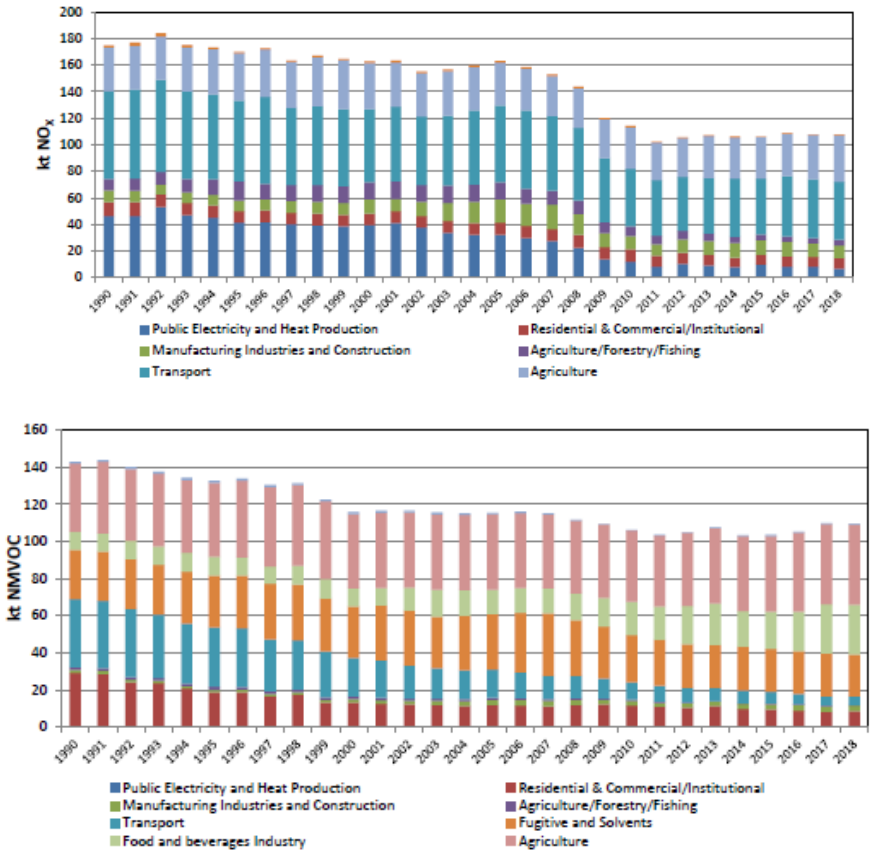

Figure 75 NOx and VOC contributions by sector from Informative Inventory Report 2020 (Duffy et al. 2020)

The MapEire.dk (https://projects.au.dk/mapeire/spatial-results/) website depicts the Irish emissions inventory according to major sources by species on a spatial resolution of 1 x 1km. The maps below show NO_x and VOC emissions from 2015 across Ireland for comparison. As NO_x is heavily associated with transport, roads and urban areas stand out. VOCs are largely associated with agriculture and industry, covering rural areas of the country, with increases in urban areas related to road use and solvents. Comparing the colour scales for the two maps shows that VOCs are considerably higher than NO_x, even in urban areas. Although these are only estimates, and the inventory is from 2015, this gives the impression that Ireland, with the exception of some very highly trafficked areas, is NO_x limited, and would explain why the model study by Menut et al. predicted a decrease in ozone for urban areas.

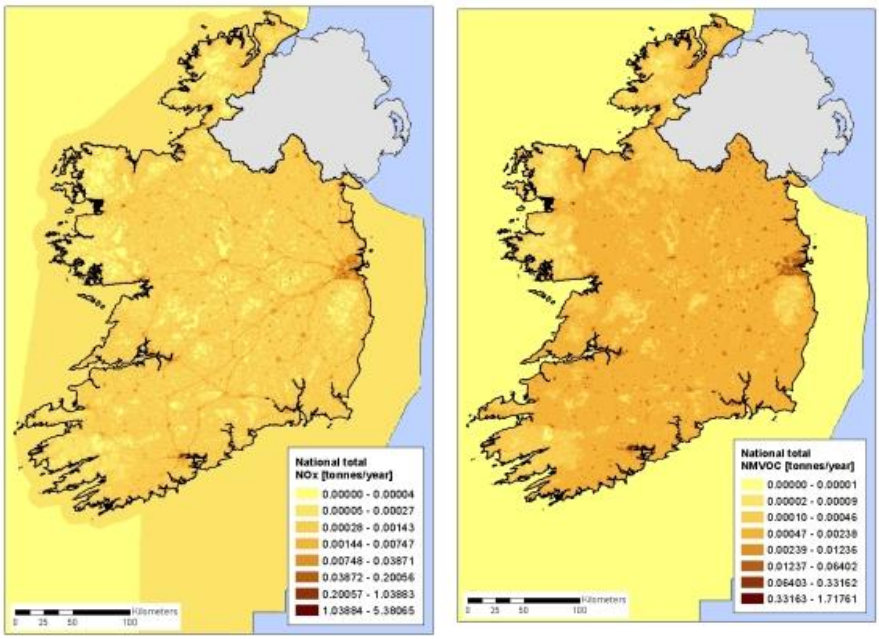

Figure 76 Spatially resolved NOx and VOC emissions for Ireland based on 2015 Inventory from MapEire.dk

The European Environmental Agency (EEA) has created a tracker system online at https://www.eea.europa.eu/themes/air/air-quality-and-covid19 where the levels of PM2.5 and PM10 can be observed on a weekly and monthly basis by country and city. On this website they note that PM2.5 has not visibly reduced across much of Europe, due to its more varied sources, including agricultural ammonia, which would not have been reduced due to Covid-19 restrictions. Home heating had also not significantly declined during this period, according to the Irish EPA, likely due to people spending more time in their homes. As the most recent Informative Inventory Report for Ireland [*Duffy et al.*, 2020] shows, transport made up only 8.7% of the total PM10 in 2018, and 13.8% of PM2.5, making it unlikely that a reduction in traffic would have a significant impact on these measurements.

Indeed, the Irish measurements of PM10 and PM2.5 do not appear to be greatly impacted by the lockdown. The percent increase/decrease was within a the standard deviation of the mean both at rural and urban sites. Even so, small changes were observed in PM1 at the rural sites. These could be related to other sources, i.e. what would normally have been traffic related might now be the result of increased home heating. The composition of PM is also very site dependent, as

the coastal sites would be heavily influenced by sea salt as shown in the mass closure experiment.

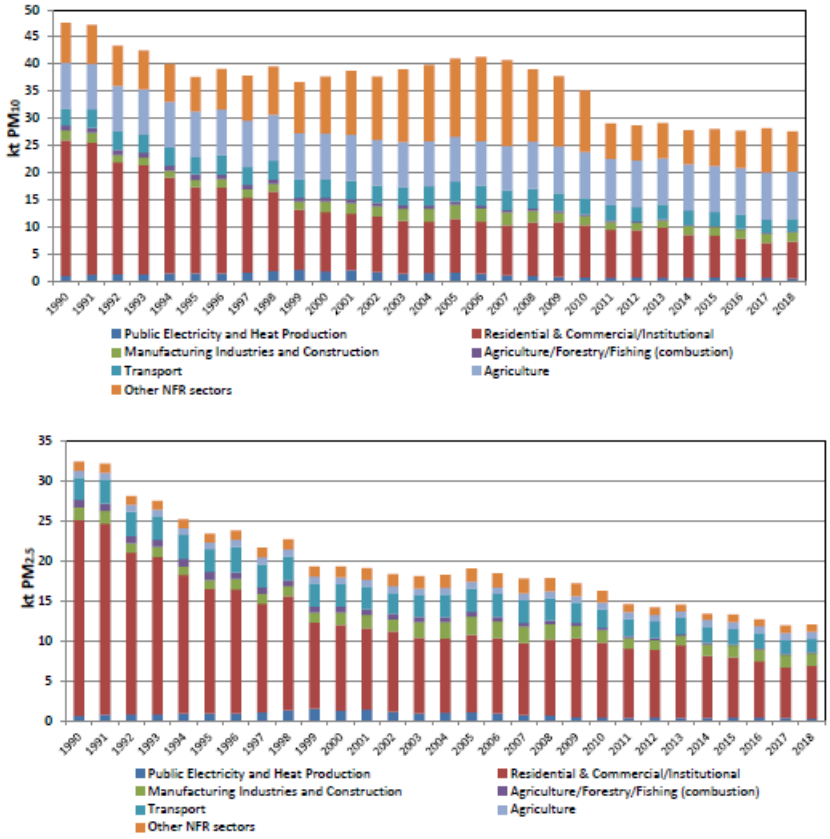

Figure 77 PM10 and PM2.5 contributions by sector from Informative Inventory Report 2020 (Duffy et al. 2020)

5.4.5 Impact of Traffic

The Traffic Infrastructure Ireland (TII) website (https://www.nratrafficdata.ie/c2/gmapbasic.asp?sgid=ZvyVmXU8jBt9PJE$c7UXt6) tracks the number and type of vehicles for thousands of locations across Ireland. When comparing various sites before and after lockdown, there is a roughly 50-60% reduction in the daily amount of traffic, mainly related to passenger vehicles. This can be seen in the plots below for the Dublin site nearest to Rathmines, where previously a daily maximum of 900 vehicles were counted, and after lockdown there were around 300 vehicles during the same late afternoon peak between 15:00-17:00, as well as a rural area such as Monaghan that previously had about 350 vehicles at the peak afternoon traffic and went down to 170 during the same period after lockdown. The level of NO_2 reduction is directly linked to the amount of traffic, due to its shorter lifetime and higher concentrations closer to the source. Other TII sites around Dublin are located on very busy motorways, such as the M50, where there were over 10,000 vehicles/hour prior to lockdown, specifically on the section leading to the airport, and traffic was reduced to just over 3,000 vehicles during the same time of day after lockdown. Monaghan on the other hand does not appear to be influenced by traffic emissions, as seen in the time series plot comparing O_3 and NO_2 at the stations. Of all the rural stations, it was the only one to show a slight (1.88%) net increase in O_3 during lockdown, small enough and within the margin of error to be considered no change, and NO_2 remained constant throughout.

Further analysis of the data showed that the Dublin site, in addition to experiencing a 60% reduction in passenger vehicles, also had the same decrease in light goods vehicles, buses, and heavy goods vehicles. Monaghan had a 50% decrease in passenger vehicles, yet the number of LGVs, buses, and HGVs did not decrease. As these types of vehicles tend to emit more pollutants, this is a possible reason that there is no visible change in NO_2 levels measured at that station after lockdown.

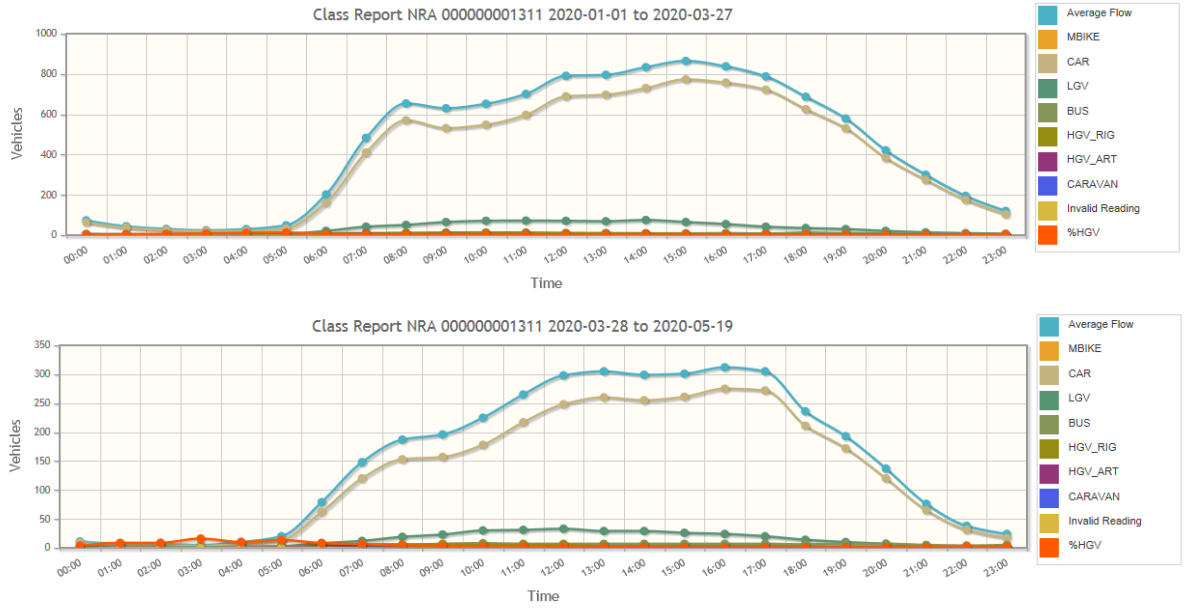

Figure 78 TII average vehicles/day by class before (top) and after (bottom) lockdown for N31 between Stillorgan and Rock Road, Blackrock, Dublin

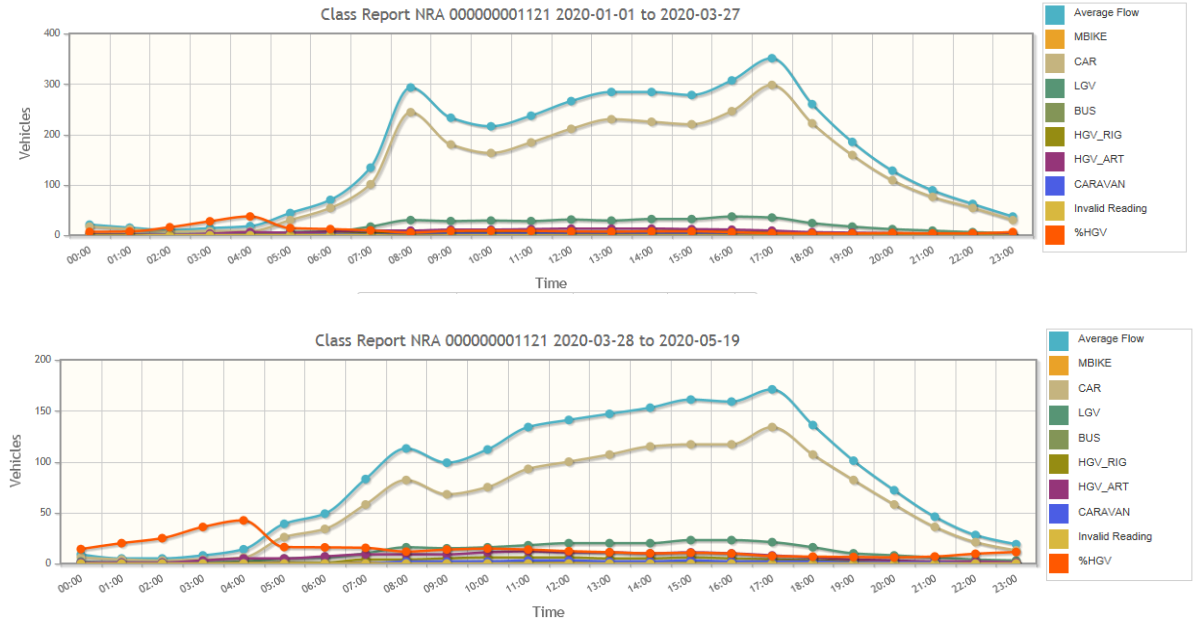

Figure 79 TII average vehicles/day by class before (top) and after (bottom) lockdown for N12 Armagh Road, Monaghan

6. Modelling

This chapter will describe on-going model related activities and present the initial findings. The first part will link model forecasts to the Covid-19 observations in the previous chapter, followed by a model validation section that explores possible reasons for the differences between models and measurements, also with an in-depth description of the models. The third section lays the groundwork for future inverse modelling by developing a method of data preparation.

6.1 Impact of Covid-19 Restrictions on Model Predictions

The previous chapter examined the impact of Covid-19 lockdown on in-situ observations, so in continuation of this, here the outcomes of model forecasts for this time period will be evaluated. NUIG's StreamAir application, which runs the WRF-Chem v4.15 forecast model (explained in more detail in section 6.2 with specifications listed in **Table 16**), has been collecting model outputs for several of the stations with real-time observations of ozone, nitrogen dioxide, PM10, and PM2.5, allowing for a comparison of model to measurements during different phases of lockdown. The model is running with "business as usual" emissions based on the TNO MACC III inventory (http://macc.copernicus-atmosphere.eu), and a reduction in emissions in measurements should lead to changes in the ratio between measurements and model. Additionally, data from the online Copernicus Atmospheric Monitoring System (CAMS) model, which runs a "lockdown" scenario with reduced emissions will be evaluated.

6.1.1 Comparison to NUIG StreamAir Model

There were no significant changes to the ratios of measurement/model PM10 and PM2.5, and a reduction in the NO_2 ratio in Cork city during lockdown, which is consistent with the results of the previous chapter where PM10 concentrations did not change compared to previous years and NO_2 was reduced by 26% in urban areas (see plots page 188 in Appendix C). The model predicts PM10 levels fairly accurately, and tends to under-predict NO_2, confirming that PM10 levels have likely not changed during the lockdown period, whereas NO_2 in the urban environment of Cork has decreased and now matches the model forecast more closely. Ballyfermot

is classified as a suburban background station, but the grid resolution of the model covers a larger area making the changes less evident. PM2.5 exhibits a slight reduction in the measured/modelled ratios after the full lockdown ends, although the ratios remain close to 1, as the model does predict the concentrations well.

Ozone measured/modelled ratios resulted in some unexpected changes during lockdown, which are more difficult to explain. The boxplot below shows the measured/modelled ratio of ozone for the various lockdown stages, and for all sites it can be seen that the ratio increases during the full lockdown. The previous section discussed how this is possible in urban/suburban areas due to the "weekend effect," however the rural stations tended to have the same, if not lower ozone compared to previous years. Oddly, the model begins to under-predict ozone at the remote sites about two weeks after full lockdown comes into effect (see plot page 189 in Appendix C).

This may be related to the proximity of the model boundaries to the stations, where the amount of initial pollutants is being fed into the model. Ozone also has a very complex chemistry in the atmosphere, with factors such as temperature, rate constants, and the disaggregation of volatile organic compounds within the model making it difficult to determine exactly what is affecting the model forecasts. Instead, in section 6.2 black carbon will be evaluated, as it is a non-reactive primary pollutant and its transport and deposition are better understood, allowing for focus on model inputs.

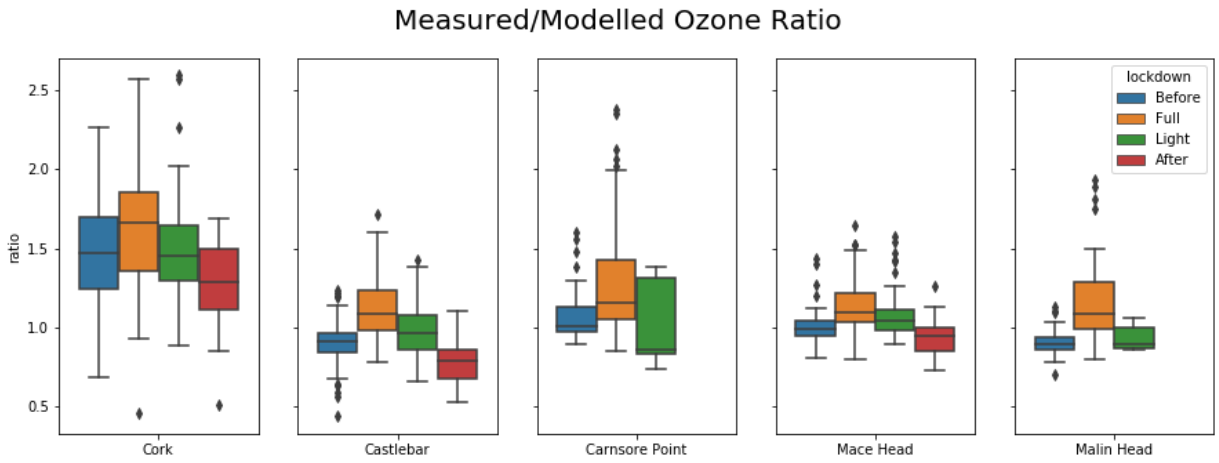

Figure 80 Measured/Modelled Ozone Ratios

6.1.2 Comparison to CAMS model

In order to see what changes occur in a model when reduced emissions are applied with all other inputs remaining the same, another model was examined. The Copernicus Atmospheric Monitoring Service [*CAMS*, 2020] has set up a webpage in support of the Covid-19 crisis, which includes a reduced emissions scenario of one of their forecast models for Europe. The chemistry transport model CHIMERE is being run by the French INERIS (Institut national de l'environnement industriel et des risques) since March with a “business as usual” and “lockdown scenario” emissions simulation based on country and sector specific reductions calculated by the Barcelona Supercomputing Center (BSC, Spain). CHIMERE is one of nine models in the CAMS Ensemble, which produces hourly air quality forecasts over Europe using the median values of all the models. Compared to the Ensemble forecast, CHIMERE tends to predict slightly higher ozone, but performs well in depicting regional distribution. The model is run on a spatial resolution of 0.1◦ on a domain covering 25W/30N/45E/72N with 9 vertical levels from the surface to 5000m. All CAMS models are routinely validated against in-situ and satellite observations, making them among the most accurate in the world.

Looking at the differences in ozone between the two CHIMERE scenarios for Carnsore Point, Mace Head, Malin Head, and Dublin over the lockdown period, a similar trend can be seen as in the previous chapter, where ozone does slightly increase in Dublin and decreases at the remote sites in the reduced emission

scenario. Due to difficulty in obtaining raw data, these ozone concentrations are estimates from a colour scale ±10µg/m^3, and are not sufficiently accurate to compare to observations, however the models appear to predict ozone more accurately in urban areas closer to emissions sources than at the rural stations, where measured ozone is consistently higher than the forecast. Due to grid resolution, model forecasts in urban areas will be closer to urban background levels such as a park or residential neighbourhood. The grid resolution may also impact the rural stations diluting the amount of ozone present across a large area.

Models all have their limitations, and constant progress is being made in improving them. This section was able to show that there were observable changes related to emissions during lockdown in the models, which mirror those in the actual observations. There are still unresolved issues in the NUIG model forecasts, and the next section will examine possible reasons for these.

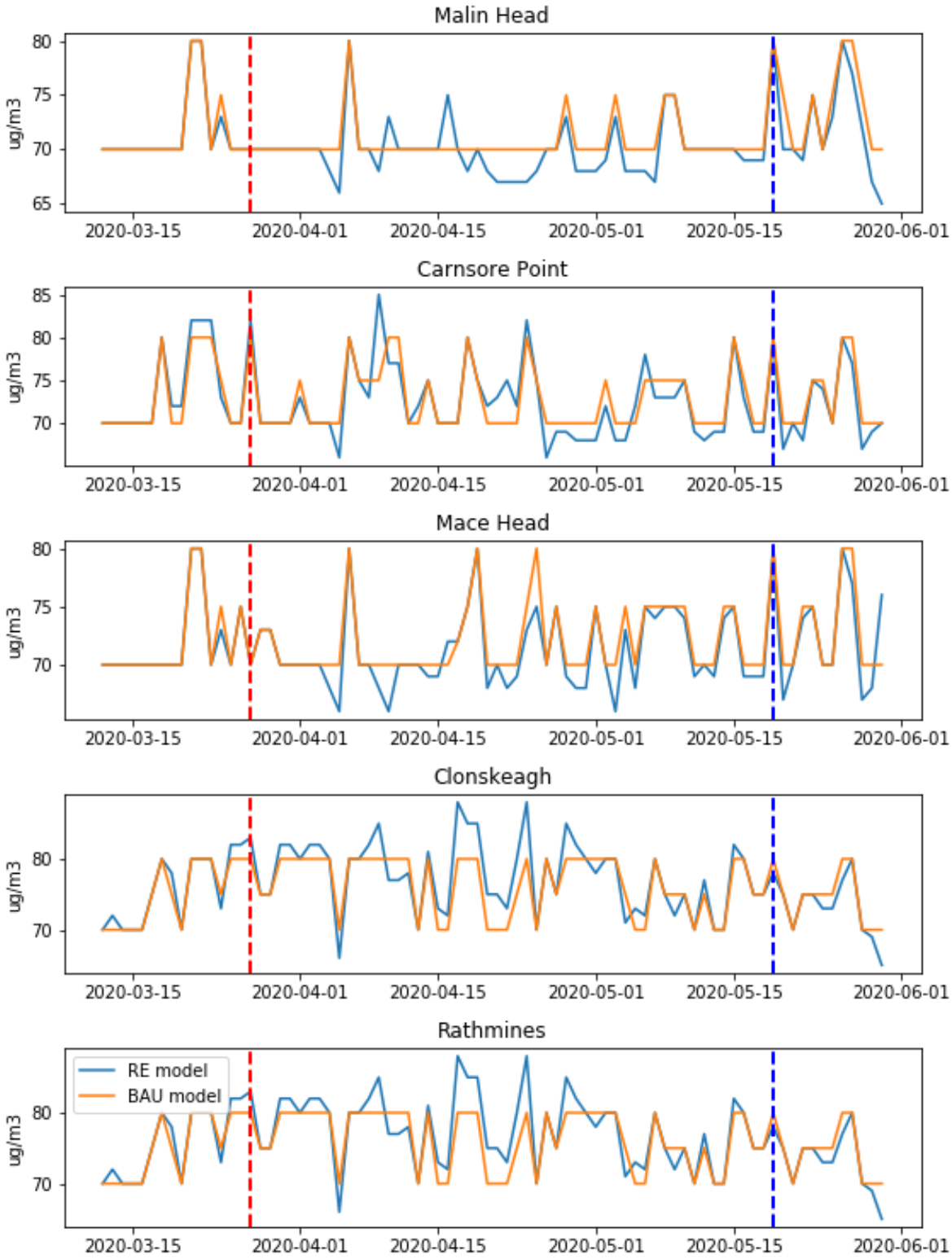

Figure 81 Daily ozone maxima of CHIMERE "business as usual" and "reduced emissions" model. Red vertical line is beginning of hard lockdown in Ireland, blue vertical line is beginning of lighter restrictions.

6.2 Forecast Model Validation

One benefit of actual measurements is the ability to validate models. NUIG recently launched its StreamAir application, using the WRF-Chem model version 4.15, with the aim of providing real-time air quality forecasts for Ireland. Many people with respiratory conditions such as asthma rely on these forecasts for health reasons, so it is important they are as accurate as possible. This section will compare the model output to the BC measurements at the stations. The process involved identifying and correcting several errors, which improved model performance. Additionally it was possible to obtain output data from a similarly configured slightly older WRF-Chem version 3.8.1 model with higher grid resolution, operated as the ManUniCast teaching tool (http://www.manunicast.com, also available as an iphone app and the first of its kind in the UK) by the University of Manchester [*Schultz et al.*, 2015], in order to compare the performance of the two models using the same emissions inventory for Ireland. A brief description of the emissions inventory and models follows.

Input data for both WRF-Chem models come from TNO (Netherlands Organisation for Applied Scientific Research), which are renowned for being among the best data available globally from the emissions inventories of individual countries but are still only estimates of emissions factors such as industry and transport with very high uncertainties of up to 300% [*Bond et al.*, 2013]. For Ireland, these estimates are reported as an annual mean in accordance with the Convention for Long-Range Transboundary Air Pollution (CLRTAP) and were most recently updated in 2019 as 1.66 Gg of total BC for 2017 according to the official reporting page at https://webdab01.umweltbundesamt.at/ which also includes a break-down by sector. As the availability of spatially resolved data for modelling is always somewhat delayed, the 2011 emissions inventory is the most recent one available, and thus being used in both models. A comparison of the 2017 to 2011 inventory showed an approximately 26% reduction in BC in the 6-year period.

WRF-Chem is the Weather Research and Forecasting model coupled to Chemistry, which is owned by the National Oceanic and Atmospheric Administration (NOAA) and freely available online at https://ruc.noaa.gov/wrf/wrf-chem/ with all

supporting documentation. It simulates the transport, mixing, and chemical transformation of trace gases and aerosols together with meteorology. The model parameters are defined in a NAMELIST file such as the ones in Appendix A and B for NUIG and Manchester WRF-Chem respectively. The key differences between the two models are summarized in **Table 16** below, followed by domain maps for each model.

Table 16 Differences between NUIG and Manchester University WRF-Chem models

	NUIG	**Manchester**
Model version	4.15	3.8.1
Coverage area	Western Europe	Mainly UK and Ireland
Grid resolution	25000m x 25000m	12000m x 12000m
Vertical resolution	30 (40 in v4.15)	45
Chemical Boundary Conditions	CAMS ECMWF-IFS	WACCM
Meteorological inputs	ECMWF	NOAA GFS
Start hour	12:00	18:00
Interval seconds	10800	21600
Restart interval	None	1440
Time step	120	60
Planetary boundary layer physics	YSU PBL scheme	Mellor-Yamada-Janjic PBL

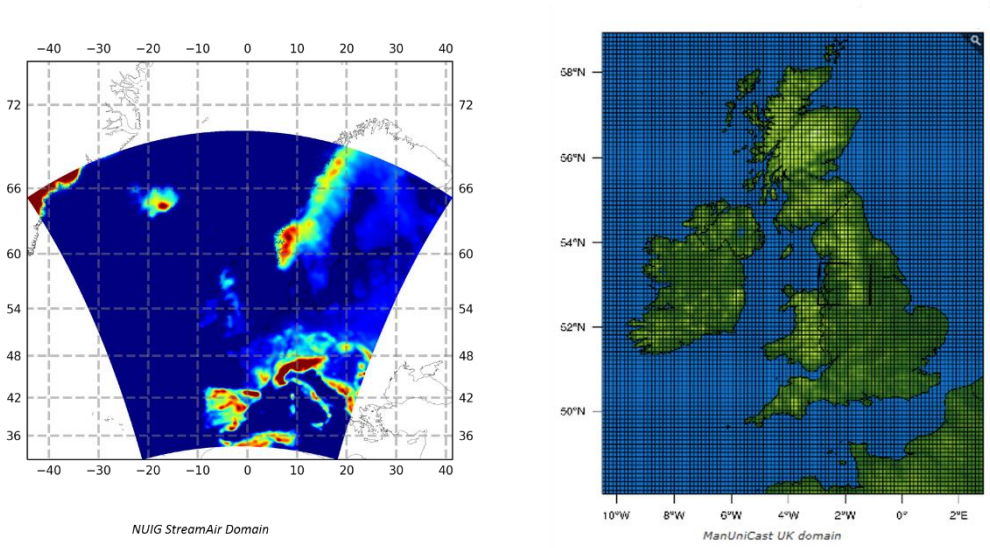

Figure 82 NUIG StreamAir and Manchester ManUniCast model domains (colour scheme in left image represents altitude above sea level, grid system in right image is 4km horizontal)

In the NUIG application, WRF-Chem runs on a 25km grid resolution covering most of Europe, as far East as the Czech Republic and as far South as Gibraltar, and uses the CRI (Common Representative Intermediates) mechanism coupled with the MOSAIC (Model for Simulating Aerosol Interactions and Chemistry) aerosol scheme and CAMS (Copernicus Atmospheric Monitoring Service) chemical boundary conditions to predict BC, organic carbon, chlorine, sodium, ammonia, nitrate, and sulfate in 8 size categories, as well as salt, NO_x, ozone, SO_2, PM10, and PM2.5 along with a wide range of meteorological parameters at one hour intervals. The TNO data are converted using a pre-processing algorithm similar to the one in [*Tuccella et al.*, 2012] which scales the annual emissions to monthly means and applies a seasonal adjustment factor which varies from country to country by region. For Ireland these scaling factors are displayed in **Figure 83** below, and are the same for PM10, PM2.5, and BC. These values were derived from a study by the University of Stuttgart, Germany (IER) as part of the GENEMIS (Generation and Evaluation of Emission data) project with the aim of providing more accurate seasonal variations in models [*Lenhart and Friedrich*, 1995], and when applied to the 2017 BC emissions in Ireland's Informative Inventory Report 2019 [*Duffy et al.*, 2019] do in fact show a distinct seasonal cycle linked to residential heating as demonstrated in **Figure 83**. The emissions categories are based on the EMEP/EEA Air Pollutant Emission Guidebook's Selected Nomenclature for Air Pollution (SNAP) as described by [*Kuenen et al.*, 2014] and shown in **Table 17**.

The same scaling factors are applied to Manchester's TNO input, making it easier to compare the models. Like NUIG, the Manchester model is also configured to use the CRI and MOSAIC modules but obtains its chemical boundary conditions from the Whole Atmosphere Community Climate Model (WACCM, https://www2.acom.ucar.edu/gcm/waccm), rather than CAMS. Meteorological inputs for Manchester come from the NOAA GFS Global Forecasting System, whereas NUIG uses the ECMWF. While it uses a one-way nested domain structure for weather forecasting, consisting of a 20km grid covering most of Europe and a 4 km grid over the UK and Ireland, the air quality forecasts for Manchester are based on a single domain of 12 km square grids covering the UK, Ireland, North Sea, and parts

of France, the Netherlands, and Germany, which is nearly double the resolution of the NUIG model over a smaller area. It also produces forecasts for 45 vertical levels, compared to NUIG's 40. The other major feature in which the models differ is the planetary boundary layer conditions, with NUIG using the YSU PBL scheme and Manchester the Mellor-Yamada-Janjic (MYJ) scheme. Some modifications were made to the Manchester model by [*Archer-Nicholls et al.*, 2014] which include adding a reduced version of CRIv2-R5 using the Kinetic Pre-Processer (KPP) interface, adding N_2O_5 heterogeneous chemistry to the existing MOSAIC framework, and allowing for primary organic aerosol to be included in sea-spray aerosol.

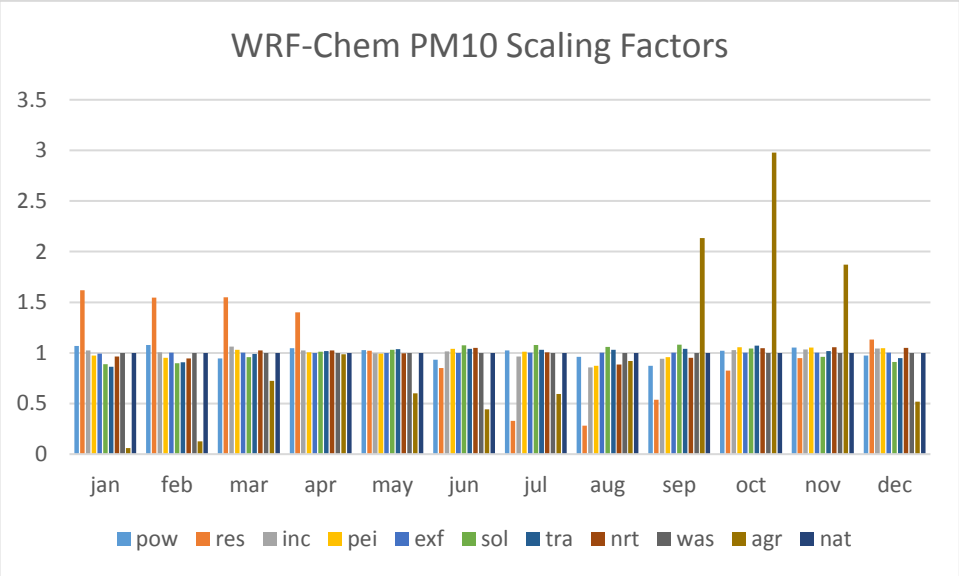

Figure 83 WRF-Chem PM10 Monthly Scaling Factors for Ireland

Table 17 SNAP sectors according to Kuenen et al. 2014 with corresponding abbreviations for Fig 83

SNAP	Sector name	
1	Energy industries	(pow)
2	Non-industrial combustion	(res)
34	Industry (combustion + processes)	(inc)
5	Extraction and distribution of fossil fuels	(exf)
6	Product use	(pei)
7	Road transport	(tra)
8	Non-road transport and other mobile sources	(nrt)
9	Waste treatment	(was)
10	Agriculture	(agr)
		(nat – natural)

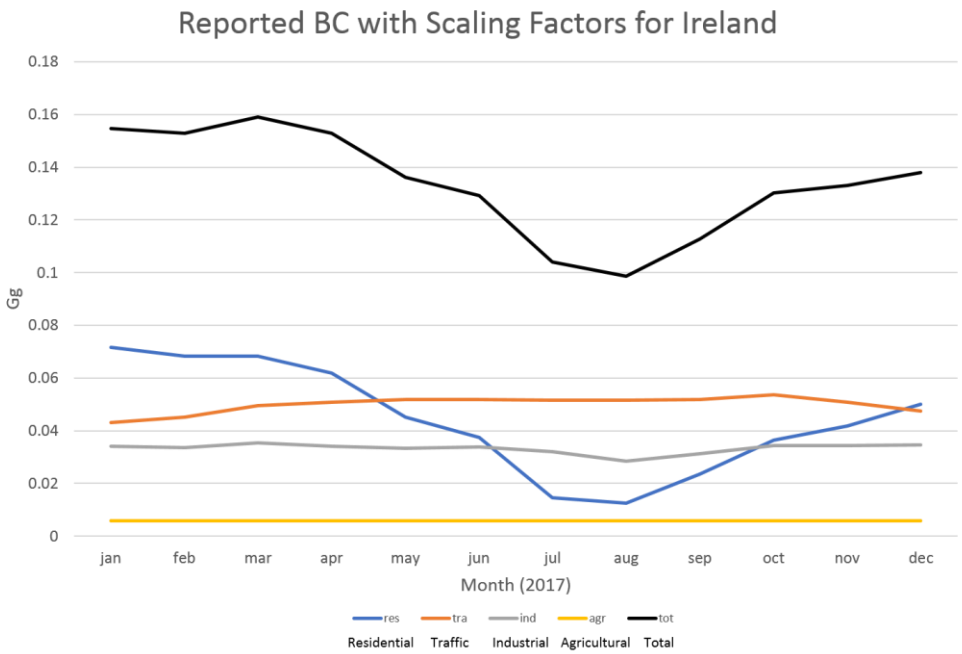

Figure 84 Seasonal variation of reported 2017 BC data with GENEMIS factors applied

As NUIG went through several iterations of WRF-Chem configuration, only limited data are available for the stations. Meanwhile, at the same time that NUIG switched to the newer WRF-Chem version 4.15 model, Manchester University began collecting their model output data for the Irish stations. The results are plotted below, showing that the NUIG model forecast for BC is consistently higher than Manchester's.

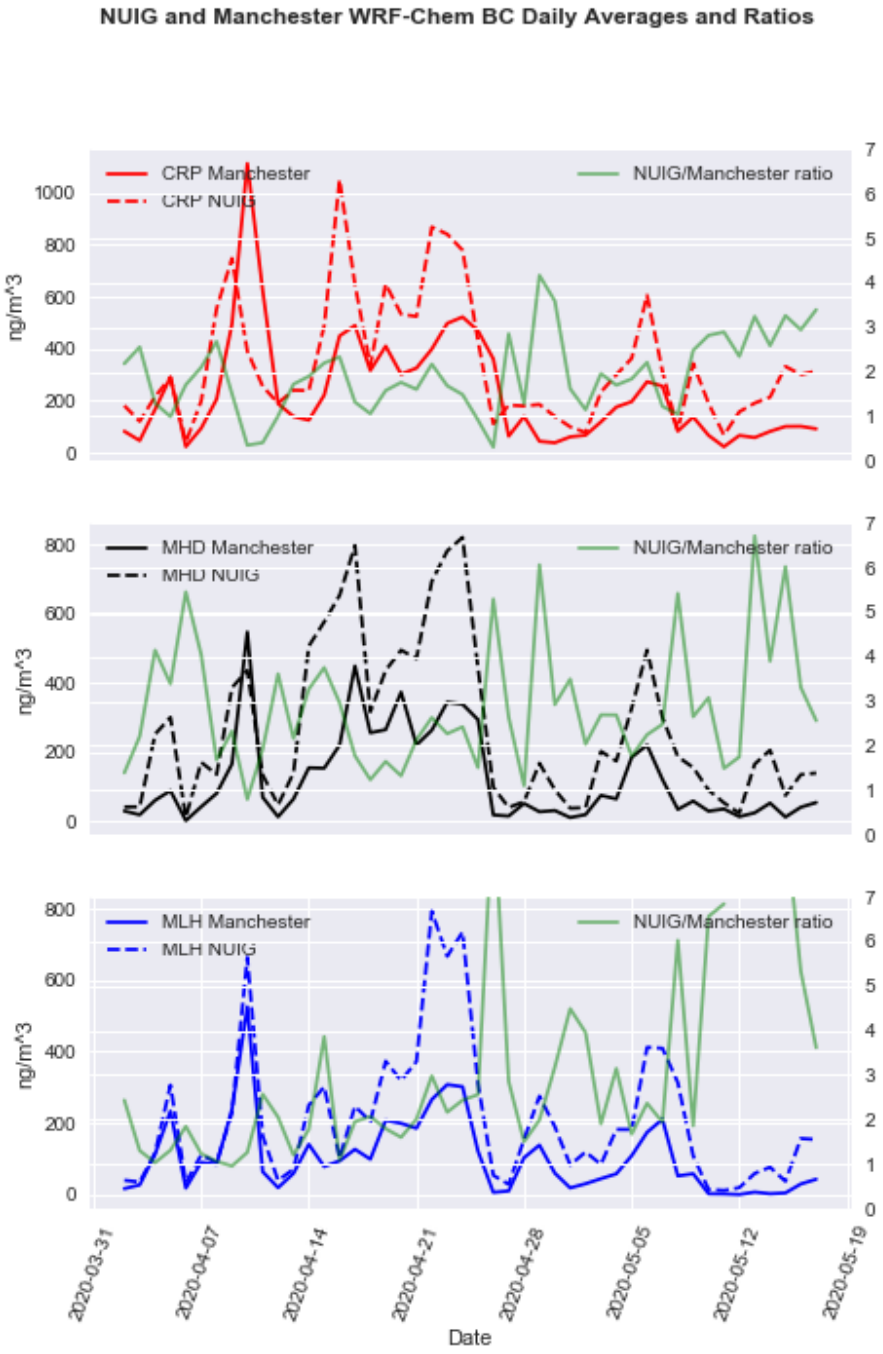

Figure 85 NUIG and Manchester WRF-Chem comparison

Looking at the wind speed and wind direction forecasts, both WRF-Chem models match the actual measured wind direction very closely despite different meteorological inputs, however the NUIG model tends to over-predict wind speed by an average factor of 1.36, whereas the average ratio of Manchester to actual wind speed is 0.98. A study by [*Brunner et al.*, 2015] found in their model inter-

comparison that the WRF-chem models tended to over-predict surface wind speed, especially in coastal areas and at lower wind speeds. Higher model forecast wind speeds would normally result in under-prediction of BC, as it would increase the rate of dispersion and mixing, so it is unlikely that wind speed or direction are the reason for the difference between the NUIG and Manchester models. Other meteorological parameters such as relative humidity, temperature, and sea level pressure matched well in both models and were consistent with actual surface conditions at MHD, indicating that the choice of meteorological inputs did not affect the output.

When comparing MHD measurements to both models, Manchester forecast BC is on average 29% higher than the measured BC. Given that BC emissions have been reduced by 26% between 2011 (the year of the model input inventory) and 2017, and the possibility of further reductions in BC concentrations between 2017 and 2020, especially since Covid-19 lockdown restrictions may be affecting the measurements now, this appears to be the most accurate possible forecast. NUIG's model, on the other hand, still forecasts an average 3.38 times the actual BC at MHD during pollution events, almost as much as it did in the original model without wet deposition. Comparing NUIG's model to the measurements before the Covid-19 lockdown showed almost 1:1 agreement during periods of clean air, which dominated during this time, but the forecast for the pollution event was again 3.4 times higher than measured. Even taking into account the reduction in emissions over time, this level of over-prediction indicates that there is still an unresolved issue affecting the BC forecasts in the NUIG model.

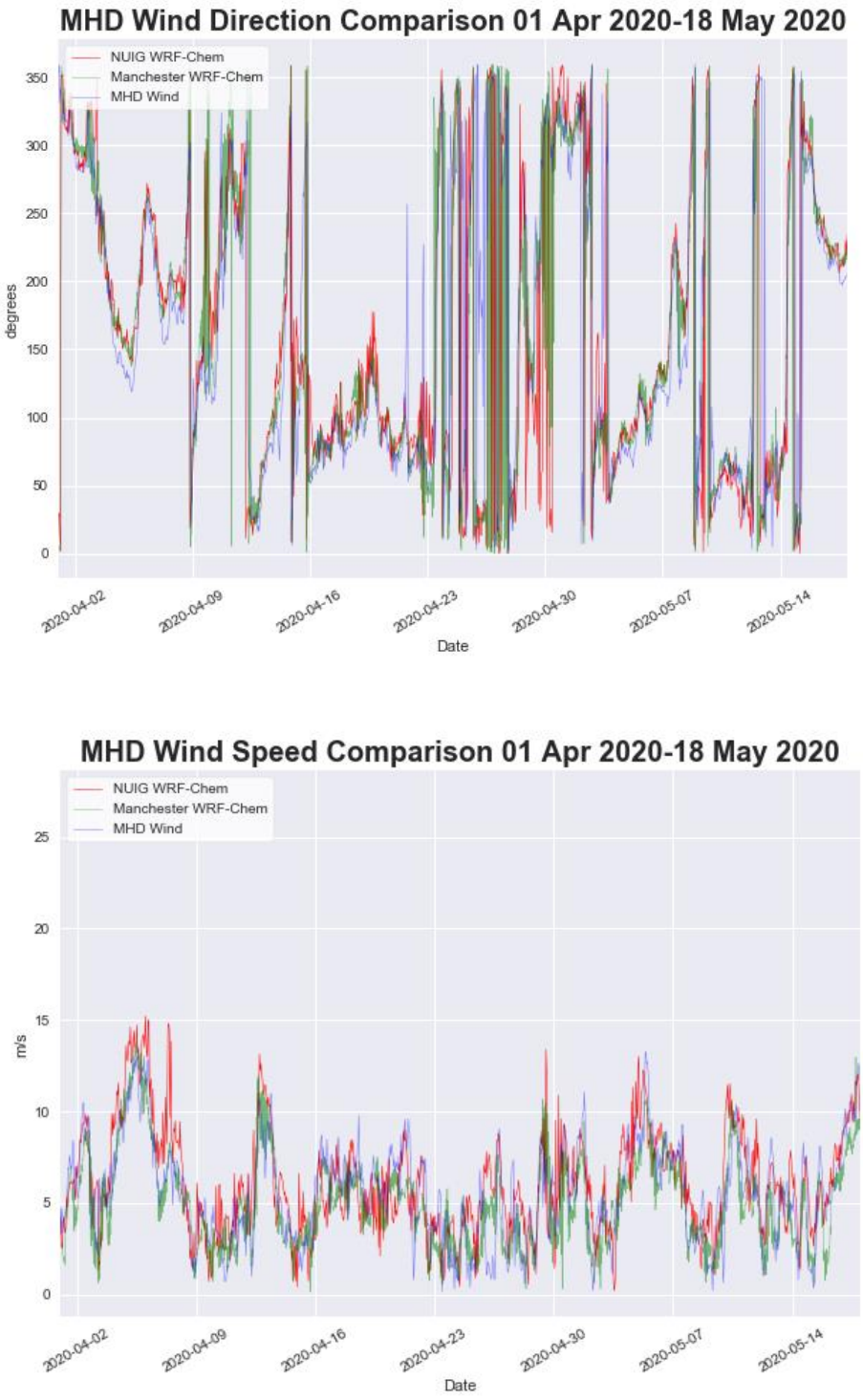

Figure 86 MHD wind direction (top) and wind speed (bottom) comparison with WRF-Chem models in hourly averages

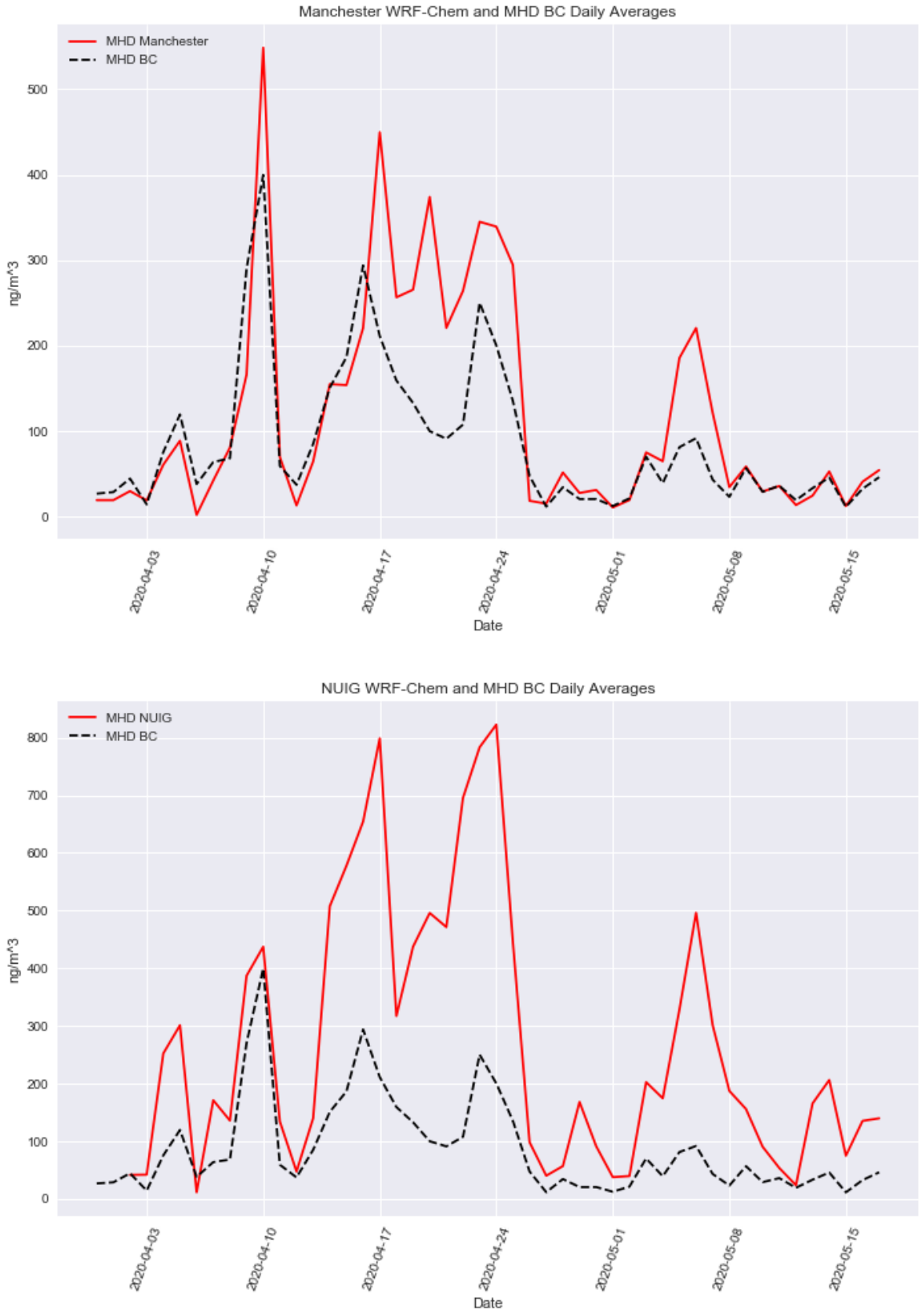

Figure 87 MHD BC compared to Manchester WRF-Chem (top) and NUIG WRF-Chem (bottom)

Model resolution may be a factor, both horizontally and vertically, as Manchester has a higher resolution than NUIG. However, studies such as [*Aligo et al.*, 2009] demonstrated that higher vertical resolution did not necessarily improve model forecasts, particularly for rain, which is the major sink for BC in the atmosphere. Indeed, it often caused the models to over-predict rain, which would lead to lower levels of BC, and is contrary to what is seen in the case of MHD.

Forecasting the amount and frequency of precipitation is a challenge using models. [*Mooney et al.*, 2016] tested the influence of different land surface, radiation physics, microphysics, and cumulus schemes on precipitation forecasts of WRF-Chem models for the British Isles. They found that of these options, land surface had the greatest impact, with the Noah scheme used by both NUIG and Manchester showing the largest over-predictions of precipitation, particularly in the summer, when convective activity is highest. The data available for comparison here are from April 2020, during which time no convective activity occurred at MHD. Comparing Manchester and NUIG rain forecasts to actual measurements, it is evident that both models under-predict rainfall amount over 0.5mm, although they tend to over-predict it at times when measured precipitation is less than that. The models also over-predict the frequency and duration of rain events, which the NUIG model does more often. While the comparison of precipitation forecasts to BC does show a drop in BC concentrations after a rain event, it is possible that BC forecasts are lower because of the wind direction, as both rain and clean air masses arrive from the west at MHD. Given the limited time period available, and that it is only for one coastal station, there is not enough information to draw conclusions from, and further evaluation will be necessary.

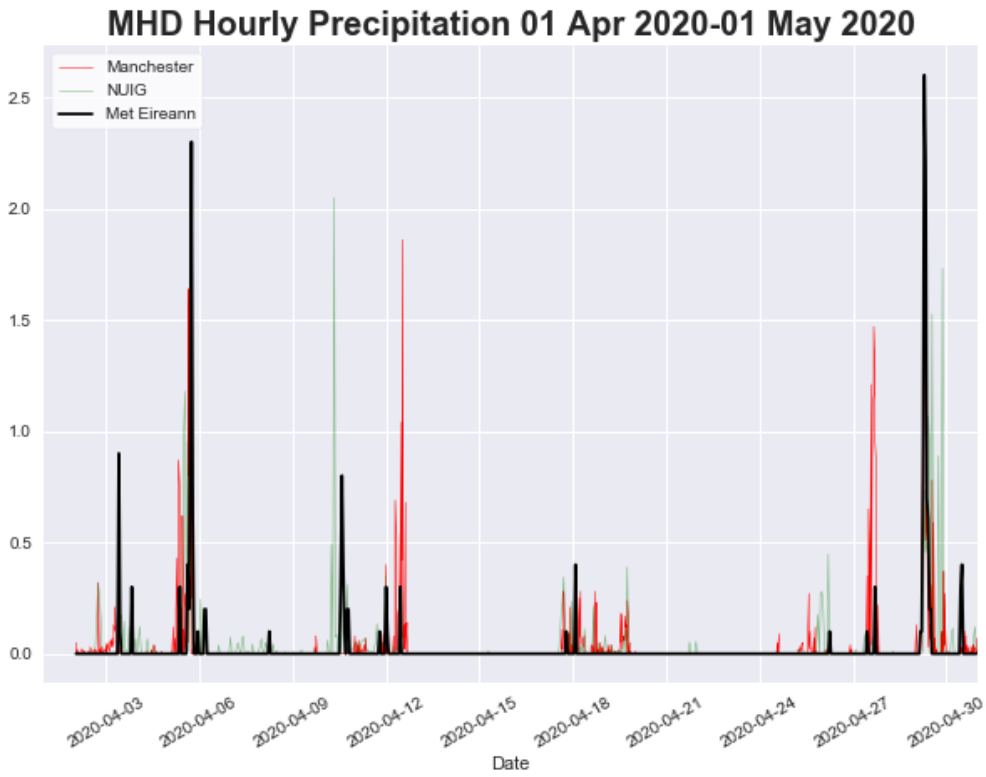

Figure 88 MHD hourly modelled and measured rainfall

A study by [*Banks and Baldasano*, 2016] examined how four different planetary boundary level (PBL) schemes impacted air quality forecasts in Spain. Two of these, the Yonsei University (YSU) and Mellor-Yamada-Janjic (MYJ) schemes are the ones being used by NUIG and Manchester respectively. All four schemes predicted a lower boundary layer than the lidar measured, and of the four, the YSU scheme was the lowest with nearly 50% lower daytime maximum. The MYJ scheme fared only slightly better. Under-predicting the boundary layer can significantly affect the aerosol concentration forecasts, as they will be less diluted in a smaller area. The study only examined ozone, NO_2, and PM10 as air quality indicators, and found the forecasts for PM10 to be least accurate when compared to measurements at urban, suburban, and rural stations, though in this case the model under-predicted the PM10 in every situation. Nevertheless, these results could be regionally dependent, as [*Hu et al.*, 2019] found the YSU scheme to outperform the MYJ scheme in predicting the boundary layer for Dublin.

Finally, the differences could well be related to the chemical boundary conditions used in the two models. Both models use real-time chemical transport models as a basis for their boundary conditions, as opposed to set values, which should lead to improved model forecasts as indicated by [*Akritidis et al.*, 2013]. The WACCM used by Manchester produces forecasts every 6 hours and is driven by meteorological fields from the NASA GMAO GEOS-5 model and include anthropogenic emissions from the Community Emissions Data System (CEDS) inventory for the year 2014 [*Hoesly et al.*, 2018], which are used for the most current CMIP6 (Coupled Model Inter-comparison Project phase 6). These global files are gridded at 0.9x1.25 degrees with 88 levels (https://www.acom.ucar.edu/waccm/download.shtml). NUIG is using the regional CAMS-IFS (Integrated Forecasting System) Reanalysis dataset [*Inness et al.*, 2018], which is the latest version covering the years 2003-2016 over Europe. It incorporates meteorological inputs from the ECMWF, as well as the Carbon Bond 2005 (CB05) chemistry scheme from the Tracer Model 5 (TM5) global chemistry transport model [*Huijnen et al.*, 2010] in conjunction with satellite data for NO_2, ozone, and aerosol optical depth (AOD). It has an 80km horizontal resolution and 3-hour temporal resolution, with 60 vertical levels. Anthropogenic emissions for this model come from the MACCity inventory [*Lamarque et al.*, 2010] used in the older CMIP5. The major distinction between CEDS and MACCity is that CEDS, in addition to better temporal resolution, is able to capture trends in fuel use, technology, and emissions controls over time by matching default estimates to specific inventories and scaling them to produce a consistent historical time series, which also allows for extrapolation of data for more recent years where no information is yet available.

As both WACCM (using the parameters described above) and CAMS (using an ensemble of 9 regional models) offer online forecasting systems based on their boundary conditions, a comparison was made between these two models for 17 April 2020, along with the corresponding outputs from ManUniCast and StreamAir. On this day, the wind was predominantly from the southeast bringing BC to Mace Head across Ireland from the southern UK and mainland Europe, and would continue until 23 April, leading to the elevated BC concentrations measured at the

station during that period. At 18:00 UTC on 17 April, the measured BC at MHD was 0.24µg/m^3 with a daily average of 0.3µg/m^3. As can be seen in the illustrations below, both WACCM and CAMS predict similar patterns of elevated BC between 0.4-0.5µg/m^3 for WACCM and 0.5-0.7µg/m^3 for CAMS over Mace Head, which translates into model outputs of between 0.5-0.7µg/m^3 and 0.7-1µg/m^3 for ManUniCast and StreamAir respectively when applying TNO emissions specific to Ireland.

To investigate this further, the 14th of May, a day with clean background air was selected, when the dominant wind was from the north at MHD, and a HYSPLIT back trajectory [*Stein et al.*, 2015] showed the air mass had not crossed land in the previous three days. On this day ManUniCast agreed with the actual measurements of 0.05µg/m^3 of BC at MHD, whereas the NUIG model predicted over 0.2µg/m^3. The CAMS model predicted about 0.5µg/m^3 at MHD that day, while WACCM forecast about 0.02µg/m^3. As indicated in a study by [*Samaali et al.*, 2009], initial chemical and lateral boundary conditions can have a profound impact on regional air quality forecasts. The differences between the chemical boundary conditions may therefore be the cause of the discrepancy between the two WRF-Chem models, with WACCM being a global model applied to the small domain over Ireland and the UK by ManUniCast and CAMS being a regional scale model for Europe, applied to an almost identical domain in the NUIG model, where the lateral boundaries are much closer to Ireland.

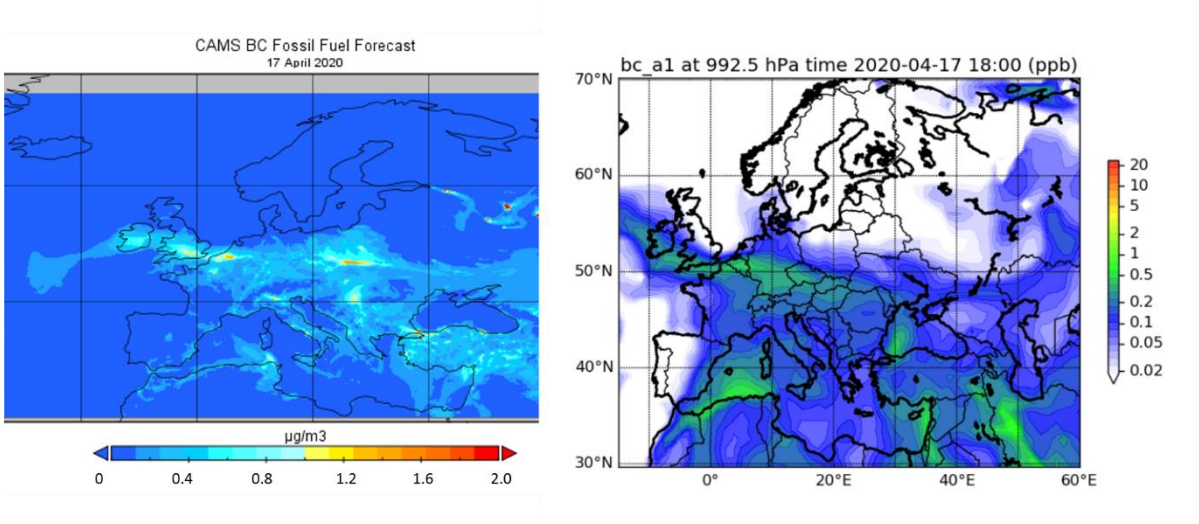

Figure 89 CAMS (left) and WACCM (right) forecast model output for BC on 17 April 2020 (zoomed in over Europe for WACCM)

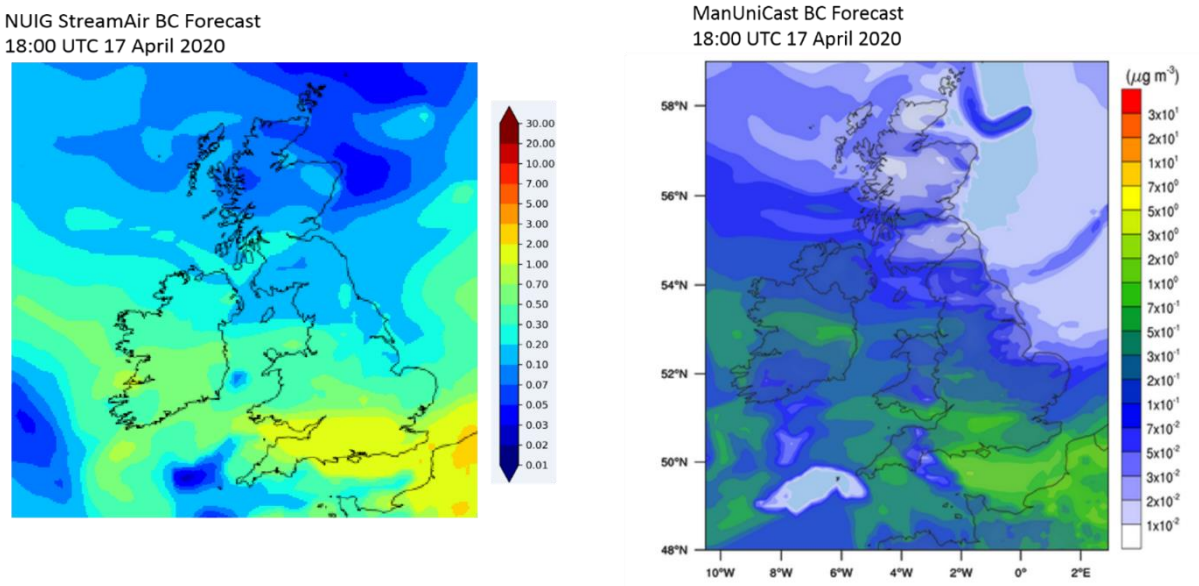

Figure 90 StreamAir (zoomed in over UK and Ireland) and ManUniCast BC forecast for 18:00 on 17 April 2020

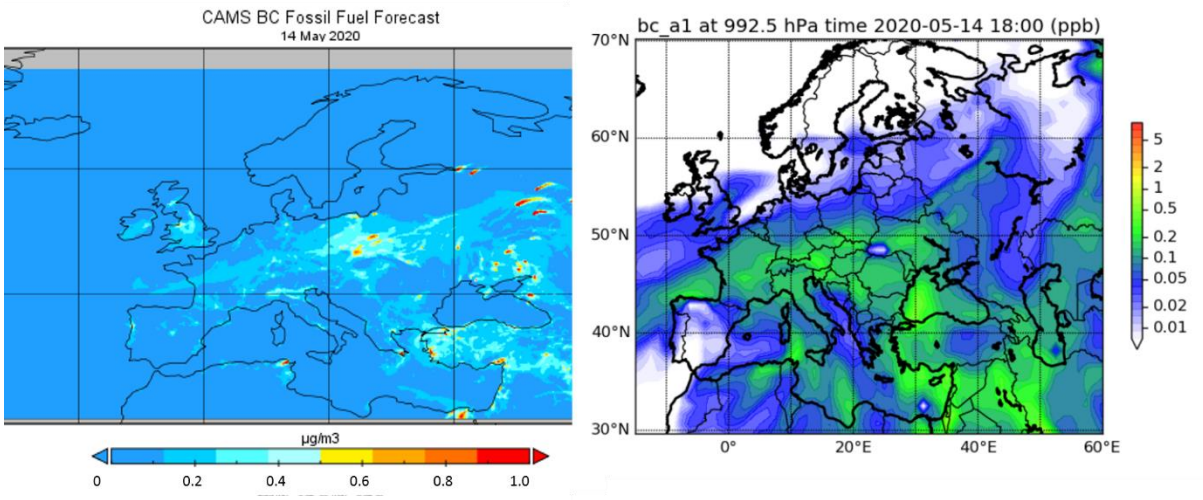

Figure 91 CAMS (left) and WACCM (right) forecast model output for BC on 14 May 2020 (zoomed in over Europe for WACCM)

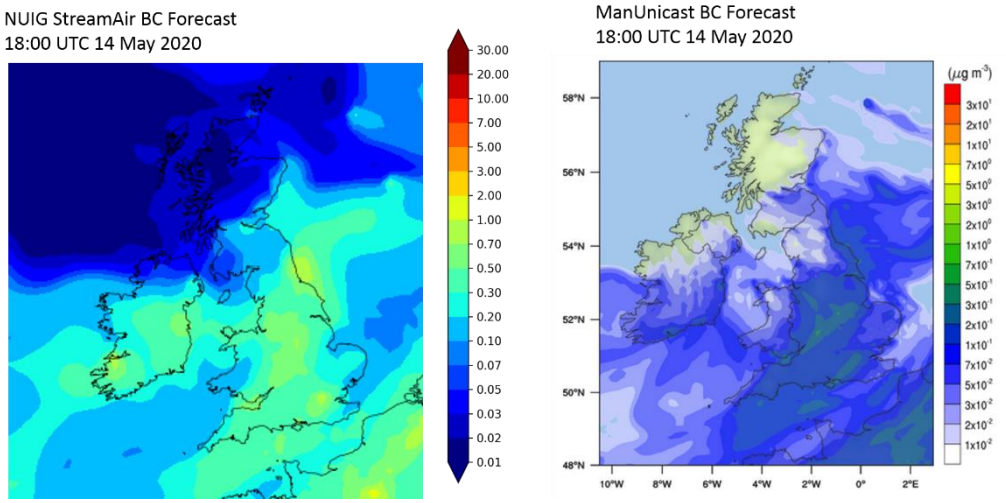

Figure 92 StreamAir (zoomed in over UK and Ireland) and ManUniCast BC forecast for 18:00 on 14 May 2020

Based on this model inter-comparison, it appears that the chemical boundary conditions may be the primary cause of the discrepancies between the models, but any of the other factors discussed could be acting either individually or in combination to cause the differences in outputs. In order to isolate these factors, further investigation in the form of sensitivity tests is required to optimize the NUIG model and obtain the best possible air quality forecasts. The network and the measurements it can provide is therefore essential not only to help validate forecast predictions affecting air quality and climate but will eventually provide valid data for more accurate emissions inventories.

6.3 Preparation for Inverse Modelling

As shown previously in the section on transboundary pollution, one of the key features of a network with stations along the borders of the country is the ability to monitor incoming and outgoing pollution. Ideally, it would be possible to track this pollution not only to a source region, but to very specific point sources. This will require sophisticated models, which take the measured data from the stations as inputs and calculate how much of a particular substance is coming from where—a technique known as inverse modelling. It works backwards from the receptor point using meteorological data and what is known about atmospheric chemistry to trace the origin of the species of interest.

Inverse modelling has been used in a variety of ways to study trace gases and aerosols in the atmosphere, and many different models exist already. A study by [*Alexe et al.*, 2015] compares four different inversion models using the same emissions data for Europe, both bottom-up (emissions inventories) and top-down (direct measurements). The four models used were TM5 [*Meirink et al.*, 2008], LMDZ [*Hourdin et al.*, 2006], TM3 [*Trusilova et al.*, 2010], and NAME-INV [*Jones et al.*, 2007]. Both TM5 and LMDZ used the 4DVAR (4 dimensional variability) application to minimise a cost factor, and TM3 employed the STILT (Stochastic Time-Inverted Lagrangian Transport Model) for finer scale resolution. NAME-INV was run using meteorological data from the UK Met Office, unlike the other models which used variations of the European Centre for Medium-range Weather Forecasts (ECMWF).

The study used two Lagrangian (NAME-INV and TM3-STILT) and two Eulerian (LMDZ-4DVAR and TM5-4DVAR) models. Lagrangian models track a parcel of air over a period of time, whereas Eulerian models iteratively model conditions at a set location.

Apart from being completely different algorithms, the models differ in grid resolution, vertical resolution, and meteorological inputs. While three out of the four models use ECWMF based met data, the format and how it is applied varies for each model.

In this study the NAME model consistently reported lower emissions than the other three models, but was closer to the IPCC estimates. This could be due to a different meteorology input than the other models, or because NAME included oceans and seas as potential sources, while the other models did not.
It is interesting to note that none of the models produced even remotely similar results, even when run using identical data inputs, meaning that there are still too many unknowns. The study concluded that a denser measurement network in addition to improved models would be required in order to obtain more consistent results.

Despite some model inconsistencies, the successful implementation of inverse modelling using measured data of GHG emissions in the UK [*Ganesan et al.*, 2015] and Netherlands [*Vermeulen et al.*, 1999] suggests that such an approach would be applicable to Ireland as well. Using a similar inversion model such as the NILU (Norsk Institutt for Luftforskning) Flexinvert [*Thompson and Stohl*, 2014; *Thompson et al.*, 2015] in conjunction with the measured data from ICOS is a viable option for obtaining more accurate emissions estimates for Ireland. This is a simple box model which determines source/receptor relationships (SSRs) based on concentration changes at the receptor. Flexinvert has been tested against the results of [*Bergamaschi et al.*, 2015], and compared favourably [*Thompson and Stohl*, 2014], as demonstrated in **Table 19**. Of course the model's resolution depends on the number of receptors, i.e. measurement stations, which implies that more stations are needed for greater accuracy, however for a start it is possible to gain a greater insight into Ireland's GHG emissions using the three existing stations.

Table 18 Thompson and Stohl (2014): Comparison of CH4 emissions (TgCH4 year−1) from this study with the range of values from an inversion ensemble for 2006 and 2007 (Bergamaschi et al., 2014). The prior and posterior emissions are shown from test S1 and include the 1SD prior and posterior uncertainties. NW Europe includes the UK, Ireland, the BENELUX, France, and Germany. E Europe includes Hungary, Poland, Czech Rep. and Slovakia, according to the definition of Bergamschi et al, 2014.

	Prior	Posterior	Bergamaschi et al. (2014)
UK + Ireland	2.66 ± 0.84	2.41 ± 0.33	2.32–4.57
BENELUX*	1.18 ± 0.80	1.09 ± 0.26	1.44–2.29
France	4.33 ± 1.37	3.14 ± 0.42	2.02–4.94
Germany	2.22 ± 1.16	2.48 ± 0.33	2.35–3.51
NW Europe	10.39 ± 4.17	9.12 ± 1.34	8.13–14.44
Hungary	0.37 ± 0.62	0.50 ± 0.17	0.34–0.73
Poland	2.81 ± 1.05	2.62 ± 0.38	1.84–2.87
Czech Republic + Slovakia	1.18 ± 0.94	1.27 ± 0.27	1.12–1.63
E Europe	4.36 ± 2.61	4.39 ± 0.82	3.59–4.90
NW + E Europe	14.75 ± 4.17	13.51 ± 2.16	11.71–19.34

Already inverse modelling is being used as part of the IMPLiCIt (IMProving inversion modeL Capability in Ireland) project to obtain a national top-down emissions inventory for greenhouse gases such as carbon dioxide and methane in Ireland, by means of the FLEXINVERT model as described in [*C O'Dowd et al.*, 2019]. In this project, methane emissions sources (fluxes) were modelled based on measurements from several European monitoring stations (receptors), including Mace Head, Malin Head, and Carnsore Point for the year 2012. The results of using the actual measurements were 30% higher than those predicted by the model using a priori data from bottom-up estimates. Given its effectiveness so far, it is hoped that this model can be applied to black carbon as well. Previous studies such as [*P Wang et al.*, 2016] have successfully used inverse modelling on BC data and found the levels of it in China to be 1.8 times higher than predicted by bottom-up estimates. These models perform best when supplied with large amounts of data from multiple receptors (in this case monitoring stations), and the AC^3 Network will be able to provide these inputs.

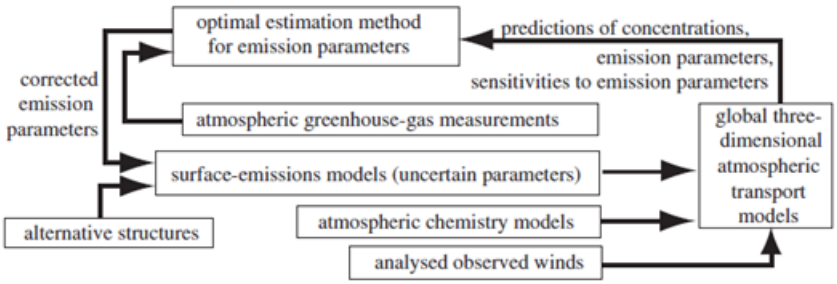

Figure 93 Schematic diagram of the FLEXINVERT system that combines observations, a priori and background information and model sensitivities to provide CH4 surface flux estimates. Source: IMPLiCIt Report, O'Dowd 2019

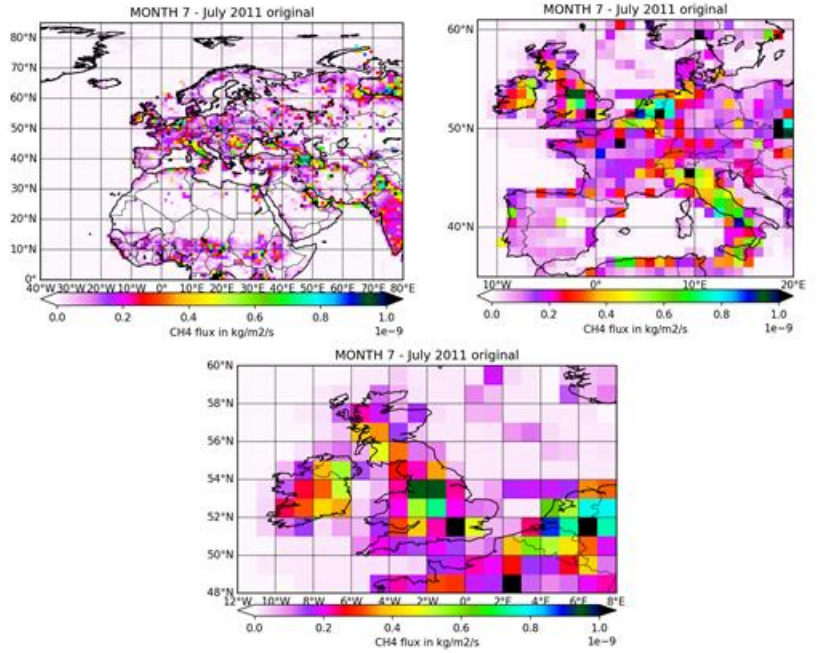

Figure 94 Example of a plot of the EDGAR 1.0x1.0_NAT created using FLEXINVERT which includes both anthropogenic and natural CH4 sources, over a wide domain (top) and zoomed into the European domain (bottom). Source: IMPLiCIt Report, O'Dowd 2019

To maximise the capability of the network, modelling techniques will be used to show how pollution is transported into and across the country from station to station. The models currently available are still quite limited in their spatial resolution, and thus require smooth datasets which do not include local sources or "spikes," which when averaged would give an inaccurate representation of the actual regional influence. This is a complex task as previous studies have shown that different methods and different control inputs can make a significant difference in the outcome. Most of the studies to date have relied on daily or even monthly data

as model inputs, however, this makes it impossible to see the daily variations in certain species such as BC.

In preparation for modelling BC transport, a statistical algorithm using the standard deviation of the background (SD) method described by [*El Yazidi et al.*, 2018] has been applied to some of the AE33 data from Malin Head, the station most affected by local influences. It involves selecting a background mean of several hours or days and removing data points that fall outside a set number of standard deviations of this mean. This method has been proven to be most effective for spike removal of local sources in other studies as well. As local spikes in BC are assumed to be short-lived, the one-minute data from the instrument are used to conduct this analysis, however, for future model inputs these data will be averaged to one hour to reduce the volume of data and further smooth the input without sacrificing too much on accuracy. The goal was to find the smoothest representation of regional background concentrations without removing too many data points or actual valid peaks not connected to local sources. This was done using Python Pandas to generate a rolling mean of black carbon for a given time interval, and then filtering out data which falls outside a set number of standard deviations of the mean. By varying the time window and standard deviation inputs to the algorithm as shown in **Table 20**, it was found that a three-day time window provided the best estimation of the average regional background, with peaks above 2 standard deviation of the background average excluded. This involved removing only 7% of the data points, and cut out the most noise, whereas higher standard deviations kept more of the extreme values, and longer time windows excluded what appear to be valid data. The results of this are shown in the plots below for a period of regional pollution in April 2018. The top plot uses a 3-day time window for the background average, removing points greater than 2 standard deviation. By contrast the bottom plot is of the same dataset using a one-week window and eliminating points higher than 1 standard deviation. Note the difference particularly around 4 and 9 April, where the second plot removes several points that are part of a definite regional pattern. Although there are still a few smaller

spikes in the one-minute data, these will be smoothed once the data are averaged to one hour without causing a significant increase to the concentration.

El Yazidi et al. also applied the SD method to data between the first and third quartile of their background averages (50% of data) and found it in their case to yield even more accurate results. This was not the case when applied to the BC data, as the background averages for any time window at the coastal station were very low and the regional pollution exceeded three times the standard deviation of the background, causing the algorithm to cut out the majority of data. This experiment shows that the spike removal algorithm will vary not only by species, but by station/location, and further fine-tuning of the models and algorithm on a case by case basis in future will be necessary to achieve the most accurate results.

Table 19 Percentage of data points removed (%rem) and BC average (avg) by background time period and standard deviation on MLH data from 4-11 April 2018

1 min avg 283 ±372	**1 std dev**		**2 std dev**		**3 std dev**	
	%rem	**avg**	**%rem**	**avg**	**%rem**	**avg**
1 day	16	225 ±235	6	245 ±255	2.5	262 ±279
3 days	18.5	194 ±180	7	235 ±238	3.3	254 ±263
1 week	23	169 ±149	8	228 ±227	3.6	250 ±255

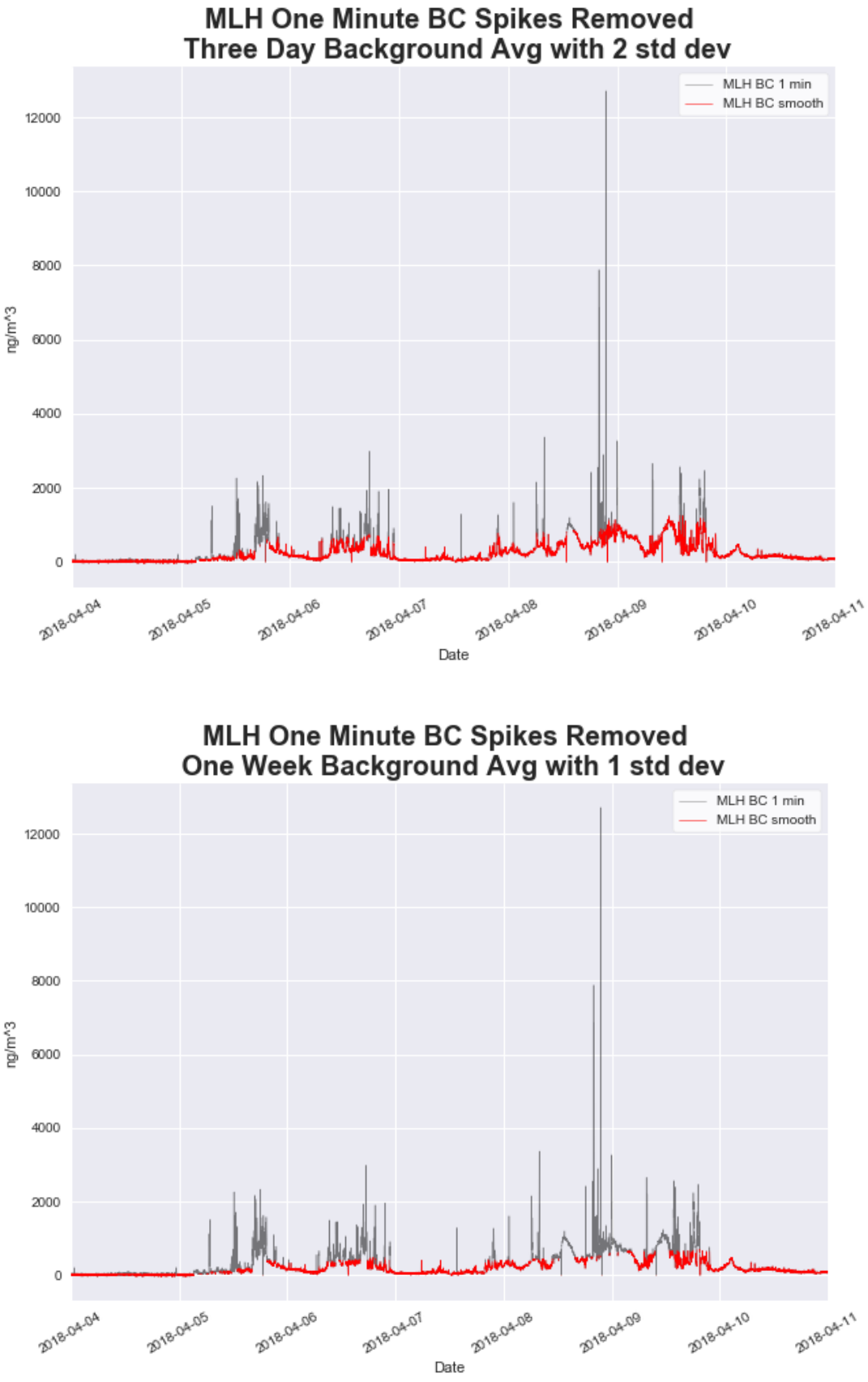

Figure 95 MLH spike removal example

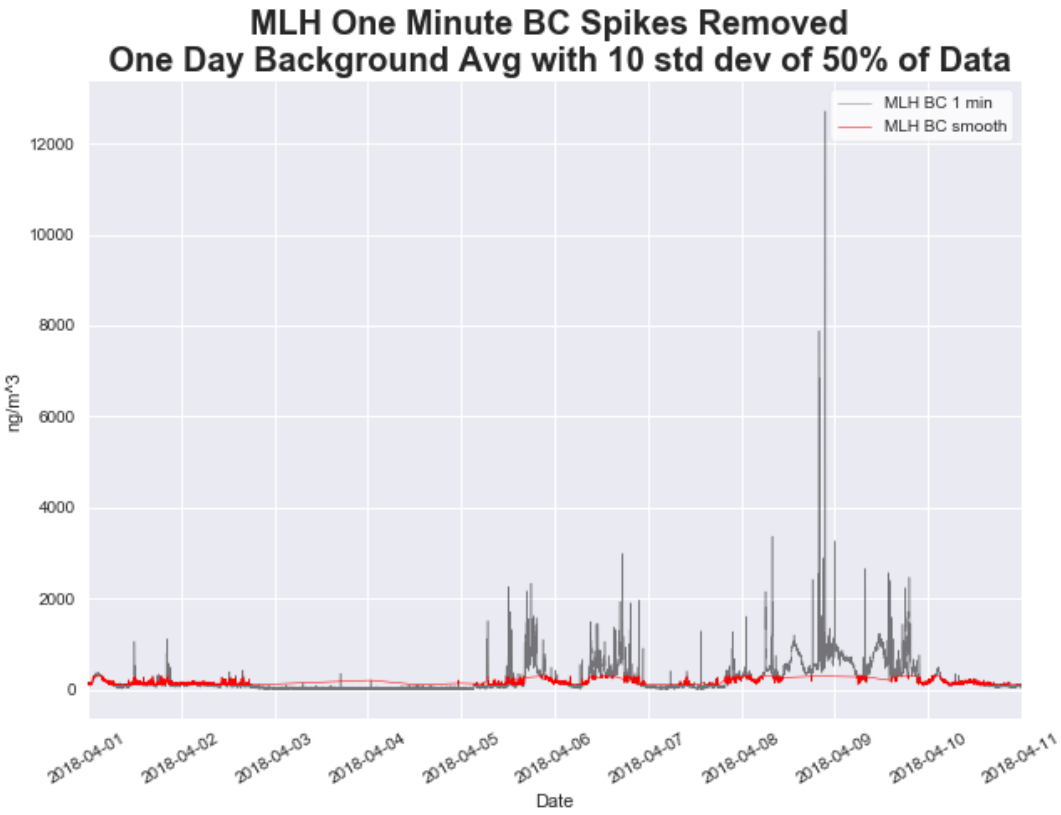

Figure 96 Spike removal using only data between the first and third quartile (50%) of a one-day time window with 10SD from the mean

Applying the formula to an entire year of data, the results are as follows. The algorithm seems to capture the most extreme spikes, only removing 4% of the data (approx. 20,000 points), as well as highlighting periods of regional pollution. It will be helpful to experiment with variations of the spike-removed data in the future inverse models to see how they affect the outcome, and select the best method based on that. As these models will be used to supply Irish emissions inventories, it is critical that the results are as close to reality as possible, because they will form the basis of important decisions regarding environmental and air quality policies.

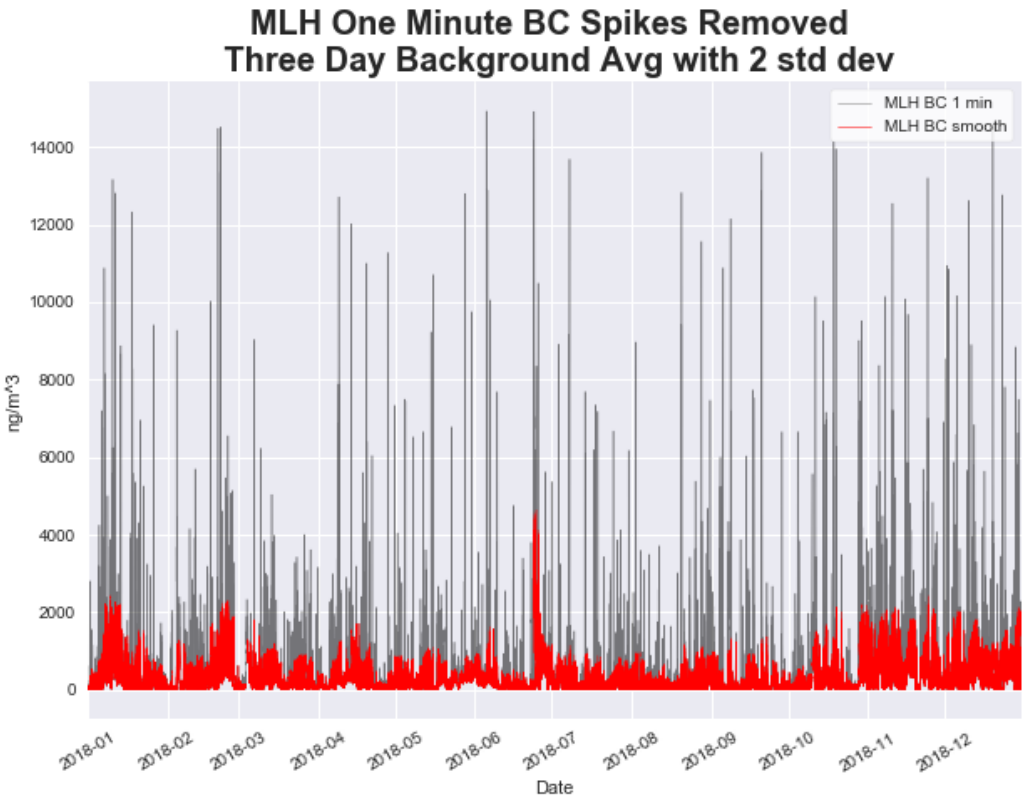

Figure 97 One year of spike-removed data for Malin Head

7. Conclusions and Future Work

It was the purpose of this study to gain a better understanding of the nature and sources of atmospheric aerosols in Ireland, using measurements from a newly established network currently consisting of three coastal sites. This was accomplished through analysis and inter-comparison of data from the same instruments at different stations, as well as different instruments at the same stations. The five main objectives outlined in the beginning have been met, and the following conclusions can be drawn from the results of this work.

Black carbon at the stations is generally low, on average 500ng/m^3 annually for Malin Head and Carnsore Point, reflecting regional pollution levels, and only around 100ng/m^3 at Mace Head due to the dominant air masses coming from the marine sector. All stations had higher average BC during the winter months, most probably as a result of home heating. The frequency distribution shows two distinct peaks at each station, one for clean air and one for regional pollution, although in winter a third peak emerges in the high pollution range, indicative of local influences. Wind sector analysis shows that the largest amount of BC at Carnsore Point comes from the east, even though the wind is only from that direction 13% of the time. At Malin Head the wind is predominantly from the south/southeast, and the majority of BC originates from this sector. Mace Head experiences the highest BC concentrations (88%) from the inland direction, although the amount is only about half as much as Carnsore Point receives from outside Ireland.

Brown carbon or biomass burning (BB) contribution is still not fully resolved, however, based on the results of this study in which levoglucosan measurements were compared to brown carbon from the aethalometer, it can be said that the instrument default settings for α_{tr} (1) and α_{wb} (2) are similar enough to those derived from levoglucosan of α_{tr} (1) and α_{wb} (2.2), and therefore adequate for estimating the BB at the coastal stations. Substituting higher or lower values, such as those used and recommended by previous studies of α_{tr} (0.9) and α_{wb} (1.68) resulted in unrealistic levels of BB, and until a better measurement technique is developed, the aethalometer model will suffice. A positive matrix factorization

(PMF) using levoglucosan measurements may help to find more exact and site-specific values in the future.

Despite the uncertainty in BB contribution, trends are clearly visible over time, and in summer the levels are nearly half those in the winter.

Transboundary pollution is evident not only from BC and BB but confirmed by measurements from the other instruments as well. The Fidas and ACSM wind roses show the highest levels of particulate originating outside of Ireland, especially in the fine particle (PM2.5 or below) range. The presence of BC and BB, which are the result of combustion, only proves that the sources are anthropogenic in nature.

Given that BC is an anthropogenic tracer, it is possible to examine periods of "clean" air in its absence, and so high particle counts measured by the CPC in summertime could be linked to tidal new particle formation events. In conjunction with SMPS measurements, it was shown that these new particle bursts are often captured by the CPC, but the particles do not always grow to a size detectable by the SMPS, and even then, do not continue to grow.

Measurements from the EMEP campaign showed that organic carbon (OC) constitutes approximately 80% of total carbon (TC) and is at least seven times higher than elemental carbon (EC). This indicates that a large quantity of the organics is comprised of secondary organic aerosol. As the MLH ACSM was measuring PM2.5 while the CRP ACSM only measured PM1, Malin Head organics were double those at Carnsore Point, and though this could be due to the generally higher local pollution levels at that station, evidence from the measurements suggests that a greater amount of organics fall into the PM2.5 and PM10 range than was previously assumed. When testing various OM/OC ratios from previous studies on the OC data from the EMEP campaign, it was found that only between 40-60% of the total OM was made up of PM1 organics, when using OM/OC ratios of 1.59 and 2.1 for UCD and MHD. These ratios are higher than the commonly accepted OM/OC ratio of 1.4, and the percentage of PM1 organics decreased as the ratios increased, which implies previous studies have been underestimating the level of total organics in the atmosphere. When the CRP total organics were calculated by doubling the PM1 organics (assuming about 50% are greater than PM1 based on

the EMEP results), they constituted approximately 8% of total PM10 mass. This was in agreement with the findings from other studies, which used OM/OC conversion factors of 1.4 and 1.5 and could mean that CRP has a similar OM/OC ratio to Dublin in the Fall/Winter. More data are necessary to determine the actual ratios, as these can vary by season and be affected by factors such as plankton blooms.

The Fidas measurements showed a distinct bi-modal distribution between PM2.5 and PM10, particularly during the summer at Malin Head. When comparing the ratios of PM2.5/PM10 by wind sector in the summer and winter, the results show very high ratios in the summer, especially to the west of the station, which may be linked to the new particle formation events occurring in the warmer months. Higher wintertime ratios tend to be from the polluted sector in the southeast due to the stronger local influence of home heating as is also indicated by the other measurements at the station.

The lockdown resulting from the on-going Covid-19 pandemic appears to have an impact on the regional pollution in Ireland. While PM10 and PM2.5 were largely unaffected, PM1 at Malin Head exhibited a decrease in the signal variability as evidenced by the reduced standard deviation of the mean, which could be related to reduced local road traffic and dust. Although NO_2 was generally lower in 2020 compared to the previous years' average, the difference increased after lockdown came into effect, with an average 50% reduction across all Dublin sites. Kilkenny was the notable exception with slightly higher NO_2 during lockdown, likely due to agricultural activity. Comparing ozone at the stations to other sites within Ireland showed that in suburban areas there was a 13.7% increase compared to the previous three-year average, and a 5.6% decrease in rural areas. This change was reflected in the CAMS model which simultaneously ran a business as usual and reduced emissions scenario during this time period. Comparison to the NUIG forecast model showed the model starting to under-predict ozone two weeks after lockdown began at urban and rural sites alike, indicating that the reduction in pollutants had enough of an impact on regional air masses to be reflected in the model.

Although the data and analysis from this study have provided a solid foundation and some insight into the nature of the atmospheric aerosols, while clearly showing a transboundary contribution of pollution reaching Ireland from other countries, much more needs to be done to understand the complexity of this topic, leaving open several opportunities for future work. The comparison of measurements and WRF-Chem forecasts identified and corrected some problems in the NUIG model setup, resulting in improved model performance, but the differences are still not completely resolved. Multiple years of data are required to accurately model the atmosphere, and this network is contributing to that purpose as well by laying a foundation for better emissions inventories.

The impact of the Covid-19 restrictions might also be looked into further, in order to evaluate the possible environmental benefits of people working from home, even after the pandemic ends, which would greatly reduce traffic and thus pollution. If it could be shown to reduce costs for businesses and employees who no longer need to provide office spaces or commute long distances, the impact on daily life would be profound.

In addition to inverse modelling of black carbon to pinpoint the actual sources of pollution, a positive matrix factorization (PMF) of the brown carbon with levoglucosan should be conducted to determine more accurate alpha values. The network will continue to expand and include other stations and more instrumentation over time, including continuous measurements of ASCM data, and instruments with the ability to measure isotopes, which will make it possible to distinguish between natural and anthropogenic sources, providing a broader overview of the atmospheric conditions in Ireland, and contributing to the global measurements of the factors influencing the climate and establishing a long-term record.

Appendix A: NUIG WRF-chem NAMELIST

```
&time_control
run_days =          0,
run_hours           =           96,
run_minutes         =           0,
run_seconds         =           0,
start_year = 2020
start_month = 04
start_day = 28
start_hour = 12
start_minute        =           00,   00,   00,
start_second        =           00,   00,   00,
end_year = 2020
end_month = 05
end_day = 04
end_hour = 12
end_minute          =           00,   00,   00,
end_second          =           00,   00,   00,
interval_seconds    =           10800
input_from_file     =           .true.,     .true.,   .true.,
history_interval    =           60,   360  ,   60,
frames_per_outfile =            1,   4,      4,
restart     =           .false.,
restart_interval    =           2880
frames_per_auxinput5        =           12,
auxinput5_interval_m        =           60, 60, 6  0,
io_form_auxinput4 =             0
io_form_auxinput5 =             2
debug_level         =           1500
/
&dfi_control
/
&domains
time_step           =           120,
time_step_fract_num         =           0,
time_step_fract_den         =           1,
max_dom             =           1
e_we      =           157,   31  ,   46,
e_sn      =           165,   22  ,   28,
e_vert    =           30,   30,   30,
num_metgrid_levels          =           21,
num_metgrid_soil_levels     =           4,
dx          =           25000,    15000,   5000,
dy          =           25000,    15000,   5000,
grid_id     =           1,   2,      3,
parent_id=          1,   1,      2,
i_parent_start      =           1,   6,      9,
j_parent_start      =           1,   6,      6,
parent_grid_ratio   =           1,   3,      3,
parent_time_step_ratio      =           1,   3,      3,
feedback =          0,          !
smooth_option       =           0
/
sfcp_to_sfcp        =           .true.
&physics
mp_physics          =           2,   2,      2,
progn     =           1,   1,      1,
ra_lw_physics       =           1,   1,      1,
ra_sw_physics       =           2,   2,      2,
radt        =           4,   40,     40,
```

```
sf_sfclay_physics  =        1,  1,     1,
sf_surface_physics =        2,  2,     2,
bl_pbl_physics     =        1,  1,     1,
bldt               =        0,  0,     0,
cu_physics         =        5,  0,     0,
cu_diag            =        1,  0,     0,
cudt               =        2,  0,     0,
ishallow           =        0,
isfflx             =        1,
ifsnow             =        1,
icloud             =        1,
surface_input_source       =        1,
num_soil_layers    =        4,
sf_urban_physics   =        1,  0,     0,
mp_zero_out        =        2,
mp_zero_out_thresh         =        1.00E-12
maxiens            =        1,
maxens             =        3,
maxens2            =        3,
maxens3            =        16,
ensdim             =        144,
cu_rad_feedback    =        .true.,
/
&fdda
/
&dynamics
rk_ord             =        3,
w_damping          =        1,
diff_opt           =        1,  1,     1,
km_opt             =        4,  4,     4,
diff_6th_opt       =        2,  0,     0,
diff_6th_factor    =        0.12,  0   .12,  0.12,
base_temp          =        290
damp_opt           =        0,
zdamp              =        5000.,     5000.,  5000.,
dampcoef           =        0.01,  0   .01,  0.01
khdif              =        0,  0,     0,
kvdif              =        0,  0,     0,
non_hydrostatic    =        .true.,    .true.,  .true.,
moist_adv_opt      =        2,  2,     2,
scalar_adv_opt     =        2,  2,     2,
chem_adv_opt       =        2,  2,     2,
tke_adv_opt        =        2,  2,     2,
time_step_sound    =        4,  4,     4,
h_mom_adv_order    =        5,  5,     5,
v_mom_adv_order    =        3,  3,     3,
h_sca_adv_order    =        5,  5,     5,
v_sca_adv_order    =        3,  3,     3,
/
&bdy_control
spec_bdy_width     =        5,
spec_zone          =        1,
relax_zone         =        4,
specified          =        .true.,    .false.,  .false.,
nested             =        .false.,   .true.,   .true.,
/
&grib2
/
&namelist_quilt
nio_tasks_per_group = 0,
nio_groups = 1,
/
&chem
```

```
kemit     =        5,
chem_opt            =        601,
bioemdt   =        15,   0,    0,
photdt    =        5,   0,     0,
chemdt    =        5,   1.2,   0,4,
io_style_emissions =        2,
emiss_inpt_opt      =        121,
emiss_opt           =        20,   0,    0,
emiss_opt_vol       =        0,   0,     0,
chem_in_opt         =        0,   0,     0,
phot_opt =         2,   3,     3,
gas_drydep_opt      =        1,   1,     1,
aer_drydep_opt      =        1,   1,     1,
bio_emiss_opt       =        1,   0,     0,
aircraft_emiss_opt =         0,   0,     0,
ne_area   =        200,
depo_fact           =        0.25,
dust_opt =         1,
dmsemis_opt         =        0,
seas_opt =         4,
gas_bc_opt          =        0,   1,     1,
gas_ic_opt          =        0,   1,     1,
aer_bc_opt          =        0,   1,     1,
aer_ic_opt          =        0,   1,     1,
gaschem_onoff       =        1,   1,     1,
aerchem_onoff       =        1,   1,     1,
wetscav_onoff       =        1,   0,     0,
cldchem_onoff       =        1,   0,     0,
vertmix_onoff       =        1,   1,     1,
chem_conv_tr        =        1,   0,     0,
conv_tr_wetscav     =        1,   0,     0,
conv_tr_aqchem      =        1,   0,     0,
biomass_burn_opt =         0,   0,     0,
plumerisefire_frq   =        120,   30  ,   30,
have_bcs_chem       =        .true.,     .false., .false.,
aer_ra_feedback     =        1,
aer_op_opt          =        0,
opt_pars_out        =        0,
diagnostic_chem     =        0,
chemdiag = 1,
n2o5_hetchem = 2,
ne_area   =        250,
/
&namelist_quilt
nio_tasks_per_group = 0,
nio_groups = 1,
/
```

Appendix B: Manchester University WRF-Chem NAMELIST

```
&time_control
run_days =          0,
run_hours           =           0,
run_minutes         =           0,
run_seconds         =           0,
start_year          =           2020,
start_month         =           04,
start_day =         28,
start_hour          =           18,
start_minute        =           00,
start_second        =           00,
end_year =          2020,
end_month           =           05,
end_day  =          01,
end_hour=           00,
end_minute          =           00,
end_second          =           00,
interval_seconds    =           21600,
input_from_file     =           .true.,
fine_input_stream   =           0,
history_interval    =           60,
frames_per_outfile =            1,
restart     =           .false.,
restart_interval    =           1440,
io_form_history     =           2,
io_form_restart     =           2,
io_form_input       =           2,
"io_form_auxinput2                              = 2"            ,
io_form_boundary =          2,
auxinput1_inname =          "met_em.d<domain>.<date>",
auxinput4_inname =          "wrflowinp_d<domain>",
auxinput4_interval =        360,
auxinput5_interval =        60,
frames_per_auxinput5        =           1,
io_form_auxinput2 =         2,
io_form_auxinput4 =         2,
io_form_auxinput5 =         2,
io_form_auxinput6 =         0,
io_form_auxinput7 =         0,
io_form_auxinput8 =         0,
iofields_filename   =       'add_remove_var.txt',
ignore_iofields_warning     =           .false.,
debug_level         =       0,
/
&domains
time_step           =       60,
time_step_fract_num         =           0,
time_step_fract_den         =           1,
max_dom             =       1,
s_we      =         1,
s_sn      =         1,
e_we      =         131,
e_sn      =         131,
e_vert    =         45,
p_top_requested   =         5000,
num_metgrid_levels          =           32,
num_metgrid_soil_levels     =           4,
dx        =         12000,
dy        =         12000,
grid_id   =         1,
```

```
parent_id=          0,
i_parent_start      =       1,
j_parent_start      =       1,
parent_grid_ratio   =       1,
parent_time_step_ratio      =       1,
feedback =          1,
smooth_option       =       0,
interp_type         =       1,
t_extrap_type       =       2,
force_sfc_in_vinterp        =       0,
use_levels_below_ground     =       .true.,
use_surface         =       .true.,
lagrange_order      =       1,
sfcp_to_sfcp        =       .true.,
/
&physics
mp_physics          =       2,
progn     =         1,
ra_lw_physics       =       4,
ra_sw_physics       =       4,
radt      =         5,
sf_sfclay_physics   =       2,
sf_surface_physics  =       2,
bl_pbl_physics      =       2,
bldt      =         0,
cu_physics          =       5,
cugd_avedx          =       1,
cudt      =         0,
isfflx    =         1,
ifsnow    =         1,
icloud    =         1,
surface_input_source        =       1,
num_soil_layers     =       4,
sf_urban_physics    =       1,
mp_zero_out         =       2,
mp_zero_out_thresh          =       1.00E-12
maxiens   =         1,
maxens    =         3,
maxens2   =         3,
maxens3   =         16,
ensdim    =         144,
cu_rad_feedback     =       .true.,
sst_update          =       1,
sst_skin  =         1,
usemonalb           =       .true.,
tmn_update          =       1,
/
&fdda
/
&dynamics
rk_ord    =         3,
w_damping           =       1,
diff_opt  =         1,
km_opt    =         4,
diff_6th_opt        =       0,
diff_6th_factor     =       0.12,
base_temp           =       290
damp_opt            =       0,
zdamp     =         5000.,
dampcoef            =       0.01,
khdif     =         0,
kvdif     =         0,
non_hydrostatic     =       .true.,
```

```
moist_adv_opt      =        2,
scalar_adv_opt     =        2,
chem_adv_opt       =        2,
tke_adv_opt        =        2,
time_step_sound    =        4,
h_mom_adv_order    =        5,
v_mom_adv_order    =        3,
h_sca_adv_order    =        5,
v_sca_adv_order    =        3,
/
&bdy_control
spec_bdy_width     =        5,
spec_zone          =        1,
relax_zone         =        4,
specified          =        .true.,
nested             =        .false.,
/
&grib2
/
&namelist_quilt
nio_tasks_per_group = 0,
nio_groups = 1,
/
&chem
kemit              =        5,
chem_opt           =        601,
bioemdt            =        15,
photdt             =        15,
chemdt             =        5,
io_style_emissions =        2,
emiss_inpt_opt     =        121,
emiss_opt          =        20,
emiss_opt_vol      =        0,
chem_in_opt        =        1,
phot_opt           =        2,
gas_drydep_opt     =        1,
aer_drydep_opt     =        1,
bio_emiss_opt      =        1,
gas_bc_opt         =        0,
gas_ic_opt         =        0,
aer_bc_opt         =        0,
aer_ic_opt         =        0,
gaschem_onoff      =        1,
aerchem_onoff      =        1,
wetscav_onoff      =        1,
cldchem_onoff      =        1,
vertmix_onoff      =        1,
chem_conv_tr       =        1,
seas_opt           =        2,
dust_opt           =        0,
dmsemis_opt        =        2,
biomass_burn_opt   =        0,
have_bcs_chem      =        .true.,
aer_ra_feedback    =        1,
chemdiag           =        1,
n2o5_hetchem       =        2,
/
```

Appendix C: Supplementary Material

ICOS station classification taken from the Atmospheric Station Specifications v1.1

Category	Gases, continuous	Gases, periodical	Meteorology, continuous	Eddy Fluxes
Class 1 Mandatory parameters	• **CO_2, CH_4, CO** : at each sampling height	• **CO_2, CH_4, N_2O, SF_6, CO, H_2, ^{13}C and ^{18}O in CO_2**: weekly sampled at highest sampling height • **^{14}C** (radiocarbon integrated samples): at highest sampling height	• **Air temperature, relative humidity, wind direction, wind speed**: at highest and lowest sampling height* • **Atmospheric Pressure** • **Planetary Boundary Layer Height****	
Class 2 Mandatory parameters	• **CO_2, CH_4** : at each sampling height		• **Air temperature, relative humidity, wind direction, wind speed**: at highest and lowest sampling height* • **Atmospheric Pressure**	
Recommended parameters***	• **^{222}Rn, N_2O, O_2/N_2 ratio** • **CO** for Class 2 stations	• **CH_4 stable isotopes, O_2/N_2 ratio** for Class 1 stations: weekly sampled at highest sampling height		• **CO_2** : at one sampling height

* Atmospheric temperature and relative humidity recommended at all sampling heights

** Only required for continental stations.

*** Recommended for its scientific value but support from ATC in terms of protocols, data base, spare analyzer will not be ensured as long as the parameters are not mandatory.

Current ICOS compliance status of Irish stations

Station	Gas Analyser	Flask Sampling	Temp.	Press.	RH	Wind Speed	Wind Dir.	PBL	Class
MHD	Picarro G2301 ●	X	PRT pt100 ●	Vaisala PTB 220 ●	Vaisala HMP 45D ●	A100L2 ●	W200P ●	Vaisala CL31 ●	1 X
CRP	Picarro G1301 ●	N/A	Rotronic MP402H ●	Young 61302 ●	Rotronic MP402H ●	Gill Windsonic ●	Gill Windsonic ●	N/A	2 ●
MLH	Picarro G2401 ●	N/A	PRT pt100 ●	Vaisala PTB 220 ●	Vaisala HMP 45D ●	A100L2 ●	W200P ●	N/A	2 ●

X Not ICOS compliant ● ICOS Compliant

Optical attenuation:	$ATN = -100 * \ln(I/I_0)$	I_0 = reference signal; I = spot signal
Flow:	$F_{in} = F_{out} * (1 - \zeta)$	F_{out} = measured flow; ζ = leakage factor
Attenuation coefficient:	$b_{atn} = \frac{S*(\Delta ATN/100)}{F_{in}\Delta t}$	S = spot area; t = time
Absorption coefficient:	$b_{abs} = \frac{b_{atn}}{C}$	C = multiple scattering parameter (Weingartner et al. 2003)
Black carbon concentration:	$BC = \frac{b_{abs}}{\sigma_{air}}$	σ_{air} = mass absorption cross-section
Loading effect compensation:	$BC = BC_{measured}/(1 - k * ATN)$	k = compensation parameter
Final equation:	$BC = \frac{S*(\Delta ATN_1/100)}{F_1(1-\zeta)*\sigma_{air}*C*(1-k*ATN_1)*\Delta t}$	

AE33 equations, taken from AE33UsersManual_Rev154.pdf

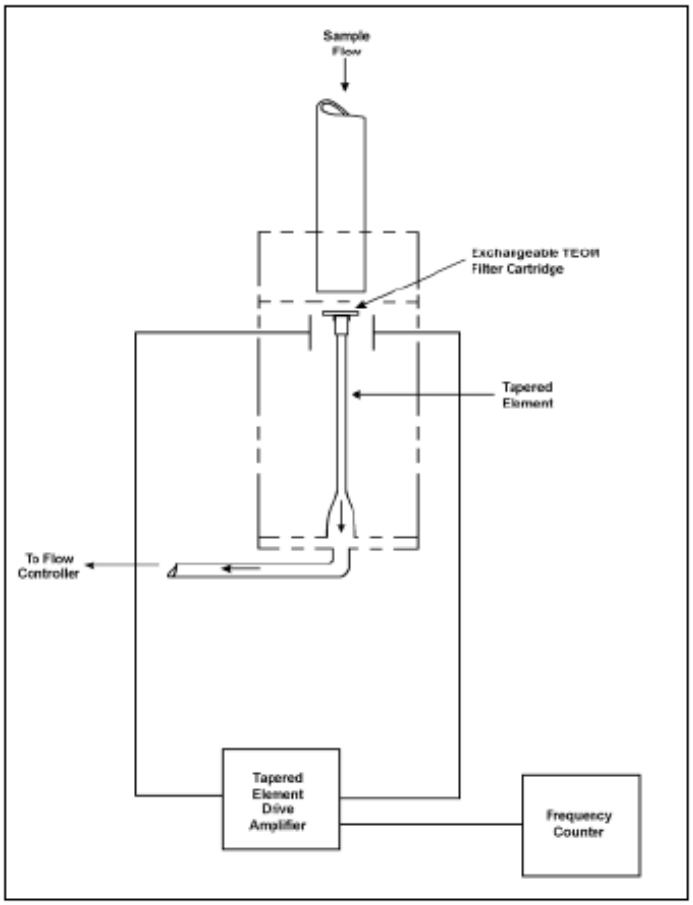

TEOM flow diagram taken from Thermo Fisher Scientific 2016 TEOM Operating Manual, illustrating the relative simplicity of this instrument.

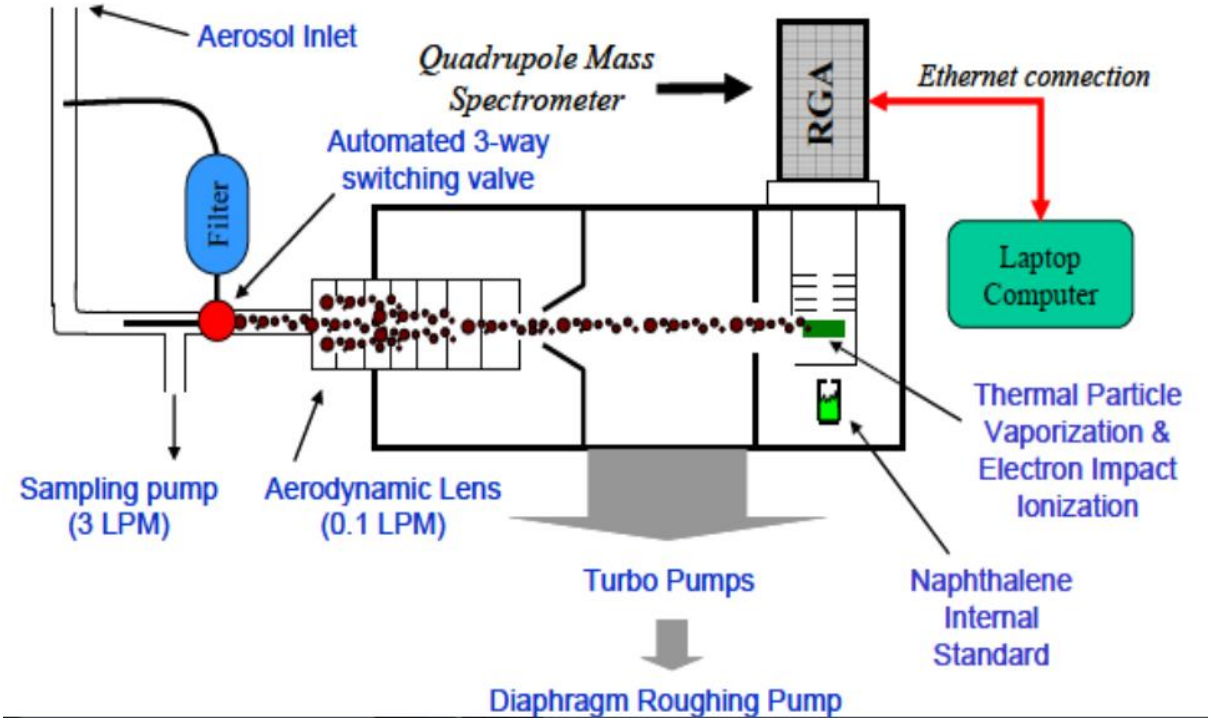

ACSM schematic taken from [Watson, 2017]

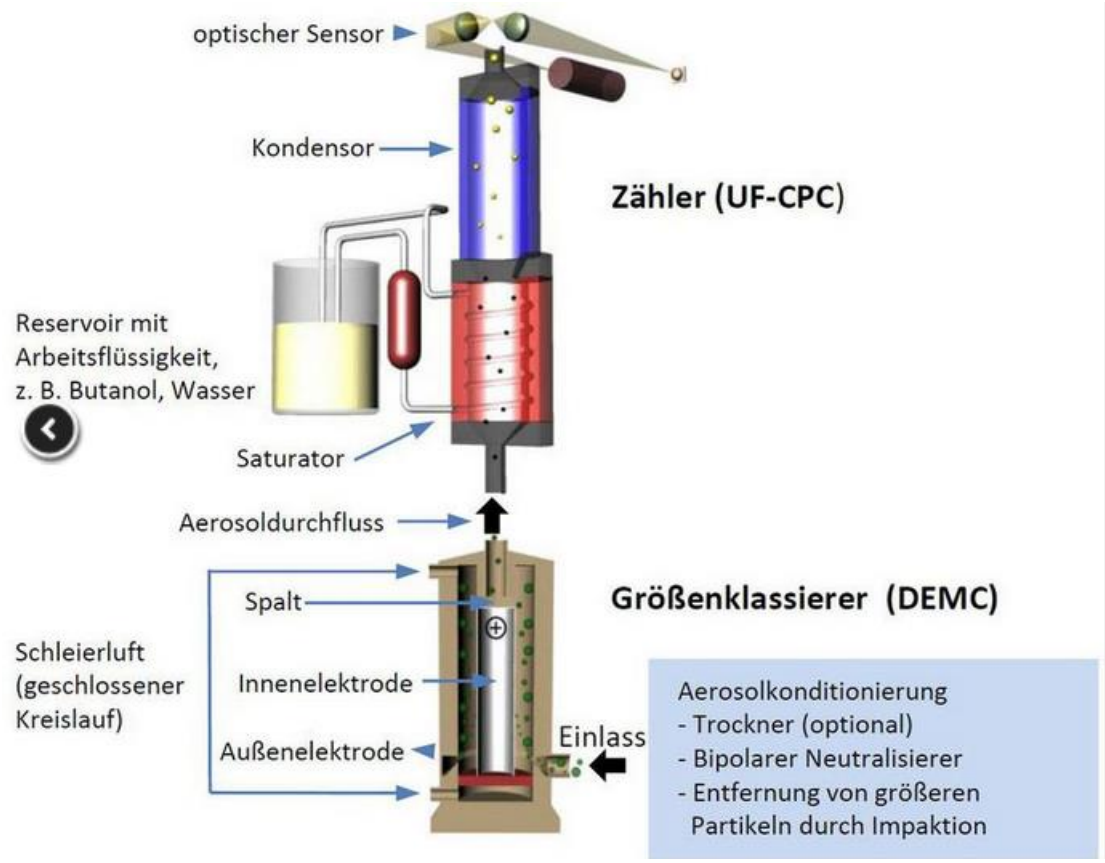

SMPS schematic taken from https://www.palas.de/en/product/usmps2050x_2100x_2200x#datasheet

AE33 Biomass Burning formula:

babs_low_WB = (babs_low-((lambda_low/lambda_high)^-alpha_TR)*babs_high) / (1-((lambda_low/lambda_high)^-alpha_TR) / ((lambda_low/lambda_high)^-alpha_WB))

babs_low_TR = babs_low - babs_low_WB

babs_high_TR = babs_high - babs_low_WB / ((lambda_low/lambda_high)^-alpha_WB)

babs_high_WB = babs_high - babs_high_TR

BC_TR_ratio_high = babs_high_TR / babs_high

BC_high = babs_high / MAC_high

BCTR = BC_high * BC_TR_ratio_high

BCWB = BC_high – BCTR

BC_WB_ratio=(1-BC_TR_ratio_high)*100

The variable inputs are:

babs_low=BC2 (450nm or lower wavelength) * 14.54 (MAC for lower wavelength)

babs_hi= BC7 (950nm or higher wavelength) * 7.19 (MAC for higher wavelength)

alphaTR= alpha for fossil fuel/traffic component

alphaWB= alpha for wood/biomass burning component

lambda_low=the lower wavelength used in calculation, ie. 450nm

lambda_hi=the upper wavelength used in calculation, ie. 950nm

MAC= mass absorption cross-section, wavelength dependent

The output gives the BCTR (traffic) and BCWB (wood burning) components in ng/m^3 as well as the percent BB (BC_WB_ratio).

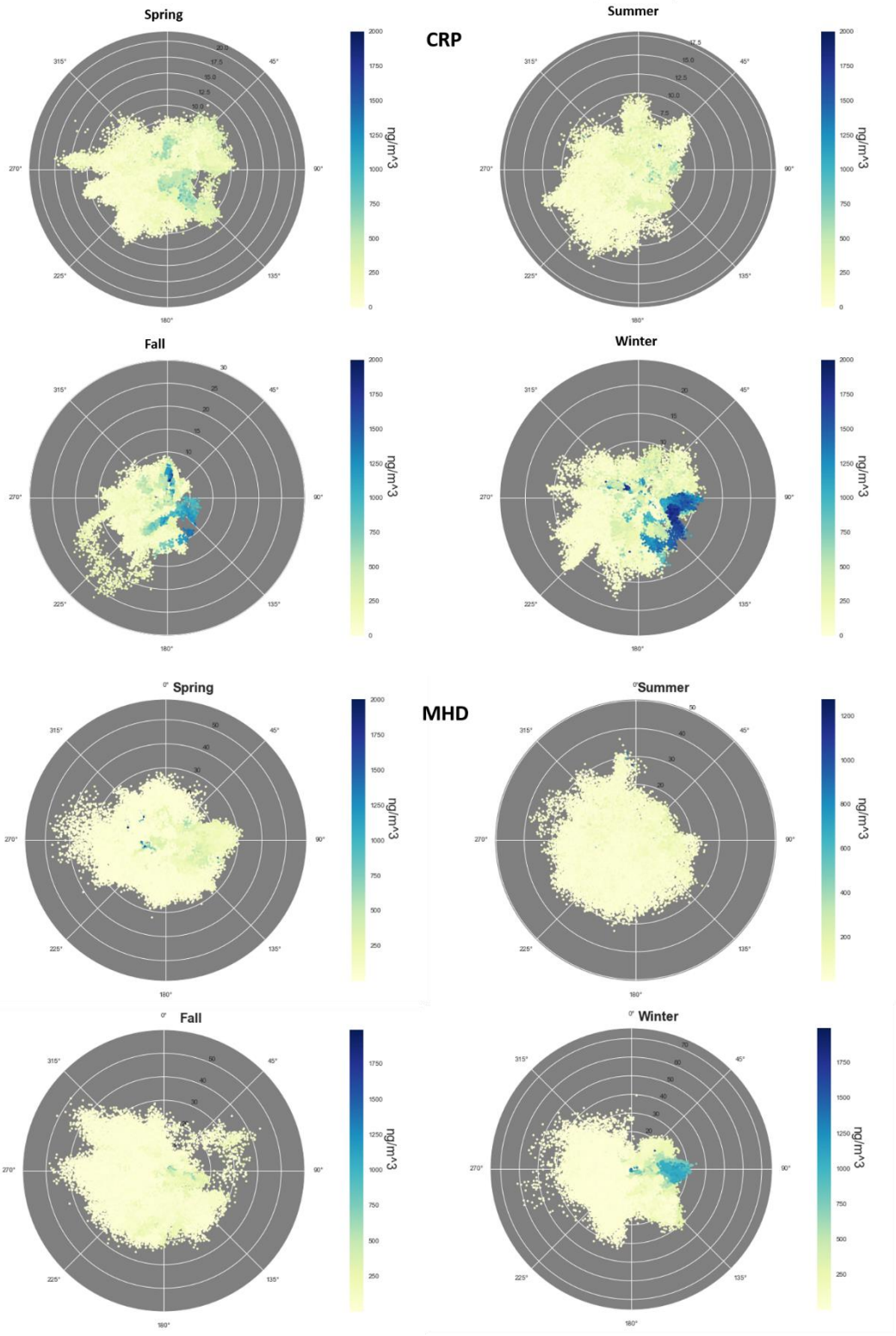
CRP
Spring
Summer
Fall
Winter
MHD
Spring
Summer
Fall
Winter
ng/m^3

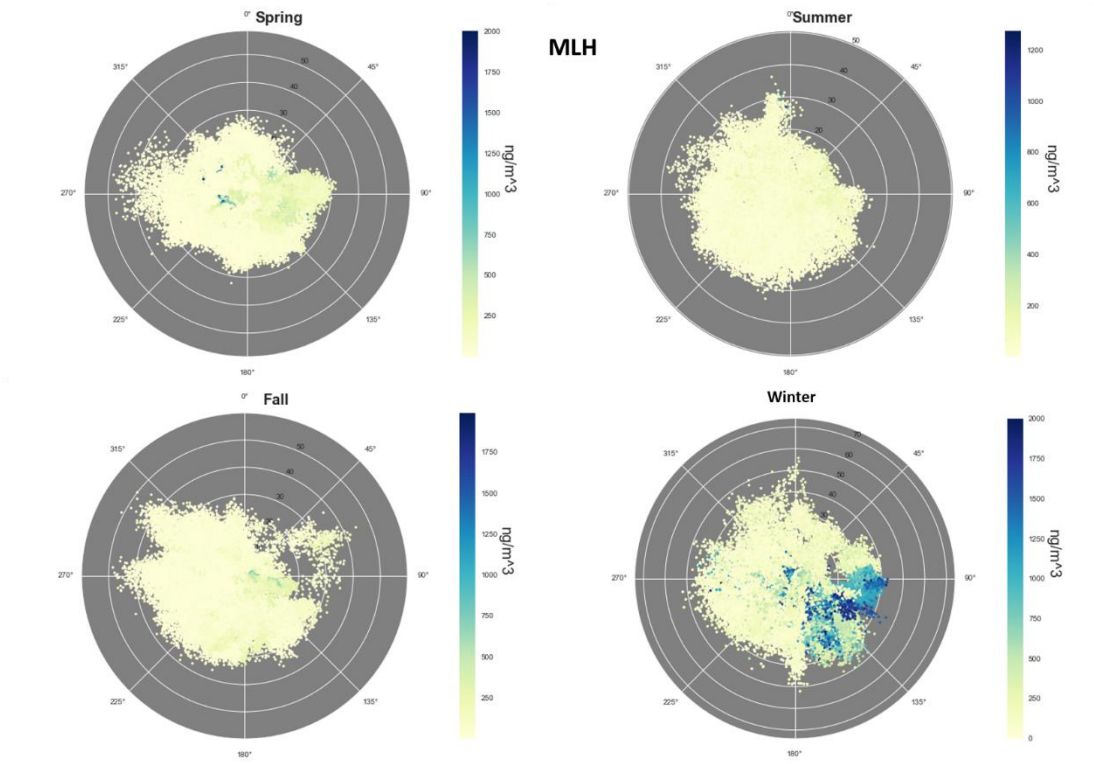

Ch 4.2 BC wind roses by season

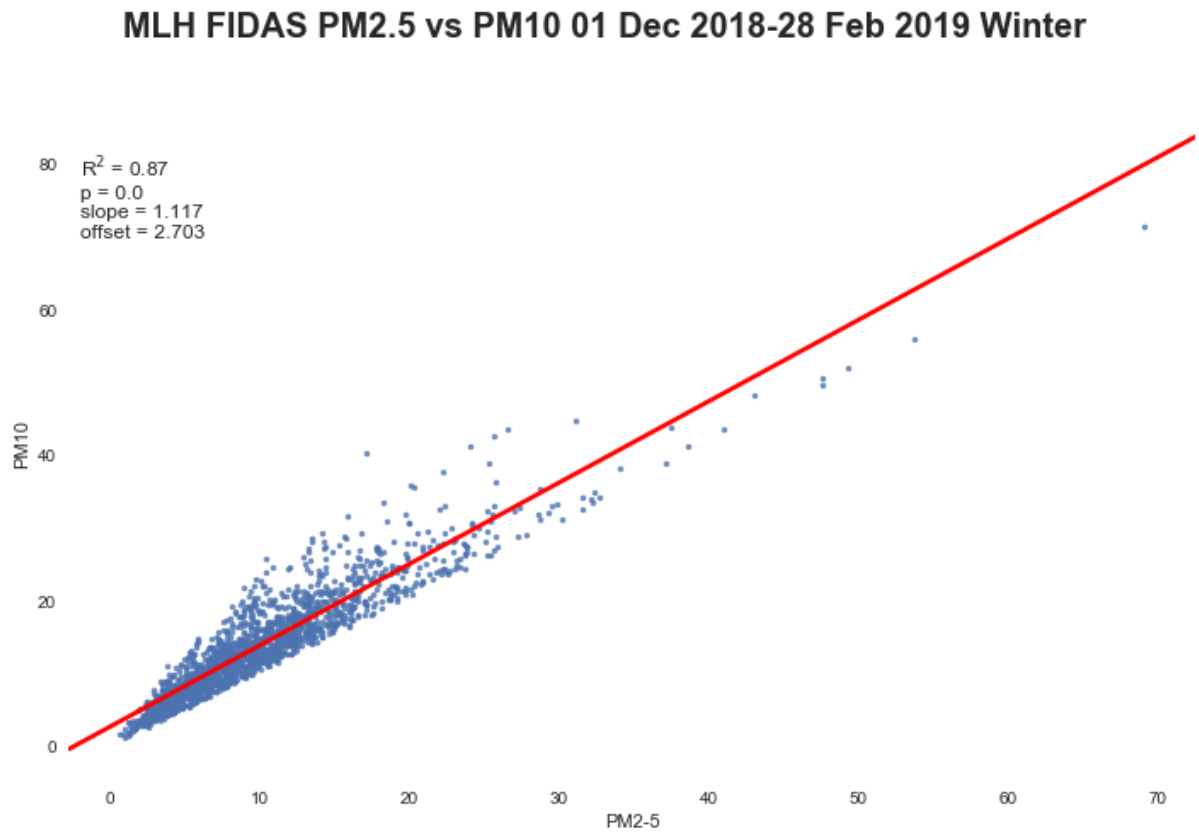

Ch 4.8.1 MLH Fidas PM10 vs PM2.5 Winter

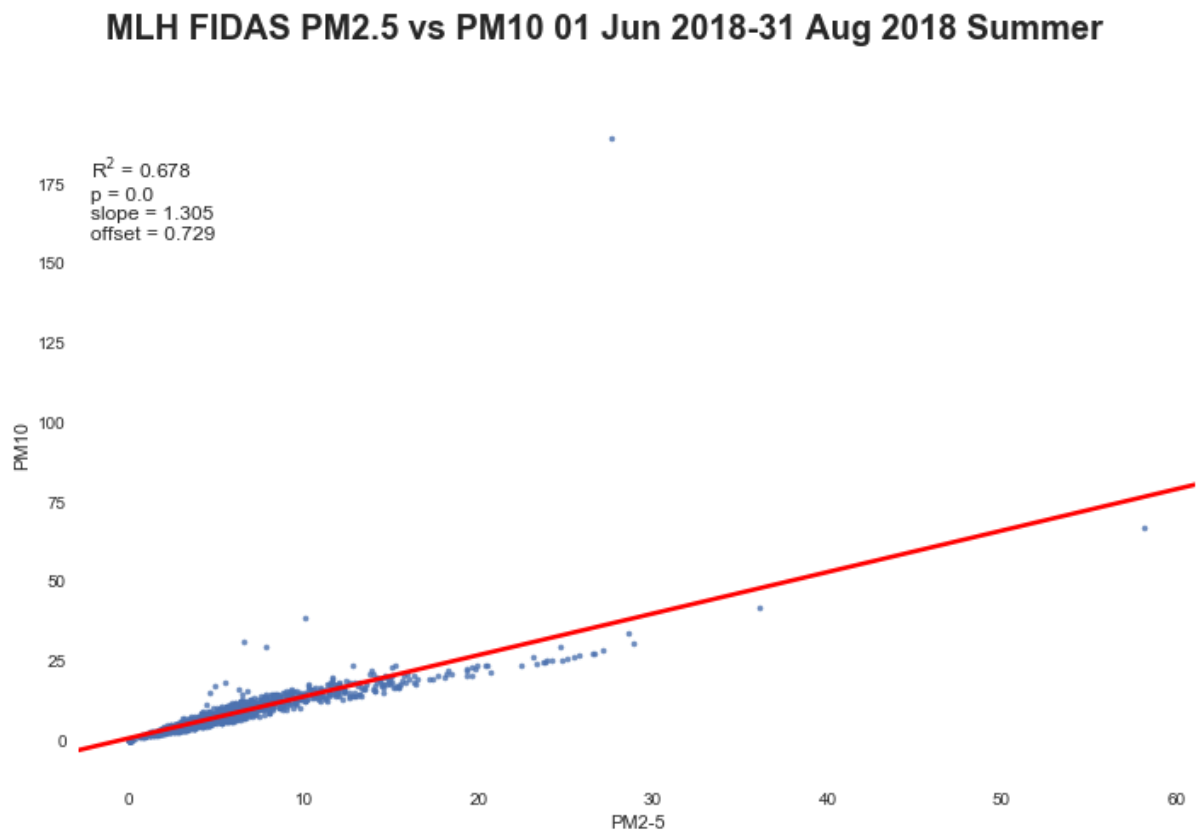

Ch 4.8.1 MLH Fidas PM10 vs PM2.5 Summer

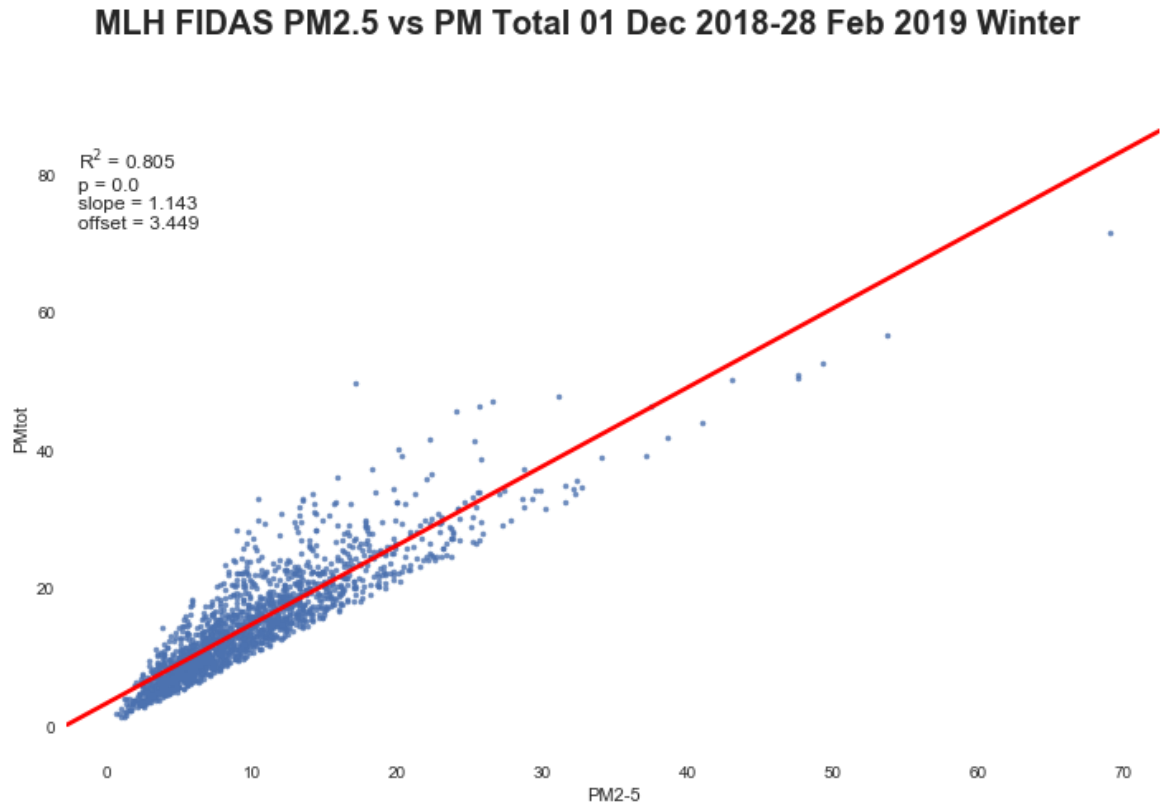

Ch 4.8.1 MLH Fidas PMtotal vs PM2.5 Winter

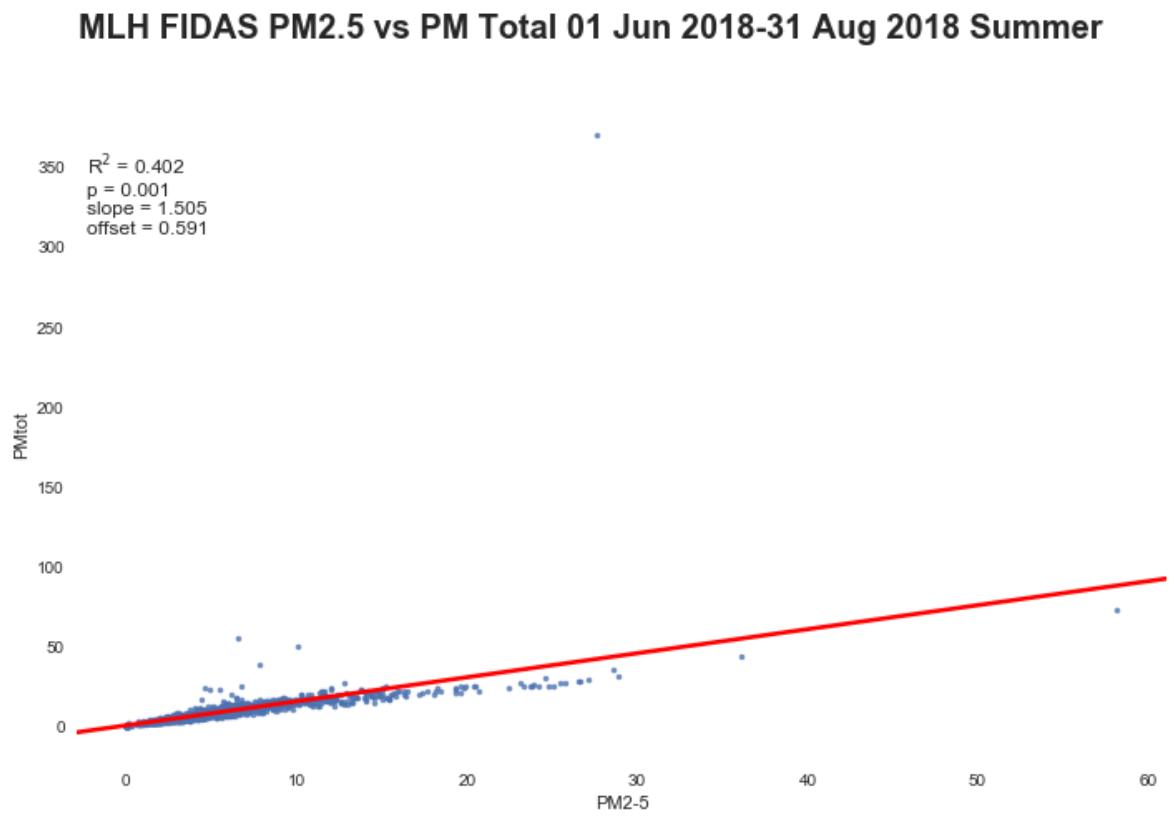

Ch 4.8.1 MLH Fidas PMtotal vs PM2.5 Summer

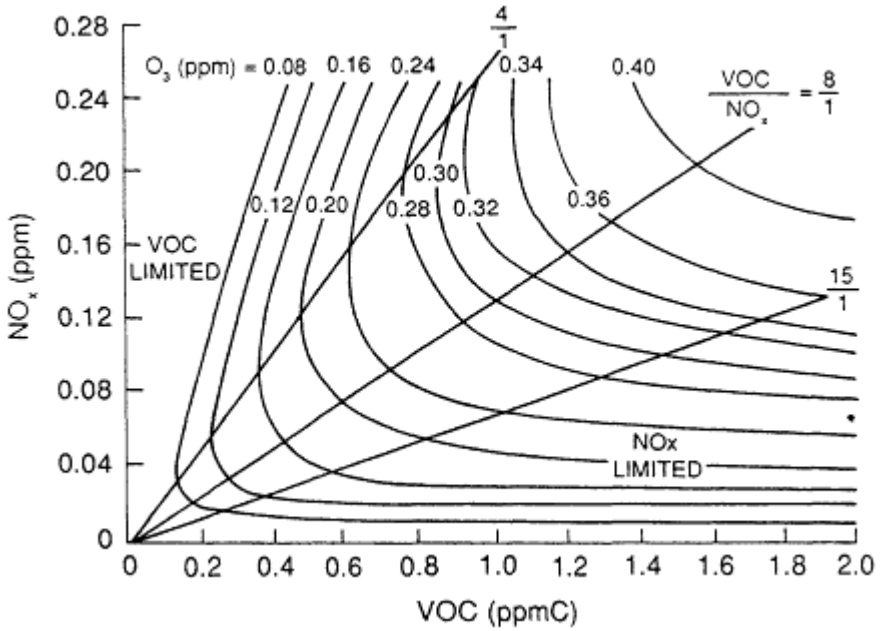

Ch 5.4.4 Ozone isopleth [Division on Earth and Life et al., 2000]

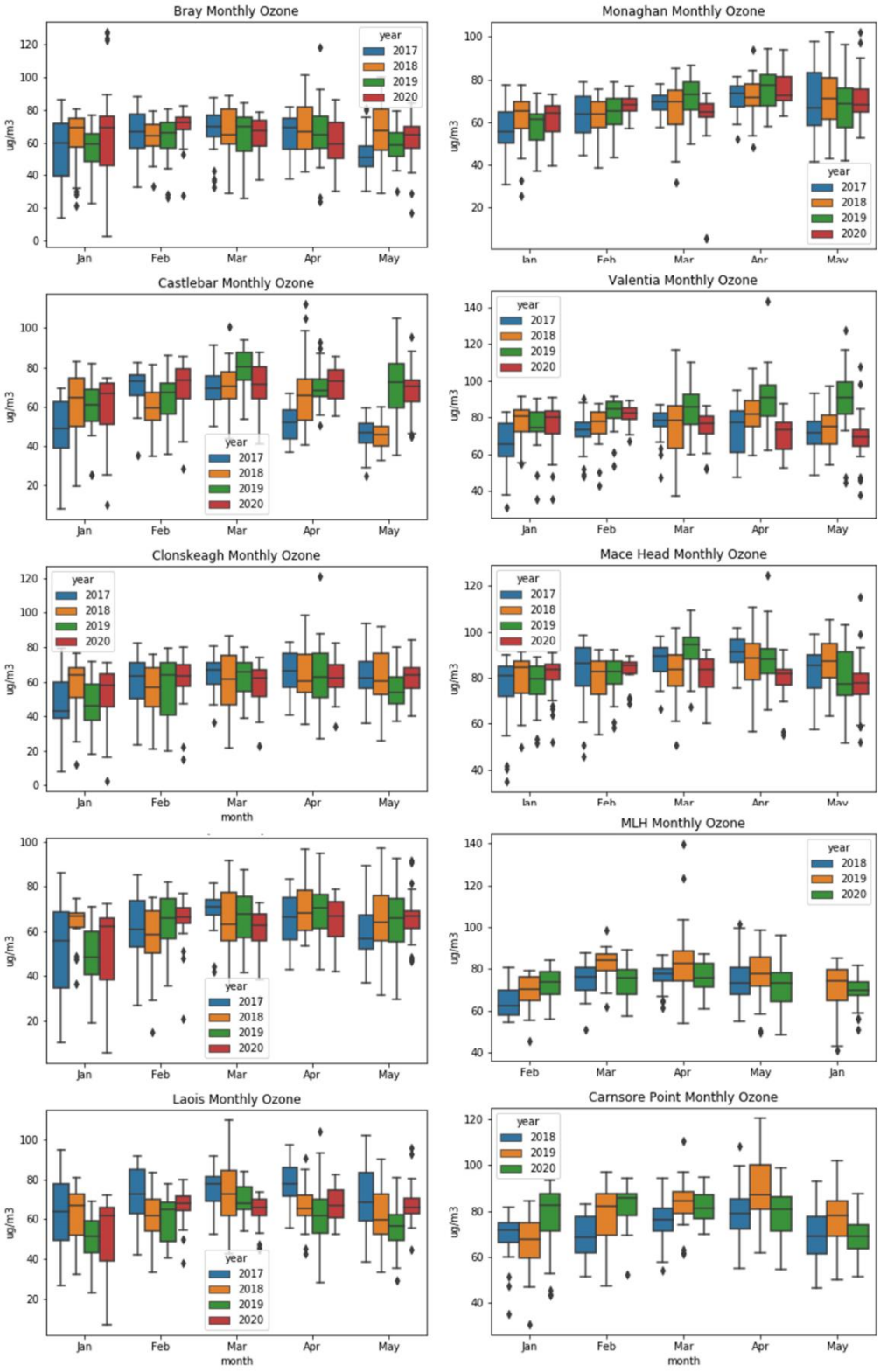

Ch 5.4.1 Suburban vs Rural Ozone

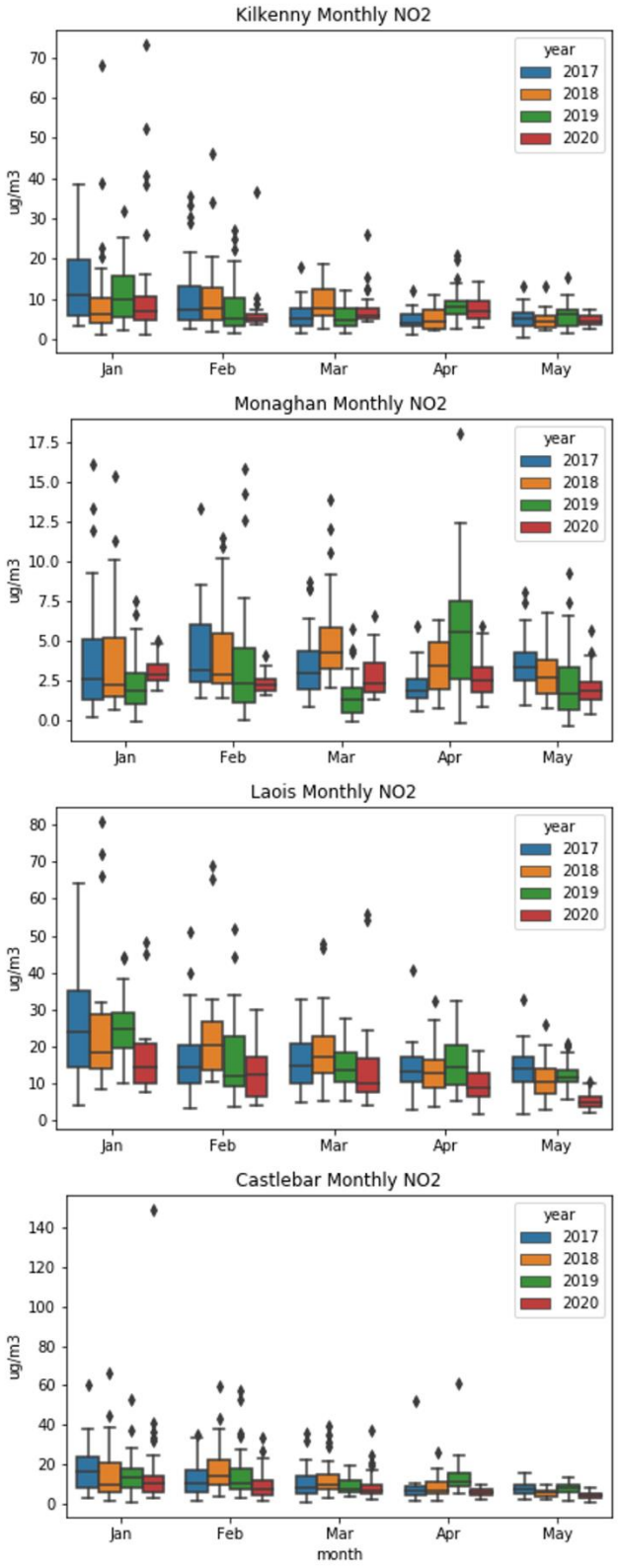

Ch 5.4.1 Suburban NO_2

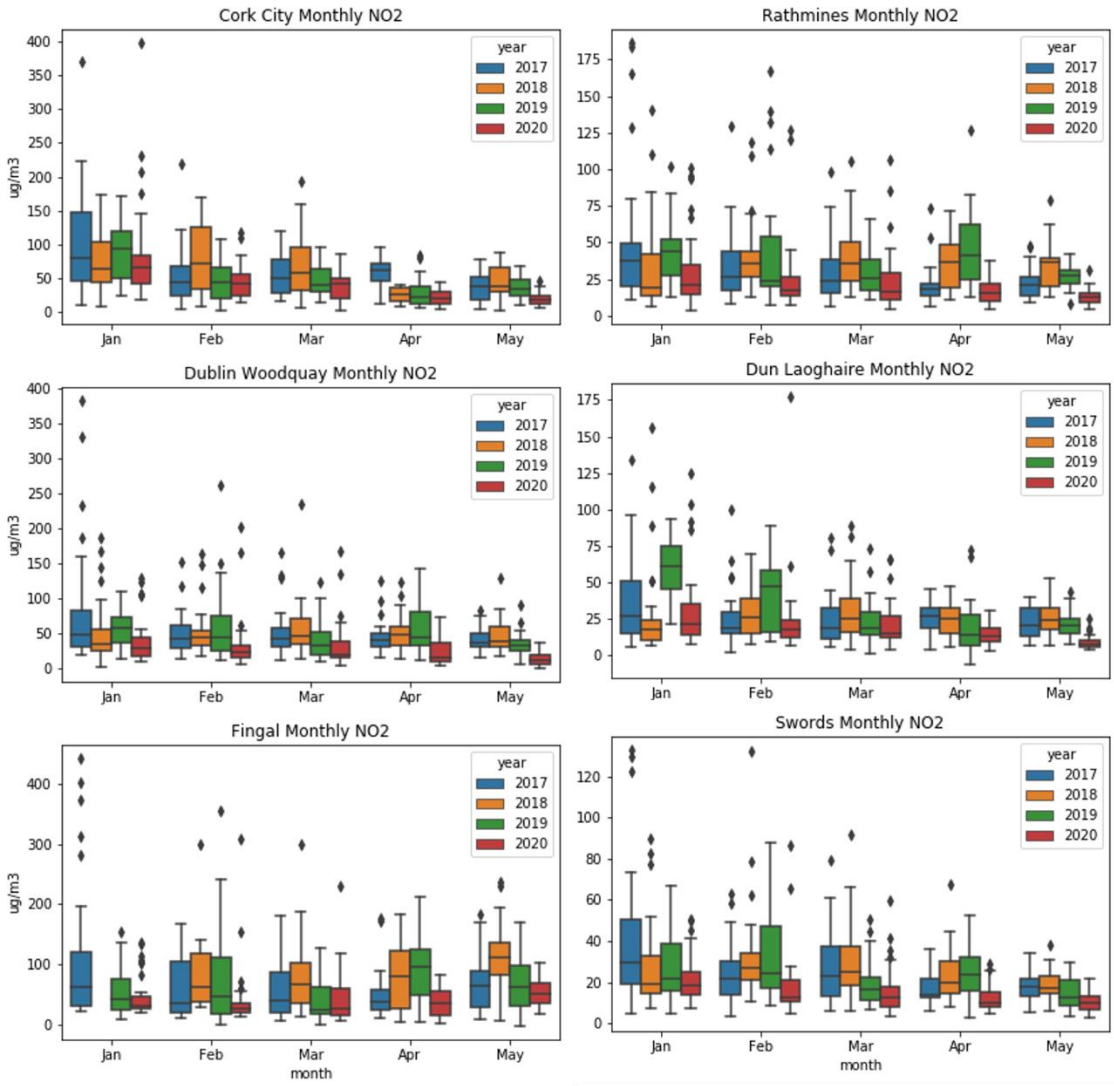

Ch 5.4.1 Urban NO_2

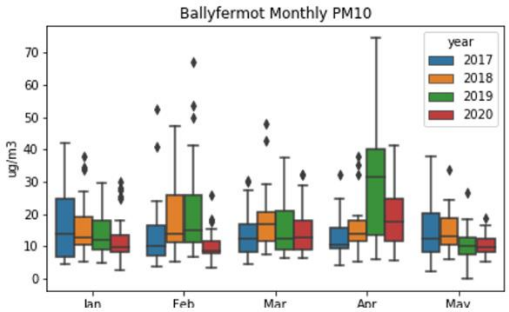
Ballyfermot Monthly PM10
year
2017
2018
2019
2020
ug/m3
0
10
20
30
40
50
60
70
Jan
Feb
Mar
Apr
May

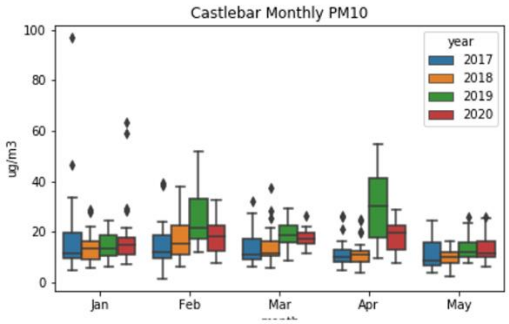
Castlebar Monthly PM10
year
2017
2018
2019
2020
ug/m3
0
20
40
60
80
100
Jan
Feb
Mar
Apr
May

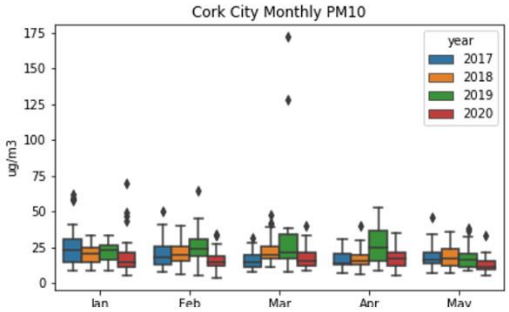
Cork City Monthly PM10
year
2017
2018
2019
2020
ug/m3
0
25
50
75
100
125
150
175
Jan
Feb
Mar
Apr
May

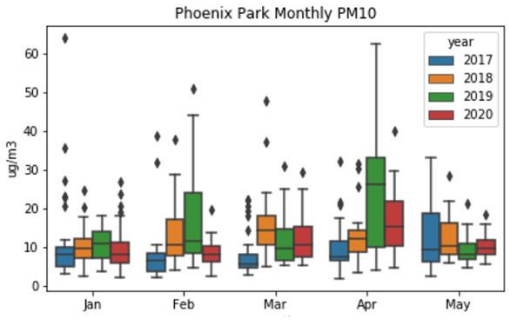
Phoenix Park Monthly PM10
year
2017
2018
2019
2020
ug/m3
0
10
20
30
40
50
60
Jan
Feb
Mar
Apr
May

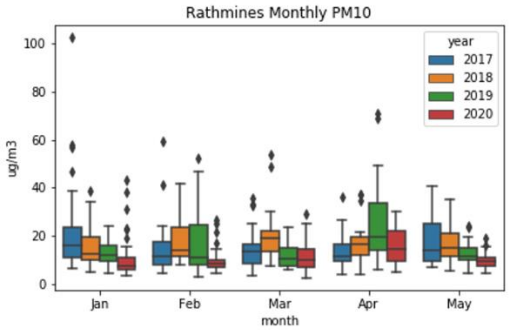
Rathmines Monthly PM10
year
2017
2018
2019
2020
ug/m3
0
20
40
60
80
100
Jan
Feb
Mar
Apr
May
month

Ch 5.4.1 PM10

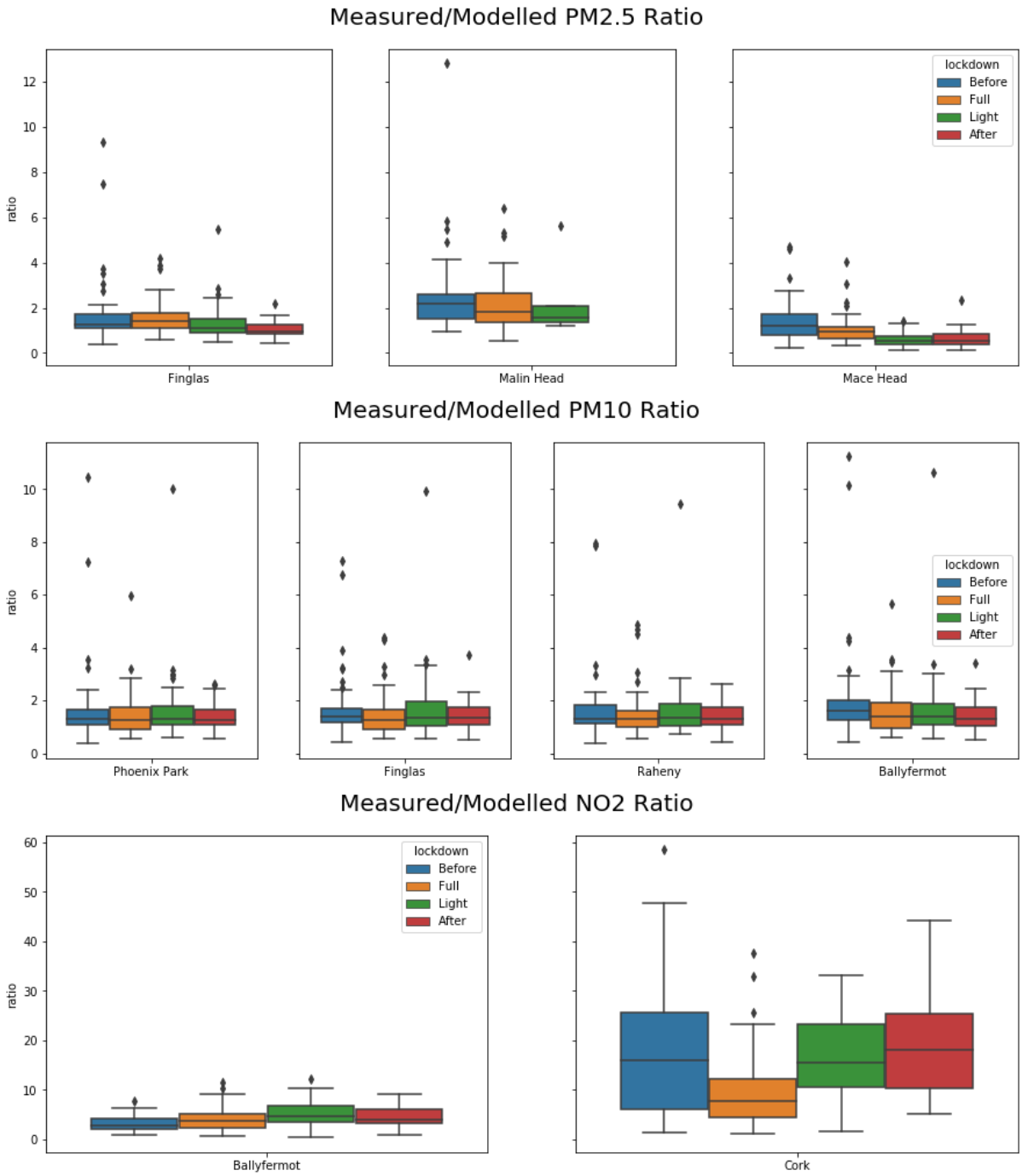

Ch 6.1 Measured/Model PM and NO_2 for the stages of lockdown

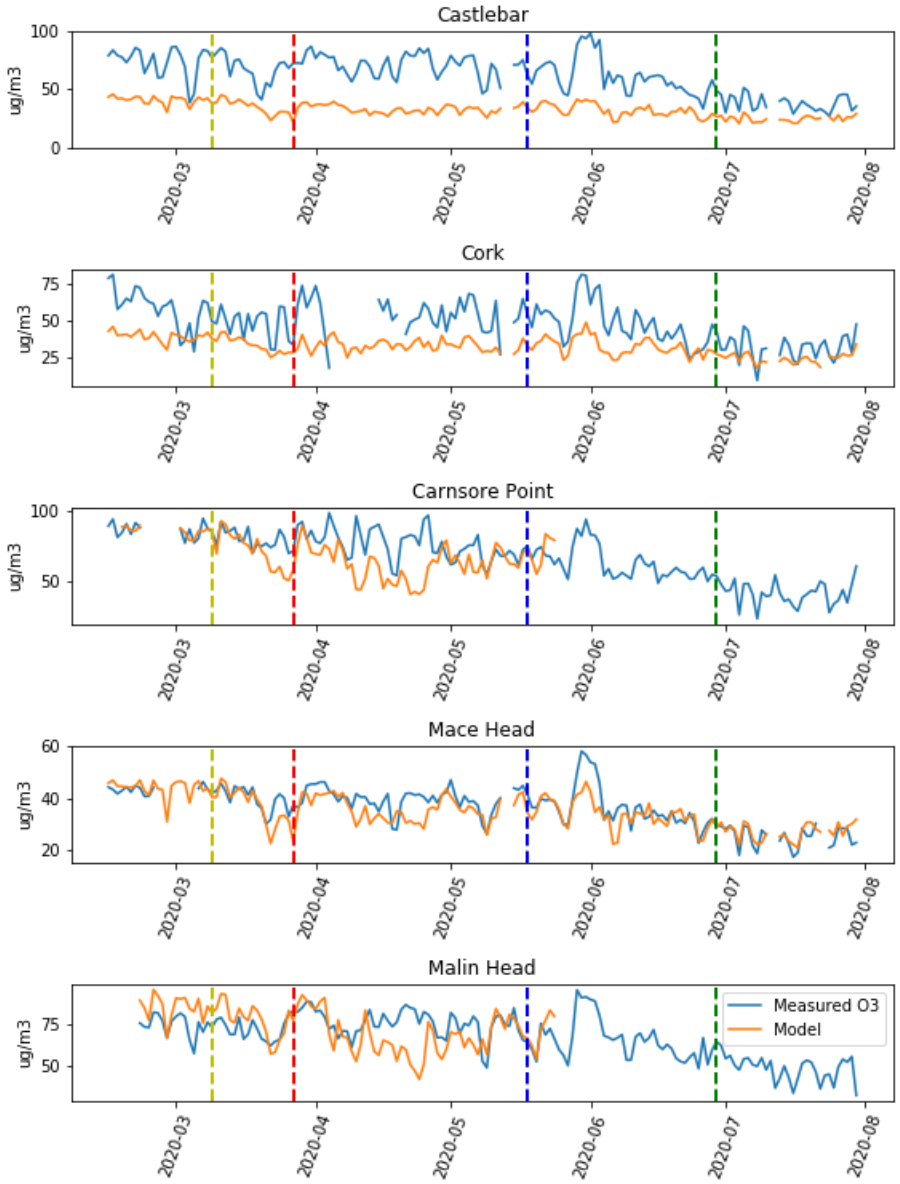

Ch 6.1 Measured and Modelled O_3 time series for the stages of lockdown

Appendix D: Course List

GS505 Graduate Research Skills

GS506 Teaching and Learning

GS509 Participation in Workshops/Courses

GS511 Research Placement

GS530 Graduate Research and Information Skills

GS057 Statistical Methods for Research

References

Aas, W., A.-G. Hjellbrekke, S. Solberg, S. M. Platt, K. E. Yttri, R. O. Rud, and K. Torseth (2018), EMEP Status Report 1/2018 Transboundary particulate matter, photo-oxidants, acidifying and eutrophying components*Rep. 1/2018*, 99-106 pp, METEOROLOGISK INSTITUTT, Norwegian Meteorological Institute.

ACMCC (2018), ACTRIS 2 (ECAC-ACMCC) Intercomparison of Aerosol Chemical Speciation Monitors, November 2018*Rep. ACSM-2018-1*7pp, Aerosol Chemical Monitoring Calibration Center.

Akritidis, D., P. Zanis, E. Katragkou, M. G. Schultz, I. Tegoulias, A. Poupkou, K. Markakis, I. Pytharoulis, and T. Karacostas (2013), Evaluating the impact of chemical boundary conditions on near surface ozone in regional climate–air quality simulations over Europe, *Atmospheric Research*, *134*, 116-130, doi:https://doi.org/10.1016/j.atmosres.2013.07.021.

Alexander, L., Allen, S., Bindoff, N. L., Bréon, F.-M., Church, J., Cubasch, U., Emori, S., Forster, P., Friedlingstein, P., Gillett, N., Gregory,, H. J., D., Jansen, E., Kirtman, B., Knutti, R., Kanikicharla, K. K., Lemke, P., Marotzke, J., Masson-Delmotte, V., Meehl, G.,, I. Mokhov, Piao, S., Plattner, G.-K., Dahe, Q., Ramaswamy, V., Randall, D., Rhein, M., Rojas, M., Sabine, C., Shindell, D., Stocker, T.,, and L. Talley, Vaughan, D. and Xie, S.-P. (2013), Climate Change 2013: The Physical Science Basis, Summary for Policymakers*Rep.*, International Panel for Climate Change.

Alexe, M., et al. (2015), Inverse modelling of CH4 emissions for 2010–2011 using different satellite retrieval products from GOSAT and SCIAMACHY, *Atmos. Chem. Phys.*, *15*(1), 113-133, doi:10.5194/acp-15-113-2015.

Aligo, E. A., W. A. J. R. Gallus, and M. Segal (2009), On the Impact of WRF Model Vertical Grid Resolution on Midwest Summer Rainfall Forecasts, *Weather and Forecasting*, *24*(2), 575-594.

Archer-Nicholls, S., D. Lowe, S. Utembe, J. Allan, R. A. Zaveri, J. D. Fast, Ø. Hodnebrog, H. A. C. Denier van der Gon, and G. McFiggans (2014), Gaseous chemistry and aerosol mechanism developments for version 3.5.1 of the online regional model, WRF-Chem, *Geoscientific Model Development*, *7*(6), 2557–2579.

Atkinson-Palombo, C. M., J. A. Miller, and R. C. Balling (2006), Quantifying the ozone "weekend effect" at various locations in Phoenix, Arizona, *Atmospheric Environment*, *40*(39), 7644-7658, doi:https://doi.org/10.1016/j.atmosenv.2006.05.023.

Banks, R. F., and J. M. Baldasano (2016), Impact of WRF model PBL schemes on air quality simulations over Catalonia, Spain, *Science of The Total Environment*, *572*, 98-113, doi:https://doi.org/10.1016/j.scitotenv.2016.07.167.

Bergamaschi, P., et al. (2015), Top-down estimates of European CH4 and N2O emissions based on four different inverse models, *Atmos. Chem. Phys.*, *15*(2), 715-736, doi:10.5194/acp-15-715-2015.

Birch, M. E., and R. A. Cary (1996), Elemental carbon-based method for occupational monitoring of particulate diesel exhaust: methodology and exposure issues, *The Analyst*, *121*(9), 1183-1190.

Bond, T. C., et al. (2013), Bounding the role of black carbon in the climate system: A scientific assessment, *Journal of Geophysical Research: Atmospheres*, *118*(11), 5380-5552, doi:10.1002/jgrd.50171.

Bougiatioti, A., P. Zarmpas, E. Koulouri, M. Antoniou, C. Theodosi, G. Kouvarakis, S. Saarikoski, T. Mäkelä, R. Hillamo, and N. Mihalopoulos (2013), Organic, elemental and water-soluble organic carbon in size segregated aerosols, in the marine boundary layer of the Eastern Mediterranean, *Atmospheric Environment*, *64*, 251-262, doi:10.1016/j.atmosenv.2012.09.071.

Brunner, D., et al. (2015), Comparative analysis of meteorological performance of coupled chemistry-meteorology models in the context of AQMEII phase 2, *Atmospheric Environment*, *115*, 470-498, doi:https://doi.org/10.1016/j.atmosenv.2014.12.032.

Buckley, P. (2019), Nature and Origin of Black Carbon in Ireland, University College Cork.

CAMS (2020), European Air Quality information in support of the COVID-19 crisis: https://atmosphere.copernicus.eu/european-air-quality-information-support-covid-19-crisis, edited, Copernicus Atmospheric Monitoring Service.

Cavalli, F., et al. (2004), Advances in characterization of size-resolved organic matter in marine aerosol over the North Atlantic, *Journal of Geophysical Research: Atmospheres*, *109*(D24), doi:10.1029/2004jd005137.

Chen, X., and J. Z. Yu (2007), Measurement of organic mass to organic carbon ratio in ambient aerosol samples using a gravimetric technique in combination with chemical analysis, *Atmospheric Environment*, *41*(39), 8857-8864, doi:10.1016/j.atmosenv.2007.08.023.

Chen, Y.-H., and R. G. Prinn (2006), Estimation of atmospheric methane emissions between 1996 and 2001 using a three-dimensional global chemical transport model, *Journal of Geophysical Research: Atmospheres*, *111*(D10), n/a-n/a, doi:10.1029/2005JD006058.

Coleman, L., J. Ovadnevaite, T. Ansari, D. Ceburnis, C. Lin, K. Fossum, P. Roche, A. Khatoon, P. Yadav, and C. O'dowd (2020), Advanced Measurements and Modelling of the Impact of Reduced Emissions on Air Quality in Dublin During Covid-19, edited.

Cooke, W. F., S. G. Jennings, and T. G. Spain (1997), Black carbon measurements at Mace Head, 1989–1996, *Journal of Geophysical Research: Atmospheres*, *102*(D21), 25339-25346, doi:10.1029/97jd01430.

Cuesta-Mosquera, A., et al. (2021), Intercomparison and characterization of 23 Aethalometers under laboratory and ambient air conditions: procedures and unit-to-unit variabilities, *Atmos. Meas. Tech.*, *14*(4), 3195-3216, doi:10.5194/amt-14-3195-2021.

De Leeuw, G., G. J. Kunz, G. Buzorius, and C. D. O' Dowd (2002), Meteorological influences on coastal new particle formation, *Journal of Geophysical Research: Atmospheres*, *107*(D19), PAR 7-1-PAR 7-11, doi:10.1029/2001JD001478.

Derwent, R. G., et al. (2006), External influences on Europe's air quality: Baseline methane, carbon monoxide and ozone from 1990 to 2030 at Mace Head, Ireland, *Atmospheric Environment*, *40*(5), 844-855, doi:http://dx.doi.org/10.1016/j.atmosenv.2005.09.077.

Dinoi, A., et al. (2017), Inter-Comparison of Carbon Content in PM2.5 and PM10 Collected at Five Measurement Sites in Southern Italy, *Atmosphere*, *8*(12), 243.

Division on Earth and Life, S., E. a. R. Commission on Geosciences, O. Committee on Tropospheric, and C. National Research (2000), *Rethinking the Ozone Problem in Urban and Regional Air Pollution*, National Academies Press, doi:10.17226/1889.

Dragomir, C. M., D.-E. Constantin, M. Voiculescu, L. P. Georgescu, A. Merlaud, and M. V. Roozendael (2015), Modeling results of atmospheric dispersion of NO2 in an urban area using METI–LIS and comparison with coincident mobile DOAS measurements, *Atmospheric Pollution Research*, *6*(3), 503-510, doi:https://doi.org/10.5094/APR.2015.056.

Drinovec, L., et al. (2014), *The "dual-spot" Aethalometer: An improved measurement of aerosol black carbon with real-time loading compensation*, 10179-10220 pp., doi:10.5194/amtd-7-10179-2014.

Duffy, P., B. Hyde, A. M. Ryan, J. Murphy, B. Quirke, and D. Fahey (2019), Ireland Informative Inventory Report 2019*Rep.*, EPA Ireland, Johnstown Castle, Wexford, Ireland.

Duffy, P., B. Hyde, A. M. Ryan, J. Murphy, B. Quirke, D. Fahey, and A. Kehoe (2020), Informative Inventory Report Ireland 2020: AIR POLLUTANT EMISSIONS IN IRELAND 1990–2018 REPORTED TO THE SECRETARIAT OF THE UNECE CONVENTION ON LONG-RANGE TRANSBOUNDARY AIR POLLUTION AND TO THE EUROPEAN UNION*Rep.*, EPA Ireland.

EEA (2020), Download of Air Quality Data, edited, https://discomap.eea.europa.eu/map/fme/AirQualityExport.htm.

Ehn, M., et al. (2010), Growth rates during coastal and marine new particle formation in western Ireland, *Journal of Geophysical Research: Atmospheres*, *115*(D18), n/a, doi:10.1029/2010JD014292.

El-Zanan, H. S., D. H. Lowenthal, B. Zielinska, J. C. Chow, and N. Kumar (2005), Determination of the organic aerosol mass to organic carbon ratio in IMPROVE samples, *Chemosphere*, *60*(4), 485-496, doi:10.1016/j.chemosphere.2005.01.005.

El-Zanan, H. S., B. Zielinska, L. R. Mazzoleni, and D. A. Hansen (2009), Analytical Determination of the Aerosol Organic Mass-to-Organic Carbon Ratio, *Journal of the Air & Waste Management Association*, *59*(1), 58-69, doi:10.3155/1047-3289.59.1.58.

El Yazidi, A., et al. (2018), Identification of spikes associated with local sources in continuous time series of atmospheric CO, CO2 and CH4, *Atmos. Meas. Tech.*, *11*(3), 1599-1614, doi:10.5194/amt-11-1599-2018.

EPA-Ireland (2016), Environmental Protection Agency Ireland, edited, p. www.epa.ie, EPA Ireland.

EPA-Ireland (2020a), Air Quality in Ireland 2019*Rep.*

EPA-Ireland (2020b), Recent trends in nitrogen dioxide (NO2) levels in air (Ireland) edited, https://www.epa.ie/newsandevents/news/pressreleases2020/name,69166,en.html.

Fagerli, H., S. Dutchak, K. Torseth, M. Amman, and M. Ritter Convention on Long Range Tranboundary Air Pollution, European Monitoring and Evaluation Programme, edited, p. EMEP website, EMEP.

Ganesan, A. L., A. J. Manning, A. Grant, D. Young, D. E. Oram, W. T. Sturges, J. B. Moncrieff, and S. O'Doherty (2015), Quantifying methane and nitrous oxide emissions from the UK and Ireland using a national-scale monitoring network, *Atmos. Chem. Phys.*, *15*(11), 6393-6406, doi:10.5194/acp-15-6393-2015.

Garg, S., B. P. Chandra, V. Sinha, R. Sarda-Esteve, V. Gros, and B. Sinha (2016), Limitation of the Use of the Absorption Angstrom Exponent for Source Apportionment of Equivalent Black Carbon: a Case Study from the North West Indo-Gangetic Plain, *Environmental Science & Technology*, *50*(2), 814-824, doi:10.1021/acs.est.5b03868.

Godec, R., M. Čačković, K. Šega, and I. Bešlić (2012), Winter Mass Concentrations of Carbon Species in PM 10 , PM 2.5 and PM 1 in Zagreb Air, Croatia, *Bulletin of Environmental Contamination and Toxicology*, *89*(5), 1087-1090, doi:10.1007/s00128-012-0787-4.

Grahame, T. J., R. Klemm, and R. B. Schlesinger (2014), Public health and components of particulate matter: the changing assessment of black carbon, *Journal of the Air & Waste Management Association (1995)*, *64*(6), 620-660, doi:10.1080/10962247.2014.912692.

Grigas, T., J. Ovadnevaite, D. Ceburnis, E. Moran, F. M. McGovern, S. G. Jennings, and C. O'Dowd (2017), Sophisticated Clean Air Strategies Required to Mitigate Against Particulate Organic Pollution, *Scientific Reports*, *7*, 44737, doi:10.1038/srep44737 https://www.nature.com/articles/srep44737#supplementary-information.

Healy, R. M., et al. (2017), Ambient measurements and source apportionment of fossil fuel and biomass burning black carbon in Ontario, *Atmospheric Environment*, *161*, 34-47, doi:https://doi.org/10.1016/j.atmosenv.2017.04.034.

Heard, D. E., et al. (2006), The North Atlantic Marine Boundary Layer Experiment(NAMBLEX). Overview of the campaign held at Mace Head, Ireland, in summer 2002, *Atmos. Chem. Phys.*, *6*(8), 2241-2272, doi:10.5194/acp-6-2241-2006.

Hegerl, G. C., S. Brönnimann, T. Cowan, A. R. Friedman, E. Hawkins, C. Iles, W. Müller, A. Schurer, and S. Undorf (2019), Causes of climate change over the historical record, *Environmental Research Letters*, *14*(12), 123006, doi:10.1088/1748-9326/ab4557.

Helin, A., et al. (2018), Characteristics and source apportionment of black carbon in the Helsinki metropolitan area, Finland, *Atmospheric Environment*, *190*, 87-98, doi:https://doi.org/10.1016/j.atmosenv.2018.07.022.

Hoesly, R. M., et al. (2018), Historical (1750–2014) anthropogenic emissions of reactive gases and aerosols from the Community Emissions Data System (CEDS), *Geosci. Model Dev.*, *11*(1), 369-408, doi:10.5194/gmd-11-369-2018.

Hourdin, F., et al. (2006), The LMDZ4 general circulation model: climate performance and sensitivity to parametrized physics with emphasis on tropical convection, *Climate Dynamics*, *27*(7), 787-813, doi:10.1007/s00382-006-0158-0.

Hu, R.-M., L. Coleman, C. Noone, C. Lin, J. Ovadnevaite, and C. O'Dowd (2019), Regionally Significant Residential-heating Source of Organic Aerosols, 170, doi:10.15344/2456-351X/2019/170.

Huang, S., R. Arimoto, and K. Rahn (2001), Sources and source variations for aerosol at Mace Head, Ireland, *Atmospheric Environment - ATMOS ENVIRON*, *35*, 1421-1437, doi:10.1016/S1352-2310(00)00368-X.

Huijnen, V., et al. (2010), The global chemistry transport model TM5: description and evaluation of the tropospheric chemistry version 3.0, *Geoscientific Model Development*, *3*(2), 445-473, doi:10.5194/gmd-3-445-2010.

ICOS (2015), ICOS Atmospheric Station Specifications, edited, ICOS.

ICOS (2016), Integrated Carbon Observation System, edited, pp. https://www.icos-ri.eu, ICOS.

Inness, A., et al. (2018), The CAMS reanalysis of atmospheric composition, *Atmospheric Chemistry and Physics Discussions*, 1-55, doi:10.5194/acp-2018-1078.

Intergovernmental Panel on Climate, C. (2006), 2006 IPCC Guidelines for National Greenhouse Gas Inventories, Prepared by the National Greenhouse Gas Inventories Programme*Rep.*, IGES.

Jennings, S. G., D. Ceburnis, A. G. Allen, J. Yin, R. M. Harrison, M. Fitzpatrick, E. Wright, J. Wenger, J. Moriarty, and J. R. Sodeau (2006), Air Pollution--Nature and Origin of PM10 and Smaller Particulate Matter in Urban Air *Rep. ERTDI Report 48*, 116 pp, EPA Ireland Dublin.

Jones, A. R., D. J. Thomson, M. Hort, B. Devenish, C. Borrego, and A. L. Norman (2007), The U.K. Met Office's next-generation atmospheric dispersion model, NAME III, *Air Pollution Modeling and its Application XVII (Proceedings of the 27th NATO/CCMS International Technical Meeting on Air Pollution Modelling and its Application)*, 580-589.

Kiss, G., B. Varga, I. Galambos, and I. Ganszky (2002), Characterization of water-soluble organic matter isolated from atmospheric fine aerosol, *Journal of Geophysical Research: Atmospheres*, *107*(D21), ICC 1-1-ICC 1-8, doi:10.1029/2001JD000603.

Kleefeld, S., A. Hoffer, Z. Krivácsy, and S. G. Jennings (2002), Importance of organic and black carbon in atmospheric aerosols at Mace Head, on the West Coast of Ireland (53°19'N, 9°54'W), *Atmospheric Environment*, *36*(28), 4479-4490, doi:http://dx.doi.org/10.1016/S1352-2310(02)00346-1.

Kroll, J. H., C. L. Heald, C. D. Cappa, D. K. Farmer, J. L. Fry, J. G. Murphy, and A. L. Steiner (2020), The complex chemical effects of COVID-19 shutdowns on air quality, *Nature chemistry*, *12*(9), 777-779, doi:10.1038/s41557-020-0535-z.

Krzysztof, K., J. Katarzyna, and C. Marianna (2017), Characterization and Seasonal Variations of Organic and Elemental Carbon and Levoglucosan in PM10 in Krynica Zdroj, Poland, *Atmosphere*, *8*(10), 190, doi:10.3390/atmos8100190.

Kuenen, J. J. P., A. J. H. Visschedijk, M. Jozwicka, and H. A. C. Denier van der Gon (2014), TNO-MACC_II emission inventory; a multi-year (2003–2009) consistent high-resolution European emission inventory for air quality modelling, *Atmos. Chem. Phys.*, *14*(20), 10963-10976, doi:10.5194/acp-14-10963-2014.

Laing, J. R., D. A. Jaffe, and I. I. I. A. J. Sedlacek (2020), Comparison of Filter-based Absorption Measurements of Biomass Burning Aerosol and Background Aerosol at the Mt. Bachelor Observatory, *Aerosol and air quality research*, *20*(4), 663-678, doi:10.4209/aaqr.2019.06.0298.

Lamarque, J. F., et al. (2010), Historical (1850–2000) gridded anthropogenic and biomass burning emissions of reactive gases and aerosols: methodology and application, *Atmospheric chemistry and physics*, *10*(15), 7017-7039, doi:10.5194/acp-10-7017-2010.

Lee, J. D., W. S. Drysdale, D. P. Finch, S. E. Wilde, and P. I. Palmer (2020), UK surface NO2 levels dropped by 42% during the COVID-19 lockdown: impact on surface O3, *Atmos. Chem. Phys. Discuss.*, *2020*, 1-27, doi:10.5194/acp-2020-838.

Leinert, S. M., F. Jennings, G. (2008), New Transboundary Air Pollution Monitoring Capacity for Ireland, edited, Environmental Protection Agency Ireland.

Lenhart, L., and R. Friedrich (1995), European emission data with high temporal and spatial resolution, *Water, Air, and Soil Pollution*, *85*(4), 1897-1902, doi:10.1007/BF01186111.

Lin, C., D. Ceburnis, S. Hellebust, P. Buckley, J. Wenger, F. Canonaco, A. S. H. Prévôt, R.-J. Huang, C. O'Dowd, and J. Ovadnevaite (2017), Characterization of Primary Organic Aerosol from Domestic Wood, Peat, and Coal Burning in Ireland, *Environmental Science & Technology*, *51*(18), 10624-10632, doi:10.1021/acs.est.7b01926.

Lin, C., et al. (2019), Wintertime aerosol dominated by solid fuel burning emissions across Ireland: insight into the spatial and chemical variation of submicron aerosol, *Atmospheric Chemistry and Physics Discussions*, 1-24, doi:10.5194/acp-2019-499.

Magee-Scientific (2017), Results of research testing and evaluation of replacement Filter Tape Media*Rep.*, Berkeley, Ljubljana.

Martinsson, J. (2014), Using the Aethalometer for Source Apportionment of Carbonaceous Aerosols*Rep.*, 10 pp, Lund University Division of Nuclear Physics, Lund, Sweden.

Masson-Delmotte, V., Zhai, P., Pörtner, P.H., Roberts, D., Skea, J., Shukla P.R.,, A. Pirani, Moufouma-Okia, W., Péan, C., Pidcock, R., Connors, S., Matthews, J. B. R., Chen, Y., Zhou, X., Gomis, M. I.,, and E. Lonnoy, Maycock, T., Tignor, M., Waterfield, T. (eds.) (2018), IPCC, 2018: Summary for Policymakers*Rep.*, 32 pp, World Meteorological Organization, Geneva, Switzerland.

Meirink, J. F., P. Bergamaschi, and M. C. Krol (2008), Four-dimensional variational data assimilation for inverse modelling of atmospheric methane emissions: method and comparison with synthesis inversion, *Atmos. Chem. Phys.*, *8*(21), 6341-6353, doi:10.5194/acp-8-6341-2008.

Menut, L., B. Bessagnet, G. Siour, S. Mailler, R. Pennel, and A. Cholakian (2020), Impact of lockdown measures to combat Covid-19 on air quality over western Europe, *Science of The Total Environment*, *741*, 140426, doi:https://doi.org/10.1016/j.scitotenv.2020.140426.

Misselbrook, T. H., J. N. Cape, L. M. Cardenas, D. R. Chadwick, U. Dragosits, P. J. Hobbs, E. Nemitz, S. Reis, U. Skiba, and M. A. Sutton (2011), Key unknowns in estimating atmospheric emissions from UK land management, *Atmospheric Environment*, *45*(5), 1067-1074, doi:http://dx.doi.org/10.1016/j.atmosenv.2010.11.014.

Mooney, P., F. Mulligan, and C. Broderick (2016), Diurnal cycle of precipitation over the British Isles in a 0.44° WRF multiphysics regional climate ensemble over the period 1990–1995, *Climate Dynamics*, *47*(9-10), 3281-3300, doi:10.1007/s00382-016-3026-6.

Munir, S. (2017), Analysing Temporal Trends in the Ratios of PM2.5/PM10 in the UK, *Aerosol and Air Quality Research*, *17*(1), 34-48, doi:10.4209/aaqr.2016.02.0081.

Murphy, P., Browne, P., Caslin B., Crosson P., Donnellan, T., Farrelly, N., Fealy, R., Finnan, J., Foley, M., Foreman, S., Gibson, M., Hennessy,M., Humphreys, J., Hyde,T., Kelly,P., Lanigan,G., Lawlor, P., Maher, P., NiFhlatharta, N., O'Brien, D., O'Donoghue,C., O'Kiely, P.,O'Mara, F.,O'Shea, R.,Richards, K., Ryan,M., Shalloo, L.,Schulte, R. (2015), Interim report on greenhouse gas emissions from Irish Agriculture*Rep.*, Teagasc Agriculture and Food Development Authority, Oak Park, Carlow.

NASA (2019), World of Change, https://earthobservatory.nasa.gov/world-of-change/decadaltemp.php, in *Decadal Temperatures*, edited, NASA GISS.

Ng, N. L., et al. (2011), An Aerosol Chemical Speciation Monitor (ACSM) for Routine Monitoring of the Composition and Mass Concentrations of Ambient Aerosol, *Aerosol Science and Technology*, *45*(7), 780-794, doi:10.1080/02786826.2011.560211.

Novakov, T., and H. Rosen (2013), The Black Carbon Story: Early History and New Perspectives, *Ambio*, *42*(7), 840-851, doi:10.1007/s13280-013-0392-8.

NUIG, A. P. R. C. (2019), MaceHead.org, edited, Atmospheric Research Cluster NUIG.

O'Dowd, C., et al. (2011), *The Eyjafjallajokull ash plume - Part I: Physical, chemical and optical characteristics*, 129-142 pp., doi:10.1016/j.atmosenv.2011.07.004.

O'Dowd, C., D. Martin, and D. Arnold (2019), IMPLiCIt IMProving inversion modeL Capability in Ireland*Rep. 2016-CCRP-MS.33*.

O'Dowd, C. D., and T. Hoffmann (2005), Coastal new particle formation: A review of the current state-of-the-art, *Environ. Chem.*, *2*(4), 245-255, doi:10.1071/EN05077.

Ovadnevaite, J., D. Ceburnis, M. R. Canagaratna, H. Berresheim, J. Bialek, G. Martucci, D. R. Worsnop, and C. O'Dowd (2012), On the effect of wind speed on submicron sea salt mass concentrations and source fluxes, *J. Geophys. Res.*, *117*(D16201), doi:10.1029/2011JD017379.

Palas (2019), Fidas 200E, edited, p. https://www.palas.de/en/product/fidas200e, Palas GmbH, Karlsruhe, Germany.

Patashnick, H., and E. G. Rupprecht (1991), Continuous PM-10 Measurements Using the Tapered Element Oscillating Microbalance, *Journal of the Air & Waste Management Association*, *41*(8), 1079-1083, doi:10.1080/10473289.1991.10466903.

Petzold, A., and M. Schönlinner (2004), Multi-angle absorption photometry—a new method for the measurement of aerosol light absorption and atmospheric black carbon, *Journal of Aerosol Science*, *35*(4), 421-441, doi:10.1016/j.jaerosci.2003.09.005.

Picarro (2019), Cavity Ring-Down Spectroscopy, in *Picarro Science Instruments*, edited, p. https://www.picarro.com/company/technology/crds, Picarro Inc., Santa Clara, California, USA.

Pio, C., M. Cerqueira, R. M. Harrison, T. Nunes, F. Mirante, C. Alves, C. Oliveira, A. Sanchez de la Campa, B. Artíñano, and M. Matos (2011), OC/EC ratio observations in Europe: Re-thinking the approach for apportionment between primary and secondary organic carbon, *Atmospheric Environment*, *45*(34), 6121-6132, doi:https://doi.org/10.1016/j.atmosenv.2011.08.045.

Querol, X., et al. (2004), Speciation and origin of PM10 and PM2.5 in selected European cities, *Atmospheric Environment*, *38*(38), 6547-6555, doi:https://doi.org/10.1016/j.atmosenv.2004.08.037.

Ramanathan, V., and G. Carmichael (2008), Global and regional climate changes due to black carbon, *Nature Geoscience*, *1*, 221, doi:10.1038/ngeo156.

Ravishankara, A., J. Daniel, and R. W. Portmann (2009), Nitrous Oxide (N2O): The Dominant Ozone-Depleting Substance Emitted in the 21st Century, *Science*, *326*(5949), 123-125, doi:10.1126/science.1176985.

Ruthenburg, T. C., P. C. Perlin, V. Liu, C. E. McDade, and A. M. Dillner (2014), Determination of organic matter and organic matter to organic carbon ratios by infrared spectroscopy with application to selected sites in the IMPROVE network, *Atmospheric Environment*, *86*, 47-57, doi:10.1016/j.atmosenv.2013.12.034.

Salako, G., et al. (2012), Exploring the Variation between EC and BC in a Variety of Locations, *AEROSOL AND AIR QUALITY RESEARCH*, *12*, 1-7, doi:10.4209/aaqr.2011.09.0150.

Samaali, M., M. D. Moran, V. S. Bouchet, R. Pavlovic, S. Cousineau, and M. Sassi (2009), On the influence of chemical initial and boundary conditions on annual regional air quality model simulations for North America, *Atmospheric Environment*, *43*(32), 4873-4885, doi:10.1016/j.atmosenv.2009.07.019.

Sandradewi, J., et al. (2008a), Comparison of several wood smoke markers and source apportionment methods for wood burning particulate mass, *Atmos. Chem. Phys. Discuss.*, *2008*, 8091-8118, doi:10.5194/acpd-8-8091-2008.

Sandradewi, J., A. S. H. Prévôt, S. Szidat, N. Perron, M. R. Alfarra, V. A. Lanz, E. Weingartner, and U. Baltensperger (2008b), Using Aerosol Light Absorption Measurements for the Quantitative Determination of Wood Burning and Traffic Emission Contributions to Particulate Matter, *Environmental Science & Technology*, *42*(9), 3316-3323, doi:10.1021/es702253m.

Sandradewi, J., A. S. H. Prévôt, E. Weingartner, R. Schmidhauser, M. Gysel, and U. Baltensperger (2008c), A study of wood burning and traffic aerosols in an Alpine valley using a multi-wavelength Aethalometer, *Atmospheric Environment*, *42*(1), 101-112, doi:10.1016/j.atmosenv.2007.09.034.

Sarangi, B., S. G. Aggarwal, and P. K. Gupta (2015), A Simplified Approach to Calculate Particle Growth Rate Due to Self-Coagulation, Scavenging and Condensation Using SMPS Measurements during a Particle Growth Event in New Delhi, *Aerosol and Air Quality Research*, *15*(1), 166-179, doi:10.4209/aaqr.2013.12.0350.

Schultz, D. M., S. Anderson, J. G. Fairman, D. Lowe, G. McFiggans, E. Lee, and R. Seo-Zindy (2015), ManUniCast: a real-time weather and air-quality forecasting portal and app for teaching, *Weather*, *70(6)*, 180-186.

Speranza, A., R. Caggiano, S. Margiotta, and S. Trippetta (2014), A novel approach to comparing simultaneous size-segregated particulate matter (PM) concentration ratios by means of a dedicated triangular diagram using the Agri Valley PM measurements as an example, *Natural Hazards and Earth System Sciences*, *14*, doi:10.5194/nhess-14-2727-2014.

Stein, A. F., R. R. Draxler, G. D. Rolph, B. J. B. Stunder, M. D. Cohen, and F. Ngan (2015), NOAA's HYSPLIT atmospheric transport and dispersion modeling system, *Bull. Amer. Meteor. Soc.*, *96*, 2059-2077, doi:http://dx.doi.org/10.1175/BAMS-D-14-00110.1.

Sugimoto, N., A. Shimizu, I. Matsui, and M. Nishikawa (2015), *A method for estimating the fraction of mineral dust in particulate matter using PM2.5-to-PM10 ratios*, doi:10.1016/j.partic.2015.09.005.

Thermo-Fisher-Scientific (2016), TEOM Technology for Particulate Matter Measurement, in *https://www.thermofisher.com/ie/en/home/industrial/environmental/environmental-learning-center/air-quality-analysis-information/teom-technology-particulate-matter-measurement.html*, edited, Thermo Fisher Scientific.

Thompson, R. L., and A. Stohl (2014), FLEXINVERT: an atmospheric Bayesian inversion framework for determining surface fluxes of trace species using an optimized grid, *Geosci. Model Dev.*, *7*(5), 2223-2242, doi:10.5194/gmd-7-2223-2014.

Thompson, R. L., et al. (2015), Methane emissions in East Asia for 2000–2011 estimated using an atmospheric Bayesian inversion, *Journal of Geophysical Research: Atmospheres*, *120*(9), 2014JD022394, doi:10.1002/2014JD022394.

TROPOS, L. I. f. T. R. (2018), Intercomparison of absorption photometer http://www.actris-ecac.eu/absorption-photometer.html, edited.

Trusilova, K., C. Rödenbeck, C. Gerbig, and M. Heimann (2010), Technical Note: A new coupled system for global-to-regional downscaling of CO₂ concentration estimation, *Atmos. Chem. Phys.*, *10*(7), 3205-3213, doi:10.5194/acp-10-3205-2010.

TSI (2007), Model 3775 Condensation Particle Counter Operation and Service Manual, edited by TSI, p. 133, Minnesota, USA.

Tuccella, P., G. Curci, G. Visconti, B. Bessagnet, L. Menut, and R. J. Park (2012), Modeling of gas and aerosol with WRF/Chem over Europe: Evaluation and sensitivity study, *Journal of Geophysical Research: Atmospheres*, *117*(D3), n/a-n/a, doi:10.1029/2011JD016302.

Turpin, B. J., and H.-J. Lim (2001), Species Contributions to PM2.5 Mass Concentrations: Revisiting Common Assumptions for Estimating Organic Mass, *Aerosol Science and Technology*, *35*(1), 602-610, doi:10.1080/02786820119445.

Vana, M., M. Ehn, T. Petäjä, H. Vuollekoski, P. Aalto, G. de Leeuw, D. Ceburnis, apos, C. D. Dowd, and M. Kulmala (2008), Characteristic features of air ions at Mace Head on the west coast of Ireland, *Atmospheric Research*, *90*(2), 278-286, doi:10.1016/j.atmosres.2008.04.007.

Vermeulen, A. T., R. Eisma, A. Hensen, and J. Slanina (1999), Transport model calculations of NW-European methane emissions, *Environmental Science & Policy*, *2*(3), 315-324, doi:http://dx.doi.org/10.1016/S1462-9011(99)00021-0.

Vingarzan, R. (2004), A review of surface ozone background levels and trends, *Atmospheric Environment*, *38*(21), 3431-3442, doi:10.1016/j.atmosenv.2004.03.030.

Wang, H., A. Junlin, B. Zhu, L. Shen, Q. Duan, and Y. Shi (2017), Characteristics of Carbonaceous Aerosol in a Typical Industrial City—Nanjing in Yangtze River Delta, China: Size Distributions, Seasonal Variations, and Sources, *Atmosphere*, *8*, 73, doi:10.3390/atmos8040073.

Wang, J., L. M. Cardenas, T. H. Misselbrook, and S. Gilhespy (2010), Development and application of a detailed inventory framework for estimating nitrous oxide and methane emissions from agriculture, *Atmospheric Environment*, *45*(7), 1454-1463, doi:10.1016/j.atmosenv.2010.12.014.

Wang, P., et al. (2016), Inverse modeling of black carbon emissions over China using ensemble data assimilation, *Atmos. Chem. Phys.*, *16*(2), 989-1002, doi:10.5194/acp-16-989-2016.

Watson, T. B. (2017), Aerosol Chemical Speciation Monitor (ACSM) Instrument Handbook, edited, U.S. Department of Energy Office of Science, Brookhaven National Laboratory.

Wavemetrics (2014), Igor Pro, edited, Wavemetrics.

Whitehead, J. D., G. Mcfiggans, M. W. Gallagher, and M. J. Flynn (2010), Simultaneous coastal measurements of ozone deposition fluxes and iodine-mediated particle emission fluxes with subsequent CCN formation, *Atmospheric chemistry and physics*, *10*(1), 255-266, doi:10.5194/acp-10-255-2010.

Xing, L., T. M. Fu, J. J. Cao, S. C. Lee, G. H. Wang, K. F. Ho, M. C. Cheng, C. F. You, and T. J. Wang (2013), Seasonal and spatial variability of the OM/OC mass ratios and high regional correlation between oxalic acid and zinc in Chinese urban organic aerosols, *Atmospheric Chemistry and Physics*, *13*(8), 4307-4318, doi:10.5194/acp-13-4307-2013.

Yttri, K. E., et al. (2007), Elemental and organic carbon in PM₁₀: a one year measurement campaign within the European Monitoring and Evaluation Programme EMEP, *Atmos. Chem. Phys.*, *7*(22), 5711-5725, doi:10.5194/acp-7-5711-2007.

Zotter, P., H. Herich, M. Gysel, I. El-Haddad, Y. Zhang, G. Močnik, C. Hüglin, U. Baltensperger, S. Szidat, and A. S. H. Prévôt (2017), Evaluation of the absorption Ångström exponents for traffic and wood burning in the Aethalometer-based source apportionment using radiocarbon measurements of ambient aerosol, *Atmospheric Chemistry and Physics*, *17*(6), 4229-4249, doi:10.5194/acp-17-4229-2017.